

Site Directed Mutagenesis Studies of
Horseradish Peroxidase.

Barry Ryan, B.Sc.

School of Biotechnology,
Dublin City University,
Glasnevin,
Dublin 9.

Under the Supervision of Dr. Ciarán Ó'Fágáin.

PhD

2006

"To know the road ahead, ask those coming back".

Anon.

"What is written without effort is, in general, read without pleasure".


Samuel Johnson

"Nihil sine labore" - Nothing without work.

Anon.

Declaration

I hereby certify that this material, which I now submit for assessment on the programme of study leading to the award of Doctor of Philosophy is entirely my own work and has not been taken from the work of others save and to the extent that such work has been cited and acknowledged within the text of my work.

Signed:  _____

ID No.: 99797874 Date: 21/12/06.

Acknowledgements.

I would like to sincerely thank my supervisor, Dr. Ciarán Ó'Fágáin, for not only giving me the opportunity to carry out this research in his laboratory, but also for always being there when I had any problems. My thanks also to his trusted "*red pen*" for all those corrections!

I wish to acknowledge the financial assistance of IRCSET (The Irish Research Council for Science, Engineering and Technology), the Vice President for Research (Dublin City University) and the School of Biotechnology (Dublin City University). All monies were greatly appreciated. Prof. Francis Arnold is thanked for supplying the HRP gene.

My deepest thanks to my parents, Noel and Maria, who supported me all the way through college. Words cannot thank you enough. Thanks also to my two sisters, Emma and Karen, who provided much needed distraction throughout the years.

Special thanks to Teresa, who has been there for me from literally day one of college! Her love is unconditional, even though I test that sometimes with "*five more minutes*" in the lab! Thanks for all the help, encouragement, motivation and support to complete this project.

A huge thank you to all the School of Biotechnology postgrads and BRS members. Great times were had throughout my studies including trips abroad and infamous "*receptions*". Special thanks to Eva, who put up with me the most! From my initial PCR phobia to little drawings on the lab whiteboard. Thanks to Sue, Sinead, Jenny Fitzgerald, Noeleen, Zelda, Caroline and Jenny Ni Mhurchu for introducing me to the concept of a "*coffee break*" and all the chats, advice and craic in between! A special mention to all the postgrad soccer crew, especially Conor, Lenny, Fred, Dennis, Barry Mc, Cormac, Dan and John, the "*Barney Cup*" will be ours some day!

A massive thank you to all the postdocs that helped me along the way. I am indebted to Paul Clarke, Paul Leonard, Jonny Finlay, Páraic Ó Cuív, Roman Vaas and Stephen Hearty for all the advice and suggestions on the molecular / protein work carried out in this project. Many thanks to Aoife Morrin, Jennifer Brennan and Neil Carolan for their help and guidance with the electrochemistry.

I wish to thank all the lecturers at the School of Biotechnology for all their help and encouragement over the last seven years, especially Dr. Mary O'Connell who introduced me to the wonders of bioinformatics! Dr. Donal O'Shea and Ms Lynne Dobson are thanked for their assistance with the imaging work in Chapter Seven. The School of Biotechnology and School of Chemistry (especially Veronica Dobbyn) technical staff are also thanked.

Many thanks to my football team, Clonard GAA. They provided many laughs along the way and always made sure I kept my feet on the ground. The long runs in the sand dunes of Curracloe were a great way to take my mind off things in the lab! Thanks also to all my drinking buddies: Sean, Karl, Barry Red, Cathal, Phillip, Shane and the rest. I'll pay back all those pints now!

Thanks also to all the friends and family who offered encouragement along the way including: Tony, Kate, Pat, Frances, Patrick, Michelle, Claire, Duncan, Maria, Anne, Elaine, David and all the others I forgotten to mention.

Abbreviations

δ ALA	Delta Aminolevulinic Acid
A ₆₀₀	Absorbance at 600 nm
AA	Amino acid (see Appendix D)
ABTS	2,2'-Azino-bis(3-ethylbenzothiazoline-6-sulfonic acid)
AFM	Atomic Force Microscopy
BCA	Bicinchoninic acid
bp	Base-pair
BSA	Bovine serum albumin
BHA	Benzhydroxamic Acid
cAMP	cyclic AMP
C ₅₀	Half Inactivation Concentration
CD	Circular Dichroism
CIP	Calf Intestinal Phosphatase
CO	Carbon Monoxide
Conc.	Concentration
CRP	cyclic AMP receptor protein
DAB	3,3'-Diaminobenzidine Tetrahydrochloride
DET	Direct Electron Transfer
dH ₂ O	Deionised water
dNTPs	Nucleotide mix
DMSO	Dimethyl sulphoxide
DNA	Deoxyribonucleic acid
DnaK/DnaJ	Co-expression chaperones
DsbA,B,C	Folding accessory proteins
DTT	Dithiothreitol
EC	Enzyme commission
EDTA	Ethylenediaminetetra acetic acid
ELISA	Enzyme Linked Immunosorbant Assay
ET	Electron Transfer
FRET	Fluorescence Resonance Energy Transfer
HRP	Horseradish Peroxidase
HRP A2	Horseradish Peroxidase, Isoform A2
HRPc	Horseradish Peroxidase, Isoform C

HRP I – V	Horseradish Peroxidase, Compounds One to Five
H ₂ O ₂	Hydrogen Peroxide
ΔG	Gibbs free energy
IMAC	Immobilised metal affinity chromatography
IPTG	Isopropyl-β-D-thiogalactopyranoside
ISH	In situ hybridisation
k_3	Apparent peroxidase k_{cat}
K'_m	Apparent peroxidase K_m
LB	Luria Bertani
MCS	Multiple cloning site
MOPS	3-(N-Morpholino)propanesulfonic acid
mRNA	Messenger RNA
NTA	Nitrilotriacetic acid
NMR	Nuclear magnetic resonance
OD	Optical density
OPD	1,2-Diaminobenzene
ORF	Open reading frame
PAGE	Polyacrylamide gel electrophoresis
PANI	Polyaniline
PEG	Polyethylene Glycol
Pt	Platinum
RBS	Ribosome binding site
rHRP	Recombinant HRP
RNA	Ribonucleic acid
RZ	Reinheitzahl
SAM	Self Assembled Monolayer
SBP	Soyabean Peroxidase
SDM	Site Directed Mutagenesis
SDS	Sodium dodecyl sulphate
SEM	Scanning Electron Microscopy
STET	Sucrose/ Triton X100/ EDTA/ Tris
$t_{1/2}$	Apparent half-life.
TAE	Tris Acetate EDTA
TEMED	<i>N, N, N, N'</i> -tetramethyl ethylenediamine

TMB	3,3',5'5-Tetramethyl Benzidine
TNBS	2,4,6-trinitrobenzenesulfonic acid
Tris	Tris (hydroxymethyl) amino methane
tRNA	Transfer RNA
UV	Ultraviolet light
V_{max}	Maximum reaction velocity
v/v	Volume per volume
w/v	Weight per volume
X-Gal	5-bromo-4-chloro-3-indolyl- β -D-galactopyranoside
% SD	Percentage Standard Deviation

Units

A	Ampere
Å	Angstrom (1.0×10^{-10} metres)
°C	Degrees celcius
Da	Dalton
g	Gram
g	g-force (relative centrifugal force - rcf)
hr	Hour
kb	Kilo base
L	Litre
m	Metre
M	Molar
min	Minute
mol	mole
s	Second
pH	Logarithm of reciprocal hydrogen-ion concentration
pI	Isoelectric point
rpm	Revolutions per minute
V	Volts
W	Watts

Prefixes

k	kilo (10^3)
c	centi (10^{-2})
m	milli (10^{-3})
μ	micro (10^{-6})
n	nano (10^{-9})
p	pico (10^{-12})

Description	Page
Declaration	I
Acknowledgements	II
Abbreviations	III
Table of Contents	VII
List of Figures	XII
List of Tables	XV
Abstract	XVI
Publications and Presentations.	XVII

Table of Contents

1	Introduction	1-39
1.1	Introduction to Peroxidases.	1
1.1.1	Heme Peroxidase Classification.	1
1.1.2	Horseradish Peroxidase Features and Crystal Structure.	2
1.1.3	Recombinant HRP Expression.	4
1.1.4	Horseradish Peroxidase Catalytic Activity.	9
1.1.5	HRP Substrates.	11
1.1.6	HRP Inhibitors.	14
1.1.7	HRP Roles and Applications.	15
1.1.8	HRP Applications: Direct electrochemical biosensors.	16
1.2	Introduction to Protein Stability.	20
1.2.1	Chemical Modification.	21
1.2.2	Genetic Modification.	21
1.2.3	Horseradish Peroxidase Stability.	23
1.3	Introduction to Protein Mutagenesis.	25
1.3.1	Site directed Mutagenesis.	25
1.3.2	Random Mutagenesis.	25
1.3.3	Combination Mutagenesis.	27
1.3.4	Rational and Semi-Rational Design.	27
1.3.4.1	Sequence Comparison.	28
1.3.4.2	Entropic Stabilisation.	28
1.3.4.3	Sequence Dipeptide Composition.	28
1.3.4.4	Tanford/Kirkwood-Bashford/Karplus Method.	29
1.3.4.5	Consensus Approach.	29
1.3.4.6	Canonical Sequence Approximation.	29
1.3.4.7	SCOPE Method.	29
1.3.5	Mutation Selection Software.	30
1.3.5.1	Homology Modelling.	31
1.3.5.2	“POPMuSiC”, algorithm.	31
1.3.5.3	“WHAT IF” algorithm.	31
1.3.6	Horseradish Peroxidase Mutagenesis.	31
1.3.6.1	Site Specific Horseradish Peroxidase Mutants.	32
1.3.6.2	Random Mutagenesis of HRP.	38
1.4	Conclusions.	39
2	Materials and Methods	41-85
2.0	Materials	41
2.0.1	Instruments.	43
2.1	<i>E. coli</i> strains, plasmids and cloning primer sequences	44
2.1.1	<i>E. coli</i> strains.	44
2.1.2	Plasmids.	45

Description	Page
2.1.3 Cloning primers: design and sequences.	47
2.2 Preparation of Microbiological Media.	48
2.2.1 Luria Bertani Broth. (LB Broth).	48
2.2.2 SOB and SOC Media.	48
2.2.3 Super Broth Medium and 50/5 Supplement.	48
2.3 Antibiotic Preparation.	48
2.3.1 Ampicillin.	48
2.3.2 Chloramphenicol.	48
2.3.3 Tetracycline.	49
2.4 Preparation of Buffers.	49
2.5 Storage and Culture of Bacteria.	52
2.6 Standard Polymerase Chain Reaction.	52
2.7 Preparation of PCR product for downstream processes.	53
2.7.1 Phenol Chloroform Extraction.	53
2.7.2 Bioline DNase Quick Clean®.	54
2.8 Plasmid Preparation.	54
2.8.1 Rapid Boiling Method.	54
2.8.2 1,2,3 Plasmid Preparation Method.	55
2.8.3 Sigma Gene Elute Plasmid Prep Mini Kit.	55
2.9 Restriction Digest of the pQE60 Vector and the PCR insert.	56
2.10 Agarose Gel Electrophoresis for DNA characterisation.	57
2.11 Preparation of RNase.	57
2.12 Preparation of Ethidium Bromide.	57
2.13 Purification of DNA from an agarose gel.	58
2.14 Ligation Reactions.	58
2.15 Preparation of High Efficiency Competent Cells.	59
2.16 Transformation of High Efficiency Competent Cells.	60
2.17 Calculation of Transformation Efficiencies.	60
2.18 Screening of Transformed High Efficiency Competent Cells.	61
2.19 Spectrophotometric analysis of nucleic acids.	61
2.20 DNA Sequencing and Protein Sequence Alignment.	62
2.21 Design of mutagenic primers.	62
2.21.1 Mutagenic Primers utilised in this study.	63
2.22 Site-Directed Mutagenic PCR.	64
2.23 Selection of Residues for Mutagenesis.	65
2.23.1 Rational Mutation Selection.	65
2.23.2 Consensus Mutation Selection.	65
2.23.3 Immobilisation Mutation Selection.	66
2.24 Recombinant Protein Expression Protocols.	66
2.24.1 Localisation of recombinant HRP expression.	66
2.24.2 Investigation of IPTG requirement for rHRP production.	67
2.24.3 Comparison of bacterial strains for rHRP production.	67
2.24.4 Investigation of rHRP expression over time.	68
2.24.5 Optimisation of <i>E. coli</i> culturing conditions.	68
2.25 Recombinant HRP Purification.	68
2.25.1 Osmotic shock and lysozyme treatment for cell lysis.	69
2.25.2 Hydrophobic Interaction Chromatography.	69
2.25.3 Size Exclusion Chromatography.	70
2.25.4 Anion Exchange Chromatography.	70
2.26 Preparation of Dialysis Tubing.	71
2.27 Gel Electrophoresis.	71

Description	Page
2.27.1 Sodium DodecylSulfate PolyAcrylamide.	71
2.27.2 Western Blotting.	72
2.27.3 Native Gel.	73
2.28 Biochemical Protein Determination, Bicinchoninic Acid Assay.	74
2.29 UV-Visible spectrum and Reinheitszahl Number determination.	74
2.30 Quantitative HRP Activity Assay, (TMB).	74
2.30.1 Optimisation of TMB assay.	75
2.31 Determination of free amino groups using the TNBS assay.	75
2.32 Thermal profile catalytic activity.	75
2.33 Thermal Inactivation Assay.	76
2.34 Organic Solvent Tolerance Assay.	76
2.35 Tolerance of Excess H ₂ O ₂ .	77
2.36 Recombinant HRP Kinetic Analysis.	77
2.37 Immobilisation Methods.	78
2.37.1 Cyanogen Bromide-Activated Matrix Immobilisation.	78
2.37.2 Pall UltraBind™ Affinity Membrane Immobilisation.	78
2.38 Electrochemical Biosensing Devices.	79
2.38.1 Screen Printed Electrode.	79
2.38.2 Microelectrode Fabrication and Preparation.	80
2.38.3 Electrochemical Cell Preparation and Analysis.	82
2.38.4 Platinum microelectrode etching.	84
2.38.5 Scanning Electron Microscopy.	84
2.38.6 Protein immobilisation onto etched Pt microelectrode.	85
3 Cloning, Expression and Purification of recombinant HRP	86-125
3.0 Introduction.	86
3.1 Cloning of HRP gene sequences into an <i>E. coli</i> expression vector.	89
3.2 Amplification of PelB Leader and HRP gene sequences by PCR.	89
3.3 Cloning of Pel B Leader Sequence.	90
3.4 Cloning of HRP gene.	91
3.5 Sequencing of the cloned PelB and HRP vector construct.	92
3.6 Out of frame cloning and His tag deletion.	93
3.7 Expression of HRP gene in <i>E. coli</i> .	95
3.7.1 <i>E. coli</i> host strain optimisation.	95
3.7.2 Determination of optimal culturing temperature.	97
3.7.3 Investigation of HRP expression over time.	98
3.8 Recombinant HRP Purification.	99
3.8.1 Recombinant HRP Nickel Affinity Purification.	99
3.8.2 Recombinant HRP Classical Purification.	100
3.8.3 Optimised Recombinant HRP Nickel Affinity Purification.	102
3.9 Recombinant HRP Characterisation.	104
3.9.1 Protein Determination.	104
3.9.2 Determination of NH ₃ groups and UV-visible spectrum.	104
3.9.3 TMB Assay Optimisation.	105
3.9.4 Thermal Activity of wild type rHRP.	107
3.9.4.1 Thermal profile of wild type rHRP.	107
3.9.4.2 Thermal inactivation of wild type rHRP.	108
3.9.5 Native Gel Electrophoresis.	109
3.9.6 Organic Solvent Tolerance.	111
3.9.7 H ₂ O ₂ Tolerance.	112
3.9.8 ABTS Kinetic Analysis.	112

Description	Page
3.9.9 Western Blot Analysis.	113
3.10 Discussion	115
3.10.1 Choice of Expression Vector and Host.	115
3.10.2 Cloning Difficulties.	116
3.10.3 Expression of HRP gene in <i>E. coli</i> .	117
3.10.4 Recombinant HRP Purification.	118
3.10.5 Recombinant HRP Characterisation.	120
3.10.5.1 Chromogenic Assay Optimisation.	120
3.10.5.2 Thermal Stability.	121
3.10.5.3 Solvent Stability.	122
3.10.5.4 H ₂ O ₂ Stability.	124
3.10.5.5 Kinetic Characterisation.	124
3.10.5.6 Western Blot Analysis.	125
4 Site-Directed Mutagenesis: Proximal Lysine Residues.	126-170
4.1 Introduction.	126
4.2 Identification of Key Amino Acid Residues.	126
4.3 Optimisation of Mutagenic PCR.	127
4.4 Wildtype reversion mutation.	128
4.5 Designed Mutations.	129
4.5.1 Lysine 174 Mutations.	129
4.5.2 Lysine 232 Mutations.	131
4.5.3 Lysine 241 Mutations	133
4.5.4 Glutamic Acid (238/239) Mutations.	136
4.5.5 Double Lysine (232/241) Mutations.	138
4.5.6 Sequencing of mutants.	140
4.6 Characterisation of Single Mutants.	141
4.6.1 Determination of Single Mutants' Concentrations.	141
4.6.2 Single Mutant Thermal Tolerance.	142
4.6.3 Single Mutant Organic Solvent Tolerance.	145
4.6.4 Single Mutant H ₂ O ₂ Tolerance.	147
4.6.5 Steady-State Kinetics of Single Lysine Mutants.	148
4.7 Characterisation of Double Mutants.	150
4.7.1 Determination of Double Mutants' Concentrations.	150
4.7.2 Double Mutant Thermal Tolerance.	150
4.7.3 Double Mutant Organic Solvent Tolerance.	151
4.7.4 Double Mutant H ₂ O ₂ Tolerance.	153
4.7.5 Steady-State Kinetics of Double Lysine Mutants.	154
4.8 Discussion.	155
4.8.1 Mutation Selection and Generation.	155
4.8.2 Thermal Stability.	156
4.8.3 Organic Solvent Stability.	161
4.8.4 H ₂ O ₂ Stability.	166
4.8.5 Kinetic Characterisation.	168
4.9 Conclusions.	170
5 Site-Directed Mutagenesis: Consensus Approach.	171-196
5.1 Introduction.	171
5.2 Generation of Peroxidase Consensus Gene.	172
5.3 Generation of the "ProteinParser" Bioinformatic Software.	172
5.4 Mutational Primer Design.	174

Description	Page	
5.5	Designed Mutations and Computer Simulations.	174
5.6	Sequencing of mutants.	178
5.7	Characterisation of Consensus Mutants.	178
5.7.1	Determination of Consensus Mutants Concentration.	178
5.7.2	Consensus Mutant Thermal Tolerance.	179
5.7.3	Consensus Mutant Organic Solvent Tolerance.	180
5.7.4	Consensus Mutant H ₂ O ₂ Tolerance.	181
5.7.5	Consensus Mutant Steady-State Kinetics.	182
5.8	Discussion.	184
5.8.1	Consensus Mutation Selection and Generation.	184
5.8.2	Thermal Stability.	185
5.8.3	Organic Solvent Stability.	187
5.8.4	H ₂ O ₂ Stability.	189
5.8.5	Kinetic Characterisation.	189
5.8.6	Failure of Consensus Approach: Bioinformatic Analysis.	190
	5.8.6.1 Consensus Methodology Validation.	190
	5.8.6.2 Class III peroxidase Bioinformatic Analysis.	193
5.9	Conclusion	196
6	Immobilisation and Sensor Development.	197-239
6.0	Introduction.	197
6.1	Identification of Key Amino Acid Residues for Immobilisation.	199
6.1.1	Visualisation and Generation of Immobilisation Mutants.	200
6.1.2	Sequencing of mutants.	200
6.2	Expression, Purification and Immobilisation of “Velcro” Mutants.	203
6.2.1	Immobilisation on Cyanogen Bromide Activated Matrix	204
6.3	Characterisation of Free and Immobilised Immobilisation Mutants.	205
6.3.1	CNBr-Immobilised HRP Thermal Tolerance.	205
6.3.4	CNBr-Immobilised Organic Solvent Tolerance.	207
6.3.3	H ₂ O ₂ Tolerance of CNBr Immobilised HRP mutants.	211
6.3.4	UltraBind™ Affinity Membrane Immobilised Activity.	212
6.4	Electrochemical Biosensors.	214
6.4.1	Plotting convention for this study.	214
6.4.4	Screen Printed Electrode.	214
6.4.3	Etched Micro-Electrode.	217
	6.4.3.1 Schematic of a microelectrode.	217
	6.4.3.2 Characterisation of Pt microelectrode in H ₂ SO ₄ .	217
	6.4.3.3 CV of a bare platinum electrode.	219
	6.4.3.4 Electrooxidation of H ₂ O ₂ at the Pt microelectrode.	220
	6.4.3.5 Etching of the Pt microwire in the microelectrode	221
	6.4.3.6 Time-current response with addition of H ₂ O ₂ .	222
	6.4.3.6 Eadie-Hofstee electrochemical kinetic analysis.	224
6.5	Discussion	226
6.5.1	Immobilisation Mutants' Free Solution Stability.	226
6.5.2	Immobilisation on CNBr-Activated Sepharose.	227
6.5.3	CNBr-Activated Immobilised Enzyme Characterisation.	228
	6.5.3.1 Thermal Stability.	228
	6.5.3.2 Solvent Stability.	229
	6.5.3.3 H ₂ O ₂ Stability.	230
6.5.4	UltraBind™ Orientated <i>Proof of Principle</i> .	232
6.5.5	Electrochemical Biosensing Devices.	234

Description	Page
6.5.5.1 Screen Print Electrode.	234
6.5.5.2 Etched Microelectrode.	236
6.6 Conclusions	239
7 Overall Conclusions.	240-242
7.0 Overall Conclusions.	240
7.1 Summary and Future Work.	242
8 References.	243-275
9 Appendices	

Figure Description.	Page
1.1 Schematic illustration of the proximal and distal calcium ions and the heme group.	4
1.2 Basic HRP catalytic reaction scheme.	9
1.3 Schematic of HRP catalytic cycle.	10
1.4 Reaction mechanism of ABTS with peroxidase.	12
1.5 Illustration of the exposed heme edge of the ferriprotoporphyrin IX.	13
1.6 Relative amino acid compositions of mesophilic and hyperthermophilic proteins.	23
1.7 Rational and directed evolution methods for enhancing protein characteristics.	27
1.8 Schematic of previously mutated HRP residues.	33
3.1 Schematic diagram of the pQE60 vector.	86
3.2 Cloning overview of the PelB leader and HRP gene.	87
3.3 Schematic representation of pQE60_PelB_HRP_His and pQE60_PelB_HRPΔHis.	88
3.4 Illustration of the initial amplification of the PelB leader sequence.	89
3.5 Illustration of the secondary amplification of the HRP gene.	90
3.6 PCR products of PelB leader and HRP sequences.	90
3.7 A 1% TAE gel of the restricted pQE60 vector and the pQE 60_PelB vector.	91
3.8 A 1% TAE gel of the restricted of the pQE 60 vector and the pQE 60_PelHRP.	92
3.9 Alignment of the pQE60_PelB_HRP construct with the published sequence.	93
3.10 Schematic of <i>Nco</i> I vector and <i>Bsp</i> HI insert digestion and in-frame ligation.	94
3.11 Sequencing results aligned against published sequences for PelB leader and HRP.	94
3.12 The optimal host strain investigation for maximal HRP production.	95
3.13 12% v/v SDS-PAGE analysis for optimal host strain.	96
3.14 Screening expression conditions for optimal catalytic activity.	97
3.15 Investigation of optimal induction conditions.	97
3.16 Minimal glucose concentration (w/v) repress HRP production.	98
3.17 Plot of HRP activity versus <i>E. coli</i> growth at 30°C, 220 rpm.	98
3.18 Plot of HRP activity versus <i>E. coli</i> growth at 37°C, 220 rpm.	99
3.19 Purification of recombinant HRP via nickel affinity chromatography.	99
3.20 A 12 % SDS PAGE of a typical rHRP purification.	100
3.21 rHRP ammonium sulphate precipitation from the bacterial cell culture medium.	101
3.22 Typical plot of hydrophobic interaction purification of wildtype recombinant HRP.	101
3.23 Typical plot of size exclusion purification of wildtype recombinant HRP.	102
3.24 Typical plot of anion exchange purification of wildtype recombinant HRP.	102
3.25 Standard curve of bovine serum albumin (BSA) for the determination of protein.	104
3.26 Standard curve of N-α-acetyl-L-Lysine for the determination of amines.	105
3.27 Plot of TMB reaction versus time for purified wild type rHRP (10 μg/L).	106
3.28 Plot of TMB reaction versus time for purified wild type rHRP (varying H ₂ O ₂).	106
3.29 Plot of TMB reaction versus time varying concentrations of rHRP.	106
3.30 Thermal profile of plant, His- and Non-His Tagged rHRP.	107
3.31 Thermal inactivation of wildtype recombinant His tagged HRP at 50°C.	108
3.32 Thermal inactivation of rHRP His tagged at 50°C, 55°C and 65°C.	108
3.33 Native gel electrophoresis of concentrated wildtype rHRP.	109
3.34 Native gel electrophoresis of empty pQE60 vector and wildtype rHRP.	110
3.35 Native gel electrophoresis of concentrated wildtype rHRP incubated at room temperature or 55°C for 15min prior to addition to native gel.	110
3.36 Native gel of XL10 Gold HRP-producing cells periplasmically lysed.	111

Figure Description.	Page
3.37 Solvent Tolerance Profile of wildtype recombinant HRP.	111
3.38 H ₂ O ₂ tolerance profile for native recombinant His tagged HRP	112
3.39 Purified native rHRP ABTS steady-state kinetic data.	113
3.40 Western blot analysis of purified wildtype rHRP.	114
3.41 Western blot analysis of various purified rHRP mutants.	114
4.1 Location of key amino acid residues, Lys 174, Lys 232 and Lys 241.	127
4.2 Schematic of alternative site-directed mutagenesis PCR.	127
4.3 Diagrammatic representation of wildtype reversion mutation.	128
4.4 <i>In silico</i> and experimental analysis of A34P revertant.	128
4.5 DeepView™ modelling of Lysine 174 mutations.	130
4.6 Diagrammatic representation of the K174 mutant restriction pattern.	131
4.7 K174 mutant screening restriction digest visualised through 1% TAE agarose.	131
4.8 DeepView™ modelling of Lysine 232 mutations.	132
4.9 Diagrammatic representation of the K232 mutant restriction pattern.	133
4.10 K232 mutant screening restriction digest visualised through 1% TAE agarose.	133
4.11 DeepView™ modelling of Lysine 241 mutations.	134
4.12 Diagrammatic representation of the K241 mutant restriction pattern.	135
4.13 K241 mutant screening restriction digest visualised through 1% TAE agarose.	135
4.14 DeepView™ modelling of Glutamic Acid 238 mutation.	136
4.15 DeepView™ modelling of Glutamic Acid 239 mutation.	137
4.16 Diagrammatic representation of the E238/239 mutant restriction pattern.	137
4.17 E238/239 mutant screening restriction digest visualised through 1% TAE agarose.	138
4.18 DeepView™ modelling of double Lysine (232/241) mutations.	139
4.19 Diagrammatic representation of the K232/241 mutant restriction pattern.	139
4.20 K232/241 mutant screening restriction digest visualised through 1% TAE agarose.	139
4.21 Sequencing results for Lysine and Glutamic Acid mutations.	140
4.22 Thermal profile of Lysine 174 mutants.	142
4.23 Thermal profile of Lysine 232 mutants.	142
4.24 Thermal profile of Glutamic Acid 238/239 mutants.	143
4.25 Thermal profile of Lysine 241 mutants.	143
4.26 Semi-log plot of a selection of single lysine mutants' thermal inactivation at 50°C.	144
4.27 DMSO and MeOH tolerance profile of single lysine mutants.	145
4.28 DMF Solvent tolerance profile of single lysine mutants.	146
4.29 H ₂ O ₂ Tolerance profile of Lysine 174 mutants.	147
4.30 H ₂ O ₂ Tolerance profile of Lysine 232 mutants.	147
4.31 H ₂ O ₂ Tolerance profile of Lysine 241 mutants.	148
4.32 H ₂ O ₂ Tolerance profile of Glutamic Acid 238/239 mutants.	148
4.33 Thermal profile of Double Lysine 232/241 mutants.	150
4.34 Semi-log plot of Double Lysine 232/241 mutants.	151
4.35 Solvent Tolerance profile of Double Lysine 232/241 mutants.	152
4.36 H ₂ O ₂ Tolerance Profile of Double Lysine 232/241 mutants.	153
5.1 GeneDoc™ illustration of aligned HRP and consensus peroxidase gene sequence.	173
5.2 DeepView™ analysis of the Threonine 102 to Alanine mutation.	174
5.3 DeepView™ analysis of the Glutamine 106 to Arginine mutation.	175
5.4 DeepView™ analysis of the Glutamine 107 to Asparagine mutation.	175
5.5 DeepView™ analysis of the Threonine 110 to Valine mutation.	175
5.6 DeepView™ analysis of the Isoleucine 180 to Phenylalanine mutation.	176
5.7 <i>In silico</i> and experimental analysis of T102A, Q106R and Q107D mutations.	176
5.8 <i>In silico</i> and experimental analysis of T110V mutation.	177
5.9 <i>In silico</i> and experimental analysis of I180F mutation.	177
5.10 Sequencing results for Consensus mutations.	178
5.11 Consensus mutants thermal profile.	179
5.12 Semi-log plot of Consensus mutants thermal inactivation at 50°C.	179
5.13 Consensus mutants DMF tolerance profile.	180
5.14 Consensus mutants DMSO and MeOH tolerance profile.	181
5.15 Consensus mutants H ₂ O ₂ Tolerance Profile.	182
5.16 3-D ribbon structure of modern day HRP and reduced phylogenetic tree.	191
5.17 DeepView™ modelling of the hypothetical archetypal peroxidase & modern day HRP.	192
5.18 Location of helices within HRP, archetypal and consensus peroxidase.	195

Figure Description.	Page
6.1 Illustration of bioelectrocatalytic reduction of H ₂ O ₂ at a peroxidase-modified electrode	198
6.2 The location of the arginine residues within HRP in relation to active site entrance.	199
6.3 Rationale and selection flowchart for arginine to lysine immobilisation mutations.	200
6.4 Location of arginine to lysine mutations and predicted tertiary structure alterations.	201
6.5 <i>In silico</i> and experimental analysis of R118K, R159K and R283K mutations.	202
6.6 Sequencing results for Immobilisation mutations.	203
6.7 Thermal inactivation curve of rHRP, <i>Velcro Plus</i> and <i>Velcro Plus(K283R)</i> at 50°C.	205
6.8 Thermal inactivation curve of <i>Velcro Minus</i> and <i>Velcro Minus(K283R)</i> rHRP at 50°C.	206
6.9 Immobilised Wildtype DMSO and MeOH tolerance profiles.	207
6.10 Immobilised Wildtype DMF, <i>Velcro Plus</i> and <i>Velcro Plus(K283R)</i> DMSO and MeOH tolerance profiles.	208
6.11 Immobilised <i>Velcro Plus</i> and <i>Velcro Plus(K283R)</i> DMF, <i>Velcro Minus</i> and <i>Velcro Minus(K283R)</i> DMSO and MeOH tolerance profiles.	209
6.12 Immobilised <i>Velcro Minus</i> and <i>Velcro Minus(K283R)</i> DMF tolerance profile.	210
6.13 H ₂ O ₂ inactivation curves of Wildtype, <i>Velcro Plus</i> , <i>Velcro PlusK283R</i> , <i>Velcro Minus</i> and <i>Velcro Minus K283R</i> .	211
6.14 Illustration of UltraBind™ Affinity Membrane Immobilisation strategy.	212
6.15 Images of spotted immobilised overnight (24 hours) DAB stained rHRP activity.	212
6.16 Images of DAB stained (0-18 hrs), spotted immobilised rHRP activity.	213
6.17 Current-potential plotting convention utilised in this study.	214
6.18 Schematic of in-house screen-printed electrode components.	215
6.19 Schematic of in-house batch cell configuration.	215
6.20 Electro-deposition of polyaniline in 1M HCl onto the surface of the SPE.	216
6.21 Current response plot of immobilised rHRP, plant HRP and BSA to H ₂ O ₂ addition.	216
6.22 Schematic cross-section of an in-house fabricated microelectrode.	217
6.23 Cyclic voltamogram of a platinum microelectrode (25µM radius) in 1.0 M H ₂ SO ₄	218
6.24 Pt microelectrodes electrochemical response in various buffering reagents.	219
6.25 Pt microelectrodes electrochemical response in various H ₂ O ₂ concentrations.	220
6.26 Scanning Electron Microscope images of non-etched and etched microelectrodes.	221
6.27 Amperometric time course curve of an etched Pt microelectrode with absorbed rHRP.	222
6.28 Linearised amperometric time curve (5.0 x 10 ⁻⁵ mol.L ⁻¹ H ₂ O ₂ additions).	223
6.29 Linearised amperometric time curve (2.5x 10 ⁻⁴ mol.L ⁻¹ H ₂ O ₂ additions).	223
6.30 Linearised amperometric time curve (5.0 x 10 ⁻⁴ mol.L ⁻¹ H ₂ O ₂ additions).	224
6.31 <i>Enzfitter</i> ™ modelled MichaelisMenten plot of recombinant HRP H ₂ O ₂ catalysis.	224
6.32 Eadie-Hofstee plot for a recombinant HRP etched electrode biosensor.	225

Table Description.		Page
1.1	Welinder's classification of the peroxidase superfamily.	2
1.2	Characteristics of <i>E.coli</i> expressed recombinant HRP.	6
1.3	Eukaryotic expression hosts of recombinant HRP.	6
1.4	Summary of HRP applications.	15
1.5	Challenges in redox protein optimisation for bioelectrocatalysis.	20
1.6	Description of common labile amino acid residues and possible fate of each residue.	22
1.7	The critical catalytic residues in HRP.	32
1.8	Detailed description of HRP site-specific mutants.	34
1.9	HRP Directed Evolution mutants towards increased activity.	38
1.10	HRP Directed Evolution mutants towards increased thermal and H ₂ O ₂ tolerance.	39
3.1	Typical purification table for lysed cell recombinant Δ His HRP.	103
3.2	Typical purification table for osmotically lysed recombinant His HRP.	103
4.1	Lys (174/232/241) and Glu (238/239) mutants A _{403nm} and calculated concentrations.	141
4.2	Lys (174/232/241) and Glu (238/239) mutants <i>k</i> -value (50°C) and half-life (t _{1/2}).	144
4.3	Lys (174/232/241) and Glu (238/239) mutants solvent inhibitory concentrations (C ₅₀).	146
4.4	Lys (174/232/241) and Glu (238/239) mutants H ₂ O ₂ inhibitory concentrations (C ₅₀).	148
4.5	Lys (174/232/241) and Glu (238/239) mutants ABTS kinetic analysis.	149
4.6	Double Lys (232/241) mutants A _{403nm} and calculated concentrations.	150
4.7	Double Lys (232/241) mutants <i>k</i> -value (50°C) and half-life (t _{1/2}).	151
4.8	Double Lys (232/241) mutants solvent inhibitory concentrations (C ₅₀).	153
4.9	Double Lys (232/241) mutants H ₂ O ₂ inhibitory concentrations (C ₅₀).	154
4.10	Double Lys (232/241) mutants ABTS kinetic analysis.	154
5.1	Consensus amino acids calculated utilising a 50% tolerance threshold.	172
5.2	Consensus mutants A _{403nm} and calculated concentrations.	178
5.3	Consensus mutants <i>k</i> -value (50°C) and half-life (t _{1/2}).	180
5.4	Consensus mutants solvent inhibitory concentrations (C ₅₀).	182
5.5	Consensus mutants H ₂ O ₂ inhibitory concentrations (C ₅₀).	183
5.6	Consensus mutants ABTS kinetic analysis.	183
6.1	Immobilisation mutants A _{403nm} and calculated concentrations.	204
6.2	Activated CNBr immobilisation rate for wildtype and immobilisation mutants.	204
6.3	Immobilisation mutants <i>k</i> -value (50°C) and half-life (t _{1/2}).	206
6.4	Immobilisation mutants solvent inhibitory concentrations (C ₅₀).	210
6.5	Immobilisation mutants H ₂ O ₂ inhibitory concentrations (C ₅₀).	211
6.6	Pt electrode geometric area, electrochemical surface area and surface roughness factor.	218

Abstract

The peroxidases are a ubiquitous subset of enzymes found in both the animal and plant kingdoms. Of all the peroxidases, the majority of research has focussed on the Class III Horseradish Peroxidase (E.C. 1.11.1.7). The basic form, HRP-C, is the most common and is utilised in this study. Recombinant HRP-C was first expressed over fifteen years ago; however, its production has been plagued by the formation of inclusion bodies and low yields. In this present study, the HRP gene and a PelB leader sequence were directionally cloned to form a fusion protein, expressed to the bacterial periplasmic envelope. By manipulating subsequent expression conditions, fully functional HRP was successfully produced, with the inclusion of a poly-Histidine tag permitting single step purification.

Site directed mutagenesis was utilised to probe the stability of the recombinant enzyme. Two methodologies were employed to select residues for mutation, initially a rational approach, based on previous knowledge proposed 16 mutations. The second method based on a peroxidase sequence alignment utilising novel bioinformatic software, proposed 6 mutations. These mutants were generated, expressed and purified via optimised conditions. All mutants were characterised based on thermal, solvent and H₂O₂ stabilities, as well as kinetic analysis. Important stabilising roles for Glutamic Acid 238, Glutamine 106 and the helical secondary structure within the HRP protein were noted. Peroxidase structure evolution could be followed via a novel archetype peroxidase sequence generated. Mutations, which increased hydrogen bonding in the Lysine 232/Lysine 241 axis, improved stability.

Genetic engineering was also employed to generate a recombinant HRP-C that permitted simple directed immobilisation (one triple mutant and one pentuple mutant), allowing maximal accessibility to the enzymes' active site. Improved immobilisation capacity was achieved, however, at the cost of free and immobilised stability. Application of wildtype recombinant HRP-C to screen-printed and etched platinum electrode biosensors was investigated. Improved direct electron transfer was noted for recombinant HRP over plant HRP for both configurations.

Publications

- Horseradish and Soybean Peroxidases: Comparable Tools for Alternative Niches?
Ryan B. J., Carolan N, Ó'Fágáin C. (2006). *Trends in Biotechnology*, 24, (8), 355-363.
- Expression and purification of His-tagged recombinant human Bfl-1: use of a modified *E. coli* expression vector enables purification by Immobilised Metal Affinity Chromatography.
Loughran S. T, Loughran N. B, **Ryan B. J.**, D'Souza B. N, Walls D. (2006). *Analytical Biochemistry*, 355, (1), 148-150.
- "ProteinParser" - A community based tool for the generation of a detailed protein consensus and FASTA output.
Ryan B. J. and Barrett R. (2006). *Computer Methods and Programs in Biomedicine*, 85, (1), 69-76.
- Failure of consensus mutations to stabilise horseradish peroxidase: insights from an ancestral protein.
Ryan B. J., O'Connell M.J. and Ó'Fágáin C. *Manuscript in Preparation*.

Presentations: Posters

- Expression and purification of His-tagged recombinant human Bfl-1: use of a modified *E. coli* expression vector enables purification by Immobilised Metal Affinity Chromatography.
Loughran S. T, Loughran N. B, **Ryan B. J.**, D'Souza B. N, Walls D. GE Healthcare Challenging Proteins European Contest for Young Scientists 2005. Paris, 16th-18th October 2005.
- Site Directed Mutagenesis of Horseradish Peroxidase, Probing Molecular Stability.
Ryan B. J. and Ó'Fágáin C. Irish Research Council for Science, Engineering and Technology National Symposium 2005. Dublin, 28th October 2005.
- Directional Cloning of Horseradish Peroxidase and Expression Vector Engineering.
Ryan B. J. and Ó'Fágáin C. Irish Research Council for Science, Engineering and Technology National Symposium 2004. Dublin, 2nd November 2004.

Presentations: Oral

- Site Directed Mutagenesis of Horseradish Peroxidase, Probing Molecular Stability.
Ryan B. J. School of Biotechnology, Dublin City University, Seminar Series. Dublin, 12th December 2005.
- Site Directed Mutagenesis Studies of Horseradish Peroxidase.
Ryan B. J. School of Biotechnology, Dublin City University, PhD Transfer Exam. Dublin, 17th August 2005.

Chapter One.

Introduction.

1.1 Introduction to Peroxidases.

The peroxidases are a ubiquitous subset of enzymes found in both the animal and plant kingdoms. This extensive distribution suggests that these enzymes maintain a pivotal role in the growth and development of living systems. Horseradish peroxidase is the most widely studied of all the peroxidases, due mainly to its ability to fulfil many diverse roles in biotechnology and associated research areas such as medicine, genetics, and histochemistry (Dunford, 1991 and Ryan et al., 2006).

1.1.1 Heme Peroxidase Classification

All heme peroxidases have a heme-based prosthetic group located at the active site. In most plant peroxidases this is ferriprotoporphyrin IX, which is composed of four pyrrole rings joined by methene bridges with iron centering the molecule (Dunford, 1999). Several attempts to classify this unique set of enzymes have been made, based mainly on the HRP amino acid sequencing work of Welinder (1979) and crystal structure (Gajhede et al., 1997). Welinder developed a classification based on structural homology, sequence homology and posttranslational modifications that divided the peroxidase superfamily into three distinct groups, as outlined in Table 1.1.

Recently, Welinder has vindicated her classification via a more bioinformatic approach focussing on the evolutionary diversity of a Class III secretory plant peroxidase, *Arabidopsis thaliana*. The phylogenetic and molecular evolution approaches developed to characterise the chosen related peroxidases yielded similar results to the earlier classification based on structure, sequence and post-translational modifications. Based on these findings, Duroux suggests that the Class III plant peroxidase gene family emerged when plants first colonised land, and that adaptive advantages were conferred through the presence of peroxidase activity, such as in cell wall metabolism and plant defence mechanisms (Duroux and Welinder, 2003).

Table 1.1: Description of Welinder's classification of the peroxidase superfamily. The divisions are based on structural homology, sequence homology and post-translational modifications (Welinder, 1992).

Class I: Prokaryotic lineage

- Intra cellular. Unique structural features such as distal Heme Helix B sequence.
- No amino terminal signal peptides.
- No disulfide bridges.
- No glycosylation.
- No structural calcium ions.
- Conservation of Tryptophan residue.

Class II: Fungal Peroxidases

- These are extracellular with amino terminal signal peptides.
- Contain four disulfide bridges, located at different positions to other peroxidases.
- Low glycosylation, normally 5%.
- One structural calcium ion present.
- Absence of tyrosine residues.

Class III: Classical Secretory plant peroxidases.

- These are secretory with amino terminal signal peptides.
 - Contain four disulfide bridges, located at different positions to other peroxidases
 - High glycosylation, between 10 - 25%.
 - Two structural calcium ions present.
-

1.1.2 Horseradish Peroxidase Features and Crystal Structure.

Horseradish Peroxidase (HRP; E.C. 1.11.17, donor: hydrogen peroxide oxidoreductase), the most commonly studied Class III peroxidase isolated from the roots of the horseradish plant (*Armoracia rusticana*), is a “hardy perennial herb cultivated mainly in temperate regions of the world, primarily for its roots” (Veitch, 2004). It is a heme peroxidase that catalyses the oxidation of a wide range of aromatic compounds, and also functions in the transfer of hydrogen peroxide from hydrogen donors (Gilabert et al., 2004). Shannon and co-workers succeeded in isolating seven isoenzymes, three acidic, two neutral, and two basic, based on the pI of the purified isoenzyme (Shannon et al., 1966). Continued studies revealed an increasing number of isoforms (Aibara et al., 1981 and Aibara et al., 1982), generating at least fifteen isoforms that can be purified by conventional techniques. However, up to forty-two isoforms can be identified via isoelectric focussing of the crude root lysate (Hoyle, 1977). Several explanations have been forwarded as to the reason behind the large number of isoforms, including

posttranslational modification by non-specific C-terminal cleavage to yield peroxidase variants (Welinder, 1979). HRP-C, a neutral isoenzyme, is the single most-studied isoform, and is also the most abundant isoform in the horseradish root.

HRP-C consists of 308 amino acid residues, four disulphide bridges (between cysteines 11-91, 44-49, 97-301, 177-209) and a single buried salt bridge, between Asp99 and Arg123. The N-terminal residue is blocked by pyroglutamate and the C-terminal is heterologous, with some molecules lacking the terminal Ser308 (Welinder, 1979). As a member of the Class III secretory peroxidases, HRP has a tendency to be highly glycosylated. There are nine potential N-glycosylation sites, with only eight of them being occupied by a sugar moiety (Wuhrer et al., 2005). Branched heptasaccharides account for up to 80% of the molecule's sugar content, with the remaining 20% formed by a variety of heterogeneous glycans. Ultimately the total glycosylation depends on the source of the enzyme, and can range from 18-22% total mass typically (Veitch, 2004). It appears that glycosylation has an important effect on the stability of the enzyme and this will be discussed later (Section 1.2.3).

The heme prosthetic group attaches to the apoprotein via the side chain of the proximal His170 (Newmyer, et al., 1996a). The second axial co-ordination site remains unoccupied during the resting phase of enzyme catalysis. It is, however, available for hydrogen peroxide binding during enzyme catalysis. Small inactive molecules such as carbon monoxide and cyanide can replace a water molecule at the second co-ordination site and yield a six co-ordinate peroxidase complex (Meunier et al., 1995). The presence of the two calcium ions was confirmed by atomic absorption spectroscopy and removal of these caused a dramatic decrease in HRP-C thermostability, probably due to structural deterioration. Removal of the calcium ions also causes decreased enzymatic activity, indicating that Ca^{2+} plays an indirect role in catalytic activity (Haschke and Friedhoff 1978). Removal of the calcium ions causes a perturbation in the heme microenvironment; however, this can be reversed by restoration of calcium which causes a conformational change in the apoprotein around the single tryptophan residue in HRP, altering the region towards a more hydrophobic environment, elongating the heme-Trp distance by 9 Å, and changing the accessibility of the heme residue (Coates et al., 1998). Howes and co-workers revealed that the proximal calcium ion is dominant in influencing catalytic activity and structure (Howes, et al., 2001a).

The total molecular weight of HRP-C is a combination of all the factors outlined above. The amino acid residues contribute 33,890 Da, the ferric heme 550 Da, the two

by induction via isopropyl- β -D-thiogalactoside (IPTG) addition. However, overexpression led to the formation of misfolded apoprotein and necessitated disrupting these protein aggregates, refolding the protein correctly and addition of the heme centre. The disruption process involved addition of EDTA to chelate ions, lysozyme and DNase to reduce viscosity of bacterial cell lysate, urea to solubilise the protein, and dithiothreitol (DTT) to break disulphide bonds. The refolding procedure required slow exchange of disrupting reagents with folding reagents such as calcium (to provide structural integrity), oxidized glutathione (to reform disulphide bridges) and bovine hemin (to form the holoprotein active site; Smith et al., 1990).

Initially *E. coli* was chosen as the recombinant HRP expression system (Table 1.2); however, expression in this system is plagued by inclusion body formation, as described above. Additional problems with recombinant HRP expression in bacterial cell lines include the reducing nature of the host cytoplasm, which does not allow the oxidation of cysteine residues to form disulphide bonds (Teilum et al., 1999). Several other peroxidases have been cloned and expressed in *E. coli*, for example, soybean peroxidase (Chen and Vierleng, 2000), lignin peroxidase (Doyle and Smith, 1996), Neutral Horseradish Peroxidase (Bartonek-Roxa and Eriksson, 1994) and *Bacillus stearothermophilus* Peroxidase Gene (Loprasert et al., 1989).

Further studies have developed other expression hosts, such as *Pichia* and *Saccharomyces*, insect cell lines (such as *Spodoperta* and *Trichoplusia*), mammalian and plant cell lines. The main advantage of expressing in a eukaryotic system is that posttranslational modifications can be carried out on the recombinant protein; however, some insect systems can hyper-glycosylate proteins and purification from animal and plant cell lines can be difficult (Morton and Potter, 2000). Several of these have been utilised in the expression of recombinant HRP (Table 1.3).

Table 1.2: Characteristics of *E.coli* expressed recombinant HRP.

Comment	Reference
Apoprotein overexpressed as inclusion bodies Non glycosylated, 2-3% total protein Refolding protocol required	Smith et al., 1990.
Strain of <i>E.coli</i> affects expression levels.	Egorov et al., 1991.
Low temperature expression with added hemin. Low level expression, 0.5 U/ml. Reverted to refolding protocol to increase yield.	Egorov et al., 1994.
Overexpressed holoprotein as inclusion bodies Non-glycosylated, periplasmic expression. PelB leader sequence for periplasmic location C-terminal His tag for purification 8-10 mg/L cell culture	Grigorenko et al., 1999.
PelB leader sequence for periplasmic location. Induced with IPTG, no ABTS activity Weak activity in absence of IPTG.	Zhanglin et al., 1999
Coexpression of foldases with HRP. Active HRP located in periplasm	Kurokawa et al., 2000.

Table 1.3: Eukaryotic expression hosts of recombinant HRP.

Expression Host	Comment	Reference
Baculovirus	High level expression Soluble, active and glycosylated HRP Identical catalytic activity to wildtype HRP	Hartmann & Ortiz de Montellano, 1992
<i>S. cerevisiae</i>	Hyperglycosylated HRP produced Enzymatically treated to remove excess sugars	Vlami-Gardikas et al., 1992
<i>S. cerevisiae</i>	Directed evolution towards increased expression. 40 fold activity increase in culture supernatant. 260 U/L culture supernatant.	Morawski et al., 2000 a
<i>P. pastoris</i>	Directed evolution towards increased expression. 85 fold activity increase in culture supernatant. 600 U/L culture supernatant.	Morawski et al., 2000 b

Table 1.3 (Cont.): Eukaryotic expression hosts of recombinant HRP.

Expression Host	Comment	Reference
<i>P. pastoris</i>	Active HRP expressed. Continuous induction with methanol Peak HRP activity after 90 hours induced growth	Morawski et al., 2001
<i>N. tabaccum</i>	CaMV-35s or Light inducible promoter. 10 fold overexpression of rHRP Natural N-terminal sequence is essential.	Kis et al., 2004
<i>Spodoperta</i>	HRP secreted into culture medium 25 mg/L without hemin addition. 41 mg/L with hemin addition Ni ²⁺ Affinity purification, RZ of 3.2	Segura et al., 2005.
<i>Beta vulgaris</i>	1.21 x 10 ⁶ U/L, 20-day incubation. Similar pH optimum to plant HRP. Increased thermal stability compared to plant HRP.	Rudrappa et al., 2005.

Peroxidase-specific methodologies have been developed to overcome the major problem of inclusion body formation during prokaryotic expression, including use of specific *E. coli* strains, inclusion of chaperones and use of leader sequences. Teilum and co-workers developed a thioredoxin reductase-negative *E. coli* strain via selective pressure protocols. This *E. coli* strain allows for the formation of disulphide bonds, and hence a fifty-fold increase in the formation of active recombinant peroxidase was noted (Teilum et al., 1999). Kondo and co-workers (2000) co-expressed Dsb folding accessory proteins and molecular chaperones with recombinant HRP and noted an increase in HRP production and activity. The foldases utilised in this study included Dsb, which aids in the transportation of proteins to the periplasm, DsbA, which catalyses disulphide bond formation, and DsbC, which initiates disulphide bond isomerisation if abnormal cysteine bonds are formed. DsbD, in conjunction with Dsb, is thought to maintain DsbA and DsbC. Active HRP production increased with coexpression of these foldases, even at high inducer concentrations, which normally caused cell death due to toxic effects. Co-expression of molecular chaperones, such as DnaK, DnaJ and GrpE, had no effect on HRP production or activity (Kondo et al., 2000; Kurokawa, et al., 2000). Gene fusion technology has also been used to ameliorate the inclusion body formation problem (Zhang et al., 1998). Leader sequences were fused in-

frame with the HRP gene to direct the protein to the periplasm where it can fold correctly in the oxidising environment (Zhanglin et al., 1999; see also Table 1.2).

Another major obstacle in the recombinant expression of HRP is the limited availability of heme and iron within a bacterial cell. Bacterial cells each contain 10^5 to 10^6 iron ions that are essential for many metabolic pathways. The low solubility of iron (III) salts at physiological pH in the presence of oxygen is a serious obstacle to any method of introducing extra iron to a bacterial system (Wandersman and Stojiljkovic, 2000). Recombinant expression of hemoproteins is often hindered by the fact that the protein produced lacks the heme prosthetic group due, in part, to the increased rate of recombinant protein biosynthesis compared with the rate of heme biosynthesis (Varnado and Goodwin, 2004). Recently, Arnold and Lin (2000) noted poor RZ (Reinheitzahl; ratio of holoprotein to apoprotein, see Section 2.29) values (between 1.2-1.9) for recombinantly-expressed HRP. Again, simple suggestions have been put forward to alleviate the problem, including slower cultivation to allow the heme biosynthesis rate equilibrate with the protein synthesis rate; however, this reduces the total yield. An alternative approach is to supplement the cells with δ -aminolevulinic acid, synthesis of which is the rate-limiting step in heme biosynthesis in bacterial cells, but this is expensive on a large scale (Woodard and Dailey 1995). Direct addition of heme to the culture broth during recombinant protein expression has been proposed as a cost effective alternative to δ -aminolevulinic acid addition but problems remain in the ability of most laboratory *E. coli* strains to use exogenous heme as an iron source. In an effort to increase the ability of *E. coli* to utilise exogenous heme, certain strains have been genetically modified to express successfully a membrane heme receptor (Perry et al., 2003). Varnado and Goodwin (2004) cited another approach to this problem where a series of co-expression plasmids contain the genes for a heme receptor protein which, once transformed with the gene of interest, allow the host cell to utilise heme in the surrounding growth medium. The heme that is bound by the host cells can then be directly incorporated into the recombinant hemoprotein without affecting the rate of protein expression (Varnado and Goodwin, 2004).

1.1.4 Horseradish Peroxidase Catalytic Activity.

HRP is classified as an oxidoreductase (E.C. 1.11.17, donor: hydrogen peroxide) and as such it functions in the transfer of hydrogen peroxide from hydrogen donors. Inherent to this transferal ability is the catalytic cycle it undertakes. Theorell noted the formation of a green solution that rapidly turned red (reviewed in Theorell, 1957), which puzzled peroxidase scientists for decades until the work of Chance and George elucidated the existence of Compounds I and II in the HRP catalytic cycle (Chance and George, 1949). Their work allowed for the formulation of the widely accepted reaction scheme:

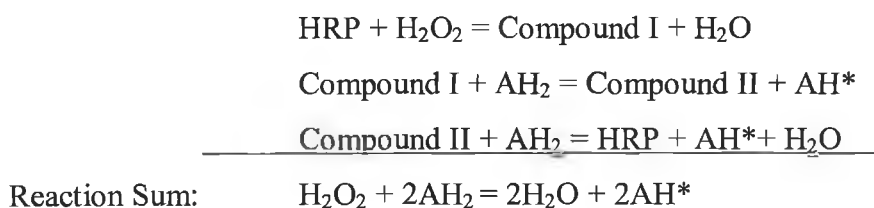


Figure 1.2: Basic HRP reaction scheme showing the formation of Compounds I and II. AH₂ is a reducing substrate, whilst AH* is the oxidised form of the substrate. (Dunford, 1999).

Continued studies concluded that the catalytic cycle of HRP is initiated by a rapid two-electron oxidation of the enzyme by hydrogen (or a similar) peroxide to yield the first intermediate, Compound I (Hiner et al., 2002) At this point, the heme iron is oxidised to its oxyferryl state [Fe(IV)=O] and a π -cation radical is located on the porphyrin ring (see Figure 1.3; Rodriguez-Lopez et al., 2000). To complete the cycle, HRPC-I is converted back to the resting enzyme via two successive single-electron reducing steps, the first yielding HRPC-Compound II, the second enzyme intermediate. HRPC-II retains the oxyferryl group but not the porphyrin cation radical. Compounds I and II are powerful oxidants, with redox potentials estimated to be close to +1.0 volts (Dunford, 1999). The site of oxidation has been investigated through the use of enzyme inactivation assays, with substrates such as cyclopropanol hydrate, nitromethane, alkylhydrazine, phenylhydrazine and sodium azide. The free radicals generated from the inactivating molecule remain in the region of activity and act as indicators to the site of oxidation. Hence, it was concluded that HRP oxidation took place at the exposed heme edge, which is composed of the C18 and C20 meso protons (Veitch and Smith, 2000). The rate of peroxidation catalysis depends on the nature of the reducing substrate, with conversion of Compound II to resting-state HRP being the rate-limiting step in the cycle. This is probably due to the longer electron transfer distance between the iron

atom of the heme group and the substrate, compared with the corresponding distance from the π -cation radical to the substrate in Compound I (Folkes and Candeias, 1997). Dunford and co-workers reported for horseradish peroxidase that Compound I formation is independent of viscosity in aqueous glycerol solutions. However, Compound I formation was a function of diffusion, influenced by such phenomena as size of the substrate and electrostatic interactions between charged reactants and the enzyme (Dunford and Hewson, 1977). Sato and co-workers described the effect of solvents on the oxidation of Compound II. Methanol and ethylene glycol (up to 50% v/v) were examined and oxidation was dramatically reduced, explained by the interaction of the hydroxy group of the solvent with the heme iron (Sato et al., 1995). Dead-end compounds, which lead to inactive enzyme, can also be formed in the presence of inhibitors. With Compound III formation a red colouration is observed, whilst with Compound IV formation a green colouration is noted (see Figure 1.3; Ryan et al., 1994). Dunford describes the Horseradish peroxidase catalytic pathway as a “*peroxidase ping-pong*” mechanism, in which the cycle is irreversible. This; combined with the fact that “*true*” peroxidase saturation cannot be achieved, prevents K_m value calculation (Dunford, 1999). However, much debate continues to surround this topic, with other mechanistic theories postulated, including van Haandels “*ping-pong-pang*” theory in which compound I formation is reversible (van Haandel et al., 1998).

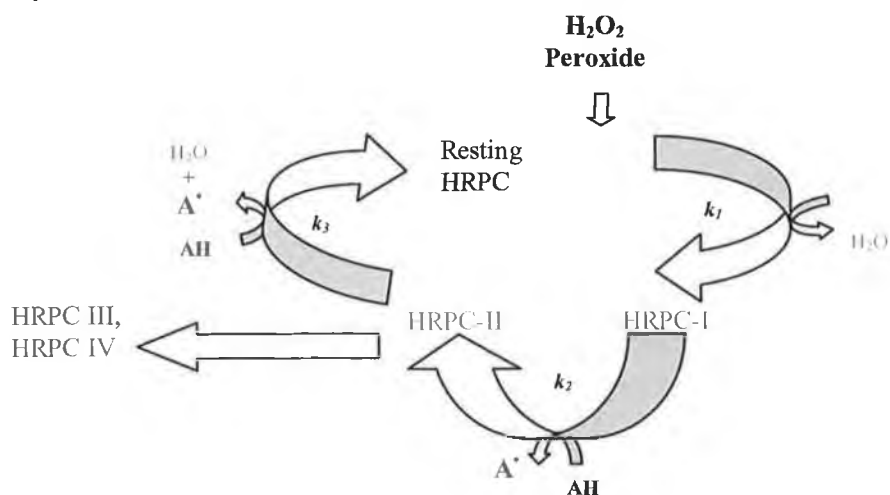


Figure 1.3: Schematic of HRP catalytic cycle, indicating the two intermediates (Compound I and II), the reaction rates k_1 , k_2 and k_3 ; and the products of the reaction, two radicals (A^*) and two water molecules. Compounds III and IV are inactive forms of HRP, often referred to as dead-end compounds.

There are several possible fates for the free radicals produced during catalysis. The radical may dimerise, react with another substrate molecule or attack another species causing co-oxidation. The radical may also reduce molecular oxygen to superoxide ($O_2^{\cdot-}$), or it may be scavenged by molecular oxygen to form a peroxy radical (HO_2^{\cdot} ; Dunford, 1991). The catalytic cycle of HRP continues to stimulate active research, including the observation of a transient intermediate Compound 0 (prior to the formation of Compound I) occurring at low temperatures in reactions between HRP and H_2O_2 (Filizola and Loew, 2000). In 2002 the catalytic cycle of horseradish peroxidase was solved by crystallography. Berglund and co-workers describe high-resolution crystal structures of the oxidation states of HRP (Resting State and HRP I-IV, as outlined in Figure 1.3); continued related studies will provide direct structural insights into redox chemistry at porphyrin-based iron centres (Berglund et al., 2002).

1.1.5 HRP Substrates.

Peroxidases are capable of catalysing the oxidation of a wide range of substrates. Fundamentally, HRP catalyses the decomposition of H_2O_2 , its natural substrate, into oxygen and water, via a two-electron transfer procedure, as outlined previously. The two-electron step requires that the HRP molecule be returned to its resting state, and this regeneration is aided by the presence of a hydrogen donor. The hydrogen donor is oxidised as the HRP molecule returns to its native state, and hence the term “oxidation/reduction reaction” is often used to describe the catalytic activity of HRP (Dunford, 1999).

Several types of hydrogen donor exist and many of these also serve as indicators for HRP activity. Indicator molecules encompass colorimetric, luminescent and fluorimetric methods of detection (Conyers and Kidwell, 1991). Not only do these molecules detect the presence of HRP, but they also indicate the rate of catalytic activity. Examples of colorimetric HRP substrates include TMB (3,3',5,5'-Tetramethylbenzidine), OPD (1,2-Diaminobenzene) and DAB (3,3'-Diaminobenzidine). However, to quantify the enzyme's catalytic activity ABTS (2,2'-Azino-bis(3-ethylbenzothiazoline-6-sulfonic acid) is a commonly cited substrate. One ABTS unit will oxidize 1 μ mol of ABTS per minute at 25°C at pH 5.0 (Sigma Aldrich, 2005).

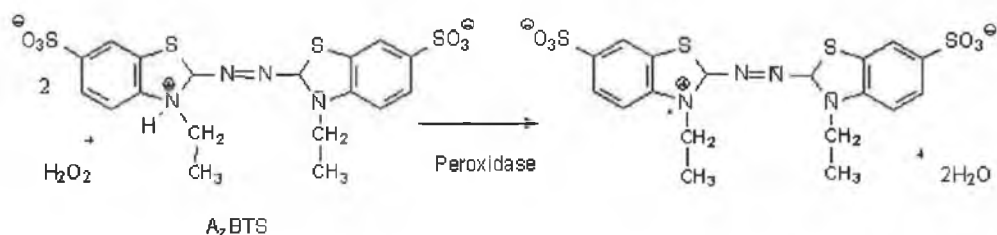


Figure 1.4: Reaction mechanism of ABTS with peroxidase results in the generation of two water molecules and a green coloured product, which can be read spectrophotometrically.

HRP can also oxidise certain chemiluminescent substrates, most commonly luminol, yielding light (Lu et al., 2004). This light emission can be measured and used to quantify HRP activity. Enhancers, such as luciferin, can be incorporated into assays to increase light emission from a flash signal to a more steady-state output and, hence, chemiluminescent techniques offer greater sensitivity compared with colorimetric assays (Azevedo et al., 2003 and Bonfils et al., 1996). Tanaka and co-workers unsuccessfully attempted to increase the active site accessibility of a recombinant HRP molecule to a luminol-based substrate to by site-directed mutagenesis as outlined Table 1.8 (Tanaka et al., 1999). HRP can also react with certain fluorimetric substrates such as 10-Acetyl-3,7-dihydroxyphenoxazine, known commercially as Amplex Red™. HRP reacts with Amplex Red™, in the presence of H₂O₂, in a 1:1 stoichiometry, to form resorfin, the fluorescent product. However, resorfin also has strong absorption, and hence it can be detected either fluorometrically (573 and 590 nm for absorption and emission respectively) or spectrophotometrically (575nm). The fluorometric assay is, however, the more sensitive method (Endo et al., 2005).

HRP can also participate in electrochemical reactions due to the inherent redox properties associated with its catalytic cycle. Here, HRP utilises a hydrogen donor that can be monitored voltametrically upon reduction. Electron donors that act as electron mediators and can be easily monitored voltametrically are essential (Sanchez et al., 1990). Electron donors employed in such situations include hydroquinone, *o*-toluidine, resorcinol and catechol. If reduction of the hydrogen donor can be measured, the concentration of hydrogen peroxide involved in the reaction can also be examined (Anh et al., 2003; Luo et al., 1997). Application of this is examined in more detail in Section 1.1.9.

HRP can also function as a catalyst in a number of other arrangements, most notably in the one-electron oxidation of phenols. Phenols such as *p*-hydroxyphenylacetate and *p*-

cresol can be converted into phenol radicals, which in turn spontaneously form polymers. The main application of this catalysis is the bioremediation of wastewater (Wanger and Nicell, 2002) as outlined in Table 1.4.

Iodine also reacts with HRP: in the presence of hydrogen peroxide, horseradish peroxidase and iodine, a simple enzyme-catalysed clock reaction occurs. In this reaction, hypoiodous acid, HOI, is reduced to form I^- ; however, in the absence of hydrogen peroxide, the remaining HOI reacts with the excess I^- to form the chromogen I_3^- . The length of time to the appearance of I_3^- is proportional to the concentration of H_2O_2 (Dunford, 1999)

HRP maintains the ability to carry out catalysis, including hydroxylations, N-demethylations and sulphoxidations, in the presence of organic solvents. Activity is maintained in organic solvents due to tightly bound nature of the water molecules within the enzyme structure (Azevedo et al., 2001). This is advantageous, as the enzyme can be used in detection systems where analytes must be dissolved in organic solvents (van de Velde et al 2001).

As can be seen, most reactions catalysed by HRP utilise reducing substrates, typically aromatic phenols, phenolic acids, indoles, amines and sulfonates (Veitch, 2004). The substrates and their products, most notably aromatic amines, can be carcinogenic and care should be taken in substrate choice (Dunford, 1991).

Substrate oxidation occurs at the exposed heme edge of the ferriporphyrin IX, at the region comprising the heme methyl C18 and heme meso C20 protons (Smith and Veitch, 1998, and Adak et al., 1996).

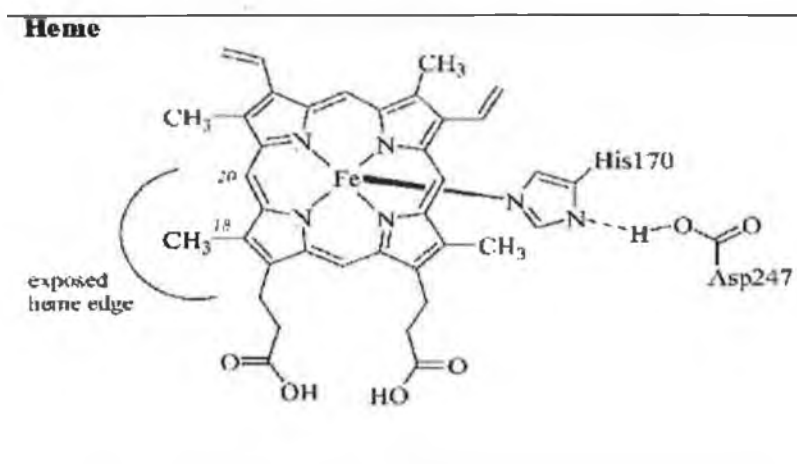


Figure 1.5: Diagrammatical representation of the exposed heme edge of the ferriporphyrin IX, adapted from Veitch (2004).

Recall that the rate-limiting step in HRP catalysis is the oxidation of the donor hydrogen molecule and the conversion of Compound II back to resting state HRP (Section 1.1.5). However, different rates of compound II conversion to resting state can be caused by substrate choice: van Haandel and co-workers (1999) noted a 3-fold difference between phenol and aniline oxidation, which was further proven by studies by Gilabert and co-workers. (Gilabert et al., 2004)

1.1.6 HRP Inhibitors.

In addition to the native substrate, phenols and aromatic amines, HRP can also bind a wide range of structurally related substrate analogs or inhibitors. Elegant suicide inhibitors have been developed that can bind to the exposed heme edge and competitively inhibit the peroxidase catalytic activity. One example of such an inhibitor is Benzhydroxamic Acid, BHA, which was utilised to elucidate the binding region of the HRP molecule, and demonstrated a hydrophobic aromatic binding pocket generated by His42, Phe68, Gly69, Ala140, Pro141 and Phe179 (Henriksen et al., 1998).

Other competitive inhibitors include 2-amino-4-nitrophenol (ANP), gallic acid (GA), 4,4'-dihydroxydiphenylsulfone (DDS) and their polydisulfides poly(ADSNP), poly(DSGA), poly(DSDDS). Metelitzka and co-workers (2004) demonstrated that the most effective competitive inhibitor, when TMB is utilised as a secondary hydrogen donor, is poly(DSGA); however, this may be due to the apparent peroxidase preference for phenol substrates. Interestingly, the polymer phenols were significantly more active inhibitors than their monomer analogs, indicating that size of the polymer phenol does not affect its binding capacity to HRP (Metelitzka et al., 2004).

Zaton and de Aspurn (1995) demonstrated that all uracils bind non-competitively to the active site of HRP; however, only thiolated uracils inhibit peroxidase activity. This inhibition could be due to the thiol residues interacting with the apoprotein, causing structural perturbation and thereby affecting activity (Zaton and de Aspuru, 1995).

Keyhani and co-workers (2003) established the inhibition of HRP by cadmium, noted as a noncompetitive or mixed inhibitor of HRP depending on the duration of incubation with HRP and on Cd^{2+} concentration. Three cadmium ions bound per HRP molecule, causing large conformational changes and a decrease in HRP activity (Keyhani et al., 2003). Similar results were noted when HRP was incubated with nickel. Four nickel ions bound to the HRP molecule, again causing structural perturbation and a dramatic decrease in activity. The enzyme remained active only over a limited metal

concentration range. Data indicated that binding of one Ni²⁺ affected the substrate binding site, binding of a second Ni²⁺ affected both substrate and peroxide binding sites, and binding of more than 2 Ni²⁺ per HRP molecule led to complete loss of enzymatic activity (Keyhani et al., 2005). Other methods of HRP inactivation, such as H₂O₂ poisoning, will be discussed in the section on protein stability (Section 1.2.3).

1.1.7 HRP Roles and Applications.

Interestingly, despite its many *in vitro* roles (Table 1.4), HRP's actual *in vivo* role has never been elucidated. Several suggestions have been based on the known roles of other plant peroxidases. Plant peroxidases are usually found in the cell wall, vacuoles, transport organelles and the rough endoplasmic reticulum, and have noted roles in lignification (Mader and Fussel, 1982), wound healing (Kerby and Sommerville, 1996) and auxin catabolism (Gazaryan et al., 1998). However, due to its intrinsic generation of free radical species during its catalysis, HRP offers a wide range of *in vitro* applications, as outlined in Table 1.4.

Table 1.4: Summary of HRP applications, with references to published work in the relevant area.

Application.	Reference.
Biosensor: This can be defined as an analytical device in which a specific biological interaction is transduced into an electrical signal. HRP is currently one of the most common biological components.	Li et al., 2004. Tang et al., 2003.
Immunoassay: Immunoassays are typically used to identify and quantify antigens and antibodies. HRP-based conjugates are commonly used in ELISA, immuno histochemistry and Western blotting immunoassays.	Dotsikas & Loukas, 2004. Shrivastav, 2003.
DNA Detection: <i>In situ</i> hybridisation (ISH) techniques are used to localise specific nucleic acid sequences within tissues or chromosomal preparations. HRP-based signal systems remain pivotal to ISH technology.	Ishii et al., 2004. van Gijlswijk et al., 2000
Bioremediation: From a variety of aromatic pollutants HRP can generate free radicals, which spontaneously polymerise and aid in the bioremediation of wastewater effluent.	Singh & Singh 2002. Wanger & Nicell, 2002.
Organic Synthesis: Peroxidases can catalyse oxidative transformations of organic reactants, utilising peroxide as the oxidant. Examples include sulfoxidations, N- and O-dealkylations and epoxidations.	van de Velde et al., 2001 Colonna et al., 1999.
Gene Therapy: HRP has been successfully used in gene-directed enzyme/prodrug therapy. An inactive precursor of the therapeutic agent is activated by the presence of HRP at specific location in the body.	Tupper et al., 2004 Greco et al., 2001.
Biomedical: Diagnostic test kits perform rapid analysis, sometimes at the bedside / point of care patient, with many containing HRP as an active component. Glucose sensors are the most common type of HRP-based diagnostic test.	Azevedo et al., 2003 Jamnicky et al., 1988.

1.1.8 HRP Applications: Direct electrochemical biosensors, a case study.

One of the fundamental areas of applied HRP research is biosensor innovation. A biosensor was recently stringently defined as “*a self contained integrated device which is capable of providing specific quantitative (or semi-quantitative) analytical information using a biological recognition element, which is in direct spatial contact with a transducer element*” (Thévenot et al., 1999). In theory, a biosensor can be tailored to match any individual analytical demand, provided the target molecule interacts selectively with a biological system. Electrochemical enzyme-based biosensors are of special interest owing to their practical advantages such as operational simplicity, low-cost fabrication, portability, potential for miniaturisation, high sensitivity and suitability for real time detection (Xu et al., 2004). In this configuration, an enzyme provides the “*biological recognition element*”, the output of which is converted to a measurable signal by electrochemical transduction. Currently, amperometric electrochemical transduction is most popular, as it offers high sensitivity in conjunction with a wide linear range (Freire et al., 2003).

Amperometric enzyme based biosensors can be classified into first, second and third generation devices. First generation biosensors relied on the electroactivity of the enzyme substrate or product. Second generation biosensors required a conducting molecule to shuttle the electrons generated at the enzyme’s active site to the electrode surface. Third generation biosensors do not require such mediators, with electrons “*hopping*” directly from the active site to the electrode surface. The area of HRP-based electrochemical sensors is too vast to review here; however, third generation, direct electrochemistry based biosensors will be summarised.

Direct enzyme-electrode electron transfer offers superior sensitivity, as it occurs during the catalytic conversion of the substrate to product. Selectivity is also increased by operating the biosensor in a potential range closer to the enzyme’s redox potential, thus reducing interfering reactions. Despite the many advantages of direct electron transfer (DET) in biosensor configurations, very few biomolecules are capable of interacting with an electrode whilst catalysing the corresponding enzymatic reaction. Typically, plant horseradish peroxidase has very slow DET, presumably due to heavy glycosylation (~20%) and the buried nature of the active site heme moiety (Ruzgas et al., 1996). Although there are reports of plant HRP-driven DET (Xu et al., 2004), these are mostly associated with carbon-based electrodes (Ferapontova, 2004a). However, DET for recombinant HRP has been noted with several electrode configurations,

including graphite rotating disk electrodes, with the improved DET being attributed to the lack of glycosylation (Lindgren et al., 1998). Marcus and Sutin (1985) postulate that electron transfer kinetics are governed by the potential difference (between the active site and the electrode), the structural rigidity of the redox species and the distance the electron has to travel (Marcus and Sutin, 1985). Mayo and co-workers (1986) further postulated that the rate of electron transfer (k) is exponentially proportional to the distance (d) the electron has to travel, and a constant (a), as given by:

$$k \propto e^{-ad}$$

In extreme cases, when the distance from the electron donor to acceptor is greater than 10 Å, the electron transfer rate drops by a factor of 10^4 (Cassidy et al., 1998). It appears that electron transfer occurs through “electron transfer channels” in the enzyme structure, as opposed to direct contact between the active site and the electrode (Lindgren et al., 1998). The pH at which the electrochemical catalysis is performed can also affect the rate of direct electron transfer. Ferapontova and Gorton (2002a) demonstrated that by decreasing the reaction pH from 8.0 to 6.0 DET is enhanced, possibly due to the involvement of a proton in the rate-determining step of electron transfer. Ferapontova (2004) recently reviewed peroxidase DET on a variety of electrode materials and concluded that DET is substantially more evident with recombinant than with plant HRP. In general, the specific catalytic requirements of HRP dictate the optimisation of bioelectrocatalysis on different electrode configurations. Adsorption is a particularly common immobilisation method for carbon-based electrodes, whilst the intrinsic structural features of the enzyme and of the electrode are crucial for metal based electrode immobilisation (Ferapontova, 2004b). Several examples of rHRP-based amperometric DET sensors are available in the literature (Ferapontova 2001, Ferapontova 2004a and references within) along with some reports of plant HRP DET sensors (Sun et al., 2004). Recombinant HRP was utilised in the movement towards bi-enzyme biosensors in work carried out by Shipovskov and co-workers (2004). In this work, a two-electrode system, comprising immobilised rHRP and cytochrome *c*, was established to detect superoxide radicals. In this arrangement, superoxide radicals ($O_2^{\cdot -}$) and H_2O_2 were simultaneously detected. A coupled bi-enzyme biosensor, in which the product of the first enzymatic reaction provides the substrate for the second, sensing, reaction is currently a vibrant area of research (Yang et al., 2004). Other peroxidases, both recombinant and native, are the

subject of DET research, including enzymes from tobacco, peanut and sweet pea (Lindgren et al., 2000, and Castillo et al., 2006).

Recent research has focussed on controlled deposition and orientation of immobilised recombinant oxidoreductases for optimal DET. As alluded to earlier, the shorter the electron transfer distance the greater the chance of DET occurring; hence, controlled directional immobilisation of enzymes is critical for the progression of third generation biosensors. Recombinant HRP demonstrates a higher percentage of correctly orientated molecules for DET in graphite rotating disk system than plant HRP; this has been ascribed to the absence of glycosylation. (Lindgren et al., 1999). Recently, Ferapontova and Dominguez (2004) demonstrated that DET could be improved by strategic manipulation of the electrode and surface charge of a recombinant HRP, presumably due to improved immobilisation. Typically, physical adsorption is utilised for peroxidase immobilisation onto a metal electrode; however, other methods such as entrapment (Yang et al., 2004) and direct covalent attachment (Castillo et al., 2005) are regularly employed.

Often, these methods lead to the formation of a randomly orientated layer, either on the surface of the electrode (metal) or within cavities (carbon). Physical adsorption may result in enzyme denaturation, due to multiple contacts with the solid phase. Binding of ligands, or substrate / product access and egress, may also be hindered, all resulting in poor bioelectrocatalytic activity (Freire et al., 2003). Self-assembled monolayers (SAM) are an attractive alternative for controlled, directed enzyme immobilisation. SAMs are highly organised monomolecular layers that form spontaneously upon submersion of a solid phase into a solution containing amphifunctional molecules. The lengthy hydrophobic chain of the SAM can be altered and terminated with a functional group that will interact only with a specific residue on an enzyme backbone (Gilardi and Fantuzzi, 2001). In this instance, a site-directed mutation could be utilised to dictate the location of the specific residue and, hence, control the orientation of the molecule (e.g additional Cys residue for thiol immobilisation; Ferapontova et al., 2002). Addition of chemically modifiable residues, preferably at the C-terminus of a protein, can simultaneously allow for improved immobilisation and DET. Ferapontova and co-workers (2002) introduced an additional Cys residue at the C-terminus of HRP, which leads to simple thiol-based immobilisation to a gold electrode and also improved DET. Redox proteins are not evolved, nor optimised, for bioelectrocatalysis. In Nature, random electron transfer is not permitted, as it would be wasteful to the organism. Also,

toxic metabolites, such as H_2O_2 , are not naturally produced in high concentrations. Further control is implemented by embedding redox-active centres deep within the insulating folds of the enzyme's backbone, and by regulating electron transfer through sophisticated control mechanisms (Wong and Schwaneberg, 2003). Protein engineering can be utilised to increase electron transfer rates and also to tailor redox proteins for specific requirements.

Researchers are faced with several challenges when attempting to optimise a redox protein for bioelectrocatalysis (see Table 1.5); however, several approaches are currently being pursued. Molecular wiring of redox proteins is an emerging field, in which electron-conductive chains can be used to link the redox centre of an enzyme to an electrode, thus providing an efficient electronic conjugation. Mutagenesis has been utilised to alter the protein backbone of azurin protein, in which a His residue was replaced with a smaller Gly, permitting direct molecular access to a buried copper ion 7 Å below the protein surface (Gilardi et al., 1994). Residues close to the active site can be mutated to allow for quicker product dissociation (lower K_m), as outlined by Davidson (2003) who replaced a bulky Phe residue in the substrate access channel of methylamine dehydrogenase with a smaller Ala; this decreased the K_m but also opened up the active site entrance. Removal of excess amino acids, not critical for structure or function, can increase access to the active site. Gelo-Pujic and co-workers (1999) removed 11 C-terminal amino acids from the Laccase protein, which improved access to the copper ion at the active site. Directed evolution also offers the potential of evolving an enzyme with a non-natural function, increased DET or long-term stability (Wong and Schwaneberg, 2003).

HRP dominates biosensor research, from the traditional voltammetric- and amperometric-based methods of detection, to nano-sized devices. Real-time quantification of hydrogen peroxide continues to be one of the main reasons for sensor development (Tønning et al., 2005), although other diverse applications include the detection of glucose (Alonso Lomillo et al., 2005), ethanol (Azevedo et al., 2005) and tumour markers *in vivo* (Lin and Ju, 2005). While a detailed account of the current applications of HRP-based sensors is beyond the scope of this review, some of the emerging trends in HRP-based biosensor development, including organic solvent compatible sensors and nano-sized sensors are highlighted.

Biosensors, including immunosensors (Penalva et al., 1999) and electro-sensors (Campanella et al., 2001), incorporating organic solvents have developed as an

expanding area of peroxidase research, primarily due to insolubility of many analytes in aqueous solutions. Recently, Konash and Magner (2006) developed a HRP-immobilised, mediated H₂O₂ sensor which demonstrated good catalytic activity in 2-butanone and ethyl acetate. Organic-solvent compatible bi-enzyme peroxidase sensors have also been cited in the literature (Castillo et al., 2003). Size reduction remains a pivotal area in sensor research. The use of nanoparticles offers increased surface area for enzyme immobilisation, whilst simultaneously reducing apparatus size (Liu et al., 2005). Currently, HRP-based nano-sensors are at the forefront of biosensor research (Ryan et al., 2006)

Table 1.5: Challenges in redox protein optimisation for bioelectrocatalysis.

Problem	Explanation.
Field Conditions	Enzymes tend to have a narrow optimal operation range, which may not suit test conditions.
Cofactor Requirement	Cofactors can be expensive and difficult to regenerate.
Enzyme Stability	Operation time can be reduced due to enzyme denaturation.
Enzyme Pretreatment	Many pre-treatment procedures (e.g. deglycosylation) can reduce enzyme activity.
Enzyme Immobilisation	Selection of suitable immobilisation technique can be an empirical process.
ET Control Processes	Naturally occurring ET control processes can be difficult to reverse.

1.2 Introduction to Protein Stability:

Protein stability is defined as “*the persistence of molecular integrity or biological function despite adverse influences or conditions, such as heat or other deleterious conditions*” (O Fágáin, 1997). Protein stability can be measured in many ways including conformational stability (which comprises monitoring protein unfolding due to deleterious conditions) and kinetic stability (which involves measuring the persistence of biological activity with time under stressful conditions; O Fágáin, 1997). In Nature, enzymes are not optimised towards stability; they are just stable enough not to be limiting for an organism (Lee and Vasmatzis, 1997). Indeed, most enzymes display a marginal stability profile regardless of size or function, and forcing the stability equilibrium towards instability is easily achieved (Taverna and Goldstein, 2002a) although sometimes apparently contradictory reports on enzyme robustness are

cited (Taverna and Goldstein, 2002b). It is clear, however, that the *in vitro* use of enzymes in biotechnological applications requires a degree of enzyme stabilisation to allow optimal enzyme function in non-natural environmental conditions (O Fágáin, 2003). Several methodologies have been developed to overcome the problems presented by protein instability, including chemical modification and genetic manipulation.

1.2.1 Chemical Modification.

Chemical modification of protein residues is a commonly utilised method in protein stabilisation. In this procedure, certain reactive amino acid R-groups are suitably changed to reduce the instability. At least eight amino acids (Cys, Lys, Asp, Glu, Arg, His, Tyr and Met) can react with specific chemical modifying reagents to form new “chemically-stabilised” proteins. These modifying reactions include crosslinking by bifunctional reagents, strengthening of hydrophobic interactions by non polar reagents, introduction of novel groups to aid in additional hydrogen bond formation, or hydrophilisation of the protein surface to reduce unfavourable surface hydrophobic contacts with water (O Fágáin, 1997). A recent example of such work includes Yoshitsune and co-workers (2005) laccase modification by use of an amphiphilic copolymer, polyalkyleneoxide-co-maleic anhydride. This strengthened the hydrophobic interactions of the enzyme, resulting in increased stability (Yoshitsune et al., 2005). A succinic anhydride modification of the lysine residues of papain reversed the charge of the lysine residue and yielded an increase in stability as well as a pH optimum shift (Roy et al., 2005). This methodology follows from the hydrophilization of protein surface concept postulated by Mozhaev and co workers (Mozhaev et al., 1988). Although chemical modification is a step above simple addition of stabilising additives, it does have many drawbacks including accessibility and the limited number of modifiable R-groups. This has led protein scientists to recombinant protein expression and genetic modification in an attempt to increase protein stability.

1.2.2 Genetic Modification.

Stable enzymes maintain features that allow the protein to function in non-optimal environments. Identifying and understanding the contributing factors to stability has been a long-standing problem. As research into protein stability continues, several attributes involved in the molecular basis of protein stability have been cited in the literature (Sterner and Liebl, 2001). The reasons for increased stability of particular

enzymes include optimal protein core packing and increased helical content, both of which increases the enzymes rigidity and reduce the risk of protein denaturation during environmental stress. Greater protein hydrophobicity allows for optimal folding of a protein structure and maintenance of this tertiary structure (Vlassi et al., 1999). The deletion or shortening of loop residues often helps increase stability. Loops are often considered the “*Achilles heel*” of protein structure and thermozymes often have shorter loops than their mesozyme counterparts (Kumar et al., 2000). The effect of increased hydrogen bonding is akin to locking the protein in position and, hence, increases protein stability; however, only certain amino acid residues can hydrogen bond (Pace et al., 2001). It has also been suggested that intramolecular salt bridges can stabilise proteins, even in a highly polar solvent. Salt bridges can also stabilise protein structure by enhancing structure rigidity (Elcock, 1998). In recent years the role of long-range electrostatic interactions in protein stabilisation has become clear (Spector et al., 2000; Sanchez-Ruiz and Makhatazde 2001; Vendruscolo 2002 and Torrez et al., 2003), contradicting previous ideas (Matthews, 1993). At a simple comparison level, thermophiles differ from mesophiles in their specific amino acid sequences, with each thermozyme capable of stabilisation by a unique combination of the attributes listed above (Sterner and Liebl, 2001). These differences, in conjunction with other biochemical studies, helped to identify certain labile amino acid residues as outlined in Table 1.6.

Table 1.6: Description of common labile amino acid residues and possible fate of each residue. (Fersht and Serrano, 1993 and Veille and Zeikus, 1996)

Asn and Gln	Deamination of amino acid residues.
Asp/Pro and Asn/Gly dipeptides	Susceptible to peptide bond hydrolysis.
Cys	β -elimination of disulphide bridges.
Cys	Oxidation of amino acid residue.
Methionine	Oxidation to sulphoxide component
Asp and Ser	Amino acids can be racemized to their D-form.
Lys	Can react with reducing sugars via Maillard reaction

Other specific amino acid residues, or patterns, were identified as labile and, as such, certain guidelines could be developed to select suitable amino acid replacements for increased stability. Statistical analysis indicates trends towards Gly→Ala and Lys→Arg substitutions. High Ala content is reflective of a high protein helical content, which, as discussed previously, leads to improved protein rigidity. There is also a notable

decrease in Val and Thr content, residues not compatible with helix formation. Hyperthermophilic proteins have a high hydrophobic and aromatic residues content, which aids packing, as does the presence of Ile: its high conformational flexibility, allows it to occupy any voids in the protein structure. In conjunction with this, Lys→Met mutants are often noted, as the bulkier side chain of Met (and Ile) aid in occupying voids in the protein core. A high Arg content is noted in hyperthermophiles: it readily forms ion pairs and hydrogen bonds with carboxylic acid residues close by. Increased Pro content is also typical of hyperthermophiles: as Pro can adopt only a few configurations, a low conformational entropy is achieved by its presence. The opposite is true for Gly the most flexible amino acid, and hence Gly→Xaa or Xaa→Pro are common substitutions in hyperthermophiles. Ultimately, these tendencies should allow rational selection of key residues for protein design, as outlined in Section 1.3 (Veille and Zeikus 2001).

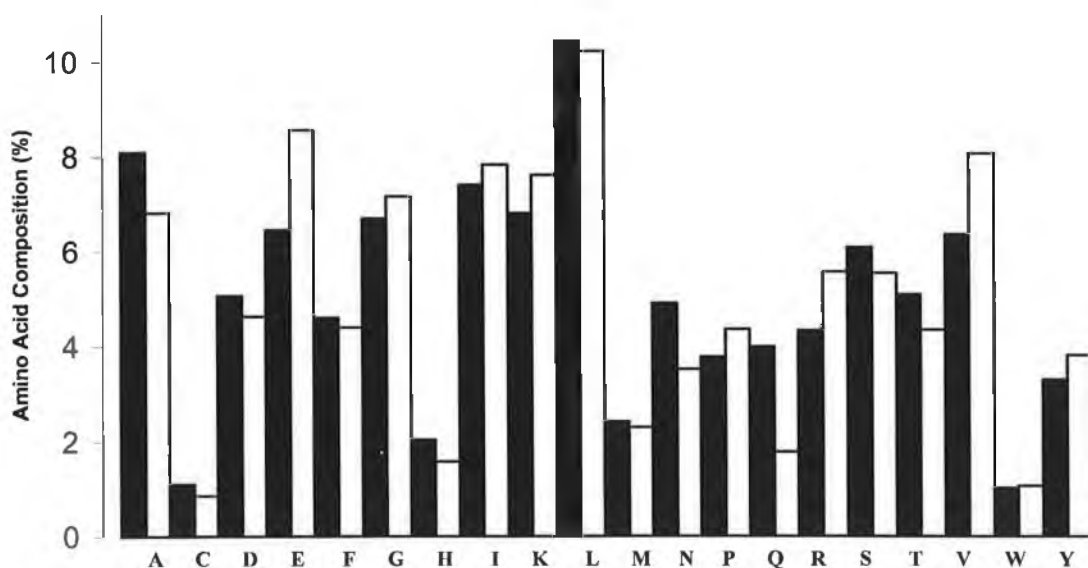


Figure 1.6: Relative amino acid compositions of mesophilic (white columns) and hyperthermophilic proteins (black columns). Sample mesophilic proteins taken from the genome sequences of; *B. subtilis*, *C. jejuni*, *E. coli*, *Haemophilus influenzae*, *Helicobacter pylori*, *Neisseria meningitidis*, *Rickettsia prowazekii* and *Synechocystis*. Hyperthermophilic proteins taken from the genome sequences of *Archaeoglobus fulfidus*, *Aquifex aeolicus*, *Aeropyrum pernix*, *Methanococcus jannaschii*, *Pyrococcus abyssi*, *Pyrococcus horikoshii* and *Thermus maritimus* (adapted from Veille and Zeikus, 2001. Single letter amino acid nomenclature used throughout.).

1.2.3 Horseradish Peroxidase Stability.

As outlined in Section 1.1.7, HRP has a wide and varied role within the life sciences and, as such, any increase in stability would afford new applications and functions for this “analyst’s friend” (Ryan et al., 1994). As with all proteins, the stability of HRP is

affected by a number of parameters including temperature (Pina et al., 2001; Chattopadhyay and Mazumdar 2000; Kaposi et al., 1999), calcium content (Kaposi et al., 1999), glycosylation (Tams and Welinder, 1998), pressure (Smeller and Fidy, 2002), irradiation (Orlaova et al., 2000), pH (Priori et al., 2000), hydrogen peroxide (Schmidt et al 2002; Nicell and Wright 1997; Arnao et al., 1990), urea (Moosavi-Movahedi and Nazari, 1994; Haque et al., 1999), guanidinium chloride (Chakrabarti and Basak, 1996) and various solvents including dimethyl sulfoxide (Santucci et al., 2002) and dimethylformamide (Machado and Saraiva, 2002). Thermal denaturation of horseradish peroxidase does not follow simple first- or second-order kinetics; instead, it tends towards a 1.5-order as outlined by Chang and co-workers (1998). Unfolding of both the apo- and holo-protein has been studied in detail, with refolding of the holo-protein proving particularly difficult. In these studies it was discovered that the protein backbone forms first, followed by calcium ion incorporation and finally by heme moiety inclusion (Pappa and Cass, 1993). Recent developments in the refolding of denatured holo-protein include the use of anti-peroxidase antibodies, which increases the refolding yield 100-fold over traditional refolding methods (Ermolenko et al., 2002).

Several attempts have been made to chemically increase the stability of this enzyme including addition of stabilising reagents (Kuhlmeyer and Klein 2003; Eremin et al., 2002), crosslinking (Liu et al., 2006; Gonera et al., 2004; O'Brien et al., 2001; Miland et al., 1996a; Ryan et al., 1994a), surface modification (Hassani et al., 2006; O'Brien et al., 2003; Liu et al., 2002; Miland et al., 1996b), attachment of PEG (Garcia et al., 1998) and carbohydrate residues modification (Bonnafe et al., 1993). Immobilisation of the enzyme has also yielded good increases in stability, as outlined by Fishman and co-workers (Fishman et al., 2002; also Azevedo et al., 2001).

To date, only one attempt has been made to genetically alter the stability of HRP by Arnold and Lin (2000), as outlined in Section 1.3.8.2. No attempt has been made to alter the stability of HRP rationally via site directed mutagenesis; however, it is clear that there is potential for this method. Wells (1990) noted that single mutational effects can have small effects on protein stability and that several small mutations can give a large cumulative increase in stability. This theory was applied when selecting suitable amino acids for HRP site-directed mutagenesis in conjunction with previous knowledge of the protein from chemical modifications, as outlined in Chapter 4.

1.3. Protein Mutagenesis

1.3.1 Site directed Mutagenesis.

Site-directed mutagenesis has become a routine laboratory technique and has since been commercialised by several biotechnology companies, for example: Transformer™ Site Directed Mutagenesis Kit (CLONTECH Laboratories, Palo Alto, CA, USA), Altered Site® II in vitro Site directed Mutagenesis Systems (Promega, Madison, WI, USA) and Quick Change™ Site-directed Mutagenesis (Stratagene, La Jolla, CA, USA). The key technique that allowed the rapid development of these site-specific mutagenesis kits was the Polymerase Chain Reaction, PCR (Mullis and Faloona, 1987). PCR methodology can be used in simple recombination mutagenesis (Jones and Winistorfer, 1997) or megaprimer-based mutagenesis (Barik, 1997). Current mutagenesis kits utilise a supercoiled vector containing the gene of interest and two synthetic oligonucleotide primers that contain the desired mutation. The oligonucleotide primers are complementary to opposite strands of the vector and are extended around the vector by a proofreading polymerase during PCR. Incorporation of the primers generates a mutated nicked plasmid which is subsequently treated with *Dpn* I restriction endonuclease to digest the parental wild type vector. The mutated plasmid is then transformed into an *E. coli* cell line lacking mismatch repair ability, where it is propagated and the gene expressed (Borns et al., 2000). The use of site directed mutation has grown exponentially due mainly to its ease of application, the vast amounts of data mutants can generate and the expansion of protein engineering, a field dedicated to developing superior enzymes through mutagenesis (Brannigan and Wilkinson, 2002).

1.3.2 Random Mutagenesis.

Initially, protein engineering and design were based on the rational and semi-rational methods outlined previously. It soon became apparent, however, that knowledge of protein structure-function relationships was insufficient to generate a consistent, robust, engineering approach; also, crystal structures had not been solved for many enzymes, thus rendering their rational design impossible (Chen, 2001). Hence, directed protein evolution has developed as an alternative mutational strategy, as it does not require precise structural information. In brief, the approach utilises accelerated protein evolution to develop the protein of interest, based on a strong selection pressure (Mössner and Pluckthün, 2001; Jermutus and Pelletier, 2001). Directed evolution

implements a simple iterative Darwinian optimisation approach, i.e. an improved mutant is used as the “parent” for the next round of evolution (Farinas et al., 2001; Petrounia and Arnold, 2000).

Directed evolution can be divided into two general approaches. Non-recombinative methods include error prone PCR, in which a small number of mutations are introduced randomly in the gene during PCR. The mutations occur due to variation in the PCR constituents, for example nucleotide concentration. The mutation frequency must be finely tuned, as beneficial mutations are rare compared to deleterious ones. This approach is limited to a small number of mutations and only mutations in the parental clone can be brought forward to the next round of mutagenesis. Recombinative methods (e.g. DNA shuffling and staggered extension process) overcome this problem. DNA shuffling involves the random fragmentation of several mutant DNA molecules followed by their reassembly by PCR into full-length molecules. This process is akin to sexual recombination; it enables mutations that are truly random and, in addition, allows for the formation of chimeric molecules. Strong selective pressure must be maintained to isolate improved mutants and evolve away from deleterious mutations. Desirable clones may be bred iteratively, thus creating offspring that contain multiple beneficial mutations (Shigeaki, 1998). DNA shuffling evolution has proven to be an especially powerful tool for the rapid functional evolution of single gene products with enhanced activity, altered substrate specificity, improved protein folding and biological pathways with improved function (Tobin et al., 2000). Other methods of library generation include the SStep Process (Zhao et al., 1998) and Iterative Somatic Hypermutation (Wang et al., 2004). The single most popular use of directed evolution is in the increase of enzyme stability and activity in non-natural environments. Improvements in these two enzymatic properties were often thought to be mutually incompatible. However, Miyazaki and co-workers (2000) enhanced both properties in a single directionally evolved mutant. Ultimately, the outcome of directed evolution is critically dependent on how a mutant library can be screened or a superior mutant selected for (Olsen et al., 2000). A system of high-throughput screening is essential for any successful random mutagenesis protocol. Current conventional methodologies (Jestin and Kaminski, 2004) compete alongside state-of-the-art concepts of phage display (Verheart et al., 2002), lipid vesicles display (Tawfik and Wells, 1999) and whole cell display (Daugherty et al., 2000).

1.3.3 Combination Mutagenesis: Site Directed Mutagenesis and Directed Evolution

The two methodologies discussed above are complementary (see Figure 1.8), with many groups demonstrating that directed evolution effectively augmented a site-directed mutant (Cherry et al., 1999; and Alltamirano et al., 2000). Recent publications suggest that targeted, “semi-rational”, evolution of enzymes might yield superior mutants in less time (Kazlauskas, 2005).

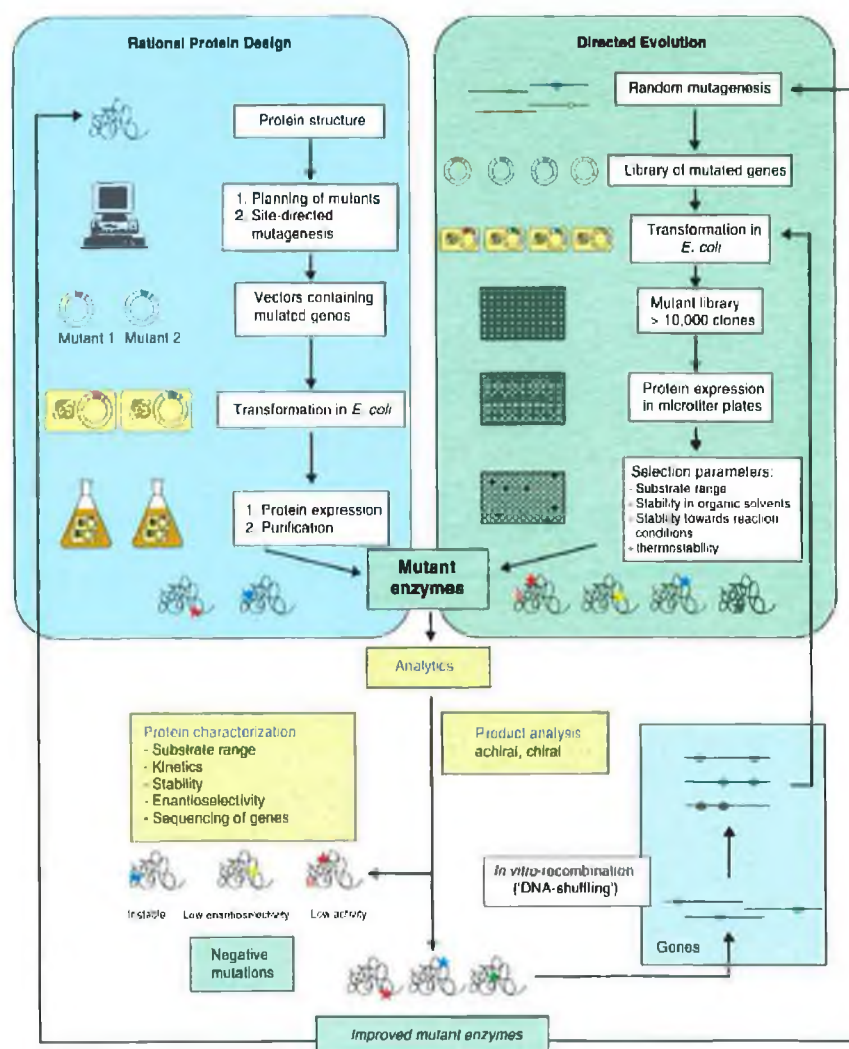


Figure 1.7: Comparison of rational (site directed mutagenesis based) and directed evolution methods for enhancing protein characteristics. The role of combination mutagenesis is also outlined (Bornscheuer and Pohl, 2001).

1.3.4 Rational and Semi-Rational Design.

Most rationally designed enzymes fail to reach their expected catalytic performances because of our limited knowledge of protein folding, dynamics and stability (van Regenmortel, 2000) e.g. subtle changes in the geometry of an active site can generate

unpredicted consequences for enzyme function (Cedrone et al., 2000). Examples of rationally based design are sequence comparison of high and low temperature-stable proteins, entropic stabilisation, sequence dipeptide composition and the “Tanford/Kirkwood-Bashford/Karplus” method. Examples of semi-rational protein design include the homology-based consensus approach, the canonical sequence approximation, SCOPE (Structure based COmbinatorial Protein Engineering) and bioinformatic based approaches, all detailed with references below.

1.3.4.1 Sequence Comparison.

One strategy for identifying thermostabilising mutations involves the comparison of stable proteins with less stable ones, with the aim of identifying amino acid sequence patterns that correlate with thermostability (Lehmann and Wyss, 2001). In this approach, statistical analysis identifies recurring amino acid replacement trends that are linked with thermal adaptation, as opposed to random genetic drift. However, there are several limitations to this methodology, including availability of sequence data and its skewed nature (Haney et al., 1999).

1.3.4.2 Entropic Stabilisation.

This approach selects regions where entropic forces within a protein molecule are sub-optimal. It is hoped that the designed mutation will influence the ΔG of unfolding by reducing the entropy of the protein in question. Unfortunately, the forces that govern protein unfolding are not completely understood and, hence, selection of critical residues is still arbitrary (van den Berg and Eijsink, 2002)

1.3.4.3 Sequence Dipeptide Composition.

Here the protein primary sequence is analysed for arrangements of certain sets of amino acids, in a specific order, that are known to degrade rapidly *in vivo*. Proline, methionine, glutamine, glutamic acid and serine occur regularly in unstable proteins and juxtaposition of these residues may lead to instability. The main disadvantage with this approach is that other factors influencing protein stability, such as disulphide bridges, ligand binding etc., are not taken into consideration (Guruprasad et al., 1990).

1.3.4.4 Tanford/Kirkwood-Bashford/Karplus. (TK-BK), Method.

This methodology is based on optimisation of long-range charge-charge interactions. The interaction energies between unit positive charges placed on the protonation sites of ionisable groups are estimated using the Tanford/Kirkwood model and, subsequently, the pairwise charge-charge interaction energies are calculated as averages over the protonation states of native protein based on the Bashford/Karplus “reduced set of sites approximation”. The results yield a W_i value (TK-BK Energy value), which is positive for groups involved in destabilising interactions and negative for groups involved in stabilising interactions. Hence, certain groups can be selected for charge deletion or charge reversal to optimise the protein’s overall W_i value (Loladze et al., 1999).

1.3.4.5 Consensus Approach.

This is based on the comparison of amino acid sequences of homologous proteins and subsequent calculation of a consensus amino acid sequence using a suitable bioinformatic package. Amino acid residues in the target protein are then mutated to the corresponding consensus residue. Utilising this approach, Lehmann and co-workers increased the thermostability of a recombinant fungal phytase by 34°C, whilst maintaining catalytic activity. Another key point to emerge from these studies was the concerted effect of single mutations, with numerous mutations yielding cumulative small stabilising effects (Lehmann et al., 2002). Success primarily relies on sufficient utilisation of non-biased sequence data sets. Also, once the regions have been selected, the labour-intensive nature of site-directed mutagenesis and the quantity of regions to be mutated may be prohibitive.

1.3.4.6 Canonical Sequence Approximation.

This approach has been primarily utilised for immunoglobulin stabilisation; however, its rationale can be generalised to any protein molecule. The hypothesis is that closely homologous proteins are derived from a common evolutionary relation, and evolved via accelerated independent local evolution. It is postulated that a protein is marginally stable and is in a state of equilibrium with respect to sequence alteration. Hence, any destabilising mutations will be neutralised so long as the overall domain stability does not fall below a certain threshold. The most probable distribution of a given amino acid at a specific position can also be statistically determined, and thus a statistical free

energy can be calculated from its frequency of occurrence. This free energy value quantitates the amino acid selection at a given position (Steipe et al., 1994).

1.3.4.7 SCOPE: Structure-based COmbinatorial Protein Engineering.

SCOPE is an example of a semi-rational combinatorial approach that combines rational and random engineering. This idea is based on the naturally occurring “exon shuffling” in which proteins are constructed by assembling blocks of coding sequences, mediated by recombination between non-coding regions of genes, introns. SCOPE utilises structural information from two proteins to design coding segments of genes that correspond to elements present in both proteins. In a series of PCR reactions, hybrid oligonucleotides act as surrogate introns to direct the assembly of coding segments to create hybrid genes, with iteration of this process enabling the synthesis of all desired combinations of structural elements (O’Maille et al., 2002).

1.3.5 Mutation Selection Software.

Bioinformatics is an emerging science in which biology, computer science and information technology converge into a single discipline. It allows vast sets of data to be analysed and predictions to be made through powerful algorithms. Examples of bioinformatic approaches to mutation region selection include homology modelling, complex algorithms such as the “PoPMuSiC” algorithm (Kwasigroch, et al., 2002) and specific computer programs such as “WHAT IF” (Vriend, 1990) (Section 1.3.5.2 and 1.3.5.3 respectively). *In silico* design methods combine the structure-based rational approach with the high throughput of random protein design, by utilising computational models to generate and screen sequences against mathematically defined criteria in order to identify mutant proteins with optimal folding energies (Dahiyat, 1999). Regarding the use of computer algorithms and programmes, it should be noted that protein engineering is a non polynomial-complete problem. This means that the problem scales non-polynomially with increasing complexity, and hence, no known algorithm can guarantee determining the optimal solution without evaluating all possible solutions. This also means that empirical random protein engineering relies on screening massive numbers of possible beneficial mutations, as outlined in Section 1.3.2, to approximate towards evaluating all possible solutions to the problem (Gustafsson, et al., 2003).

1.3.5.1 Homology Modelling.

Homology modelling utilises the same sequence alignments as in the sequence comparison approach. However, computer generated structural models are then developed for both thermophile and mesophile sequences, and regions for increased stability are then inferred from structure comparison. Modelling allows for specific regions, such as solvent-exposed loops and salt bridges, to be studied in detail and, hence, selection of key residues for this particular region is optimised (Chakravarty and Varadarajan, 2002)

1.3.5.2 Prediction Of Protein Mutation Stability Changes, “POPmuSiC”, algorithm.

A powerful algorithm is utilised in this bioinformatic package to perform *in silico* all possible point mutations in a given protein or protein region. The programme then estimates the stability changes with linear combinations of database-derived potentials, the coefficients of which depend on the solvent accessibility of the mutated residues. The results generated are presented in the form of stabilising, destabilising and neutral mutations (Kwasigroch et al., 2002).

1.3.5.3 “WHAT IF” Computer Program.

This is a much-cited (Eijsink et al., 2004 and references therein) computer programme designed for macromolecular modelling and drug design, with the added ability to mutate specific residues and ascertain the effect on the protein *in silico*. Within the programme there are two mutational methods, the first being a database comparison approach, while the second is an algorithm procedure. This algorithm employs statistically significant correlations between observed frequencies of occurrence of side chain torsion angles to predict the optimal mutation. A conformational search can be completed to minimise the spatial overlap with neighbouring residues, whilst a fragment search can be implemented to ascertain potentially beneficial deletions, insertions or loop transplantations (Vriend, 1990).

1.3.6 Horseradish Peroxidase Mutagenesis.

Mutagenesis studies on Horseradish Peroxidase began with the successful cloning of a synthetic HRP gene and its subsequent expression, purification and refolding to yield an active recombinant HRP molecule (Smith et al., 1990). Prior to the elucidation of the

crystal structure in 1997, (Gajhede et al., 1997) the majority of the mutants focused on ascertaining the key residues in the active site.

1.3.6.1 Site Specific Horseradish Peroxidase Mutants.

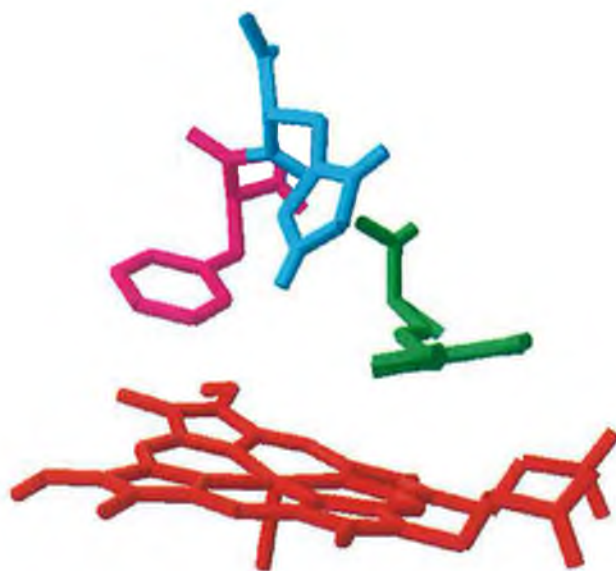
Before solution of the HRP crystal structure, researchers based their assumptions on the structures of closely related peroxidases (such as cytochrome *c* peroxidase), which suggested residues 38 through 42 as key catalytic residues. Primarily, mutants focussed on Arginine 38, Phenylalanine 41 and Histidine 42, with all mutants revealing a dramatic decrease in peroxidase catalytic activity (see Table 1.7). However, some Phe 41 mutants revealed an augmented thioester sulfoxidation activity, due to increased access channel area (see Table 1.8; Ozaki and Ortiz de Montellano, 1994).

Through continued studies, asparagine 70 was also noted as being an important residue in HRP catalysis, although it was not located in the active site. Mutations in this region also caused decreased HRP activity and a re-orientation of active site residues. Phenylalanine 221 was also mutated and was shown to alter the resting state of enzyme to a quantum mechanically mixed-spin heme species. Tryptophan 117 mutations revealed the role of this residue in protein folding and electron transfer within the enzyme. Mutations within the active site entrance revealed the key role of Phe 142 in binding aromatic molecules, whilst mutations within the proximal region of the enzyme disclosed the role of Phe 179 in aromatic molecule binding and the role of His 170 in heme group anchorage. From the site directed mutation studies the roles of the various catalytically important residues can be described (Veitch, 2004), as set out in Table 1.7.

Table 1.7: Summary table listing the critical role of catalytic residues in HRP as elucidated by site directed mutagenesis.

Residue	Role
Arg 38	Formation and Stabilisation of Compound I. Binding and stabilisation of ligands and aromatic molecules.
Phe 41	Prevents substrate access to the ferryl oxygen of compound I.
His 42	Formation of Compound I Binding and stabilisation of ligands and aromatic molecules
Asn 70	Maintains basicity of His 42 side chain through hydrogen bond network.

A



B

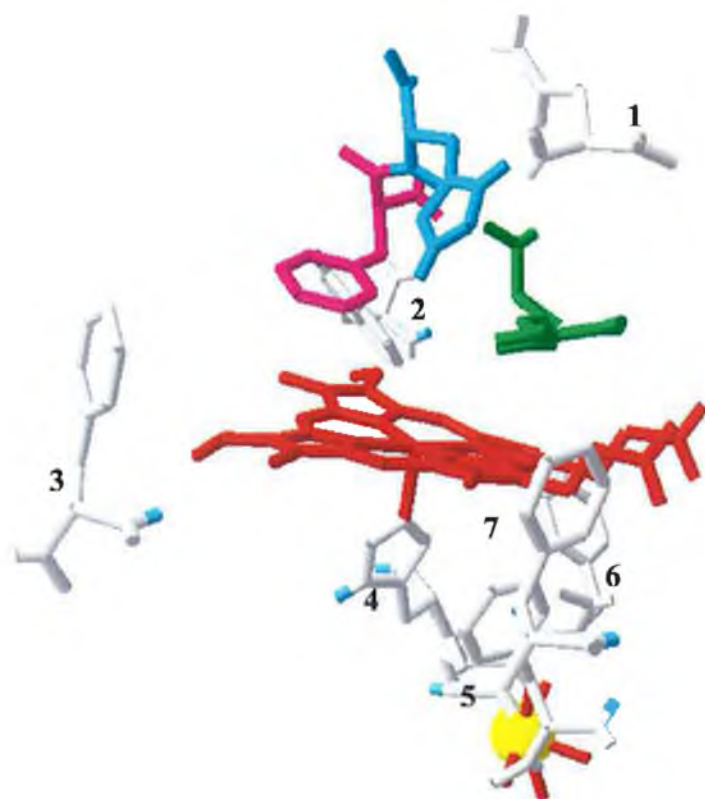


Figure 1.8: Part A illustrates the catalytically active residues in HRP; ■, Arg 38; ■, Phe 41; ■, His 42. Part B shows the remaining residues discussed in Table 1.8; 1, Asn 70; 2, Trp 117; 3, Phe 143; 4, His 170, 5, Thr171; 6, Phe 172; 7, Phe 221. The proximal calcium is shown as a yellow sphere.

Table 1.8: Detailed description of HRP site-specific mutants. The region of mutation, its effect, the expression host and purification methodology are also outlined. Expression host: \diamond , *E. coli*; \ast , *Spodoptera frugiperda*; \times , *Trichoplusia ni*. All mutants purified by refolding of inclusion bodies unless otherwise noted: \square , S Fast Flow Q Fast Flow; \odot , Mono Q anion Exchange; Chelating Fast Flow Sepharose Thiophilic gel or $\text{\textcircled{H}}$, Nickel Affinity.

Primary Author	Mutation	Effect
Active Site Region		
$\text{\textcircled{H}}$ Asokan et al., 2001	His 42 Ala.	Wildtype NMR structure was indistinguishable from that of the solved crystal with the exception of Phe68 reorientation within the substrate-binding pocket. Adjacent residues Ile53 and Leu138, reoriented slightly in H42A mutant.
Howes et al., 2001c	Phe179Ala, His42Glu, His42 Glu/Arg38 Leu.	Mutation of His42 leads to an increase of 6-coordinate aquo heme forms at the expense of the 5-coordinate heme state. The His42Glu:Arg38Leu double mutant displays an enhanced proportion of the pentacoordinate heme state, similar to the single Arg38Leu mutant, whilst the Phe179 is unaffected. His 42 and Arg 38 play a more important role in BHA binding than Phe179.
\diamond Feis et al., (1998)	His 42 Leu, Arg 38 Leu.	Mutants do not have an effect on CO bound HRP structure at acid pH; however, Arg 38 Leu is less stable at alkaline pH, as CO is H-bound to the Arg residue in the wildtype CO bound structure.
$\text{\textcircled{H}}$ Savenkova et al., (1998b)	His 42 Ala, Phe 41 His, Arg 38 His, Asn 70 Asp.	His 42 Ala mutation greatly reduces the peroxidase activity, as His 42 deprotonates the H ₂ O ₂ and facilitates O-O bond cleavage. Asn 70 is involved in hydrogen bonding to His 42 and locks it in position, Asn 70 Asp cannot participate as a surrogate catalytic residue in His42 Ala, probably due to distance from the active site. His 42 Ala/Asn 70 Asp double mutant has a higher peroxidase activity than His 42 Ala.
\diamond Meunier et al., (1998)	His 42 Leu, His 42 Ala, Arg 38 Leu.	His 42, with its pK modulated by Arg 38, provides the protonation site on the reduced enzyme, which is reasonable for the pH dependencies of HRP. Mutants bind cyanide differently than wildtype and binding is affected by pH. However, His 42 Ala mutation binds cyanide similarly to wildtype. Mutants also affect access channel for carbon monoxide.
$\text{\textcircled{H}}$ Savenkova et al., (1998a)	Arg 38 Ala, Arg 38 His, Arg 38 His/His 42 Val.	The rate of compound I formation for all the mutants was significantly decreased. Arg 38 mutant is reduced to its resting state without compound II formation. All mutants oxidise guaiacol and ABTS slower than the wildtype. Arg 38 Ala and Arg 38 His/His 42 Val are 190 and 1400 times more efficient as sulfoxidation catalysts, and both are 25 times more efficient as styrene catalysts, than the wildtype. Arg 38 is also important in compound I stabilisation.
\diamond Rodriguez-Lopez et al., (1997a)	His 42 Leu, His 42 Arg, Arg 38 Leu, Arg 38 Lys, Arg 38 Ser, Arg 38 Gly.	His 42 Leu and Arg increase the binding of dioxygen by less than one order of magnitude, His 42 Arg mutant increases binding of dioxygen by more than two orders of magnitude. All mutants, except Arg 38 Ser, had greater O ₂ dissociation than wild type. Arg 38 Ser had essentially irreversible binding. Provides evidence for the role of Arg 38 and His 42 as dioxygen-heterolytic cleavers. Also, both amino acids serve to decrease the lability of the ferric enzyme-dioxygen in order to suppress the formation of the inactive ferrous state.
\diamond Howes et al., (1997)	His 42 Leu, His 42 Arg, Arg 38 Gly, Arg 38 Glu.	The mutants displayed a diverse heme spin state, differentiated by the bonding of the iron bound water molecule and the Arg 38 or His 42 residue. The mutants identify a concerted role of His 42 and Arg 38 in BHA binding, although Arg 38 plays the more critical role.
\diamond Tanaka et al., (1997a)	His 42 Glu, His 42 Gln.	His 42 Glu compound I formation is greater than His 42 Gln, which suggests that the Glu residue could play a role as an acid base catalyst; however, both mutants are much less active than wildtype HRP. It was also noted that the basicity of the Glu mutant is lower than that of the wildtype and the Glu residue was not orientated correctly, both of which would destabilise the heme O ₂ distal Glu ternary intermediate. However, enhanced peroxxygenase activity was noted in the Glu mutant.

Table 1.8: Continued.

Primary Author	Mutation	Effect
Active Site Region		
◆ Rodriguez-Lopez et al., (1996)	Arg 38 Leu.	Mutation reveals pivotal roles of Arg 38. It is involved in the rapid binding of H ₂ O ₂ to HRP and the cleavage of O-O. It plays a role in the affinity of HRP for certain substrates, such as guaiacol, and it modulates the reactivity of HRP to compound I. Arg 38 serves as a charge stabiliser for the acid/base catalysis initiated by His 42.
◆ Newmyer et al., (1996a)	His 42 Ala.	Mutant demonstrates acid/base catalysis role of His 42. Exogenous His can function as surrogates for the mutant, with similar formation of compound I as Native HRP. Neutral imidazoles serve this role best compared to protonated residues. Imidazole has a role in deprotonating H ₂ O ₂ and facilitates the formation of the Fe-OOH complex.
✖⌘ Savenkova et al., (1996)	His 42 Ala, Phe 41 His, His 42 Ala / Phe 41 His.	His 42 Ala mutation greatly reduces the peroxidase activity, by a factor of 10 ⁶ . Phe 41 His substitutes, slightly imperfectly, for His 42 and allows for peroxidase catalytic activity. The Phe 41 His mutant does not H-bond in the same fashion as the wild type His, which causes Compound II instability. The double mutant, His 42 Ala/Phe 41 His, is a considerably better thioanisole sulfoxidation and styrene epoxidation catalyst than wild type or the single His 42 Ala mutant.
◆ Tanaka et al., (1996)	His 42 Glu.	Mutant can still carry out, at much lower levels, catalytic activity compared with other hydrophobic mutants. Possible role as acid-base catalyst for peroxidase reaction cycle if the carboxyl group of Glu can be fixed in optimum position.
◆ Gazaryan et al., (1995)	Phe 41 His, Phe 143 Glu.	Mutants display a low specific activity. Phe 41 His destroys active site hydrophobicity. ABTS activity noted for Phe 143 Glu mutant. Role of Phe 41 and 143 is to form a hydrophobic pocket for the non-covalently bound heme and provide an entrapment mechanism for the heme.
✖⊙ Ozaki and de Montellano, (1995)	Phe 41 Leu, Phe 41 Thr.	Both mutants have a higher V _{max} for sulfoxidation of phenyl alkyl thioesters. Both catalyse the epoxidation of styrene and cis-β-methylstyrene. Phe 41 Leu yields sulphoxides with higher enantioselectivity than native HRP. Both mutations greatly enhance the peroxygenase activity of HRP.
◆ Hiner et al., (1995)	Phe 143 Ala, Arg 38 Lys.	Both mutants were inactivated by H ₂ O ₂ quicker than native recombinant and wild type HRP. Inactivation by m-chloroperoxybenzoic acid was almost uniform across the mutants, native recombinant and wild type HRP. The affinity of Compound I for H ₂ O ₂ leading to the formation of a transitory intermediate decreased in the order wild type HRP, native recombinant, Phe 143 Ala, Arg 38 Lys.
✖⌘ Newmyer et al., (1995)	His 42 Ala, His 42 Val, Phe 41 Ala.	Mutants compromise the catalytic activity. His 42 Val destabilises compound II formation, due to breaking of hydrogen bonds with the ferryl oxygen. The Phe residue plays a role in shielding the ferryl species and also sterically hinders access to the active site. Peroxygenase activity noted for mutants due to increased access to active site.
◆ Meunier et al., (1995)	His 42 Leu, His 42 Arg, Arg 38 Leu.	The His mutants allow for carbon monoxide recombination similar to wild type; however, Arg 38 Leu mutation increases the recombination rate by 10 ³ -fold. Cyanide could not bind to any of the mutants. This can be attributed to the charged anionic nature of cyanide compared to neutral carbon monoxide. Their differing distal heme pockets can, in part, explain differences between peroxidases and globins.

Table 1.8: Continued.

Primary Author	Mutation	Effect
◆ Gazaryan et al., (1994)	Phe 41 His, Phe 143 Glu.	Phe 41 and 143 have essential roles in the HRP catalytic mechanism. Phe 41 acts as a hydrophobic barrier between the two His in the active site and also provides a hydrophobic binding site for the porphyrin ring. Phe 143 is located at the entrance to the active site and mutations here generally cause steric hindrance for substrate entrance.
◆ Smulevich et al., (1994)	Phe 41 Val, Phe 41 Trp, Arg 38 Lys	Phe 41 Val and Trp show an increase in 6 coordinate high spin heme content, whilst Arg 38 Lys shows an increase in both 6 coordinate high and low spin. Results suggest that the distal heme pocket is different to cytochrome C peroxidase. Distal mutations affect ability to bind BHA, suggesting that BHA binds close to the distal region.
◆ Sanders et al., (1994)	Arg 38 Lys.	Decrease in pH to 4 causes Arg 38 Lys mutant to display different enzyme intermediates, as compared to wildtype HRP.
✱⊙ Ozaki and de Montellano, (1994)	Phe 41 Leu.	Mutant increases the rate and enantioselectivity of thioester sulfoxidation, whilst maintaining catalytic activity. Increase in sulfoxidation is due to increased active site access and maintenance of active site hydrophobicity.
◆ Veitch et al., (1992)	Phe 41 Val, Arg 38 Lys.	Phe 41 and Arg 38 have complex hydrogen bonding roles in the active site; binding of BHA affects the properties of the heme pocket as a whole.
◆ Smith et al., (1992)	Phe 41 Val.	Eight-fold decrease in activity for the formation of compound I, 2.5-fold for compound II and 1.3-fold for compound III with H ₂ O ₂ and para-aminobenzoic acid as substrates. A decrease in ABTS activity was also noted. Mutations in the distal region affect reactivity towards different reducing substrates.
◆ Tanaka et al., (1999)	Ser 35 Lys, Gln 176 Glu, Ser 35 Lys/ Gln 176 Glu.	The double Ser 35 Lys/Gln 176 Glu mutant, showed a decreased V _{max} /K _m for hydroquinone. However Ser 35 Lys showed an increase in ABTS V _{max} /K _m , while Gln 176 Glu showed a decrease and the double mutant showed no variation. The reduction potentials for compound II of Ser 35 Lys and Gln 176 Glu were higher than wildtype. Mutants did not bind luminol effectively, due to hydrophobic nature of binding pocket, steric hindrance from Phe residues and the orientation of the distal catalytic residues. Changes in NMR spectra revealed that luminol binds via electrostatic interactions in the binding cavity.
◆ Veitch et al., (1995)	Phe 142 Ala, Phe 143 Ala.	Phe 142 Ala, but not Phe 143 Ala, alters the aromatic donor molecule binding site. Phe142 plays an important role in aromatic molecule binding in HRP as Phe 142 Ala binds BHA three times less effectively.
◆ Mukai et al., (1997)	Asn 70 Val, Asn 70 Asp.	Mutants demonstrated six co-ordinate high-spin structure, whilst wild type maintained a five co-ordinate high-spin structure. Asn 70 serves as a hydrogen bond acceptor from His 42. Mutants have dramatically decreased activity. The pH range of the mutants is also decreased due to reduced pKa of the His residues lacking a hydrogen bond sink.
◆ Tanaka et al., (1997b)	Asn 70 Asp.	Mutant displayed similar CD spectra and redox potential to that of the native enzyme. Paramagnetic NMR spectrum indicated lack of a hydrogen bond between His 42 and Asp 70. A H-bond did not form between the His 42 and the mutant Asp residue, despite the presence of a carboxy group on the Asp residue. The non-formation of the hydrogen bonds results in improper positioning of the distal His and causes cleavage of the other hydrogen bonds surrounding the distal region, resulting in a substantial decrease in catalytic activity but without large structural alterations to the global structure of the enzyme.

Table 1.8: Continued.

Primary Author	Mutation	Effect
Asparagine 70		
◆ Nagano et al., (1996)	Asn 70 Val, Asn 70 Asp.	The mutants were spectroscopically similar to wildtype; however, compound I formation was decreased by 90%, as were the reduction rates of compound I and II due to decreased basicity of the distal His. However, ABTS oxidation was substantially increased in the mutants due to higher-than-wildtype redox potentials of compound II caused by the altered hydrogen bond network.
◆ Nagano et al., (1995)	Asn 70 Val.	Disrupts hydrogen bond network to substrates. Compound I formation is reduced by two orders of magnitude. At neutral pH, Compound II formation is not noted in mutant; however, stable compound II is noted at alkaline pH. This pH effect may be due to the altered basicity of the distal His caused by disrupted H-bonding.
Tryptophan 117		
◆ Ignatenko et al., (2000)	Trp 117 Phe.	Role of Trp 117 in ABTS and guaiacol oxidation, via electron transfer, elucidated with a decreased product dissociation constant noted for mutant. Trp 117 Phe mutation increased enzyme stability in acid media possibly due condensed heme region. However, Trp 117 plays a role in HRP folding and Trp 117 mutants required changes in refolding conditions as compared to wild type.
◆ Gazaryan et al., (1999)	Trp 117 Phe.	Mutant is more acid (removal of a radical trap) and irradiation-stable (due to removal of irradiation-labile Trp residue). Trp 117 is noted to have a role in electron transfer pathways within the enzyme. Trp 117 is important in HRP folding but not in stability.
Threonine 171		
Howes et al., (2005)	Thr171Ser.	Proximal structural alteration, affects proximal pocket hydrogen bonding. Methyl group of Thr171 interacts with other core proximal residues, linking the proximal Ca ²⁺ and the heme ligand. Significant change noted in the Fe ₂₊ /Fe ₃₊ redox potential of the mutant.
Phenylalanine 221		
◆ Howes et al., (2001b)	Phe 221 Met.	Changes resting state of enzyme to quantum mechanically mixed-spin heme species, decreases the enzymes pI, decreases enzyme stability in alkaline conditions.
◆ Morimoto et al., (1998)	Phe 221 Trp.	Mutant is based on cytochrome <i>c</i> peroxidase. Trp mutant allows for the formation of Trp radical from Compound I, as opposed to the π -cation radical in native HRP. The Trp radical is unstable due to the amino acid environment in its vicinity and a cationic Ca ²⁺ ion close by. The amino acid residues used to control radicals can be a key factor in discriminating the functions of peroxidases.
Proximal Region		
◆ Veitch et al., (1997)	Phe 179 Ala, Phe 179 His, Phe 179 Ser.	The mutants displayed an altered NMR spectrum, indicating that the Phe 179 side chain is in close proximity to the exposed heme edge. All mutants have decreased affinity for BHA, with Phe 179 having the lowest, followed successively by Phe 179 Ser and Phe 179 His, indicating that Phe 179 maintains a pivotal role in BHA binding, as opposed to other nearby by Phe residues (Phe 68, Phe 142). The mutants could be used to ascribe a reason for decreased BHA binding in other isoforms of HRP.
⊗ Newmyer et al., (1996b)	His 170 Ala.	Mutant is catalytically active in the presence of a reducing substrate. It is spectroscopically different to the wildtype, being hexacoordinate with a low-spin heme species. Mutant activity is lower than wildtype and is partially rescued by addition of exogenous imidazole. It is shown that the major function of the proximal His is to tether the heme iron, to maintain it in a pentacoordinated state and to prevent its coordination to the distal His.

Table 1.8: Continued.

Primary Author	Mutation	Effect
✘ Miller et al., (1995)	Phe 172 Tyr.	Distal site not altered by this mutation. Compound I decays to a compound II state in the presence of H ₂ O ₂ and absence of any other reducing substrate. An electron radical is formed, located at the Tyr mutation, possibly due to Tyr being in a more oxidisable state.

1.3.6.2 Random Mutagenesis of Horseradish Peroxidase.

As stated previously, the most common application of random mutagenesis is enhancement of protein characteristics such as thermostability, resistance to inactivation by inhibitors and stability in non-natural environments such as organic solvents. HRP has many biotechnological applications (see Table 1.5) and as such, increasing the stability has many potential benefits.

Arnold and Lin (2000) carried out directional evolution on native HRP with the aim of increasing activity and stability. Error-prone PCR, utilising an unbalanced concentration of nucleotides and a decreased concentration of MnCl₂, was used to generate random mutations, with many thousands of colonies screened for superior properties. The mutational protocol was optimised to produce approximately one mutation per gene. The parent gene, designated HRP1A6, was randomly mutated and expressed in *Saccharomyces cerevisiae*. Three rounds of random mutagenesis were carried out to improve expression of the protein in the yeast host (see Table 1.9). One round of mutagenesis was also carried out to improve stability (see Table 1.10; Arnold and Lin, 2000).

Table 1.9: Directed Evolution of the HRP protein towards increased activity. Error-Prone PCR was utilised to generate random mutants. ABTS, in standard assay conditions, was used as the reducing substrate. Silent mutations are also noted. The previous multiple mutant was utilised as the parent for subsequent round of mutagenesis in multi-round mutagenesis protocols.

Mutation(s)	Name	Effect
Round One Mutation: Selection for Increased Activity. Parent (HRP1A6)		
L131P, N135N, L223Q, T257T	HRP1-117G4	Increased soluble activity to 147 U.L ⁻¹ .
L37I	HRP1-77E2	Greater ABTS activity than parent clone.
Round Two Mutation: Selection for Increased Activity. Parent (HRP1-117G4)		
T102A, L131P, N135N, L223Q, P226Q, T257T.	HRP2-28D6	Increased soluble activity to 410 U.L ⁻¹ .
Round Three Mutation: Selection for Increased Activity. Parent (HRP2-28D6)		
N47S, T102A, G122G, L131P, N135N, L223Q, P226Q, K241K, T257T.	HRP3-17E12	Increased soluble activity to 1080 U.L ⁻¹ .

Table 1.10: Directed Evolution of the HRP protein towards increased thermal stability and H₂O₂ tolerance. Error-Prone PCR was utilised to generate random mutants. ABTS, in standard assay conditions, was used as the reducing substrate.

Mutation(s)	Title	Effect
Round One Mutation: Selection for Increased Stability. Parent (HRP1-117G4)		
L37I, K232M	HRP1-4B6	6°C increase in T ₅₀ compared to parent.
L37I, F221L	HRP1-28B11	Increased thermostability at 50°C compared to parent.
L37I, L131P	HRP1-24D11	Equally as thermostable as parent, 65% more stable in 25mM H ₂ O ₂ .

After three rounds of directed evolution towards increased activity, a nine-position HRP mutant displayed an 85-fold increase in HRP activity over the original HRP1A6 parent. Additionally, after one round of random mutagenesis towards increased thermal stability and H₂O₂ tolerance, three mutants were produced that were more stable than the parental gene in relation to both temperature and H₂O₂ tolerance.

The mutants were then subcloned into an expression vector for *Pichia pastoris* expression. Recombinant protein expression in *P. pastoris* has several advantages: it has a strong, inducible promoter, it is capable of generating post-translational modifications and isolation of foreign protein is facilitated by the fact that *P. pastoris* does not secrete its own proteins (Cregg et al., 1993) These advantages lead to a final mutated HRP yield of 6,500 U.L⁻¹ after 55 hours growth, which was a 6.5 fold increase on expression in *S. cerevisiae* (Arnold and Lin, 2000).

1.4 Conclusions and Project Outline.

As outlined, HRP is a widely studied and very important oxidoreductase with many applications in the life sciences and beyond. In the quest to increase the scope of HRP's potential applications, it has been subjected to many stabilisation protocols. Chemical modifications have been effective in stabilising HRP activity against varying organic solvents, whilst both chemical and directed evolution have been successfully utilised to increase its thermostability (Arnold and Lin, 2000). Since the cloning of the HRP gene (Smith et al., 1990) a large body of work has been produced on site directed mutants of HRP. Initially, site specific mutants were produced with the aim of elucidating the key residues involved in catalytic activity, while in more recent years researchers have utilised site directed mutagenesis to alter functions of the HRP molecule (Tanaka et al., 1999). Directed evolution has proven that the HRP molecule can be stabilised against thermal denaturation; however site specific, rationally designed, mutants aimed at

increasing HRP thermostability have yet to be investigated. As alluded to previously, the selection of residues for site-specific mutation is the key step in any rational design experiment. Hence, previous knowledge from chemical stabilisation of HRP will provide candidate residues for mutation (O'Brien et al., 2001). Further residues will be selected utilising the consensus approach, which is simple to implement, yet has yielded large increases in the thermostability (Lehmann et al., 2001). It is hoped that judicious selection of residues for site directed mutagenesis will yield a more stable recombinant form of this classical enzyme. Stabilised, directionally-orientatable recombinant HRP would find many applications in the biosensor field. Direct electrochemistry afforded by the optimal use of rHRP would aid further development of third-generation biosensors, particularly in H₂O₂ sensing. Incorporation of rHRP into bi-enzyme sensors would extend its potential application and enhance its pivotal role in advancing biotechnology. This thesis describes the generation and characterisation of HRP mutants at residues identified (i) through chemical stabilisation, (ii) by consensus approach and (iii) for directional binding and immobilisation.

Chapter Two.

Materials and Methods.

2.0 Materials.

Alpha Technologies, The Leinster Technology Centre, Blessington Industrial Estate, Blessington, Co. Wicklow, Ireland.

Ethidium Bromide Destaining Bags

Bioline, Allenwood Business Park, Naas, Kildare, Ireland.

DNase Quick Clean.

Bio-sciences (Invitrogen), 3 Charlemount Tce, Dun Laoghaire Co. Dublin, Ireland.

T₄ Ligase, *Not* I, *Nco* I.

Biomedics, Parque Tecnológico De Madrid, 28760 Tres Cantos, Madrid.

Nutrient Agar.

Cosmo Bio Company Ltd, Tokyo 135-0016, Japan.

δ-ALA (delta aminolevulinic acid).

Fisher Chemicals, Slaney Close, Dublin Industrial Estate, Dublin 11, Ireland.

Na₂-EDTA, glacial acetic acid, glycerol, hydrogen peroxide, methanol, sodium chloride, sodium hydroxide, Tris buffer.

Fusion Antibodies Ltd, Queens University Belfast, Grosvenor Road, Belfast, BT12 6BN, Northern Ireland.

Plasmid sequencing.

Isis (New England Biolabs), Boghall Road, Bray, Co. Wicklow Ireland.

*Bam*H I, *Bsp*H I, *Cla* I, *Dpn* I, *Eco*r I, *Hind* III, *Hpa* I, *Nae* I, *Pst* I,

Melford Chemicals, Chelsworth, Ipswich, IP7 7LE, United Kingdom.

Isopropyl-β-D-thiogalactopyranoside.

Medical Supply Company (Promega), Damastown, Mulhuddart, Dublin 15, Ireland.
dNTP Mixture, Pierce Bicinchoninic Acid assay.

MWG Biotech (Germany), Anzingerstr. 7a, 85560 Ebersberg, Germany.
All primers and some plasmid sequencing.

Oxoid, Basingstoke, Hampshire, RG24 8PW, England.
Tryptone, Yeast Extract

Sigma Aldrich, Airton Road, Tallaght, Dublin 24, Ireland.

ABTS (2,2'-Azino-bis(3-Ethylbenz-thiazoline-6-sulfonic acid), agarose, ammonium sulphate, ampicillin, δ -ALA, β -mercaptoethanol, bis-acrylamide, bromophenol blue, calcium chloride, chloramphenicol, dialysis tubing, diethylaminoethyl (DEAE) SepharoseTM, ethidium bromide, GeneEluteTM plasmid prep kit, glycine, lysozyme, MOPS, N- α -acetyl-L-Lysine, Nickel-N-nitrotriactic acid (Ni-NTA) resin, phenol phloroform isoamylalcohol, phenyl SepharoseTM, potassium acetate, ribonuclease A, rubidium chloride, SephacrylTM S-300-HR, sodium acetate, sucrose, *Taq* polymerase and PCR buffers, tetracycline, 3,3',5,5'-Tetramethylbenzidine dihydrochloride (TMB), 2,4,6-trinitrobenzenesulphonic acid (TNBS), xylene cyanol.

Technopath (Stratagene), Rosse Centre, Holland Road, Plassey, Limerick, Ireland.
Dpn I, *Quickchange*TM Site directed Mutagenesis Kit, XL-10 Gold cell line.

Unitech (Eppendorff), Airton Road, Tallaght, Dublin 24, Ireland.
Perfect Prep Gel Clean up Kit.

VWR International (AGB scientific), Dublin Industrial Estate, Glasnevin, Dublin 11, Ireland.
Macrosep centrifugal concentrators, Pall UltraBindTM US450 modified polyethersulfone affinity membranes.

2.0.1 Instruments.

BioRad Powerpack 1000 (Alpha Technologies, Wicklow, Ireland),

Beckman J2-21 Centrifuge (VWR International, Dublin Ireland),

Corning 240 pH meter (VWR International, Dublin Ireland),

Enzfitter® Programme (Biosoft, Cambridge, CB2 1NS, United Kingdom),

Eppendorff 5415D microfuge (Unitech, Dublin, Ireland.),

Labsystems multiscan MS platereader (Medical Supply Company Dublin, Ireland),

MT and C6CP Lauda water baths, (VWR International, Dublin Ireland)

ProteinParser consensus protein software, (This Study)

Unicam UV2 spectrophotometer (with Vision 1.3 software), (Brennan, Dublin Ireland),

UV transilluminator (Pharmacia Biotech AB, Dublin, Ireland),

Vibra Cell Sonicator (Fisher Scientific, Dublin, Ireland),

660A CHi Potentiostat and CHi 660A software (CH Instruments, Texas, USA).

2.1 *E. coli* strains, plasmids and cloning primer sequences.

2.1.1 *E. coli* strains.

The *E. coli* strains utilised in this study are described in below:

Strain	Phenotype/Genotype	Source
NovaBlue	<i>endA1</i> , <i>hsdR17</i> (r_{K12}^- , m_{K12}^+), <i>supE44</i> , <i>thi-1</i> , <i>recA1</i> , <i>gyrA96</i> , <i>relA1</i> , <i>lac</i> [F', <i>proA</i> ⁺ B ⁺ <i>lacI</i> ^q ZΔM15 ::Tn10(tet ^R)]	Novagen
JM109	<i>e14</i> (<i>mcrA</i> ⁻), <i>recA1</i> , <i>endA1</i> , <i>gyrA96</i> , <i>thi-1</i> , <i>hsdR17</i> (r_K^- m_K^-), <i>supE44</i> , <i>relA1</i> , λ^- , Δ (<i>lac-proAB</i>), [F' <i>traD36</i> , <i>proAB</i> , <i>lacI</i> ^q ZΔ M15].	Stratagene
Sure II	<i>e14</i> (<i>mcrA</i> ⁻), Δ (<i>mcrCB-hsdSMR-mrr</i>)171, <i>endA1</i> , <i>supE44</i> , <i>thi-1</i> , <i>gyrA96</i> , <i>relA1</i> , <i>lac</i> , <i>recB</i> , <i>recJ</i> , <i>sbcC</i> , <i>umuC</i> ::Tn5(Kan ^r), <i>uvrC</i> , [F' <i>proAB</i> , <i>lacI</i> ^q ΔM15, Tn10(Tet ^r), Amy, Cam ^r].	Stratagene
TOP 10	F ⁻ , <i>mcrA</i> , Δ(<i>mrr-hsdRMS-mcrBC</i>), Φ80 <i>lacZ</i> ΔM15 Δ <i>lacX74</i> , <i>deoR</i> , <i>recA1</i> , <i>araD139</i> Δ(<i>ara-leu</i>)7697 <i>galU galK</i> , <i>rpsL</i> (Str ^R), <i>endA1</i> , <i>nupG</i>	Invitrogen
XL-1 Blue	<i>recA1</i> , <i>endA1</i> , <i>gyrA96</i> , <i>thi-1</i> , <i>hsdR17</i> (r_K^- , m_K^+), <i>supE44</i> , <i>relA1</i> , λ^- , <i>lac</i> ⁻ , [F' <i>proAB</i> , <i>lacI</i> ^q ZΔ M15, Tn10(Tet ^r)].	Stratagene
XL 10-Gold	Tet ^R , Δ($\mu\chi\rho A$)183 Δ(<i>mcrCB-hsdSMR-mrr</i>)173, <i>endA1</i> , <i>supE44</i> , <i>thi-1</i> , <i>recA1</i> , <i>gyrA96</i> , <i>relA1</i> , <i>lac</i> Hte[F' <i>proAB lacI</i> ^q ZΔM15 Tn10(tet ^R) Amy Cam ^R]	Stratagene
ER2925	<i>ara-14 leuB6 fhuA31 lacY1 tsx78 glnV44 galK2</i> <i>galT22 mcrA dcm-6 hisG4 rfbD1</i> R(<i>zgb210</i> ::Tn10)TetS <i>endA1 rpsL136 dam13</i> ::Tn9 <i>xylA-5 mtl-1 thi-1 mcrB1 hsdR2</i>	New England Biolabs

2.1.2 Plasmids.

The plasmids utilised in this study are outlined below:

Plasmid	Description	Source
pUC18	Cloning vector. Ampicillin resistant. <i>LacZα</i>	Amersham
pQE 60	High copy number expression vector. Ampicillin resistant. T5 promoter/lac operon. 6xHis sequence at 3' end of MCS.	QIAGEN
pQE 60 based plasmids.		
pQE_PelB	pQE vector with PelB leader inserted via <i>Nco</i> I – <i>Bam</i> HI directional cloning.	This Study
pQE_PelB_HRP	pQE_PelB vector with HRP gene inserted via <i>Not</i> I – <i>Hind</i> III directional cloning.	This Study
pQE_PelB_HRP_His	pQE vector with PelB – HRP fusion construct inserted via <i>Bsp</i> HI – <i>Bam</i> HI directional cloning in frame with C-terminal His ₆ purification tag.	This Study
pQE_PelB_HRP_ΔHis	pQE vector with PelB – HRP fusion construct inserted via <i>Bsp</i> HI – <i>Hind</i> III directional cloning.	This Study
pBR_I	pQE_PelB_HRP_His vector with wildtype HRP gene present. Generated via Pro 34 Ala mutation.	This Study
pBR_I based site-directed mutagenesis plasmids.		
pBR_K174A/E/N	pBR_I plasmid with Lys 174 on the HRP gene replaced by an Ala/Glu/Asn..	This Study
pBR_K232A/E/N/Q/F	pBR_I plasmid with Lys 232 on the HRP gene replaced by an Ala/Glu/Asn/Gln/Phe.	This Study
pBR_E238Q	pBR_I plasmid with glutamic acid 238 on the HRP gene replaced by a glutamine.	This Study
pBR_E239N	pBR_I plasmid with glutamic acid 239 on the HRP gene replaced by an asparagine.	This Study
pBR_K241A/E/N/Q/F	pBR_I plasmid with Lys 241 on the HRP	This Study

pBR_K232Q/241Q	gene replaced by an Ala/Glu/Asn/Gln/Phe. pBR_I plasmid with Lys 232 and 241 on the HRP gene replaced by a Gln.	This Study
pBR_K232N/241N	pBR_I plasmid with Lys 232 and 241 on the HRP gene replaced by an Asn.	This Study
pBR_K232F/241N	pBR_I plasmid with Lys 232 and 241 on the HRP gene replaced by Phe and Asp respectively.	This Study
pBR_T102A	pBR_I plasmid with Thr 102 on the HRP gene replaced by an Ala.	This Study
pBR_Q106R	pBR_I plasmid with Gln 106 on the HRP gene replaced by an Arg.	This Study
pBR_Q107D	pBR_I plasmid with Gln 107 on the HRP gene replaced by an Asp.	This Study
pBR_T110V	pBR_I plasmid with Thr 110 on the HRP gene replaced by a Val.	This Study
pBR_I180F	pBR_I plasmid with Ile 180 on the HRP gene replaced by a Phe.	This Study
pBR_R118K	pBR_I plasmid with Arg 118 on the HRP gene replaced by a Lys.	This Study
pBR_R118K_159K (<i>Velcro Plus K283R</i>)	pBR_R118K plasmid with Arg 159 on the HRP gene replaced by a Lys.	This Study
pBR_R118K_159K_K232F _K241N (<i>Velcro Minus K283R</i>)	pBR_R118K_159K plasmid with Lys 232 and 241 on the HRP gene replaced by Phe and Asn respectively.	This Study
pBR_R118K_159K_R283K (<i>Velcro Plus</i>)	pBR_R118K_159K plasmid with Arg 283 on the HRP gene replaced by a Lys.	This Study
pBR_R118K_159K_R283K K232F_K241N (<i>Velcro Minus</i>)	pBR_R118K_159K_R283 plasmid with Lys 232 and 241 on the HRP gene replaced by Phe and Asn respectively.	This Study

2.1.3 Cloning primers: design and sequences.

Primers were designed for amplification and final ligation of PCR products into the *QIAexpress* type ATG vector construct pQE 60, commercially available from Qiagen. To amplify the specific regions (namely the PelB leader and the HRP gene) from the donated unknown vector, primers were designed based on the sequence determined from di-deoxy sequencing carried out commercially by MWG Biotech, Germany. The multiple cloning site of pQE 60 contains three unique restriction sites: *Nco* I, *Bam*H I and *Bgl* II, with *Nco* I located closest to the Ribosomal Binding Site (RBS). The restriction site *Hind* III is located directly 3' to the stop codon downstream of the poly His tag. However, due to the nature of the cloning strategy, none of these restriction sites could be utilised for HRP gene cloning, so judicious establishment of unique restriction sites was required. Introduction of the PelB leader allowed for the development of a unique restriction site, *Not* I. Therefore, the PelB leader sequence forward primer included the *Nco* I restriction sequence, while the Pel B reverse primer contained *Bam*H I and 5' *Not* I restriction sequences. Consequently the HRP forward primer contained *Not* I binding site sequence and the reverse primer contained a polyHis tag sequence and a 3' *Hind* III binding site sequence. Forward primers were designed using the same bases found in the original sequence of the required gene, whilst the reverse primers were designed using the complementary bases from the 3' to the 5' end of the bases. The amplification primers utilised in this study are listed in below:

pELB_For	CATGCCATGGATGAAATACCTGCTGCCGACCGC
BspH I For	ATATCATGAGCAAATACCTGCTGCCGACCG
pELB_Rev	CGGGATCCGCGGCCGCGGCCATCGCCGGCTGGG
HRP_For:	AAGGAAAAAAGCGGCCGCCATGCAGTTAACCCTACATTCTACGAC
HRP_His_Rev:	CCAAGCTTAGTGATGGTGATGGTGATGAGAGTTGCTGTTGACCACTC
HRP Δ His_Rev:	CCCAAGCTTAGAGTTGCTGTTGACCACTCTGCAG
HRP_Rev:	CGCGGATCCGCTGTTGACCACTCTGCAG

2.2 Preparation of Microbiological Media.

2.2.1 Luria Bertani Broth. (LB Broth)

LB medium contained 10 g.L⁻¹ tryptone, 10 g.L⁻¹ sodium chloride and 5 g.L⁻¹ yeast extract. Glassware was cleaned prior to addition of media components, and distilled water (dH₂O) was used throughout. Once the components were reconstituted with dH₂O, the pH was adjusted to pH 7 and the medium was autoclaved immediately at 121 °C and 1.5 bar for 15 min. No antibiotics were added prior to autoclaving, as these are heat labile. Filter-sterilised glucose, 2% w/v, was added to the LB to repress recombinant expression (after autoclaving, to avoid caramelisation of the glucose).

2.2.2 SOB and SOC Media

SOB medium contained 20 g.L⁻¹ tryptone, 5 g.L⁻¹ yeast extract, 0.5 g.L⁻¹ sodium chloride, 2.5 mM potassium chloride and prepared as per 2.2.1 above. After making SOB medium (1 L as outlined above) and allowing it to cool to less than 50 °C, 50 µL of sterile 2M MgCl₂ and 200 µL of sterile 1 M glucose were added, to give final concentrations of 10 mM and 20 mM respectively.

2.2.3 Super Broth Medium and 50/5 Supplement.

Super broth medium contained 30 g.L⁻¹ tryptone, 20 g.L⁻¹ yeast extract and 10 g.L⁻¹ MOPS and prepared as per 2.2.1 above. After making Super broth medium (outlined above) and allowing it to cool to less than 50 °C, sterile glycerol and glucose were added to final concentrations of 50% v/v and 5% w/v, respectively. 2mM MgCl₂ (final concentration) can also be added to increase cell density.

2.3 Antibiotic Preparation.

Antibiotics were prepared to the various concentrations outlined below and stored at – 20 °C.

2.3.1 Ampicillin.

Ampicillin (100 mg.mL⁻¹) was prepared in dH₂O and was used in liquid broth and solid agar at a final concentration of 100 µg.mL⁻¹.

2.3.2 Chloramphenicol.

Chloramphenicol (125 mg.mL⁻¹) was prepared in 100% (v/v) ethanol and was used in liquid broth and solid agar at a final concentration of 125 µg.mL⁻¹.

2.3.3 Tetracycline.

Tetracycline (125 mg.mL^{-1}) was prepared in 50% (v/v) ethanol and was used in liquid broth and solid agar at a final concentration of $125 \mu\text{g.mL}^{-1}$.

2.4 Preparation of Buffers.

DNA Electrophoresis Buffers

50X TAE Buffer.

EDTA	50 mM
Glacial acetic acid	57 mL
Tris	242 g
dH ₂ O	to 1 L
pH	8.0

6X DNA Gel loading Dye.

Bromophenol Blue	0.25% w/v
Xylene Cyanol	0.25% w/v
Sterile Sucrose	20% w/v
Made up in sterile dH ₂ O, stored at 4°C.	

Buffers One and Two for Competent Cell Production.

Buffer One (60mL):

Make up in **UltraPure Water**

Potassium Acetate	30 mM
Calcium Chloride	10 mM
Glycerol	15 % (v/v)
Rubidium Chloride	100 mM
Adjust pH with dilute HCl to 5.8.	
Manganese Chloride	50 mM

Filter sterilise into a sterile container.

Store at 4°C.

Buffer Two (8mL):

Make up in **UltraPure Water**

Rubidium Chloride	10 mM
MOPS	10 mM
Calcium Chloride	75 mM
Glycerol	15 % (v/v)
Adjust pH with dilute KOH to 6.8.	

Filter sterilise into a sterile container.

Store at 4°C.

Buffers for 1.2.3 Plasmid Preparation.

Solution One:

Glucose	1 mL 0.5 M
Na ₂ -EDTA (pH 8)	1 mL 0.1 M
Tris HCl (pH 8)	1 mL 1 M
dH ₂ O	7 mL

TE Buffer

Tris-HCl (pH 8)	10 mM
Na ₂ -EDTA (pH 8)	1 mM

Solution Two:

NaOH	2 mL 1 M
SDS	1 mL 10%
dH ₂ O	7 mL

Solution Three:

Potassium acetate	60 mL 5 M
Glacial acetic acid	11.5 mL
dH ₂ O	28.5 mL

Buffers for Sodium Dodecyl Sulfate PolyAcrylamide Gel Electrophoresis

Buffer A

2M Tris/HCl, pH 8.8	750 ml
10% (w/v) SDS	40 ml
dH ₂ O	210 ml

Buffer B

1M Tris/HCL, pH 6.8	500 ml
10% (w/v) SDS	40 ml
dH ₂ O	460 ml

4X Loading Buffer

dH ₂ O	20 mL
Tris/HCl, pH 6.8, 0.5M	5 mL
Glycerol (neat)	4 mL
SDS (10% w/v)	8 mL
β-mercaptoethanol (neat)	2 mL
Bromophenol Blue (1% w/v)	1 ml

10X Running Buffer

Tris/HCl	30.25 g
Glycine	144 g
SDS 10% (w/v)	100 ml.

Make up to 1 litre with dH₂O.

Dissolve in a waterbath set to 55°C.

Staining Solution:

Acetic Acid (neat)	100 mL
Methanol (neat)	250 mL
dH ₂ O	250 mL
Bromophenol Blue	2.5 g

Destaining Solution

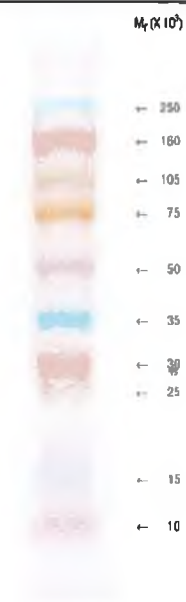
Acetic Acid (neat)	10 mL
Methanol (neat)	450 mL
dH ₂ O	450 mL

The molecular weight standards used in SDS-PAGE are:

Sigma Wide Range Markers

Myosin, rabbit muscle	205 kDa
β -Galactosidase, <i>E. coli</i>	116 kDa
Phosphorylase b, rabbit muscle	97 kDa
Fructose-6-phosphate Kinase	84 kDa
Albumin, bovine serum.	66 kDa
Glutamic Dehydrogenase, bovine liver.	55 kDa
Ovalbumin, chicken egg.	45 kDa
Glycer Phos Dehyd, rabbit muscle.	36 kDa
Carbonic Anhydrase, bovine erythrocytes.	29 kDa
Trypsinogen, bovine pancreas.	24 kDa
Trypsin Inhibitor, soybean.	20 kDa
α -Lactalbumin, bovine milk.	15 kDa
Aprotinin, bovine lung.	6.5 kDa

Amersham Rainbow Markers



Buffers for Non Denaturing Gel Electrophoresis

4x Buffer C

1.5M Tris/HCl, pH 8.8 100 ml

4x Buffer D

0.5M Tris/HCl, pH 6.8 100 ml

1x Running Buffer (pH to 8.8).

Tris/HCl 3.25 g

Glycine 14.4 g

Make up to 1 litre with dH₂O.

4X Loading Buffer

dH₂O 15 mL

1M Tris/HCl, pH 6.8, 5 mL

Glycerol (50% v/v) 4 mL

Bromophenol Blue (1% w/v) 1 ml

Staining Solution:

TMB Assay as outlined in Section 2.29

Buffers for Western Blots.

1x Transfer buffer

Tris-HCl	25 mM
Glycine	150 mM
Methanol	10% (v/v)

TBS-Tween buffer (pH 7.5)

Tris-HCl	20 mM
NaCl	500 mM
Tween 20	0.05% (v/v)
Triton X-100	0.2% (v/v)

TBS buffer (pH 7.5)

Tris-HCl	10 mM
NaCl	150 mM

Blocking Buffer.

5% w/v MarvelTM milk powder in TBS

2.5 Storage and Culture of Bacteria.

All bacterial strains were stored as 50% v/v glycerol stocks at -80°C . The stocks were prepared by aseptically adding 0.5 mL of late log phase bacteria to 1.0 mL of 80% (v/v) sterile glycerol in a sterile microcentrifuge tube. The contents were then mixed and the stock was stored at -80°C for long-term storage, while an identical stock was also stored at -20°C for medium term storage. Short-term storage was on agar plates containing the selective antibiotic, stored at 4°C .

To culture bacteria from the medium- and long-term storage conditions, the uppermost layer of the frozen cell mass was allowed to defrost and this was aseptically used to inoculate fresh LB broth supplemented with the correct antibiotic. The LB broth was then incubated at 37°C , 220 rpm, overnight.

2.6 Standard Polymerase Chain Reaction.

Polymerase Chain Reaction was utilised to amplify the DNA for both the PelB leader and the HRP gene. A standard PCR reaction (stock concentrations indicated) was set up as follows:

1 μL	dNTP 10 mM mix
5 μL	10x Red <i>Taq</i> PCR Buffer containing 500mM MgCl_2 .
1 μL	Forward Primer (100 pMol)
1 μL	Reverse Primer (100 pMol)
1 μL	Template DNA (varying concentration)
38.5 μL	Sterile H_2O

The reaction tube contents were then gently mixed by flicking the tube repetitively. The solution was collected at the bottom of the tube by a short centrifugation. Finally,

2.5 μ L RedTaq[®] Polymerase

was added, and again the mixture was mixed and collected as outlined above. A negative control was also set up as above but without template DNA.

The following PCR cycle was utilised for DNA amplification:

Stage One: Denaturation.		
95 °C	2 min 30 s	1 cycle
Stage Two: Cycling		
95 °C	50 s	18 cycles
T _{anneal}	50 s	
72 °C	1 min/kb	
Stage Three: Final Elongation		
72 °C	5 min	1 cycle

If the optimum annealing temperature was to be determined, the T_{anneal} was varied based on the theoretical T_{anneal} calculation:

$$T_{\text{anneal}} = [2x (\text{A/T content}) + 4x (\text{G/C content})] - 5 \text{ } ^\circ\text{C. (Maniatis et al., 1989)}$$

2.7 Preparation of PCR product for downstream processes.

Once the PCR was complete, the amplified DNA was cleaned for further downstream processes. This cleaning process removed the RedTaq, primers etc. from the amplified DNA. Two methods were used to purify the amplified DNA:

2.7.1 Phenol Chloroform Extraction.

The volume of the PCR reaction mixture was increased to 400 μ L by adding TE buffer. 400 μ L of Phenol:Chloroform:Isoamylalcohol [25:24:1] was then added to the reaction tube. The mixture was vortexed and centrifuged at 10,400 x g for 5min in a microfuge. The aqueous layer was removed to a clean Eppendorf tube. One volume of ice-cold isopropanol was added to aqueous layer. One-tenth volume of 3M sodium acetate (pH5.5) was added to the aqueous layer and alcohol. Repeated inversion of the mixture led to homogeneity. The mixture was stood upright at -20 °C for 2 hours.

Centrifugation at 10,400 x g for 15 min produced a pellet and supernatant, which latter was removed. The resultant pellet was washed with 400 μ L of 70% v/v ethanol. This mixture was again centrifuged at 10,400 x g for 10 min and the supernatant removed. The pellet was resuspended in an appropriate volume of TE buffer. A TAE agarose gel was run to confirm adequate cleaning of PCR product and to estimate DNA concentration for further downstream applications.

2.7.2 Bioline DNase Quick Clean®.

DNase Quick Clean® is a commercially available size exclusion method for cleaning DNA used to concentrate double stranded DNA from PCR reactions and enzymatic reactions. The procedure was followed as per the manufacturer's protocol. In short, 1 volume of DNase Quick Clean® was added to a sample of DNA, mixed thoroughly by vortexing and statically incubated at room temperature for 5 min. The microcentrifuge tube containing the mixture was then centrifuged at 10,400 x g for 10 min and the supernatant discarded. The DNA pellet was then washed with 70% v/v ethanol to remove any residual salts etc., and again the microcentrifuge tube was centrifuged for 10 min and the ethanol removed. The DNA pellet was then resuspended in the desired volume of TE buffer or molecular grade water for further downstream applications.

2.8 Plasmid Preparation.

2.8.1 Rapid Boiling Method.

This method is similar to that of Holmes and Quigley (1981) and can be utilised to screen large number of transformants. However, the resulting preparation is very crude and unsuitable for digestion experiments. A 1.5mL aliquot of an overnight culture was centrifuged at 10,400 x g in a microfuge and the supernatant removed. The cell pellet was resuspended in 350 μ L of STET buffer. A 20 μ L aliquot of a 10 mg.mL⁻¹ lysozyme solution (freshly prepared in STET buffer) was added and the microfuge tube incubated at 30 °C for 10 min. The tube was then placed in boiling water for 30 s and immediately centrifuged at 10,400 x g for 10 min. The supernatant was removed to a fresh tube and an equal volume of isopropanol was added to precipitate the DNA. The tube was left at room temperature for 10 min and the plasmid DNA was pelleted by centrifugation at 10,400 x g for 10 min. The pellet was dissolved in 70 % v/v ethanol, air dried and then dissolved in 50 μ L of TE buffer. This preparation was stored at 4 °C until required.

2.8.2 1,2,3 Plasmid Preparation Method.

This rapid and inexpensive method based on Birnboim and Doly (1979) produces a reasonably pure plasmid preparation. Cells from an overnight culture (4.5 mL) were pelleted via centrifugation at 10,400 x g. The LB was removed and the cells were resuspended in 100µL of Solution One (Section 2.4) and statically incubated at room temperature for 5 min. Solution Two (200 µL) was then added and the tube was mixed by inversion and stood on ice for 5 min. Solution Three (150 µL) was then added and again mixed by inversion and stood on ice for 10 min. Chromosomal DNA precipitated out of solution and was pelleted by centrifugation at 10,400 x g. The supernatant was removed and placed into a clean eppendorff, 450µL of phenol:chloroform:isoamylalcohol (25:24:1) was added and the solution mixed by vortexing. The mixed solution was then centrifuged for 5 min at 10,400 x g and the upper aqueous layer removed to a fresh tube. An equal volume of isopropanol was then added to the supernatant; the solution was mixed and incubated at room temperature for 10 min. The mixture was again centrifuged at 10,400 x g for 10 min; this pelleted the plasmid DNA. The pellet was washed with 70% v/v ethanol and the ethanol was allowed to evaporate. The pellet was resuspended in 50 µL of TE Buffer and 0.1 µL RNAase (10 mg.mL⁻¹) was added. The preparation was stored at -20 °C.

2.8.3 Sigma Gene Elute Plasmid Prep Mini Kit.

A single *E.coli* colony bearing the pQE 60 vector was picked from a LB agar plate containing 100 µg.mL⁻¹ ampicillin and was grown overnight (16 hours) in 10 mL of LB broth containing 100 µg mL⁻¹ ampicillin at 37 °C, shaken at 220 rpm. The pQE 60 vector was then purified via the Sigma Gene-Elute™ Kit as per manufacturer's instructions. Briefly, 4.5 mL of cells from an overnight culture were pelleted via centrifugation at 10,400 x g. The LB was removed and the cells were resuspended in 200 µL of Resuspension Solution, containing RNase A. The cells were vortexed to ensure complete cell resuspension. Lysis solution (200 µL) was added and the mixture was inverted 4-6 times to ensure correct mixing. The solution was allowed to clear for ≤5 min. Once the lysate had cleared, 350 µL of Neutralisation Buffer was added and the mixture inverted 4-6 times. The cell and chromosomal debris was then pelleted by centrifugation at 10,400 x g for 10 min. The spin-cup based Binding Column was

prepared by adding 500 μ L of Column Preparation Solution to the spin cup. The cup was spun at 10,400 x g for 1 min. The cleared lysate was then transferred to the prepared Binding Column and the contents were spun through the column at 10,400 x g for 1 min, with the flow-through being discarded. The Binding Column was then washed with 750 μ L of Wash Solution, containing ethanol, and the column centrifuged for 1 min at 10,400 x g. The column was then spun for an additional minute to ensure dryness. The Binding Column was then transferred to a new collection microcentrifuge tube, and 100 μ L of Elution Buffer was added to the column. The column was spun at 10,400 x g and the plasmid was eluted into the collection microcentrifuge tube. If the plasmid preparation was not used immediately, it was stored at -20°C .

2.9 Restriction Digest of the pQE60 Vector and the PCR insert.

A restriction digest was typically carried out on the pQE 60 vector and the relevant insert, for directional cloning or mutant screening purposes. The restriction enzymes utilised depended on the insert, and ultimately on the primers, as outlined in Section 2.1.3.

A standard double digest (stock concentrations noted) of the pQE 60 vector to prepare for PelB insertion is outlined below:

20 μ L	Freshly prepared pQE 60 vector.
2.25 μ L	10x Restriction Enzyme Reaction Buffer.
1.25 μ L	<i>Nco</i> I Restriction Enzyme (10,000 U.mL ⁻¹)
1.25 μ L	<i>Bam</i> H I Restriction Enzyme (10,000 U.mL ⁻¹)

A standard double digest (stock concentrations noted) of the pQE60_PelB vector to prepare for HRP insertion was as follows:

20 μ L	Freshly prepared pQE60_PelB vector.
2.25 μ L	10x Restriction Enzyme Reaction Buffer.
1.25 μ L	<i>Not</i> I Restriction Enzyme (10,000 U.mL ⁻¹)
1.25 μ L	<i>Hind</i> III Restriction Enzyme (10,000 U.mL ⁻¹)

The inserts were also digested with the appropriate restriction enzyme, *Nco* I and *Bam*H I for the PelB insert and *Not* I and *Hind* III for the HRP insert, in a similar set-up to those above. Once the reaction mixture had been prepared the contents were gently

mixed and centrifuged. All digestions were carried out at 37 °C for 3.5 hours to ensure complete restriction. The restricted DNA fragment (vector or insert) was then gel purified (Section 2.10) for further processing or visualised to ensure correct restriction.

2.10 Agarose Gel Electrophoresis for DNA characterisation.

DNA was analysed by running on agarose gels in a horizontal gel apparatus. Agarose gels were prepared by dissolving low melting point agarose (typically 0.7% to 1.2% w/v) in 1 X TAE buffer and boiling until the solution became translucent. The 1 X TAE buffer was also utilised as the running buffer. Once the boiled agarose had cooled sufficiently, the gel was poured into the mould and the comb added to form loading wells for the DNA. A tracker dye was also incorporated into the DNA samples to aid loading into the wells and to estimate migration rate of DNA through the gel. On a 1% agarose gel, bromophenol blue and xylene cyanol migrate approximately with the 300 bp and 4000 bp fragments respectively. However, where Sigma RedTaq® was used, no tracking dye was added, as this was included in the RedTaq® mixture. Mini gels were frequently run at 100 Volts for 1 hour or until the tracker dye reached the end of the gel. Gels were stained by immersion in a bath of ethidium bromide (Section 2.12) for 20min. Gels were then visualised on a UV transilluminator and photographed using a UV image analyser.

2.11 Preparation of RNase.

Ribonuclease A (DNase free) was dissolved at a concentration of 10 mg.mL⁻¹ in 10 mM Tris-HCl (pH 7.5) and 15 mM NaCl. The solution was aliquoted and stored at -20 °C.

2.12 Preparation of Ethidium Bromide.

A 10 mg.mL⁻¹ stock solution of ethidium bromide was prepared by dissolution in dH₂O. This stock solution was stored in the dark at 4 °C. A 100 µL aliquot of the stock solution was added to 1 L of dH₂O for TAE gel staining. Gloves, lab coat and glasses were worn at all times when handling solutions of ethidium bromide. Once the staining capacity of the ethidium bromide solution had degenerated, one ethidium bromide destaining bag (Alpha Technologies, Wicklow), was added to the bath and allowed to absorb the ethidium bromide overnight. The clear solution was then disposed of

normally and the solids contained in the ethidium bromide destaining bag were incinerated.

2.13 Purification of DNA from an agarose gel.

DNA was purified from agarose gels using a DNA Gel Purification Kit (PerfectPrep, Eppendorff), utilised as per manufacturer's instructions. After electrophoresis, the gel of interest was stained in ethidium bromide for 20 min and viewed under 70% UV illumination. As with the preparation of ethidium bromide (Section 2.12), gloves, glasses and lab coat were worn at all times during agarose manipulation. The time of exposure was minimised as UV light is a known DNA mutagen. The DNA band of interest was excised utilising a sterile scalpel blade, and the agarose slice was transferred to a sterile 1.5 mL microcentrifuge tube. Three volumes of solubilising buffer were added and the tube was incubated at 55 °C with regular gentle vortexing until the gel slice had completely dissolved. One volume of isopropanol was added to the tube and mixed thoroughly. Eight hundred microlitres of this solution was transferred into a spin cup and spun at 10,400 x g for 1 min. The flow-through was discarded and 750 µL of Washing Solution (containing ethanol) was added and centrifuged for a further minute at 10,400 x g. The flow-through was discarded and the cup was centrifuged for a further minute to ensure it was completely dry. The spin cup was then transferred to a fresh microfuge tube and 50 µL of TE was added to the cup. The cup was then centrifuged for one minute at 10,400 x g to elute the DNA. A ligation reaction was set up immediately.

2.14 Ligation Reactions.

In this project directional cloning was utilised and, hence, a cohesive ligation strategy was implemented. A typical reaction was carried out as outlined below:

9 µL	Gel Purified Restricted Insert
3 µL	Gel Purified Restricted Vector
4 µL	T ₄ Ligase Buffer (5 X)
3 µL	Sterile dH ₂ O
1 µL	T ₄ Ligase (1U.µL ⁻¹)

Generally, a 3:1 Insert:Vector ratio was implemented, as suggested by T₄ Ligase manufacturer (Invitrogen). The ratio was judged from a 1% TAE gel. The ligation was

allowed to proceed overnight at $\sim 17^{\circ}\text{C}$. Once the reaction was completed, the ligated products were stored at -20°C until transformation was carried out.

2.15 Preparation of High Efficiency Competent Cells.

The calcium chloride method was utilised for competent cell preparation as described by Inoue and co-workers (1990). A frozen stock of *E.coli* strain XL-10 Gold was slowly defrosted and streaked onto an LB agar plate containing $12.5\ \mu\text{g}\cdot\text{mL}^{-1}$ tetracycline and $10\ \mu\text{g}\cdot\text{mL}^{-1}$ of chloramphenicol. The plate was incubated overnight at 37°C . One colony was picked from this plate and was used to inoculate 10 mL of LB broth, again containing $12.5\ \mu\text{g}\cdot\text{mL}^{-1}$ tetracycline and $10\ \mu\text{g}\cdot\text{mL}^{-1}$ of chloramphenicol. This culture was grown overnight at 37°C , 220 rpm. Two millilitres of overnight culture was taken and used to inoculate 200 mL of sterile LB broth without any antibiotics present. This culture was grown at 37°C , 220 rpm. The growth was monitored carefully and once the $\text{OD}_{600\text{nm}}$ reached 0.475 (approximately 2-3hrs), the flask was removed, placed on ice and gently swirled for 5 min. The culture was then transferred to a chilled sterile centrifuge tube and the cells were collected by centrifugation at low speed (5 min, $800 \times g$) in a previously cooled (4°C) centrifuge, (Beckman J2-21). After centrifugation, the supernatant was carefully discarded, as per Class I licence standards, whilst maintaining the cells continuously on ice. The cell pellet was carefully resuspended in 60mL of ice cold Buffer One via swirling in a container of ice water. Once the pellet was resuspended, the container was buried in ice and statically incubated at 4°C for 90 min. The chilled cells were then collected in a previously cooled (4°C) centrifuge operated at low speed (5 min, $800 \times g$). After centrifugation, the supernatant was again carefully discarded whilst maintaining the cells continuously on ice. The cell pellet was carefully resuspended in 8mL of ice cold Buffer Two via swirling in a container of ice water. Once the pellet is resuspended, the cells are quickly and aseptically aliquoted into sterile chilled eppendorffs in $800\ \mu\text{L}$ fractions. The cell fractions are then flash frozen by dipping the eppendorff in ethanol, stored at -80°C overnight, for 1 min. Once frozen, the cells were transferred to the -80°C freezer for long term storage. Cells prepared in this manner frequently gave transformation efficiencies in the order 10^7 transformants/ μg DNA.

2.16 Transformation of High Efficiency Competent Cells.

A microcentrifuge tube of high efficiency competent cells prepared according to 2.15 above was allowed to thaw slowly on ice and 2 μL of transformation reaction mixture was carefully pipetted into 100 μL of cells. A 1 in 5 dilution of the transformation reaction was also added to a separate 100 μL vial of cells. Finally, positive and negative control reactions were also set up, by adding 2 μL of restricted vector and either 2 μL of $0.01\text{ng}\cdot\mu\text{L}^{-1}$ of pUC 18 vector (positive) or 2 μL of TE buffer (negative), to separate vials (100 μL) of cells. Once the transformation (or control) additions were made, the mixture was gently mixed by flicking the microcentrifuge tube. The tubes were then incubated on ice for 30 min. The cells were then heat shocked for 45 s in a 42°C water bath and immediately placed back on ice. SOC medium (900 μL , room temperature) was aseptically added to each of the tubes. The cells were then allowed to recover for 1 hour by horizontal shaking at 37°C at 220 rpm. After one hour the cells were collected by centrifugation at $10,400 \times g$ and 900 μL of supernatant was removed. The remaining 100 μL was utilised to resuspend the cells. From each 100 μL vial, 20 μL and 80 μL were aseptically spread onto LB agar plates containing $100 \mu\text{g}\cdot\text{mL}^{-1}$ ampicillin. The plates were inverted and grown overnight at 37°C .

2.17 Calculation of Transformation Efficiencies.

Cells prepared as outlined in Section 2.15 were transformed with a known concentration of plasmid DNA, to ascertain the transformation efficiency for the batch of cells. Typically, 2.5 pg of pUC 18 plasmid DNA was utilised in the transformation, with the transformed cells being plated on LB agar supplemented with $100 \mu\text{g}/\mu\text{L}$ ampicillin. The cells were allowed to grow overnight (18 h) and total colonies counted. The following equation (Maniatis et al., 1989) was utilised to calculate the transformation efficiency:

$$\frac{CFU}{\mu\text{L}_{\text{Cells}}} \times \frac{1000\mu\text{L}}{2.5\text{pg}_{\text{DNA}}} \times \frac{1 \times 10^6 \text{pg}}{1\mu\text{g}} = CFU / \mu\text{gDNA}$$

Transformation efficiencies in the range of 1×10^7 CFU/ μg DNA were regularly achieved by the methods outlined in Section 2.15.

2.18 Screening of Transformed High Efficiency Competent Cells.

Following overnight growth, a representative number of colonies (usually 5-7) was picked from each plate. These colonies were inoculated into 10 mL of LB Broth supplemented with 100 µg/mL ampicillin. The cultures were grown overnight and a plasmid preparation was carried out the following day via the 1,2,3 Method. The plasmid preparations were then restricted at a unique restriction site, only present if the insert had been correctly incorporated into the vector (*Not* I in the case of PelB Insertion and *Pst* I in the case of HRP insertion). This screening methodology was also implemented for mutant plasmid screening.

A standard screening digest of the pQE60pelBHRP vector (with stock concentrations noted) was set up as follows:

8 µL	Freshly prepared pQE60pelBHRP vector.
1 µL	10x Restriction Enzyme Reaction Buffer.
1 µL	<i>Pst</i> I Restriction Enzyme (10000 U.mL ⁻¹)

Once the reaction mixture had been prepared, the contents were gently mixed and collected by centrifugation. All digestions were carried out at 37 °C for 1 hour to ensure complete restriction. The restricted DNA fragment was then visualised under UV light after DNA electrophoresis and suitable staining in ethidium bromide. Colonies that produced a suitably digested vector were then chosen for further restriction analysis and, ultimately, DNA sequencing.

2.19 Spectrophotometric analysis of nucleic acids.

DNA concentration was determined by measuring the absorbance at 260 nm, where nucleic acids absorb maximally. To calculate the concentration of DNA the formula (Maniatis et al., 1989) below was utilised:

$$DNA_{con}^c \left(\frac{\mu g}{\mu L} \right) = \frac{A_{260nm} \times 50 \times Dil^n \times Factor}{1000}$$

A 50 µg.mL⁻¹ preparation of pure DNA has an absorbance of 1 unit at 260nm; the formula is divided by 1000 to convert to µL. The purity of the DNA solution was determined by reading the absorbance at 260 nm (λ_{max} for nucleic acids) and the absorbance at 280 nm (λ_{max} for proteins) and estimating their ratio. Pure DNA has an A_{260nm}/A_{280nm} of approximately 1.8.

2.20 DNA Sequencing and Protein Sequence Alignment.

Once a suitable clone had been elucidated from restriction analysis, a fresh plasmid preparation was produced. The concentration of the DNA in the preparation was calculated as outlined previously (Section 2.19), and was suitably adjusted by dilution to 2 µg/µL for the Value Read and 10 µg/µL for the Comfort Read, both commercially available from MWG Biotech, Germany. Fusion Antibodies Ltd, Northern Ireland, required 5 µg/µL concentration of plasmid DNA for sequencing. Standard pQE sequencing primers were utilised for the sequencing of the clones, these primers are outlined as follows:

pQE For: GTA TCA CGA GGC CCT TTC GTC T

pQE Rev: CAT TAC TGG ATC TAT CAA CAG GAG

Sequencing results were obtained via e-mail. Nucleotide sequences were translated to amino acid sequences via the ExPASy Translate Tool (<http://us.expasy.org>). The amino acid code was aligned with the HRP sequence available in Genbank (PDB Accession Number: 1ATJ) utilising the ClustalW bioinformatic program (Thompson et al., 1994). Finally, aligned sequences were imported into Genedoc for further sequence manipulation.

2.21 Design of mutagenic primers.

Individual primers for each mutagenic PCR were manually designed. Both mutagenic primers (forward and reverse) incorporated the desired mutation and also a silent mutation that would introduce a new restriction site. The inclusion of a new restriction site would allow for cost effective screening of multiple mutant clones. Both primers in a single mutagenic PCR were also designed to have a similar melting temperature. Primers were typically between 33 and 41 basepairs in length and had melting temperatures greater than 78 °C, estimated utilising the following formula (Borns et al., 2000):

$$T_m = 81.5 + 0.41(\%G/C) - 675/N - \% \text{ mismatch.}$$

Where N is the primer length and all % are whole numbers. The desired mutation was located in the centre of the primer and primers terminated in a G or C base to ensure efficient binding to the template DNA.

2.21.1 Mutagenic Primers utilised in this study.

The amino acid substitution sites are emboldened and underlined, whilst silent mutants are emboldened. The mutation achieved by each primer is also tabulated. All primers were supplied by MWG Biotech, Germany.

Primer Name	Primer Sequence	Mutation
pBR_I P34A_F	GATCCGATCCCAGGATCCCAG <u>GCT</u> TCAATATTACGTC	P34A
pBR_I P34A_R	GACGTAATATTGAAGCAG <u>CGA</u> TCCTGGGATCGGATC	P34A
pBR_I K174A_F	CTGTCCGGTGGCCACACATTTGGAG <u>GCG</u> AACCAGTGTAGG	K174A
pBR_I K174A_R	CCTACACTGGTT <u>CGC</u> TCCAAATGTGTGGCCACCGGACAG	K174A
pBR_I K174E_F	CTGTCCGGTGGCCACACATTTGGAG <u>GAGA</u> AACCAGTGTAGG	K174E
pBR_I K174E_R	CCTACACTGGTTCT <u>CT</u> TCCAAATGTGTGGCC <u>A</u> CCGGACAG	K174E
pBR_I K174N_F	CTGTCCGGTGGCCACACATTTGGAA <u>AT</u> AACCAGTGTAGG	K174N
pBR_I K174N_R	CCTACACTGGTT <u>A</u> TTTCCAAATGTGTGGCC <u>A</u> CCGGACAG	K174N
pBR_I K232A_F	CCATCTTCGATAAC <u>CG</u> GTAATATGTGAATCTCGAGGAGCAG	K232A
pBR_I K232A_R	CTGCTCCTCGAGATTCACATAGT <u>ACCG</u> GTTATCGAAGATGG	K232A
pBR_I K232E_F	CCATCTTCGATAAC <u>GAG</u> TACTATGTGAATCTCGAGGAGCAG	K232E
pBR_I K232E_R	CTGCTCCTCGAGATTCACATAGT <u>ACTCG</u> GTTATCGAAGATGG	K232E
pBR_I K232N_F	CCATCTTCGATAACA <u>ATT</u> TACTATGTGAATCTCGAGGAGCAG	K232N
pBR_I K232N_R	CTGCTCCTCGAGATTCACATAGT <u>ATTG</u> TTATCGAAGATGG	K232N
pBR_I K232F_F	CCATCTTCGATAAC <u>TTTT</u> TACTATGTGAATCTCGAGGAGCAG	K232F
pBR_I K232F_R	CTGCTCCTCGAGATTCACATAGT <u>AAA</u> GTTATCGAAGATGG	K232F
pBR_I K241A_F	GTGAATCTCGAGGAGCAG <u>GCG</u> AGGCCTGATACAG	K241A
pBR_I K241A_R	CTGTATCAGGCCT <u>GC</u> CTGCTCCTCGAGATTCAC	K241A
pBR_I K241E_F	GTGAATCTCGAGGAGCAG <u>GGA</u> AGGCCTGATACAG	K241E
pBR_I K241E_R	CTGTATCAGGCCT <u>TC</u> CTGCTCCTCGAGATTCAC	K241E
pBR_I K241N_F	GTGAATCTCGAGGAGCAG <u>AAT</u> GGCCTGATACAG	K241N
pBR_I K241N_R	CTGTATCAGGCC <u>ATT</u> CTGCTCCTCGAGATTCAC	K241N
pBR_I K241F_F	GTGAATCTCGAGGAGCAG <u>TTT</u> GGCCTGATACAG	K241F

Primer Name	Primer Sequence	Mutation
pBR_I K241F_R	CTGTATCAGGCC AA ACTGCTCCTC G AGATTAC	K241F
pBR_I K232Q_F	GATAACC C AGTACTATGTGAATCT C GAGGAGAACCAG	K232Q
pBR_I K232Q_R	CTGGTTCTCCTC G AGATTACATAGTACT G GTTATC	K232Q
pBR_I K241Q_F	GTGAATCT A GAGGAG C AGCAGGGCCTGATACAG	K241Q
pBR_I K241Q_R	CTGTATCAGGCCCT G C T G CTCCTC T AGATTAC	K241Q
pBR_I T102A_F	GTCAGTTGTGCAGAT T CTGCTG G C G ATAGCTGCGCAACAG	T102A
pBR_I T102A_R	CTGTTGCGCAGCTAT C G C CAGCAG A TCTGCACAAC T GAC	T102A
pBR_I Q106R_F	GCAGAT T CTGCTGACTATAGCTGCGC G T C AGAGCGTGAC	Q106R
pBR_I Q106R_R	GTCACGCTCT G A C G CGCAGCTATAGTCAGCAG A TCTGC	Q106R
pBR_I Q107N_F	GCAGAT T CTGCTGACTATAGCTGCGCA A G ATAGCGTGAC	Q107N
pBR_I Q107N_R	GTCACGCT A T C TTGCGCAGCTATAGTCAGCAG A TCTGC	Q107N
pBR_I T110V_F	GCGCAACAGAGCGTG G T T CTTGCC G CGGACCGTCCTGG	T110V
pBR_I T110V_R	CCAGGACGGTCCGCC G G C AAG A ACCACGCTCTGTTGCGC	T110V
pBR_I I180F_F	CCAGTGTAGGTT C T T T ATGGAT C G A TCTACAATTT C	I180F
pBR_I I180F_R	GAAATTGTAGA A T C GATCCAT A A A GAACCTACACTGG	I180F
pBR_I E238Q_F	CAAGTACTATGTGAATCT A C A G G AGCAG A AAGGCCTG	E238Q
pBR_I E238Q_R	CAGGCCTTT C T G CTC C T G TAGATTACATAGTACTTG	E238Q
pBR_I E239N_F	CTATGTGAATCT C GAG A ACCAGAAAGGCCTGATACAGAG	E239N
pBR_I E239N_R	CTCTGTATCAGGCCTTTCT G T T CTC G AGATTACATAG	E239N
pBR_I R118K_F	GACTCTTGCAGGCC C G C CGTCC T GG A AA G TGCCGCTCGG	R118K
pBR_I R118K_R	CCGAGCGGCAC T T T CCAGGACGG C C G GCCTGCAAGAGTC	R118K
pBR_I R159K_F	CGTGGGTCTGAAT A A A TCG T CAGATCTTGTGGCTCTGTC	R159K
pBR_I R159K_R	GACAGAGCCACAAG A T C T G ACGAT T T T ATT C AGACCCACG	R159K
pBR_I R283K_F	CATGGAC A A A ATGGGTAACATTACCC C G T A ACGGGTAC	R283K
pBR_I R283K_R	GTACCCGT T A C GGGGTAATGTTACCCAT T T T GTCCATG	R283K

2.22 Site-Directed Mutagenic PCR.

Mutagenic PCR was carried out as described by Wang and Malcom (1999) using complementary primers. Briefly, this involved two individual mutagenic polymerase chain reactions, each using a single primer (forward or reverse). The use of a single primer method increases the mutagenic efficiency, as primer-dimer formations are eliminated. Each 50 μ L PCR contained 10-100 ng of plasmid template DNA isolated from a *dam*⁺ (methylating) *E. coli* strain (typically XL-10 Gold), 0.5 μ M of each

mutagenic primer, 200 μ M of each dNTP, 1 unit of *pfuTurbo* DNA polymerase, 5 μ L of specific 10x enzyme buffer and 3 μ L of Stratagene “*Quick-Solution*”. The thermocycling conditions were as follows:

Stage One: Denaturation.		
95 °C	2 min 30 s	1 cycle
Stage Two: Cycling		
95 °C	50 s	10 cycles
60°C	50 s	
68°C	1 min/kb	
Stage Three: Final Elongation		
68 °C	10 min	1 cycle

After primary thermocycling, the two separate reactions were combined in equal amounts to a final volume of 50 μ L. An additional 1 U of *pfuTurbo* DNA polymerase was added to the mixture and the PCR was repeated as above; however, stage two consisted of 18 cycles. After secondary thermocycling, the reaction mixture was cooled to <37 °C and the template DNA was removed by digestion with 20 U of *Dpn* I endonuclease at 37 °C for at least 2h. *Dpn* I selectively digests methylated DNA; hence, it will digest the template DNA but not the newly synthesised DNA. The remaining DNA was transformed into XL-10 Gold cells, as outlined in Section 2.16. These transformed cells were grown on selective LB agar, yielding single colonies. Typically, 15 colonies were selected and the plasmids contained within these cells were analysed, by endonuclease digestion, for the desired restriction pattern. Potential mutants were verified by commercial DNA sequencing: see Section 2.20.

2.23 Selection of Residues for Mutagenesis.

2.23.1 Rational Mutation Selection.

Residues for mutation were rationally selected based on prior art that had pinpointed key residues influencing the stability of HRP. Previous cross-linking experiments on plant HRP identified Lysines 174, 232 and 241 as important residues (O’ Brien et al., 2001).

2.23.2 Consensus Mutation Selection.

Sequences were identified utilising a search Boolean, and downloaded from the NCBI gene repository (www.ncbi.nlm.nih.gov). These sequences (100) were then aligned using the default alignment parameters of the Clustal W server (Thompson et al.,

1994). The alignment was saved as a “.aln” file and subsequently processed by the “*ProteinParser*” software. “*ProteinParser*” is a novel bioinformatic software package that allows the user to rapidly elucidate key residues in a protein alignment via a frequency counting algorithm. A tolerance level of “50% Consensus” was set (i.e. $\geq 50\%$ frequency of occurrence of a particular amino acid) and the consensus sequence was subsequently generated (Ryan and Barrett, in press).

2.23.3 Immobilisation Mutation Selection.

Immobilisation, via covalent attachment, to an activated solid phase has been shown to improve protein stability. Directional immobilisation, via specific chemically reactive amino acid R-groups, offers many potential applications. In this study lysine was selected as the amino acid of choice, since it possesses one of the most reactive side chains of the twenty proteogenic amino acids. Wild-type arginine residues were selected for lysine replacement, as this is a conservative mutation: both size and charge are similar, and should result in minimal secondary structure rearrangement. The twenty-one arginine residues present in the HRP protein were viewed in Deep ViewTM (Guex and Peitsch, 1997) and analysed based on secondary structure and location. Beta sheet-forming residues were preferred over helical ones, and surface-exposed residues were selected in preference to buried ones.

2.24 Recombinant Protein Expression Protocols.

2.24.1 Localisation of recombinant HRP expression.

10 mL of LB broth supplemented with ampicillin ($100 \mu\text{g}\cdot\text{mL}^{-1}$), was inoculated with 200 μL of XL-10 Gold cells transformed with pBR_I and the culture grown overnight at 37 °C, 220 rpm. This 10 mL overnight culture was utilised to inoculate 100mL of LB broth supplemented with ampicillin ($100 \mu\text{g}\cdot\text{mL}^{-1}$), to 1% (v/v) inoculum. This 100 mL culture was grown until the $\text{OD}_{600\text{nm}}$ reached approximately 0.5. At this time, a 1 mL sample was taken and stored at -20 °C. The culture was then either induced with IPTG (final concentration of 50 μM) or no IPTG was added, and a 1 mL sample was taken at every time point. Each 1 mL sample was centrifuged at 10,400 x g for 1 min, the supernatant removed and saved for later analysis (S1). The pellet was resuspended in the 50mM sodium phosphate (pH 7.5). The samples were then sonicated for 30 s, at amplitude 40 and wattage output 100, using a microtip Vibra Cell Sonicator. The

sonicated cell debris was removed via centrifugation at 10,400 x g for 2 min. Fifty microlitres each of the cell lysate supernatant (S2) and the cell culture supernatant (S1) was utilised in the TMB peroxidase activity assay to ascertain recombinant HRP production and location.

2.24.2 Investigation of IPTG requirement for optimal recombinant HRP production.

The requirement for IPTG induction was investigated by following a simple time course assay over an 18-hour growth time. Cells harbouring the pBR_I plasmid were cultured to an OD_{600nm} of approximately 0.5 in the presence of the relevant antibiotics and sterilised glucose, at a concentration of 2% w/v. The cells were then centrifuged and resuspended in glucose-free LB broth, supplemented with 1 mM δ -ALA, 2mM CaCl₂ and 100 $\mu\text{g mL}^{-1}$ ampicillin. The cells were then induced with IPTG to final concentrations, ranging from 0 mM to 1 mM (0 mM, 0.05 mM, 0.1 mM, 0.5 mM and 1 mM) and the cells grown for a further 18 hours at 37 °C and 30 °C, each at 220 rpm. At 0 h, 4 h, and 18 hours post induction, a 1mL aliquot was removed and the cells were centrifuged at 10,400 x g for 1 min. The cell culture supernatant (S1) was retained for further analysis. The cell pellet was resuspended in 200 μL of 50 mM sodium phosphate (pH 7.5) and the suspension sonicated for 30 s, at an amplitude 40 and watt output 100, using a microtip Vibra Cell Sonicator. The cell debris was removed and 50 μL each of the cell lysate supernatant (S2) and the cell culture supernatant (S1) was utilised in the TMB Peroxidase activity assay to ascertain recombinant HRP production and location. Sterilised glucose (final concentration 2% w/v) was added to the negative control to block any leaky expression by the lac promotor.

2.24.3 Comparison of bacterial strains for recombinant HRP production.

Various *E. coli* derived strains were compared for their ability to express recombinant HRP. Competent cells for each strain were produced as per Section 2.15, and each cell line was transformed with 1 μg of pBR_I and a single colony bearing this plasmid was inoculated into 10 mL of LB broth supplemented with ampicillin (final concentration 100 $\mu\text{g mL}^{-1}$). Recombinant HRP expression was carried out as outlined in Section 2.24.2; however, only repressed, non-induced and 50 μM IPTG conditions were investigated.

2.24.3 Investigation of rHRP expression over time.

A single colony, transformed with pBR_I, was inoculated into 10 mL of LB broth supplemented with ampicillin (final concentration $100 \mu\text{g}\cdot\text{mL}^{-1}$) and was grown overnight at 37°C , 220 rpm. This overnight culture was used to inoculate 10 mL LB broth, supplemented with 1 mM δ -ALA, 2 mM CaCl_2 and $100 \mu\text{g}/\text{mL}$ ampicillin, to a final theoretical optical density of 0.01 at 600 nm. Replicate 10 mL cultures were set up in this manner and one 10 mL sample was taken at the appropriate time-points throughout the experiment and centrifuged. Cells were prepared for analysis as previously outlined, Section 2.24.1, and assayed for activity via TMB assay (Section 2.30). Absorbances at OD_{620nm} were plotted against time, to determine the optimal *E.coli* growth time.

2.24.4 Optimisation of *E. coli* culture conditions for maximal HRP production.

An overnight culture was set up as per Section 2.24.1 and 10 mL LB, 1 mM δ -ALA, 2 mM CaCl_2 and $100 \mu\text{g}\cdot\text{mL}^{-1}$ ampicillin was inoculated to a final theoretical OD_{600nm} of 0.01. The pBR_I-containing cells were grown in the presence of glucose (2% w/v) until an OD_{600nm} of approximately 0.5 was achieved. The cells were then removed from the glucose-containing medium by centrifugation at $2,000 \times g$ for 10 min, and resuspended in the same LB minus glucose. Cells were either induced with $50 \mu\text{M}$ IPTG or grown non-induced at 30°C , at 220 rpm for 18 hours. Cells were prepared for analysis as previously outlined (Section 2.24.1) and assayed for activity via TMB assay (Section 2.30). Absorbances at 620nm were plotted against time to determine the optimal *E.coli* culture conditions.

2.25 Recombinant HRP Purification

Initially Immobilised Metal Affinity Chromatography (IMAC) was utilised as the purification procedure for the recombinant HRP. The Ni-NTA resin was washed extensively in running buffer (50 mM sodium phosphate, pH7.5) to remove any traces of storage ethanol. In brief, the method involved the gentle mixing of 1mL of Ni-NTA resin with 10 mL of cleared cell lysate, containing 200 mM Gn HCl and 1 M NaCl, in a sterile universal for at least one hour at 4°C . The resin was collected by a slow ($1,000 \times g/10$ min) centrifugation, yielding the “run through” fraction. The resin was then washed with 50mM sodium phosphate, pH 7.5, to yield the “wash” fraction. Bound

recombinant protein was eluted by a pH shift, using 50 mM sodium acetate pH 4.5 to reverse the positive charge of the 6 X His tag. Eluted fractions were neutralised via dialysis against 50 mM sodium phosphate, pH 7.5. All fractions were analysed for peroxidase activity via the TMB assay (Section 2.30) and protein concentration via the BCA assay (Section 2.28). Purified fractions containing HRP were concentrated (MacrosepTM centrifugal concentrators) and filter sterilised and stored at 4 °C.

The Ni-NTA resin could be regenerated up to five times. Used resin was poured into a universal container and washed with 2 column volumes of distilled water followed by 2 column volumes 50% v/v ethanol. The resin was stripped with 3 column volumes of 100 mM EDTA, pH 8.0, then washed with 2 column volumes of 500 mM NaCl followed by 2 column volumes of distilled water. The resin was re-charged with 2 column volumes of 100 mM NiSO₄, washed with 2 column volumes of distilled water, transferred to a clean sterile container and stored at 4 °C in 20% v/v ethanol.

2.25.1 Osmotic shock and lysozyme treatment for cell lysis.

Proteins were released from the periplasmic envelope by a method similar to that described by French et al., (1996). The fractionation buffer (F1) comprised (final concentrations) 500 µg/mL lysozyme, 20% w/v sucrose, 1 mM EDTA (pH 8.0), 200 mM guanidine hydrochloride and 200 mM Tris-HCl (pH8.0) at room temperature. The cells to be disrupted were pelleted by centrifugation at 10,400 x g for 3 min. The pellet was resuspended in F1 buffer in 20% of the original culture volume. The resuspended cells were statically incubated at room temperature for 15 min, after which time an equal volume of ice-cold water was added. Once again, the mixture was allowed to stand for 15 min at room temperature. The cell debris was then removed by centrifugation at 10,400 x g for 10 min. The supernatant was carefully transferred to a clean container and prepared for further purification steps.

The recombinant non-His tagged HRP was purified through a three-step purification procedure, which utilises the inherent physio-chemical properties of the enzyme.

2.25.2 Hydrophobic Interaction Chromatography (HIC).

The column was set up by pouring approximately 30 ml Phenyl SepharoseTM into a clean, dry column (8 cm x 3 cm). The resin was allowed to settle and the storage ethanol was separated from the resin. The resin was then equilibrated with 100 ml (>3

column volumes) of 30% w/v $(\text{NH}_4)_2\text{SO}_4$ in 50mM sodium phosphate, pH 7.5. Prior to the addition of cell lysate, an aliquot of the loading sample (no salt) was saved for analysis. The sample was loaded in 30% $(\text{NH}_4)_2\text{SO}_4$ (w/v; based on original volume with no adjustment made for increased volume due to salt addition) and 5mL fractions were immediately collected. After loading the sample, the column was washed with 90 ml of 30% (w/v) $(\text{NH}_4)_2\text{SO}_4$, with the fractions collected during this wash being labelled as “salt-wash fraction”. A salt gradient of 30%-0% (w/v) $(\text{NH}_4)_2\text{SO}_4$ was then run, with collected fractions labelled as “salt-gradient fractions”. Finally, the column was washed with 50 mM Sodium Phosphate (pH 7.5) and the collected fractions were labelled as “buffer-wash fractions”. The fractions displaying the most peroxidase and protein activity were determined by the TMB (Section 2.30) and BCA (Section 2.28) assays respectively. The fractions containing the most peroxidase activity were pooled and the final volume noted. An aliquot of post-HIC sample was retained for further analysis. The column was cleaned via a 100% ethanol wash (at least 90 ml), and stored in 20% v/v ethanol.

2.25.3 Size Exclusion Chromatography.

The column was set up by pouring approximately 100 mL of Sephacryl S-300-HRTM into a clean, dry column (53 cm x 2.5 cm). The resin was allowed to settle and the storage ethanol was separated from it. The resin was then equilibrated with 300 ml (>3 column volumes) 50 mM sodium phosphate (pH 7.5). A maximum of 5 mL sample was loaded onto the column; larger volume samples were concentrated via reverse osmosis. The sample was loaded in 50 mM sodium phosphate (pH 7.5) and 5 mL fractions were collected immediately. The column was washed with 100 mL 50 mM sodium phosphate (pH 7.5). The fractions displaying the most peroxidase and protein activity was determined by the TMB (Section 2.30) and BCA (Section 2.28) assays respectively. The fractions containing the most peroxidase activity were pooled and the final volume noted. An aliquot of post-size exclusion sample was retained for further analysis. The column was cleaned using 50 mM sodium phosphate (pH 7.5) wash (at least 200 mL), and stored in 20% v/v ethanol.

2.25.4 Anion Exchange Chromatography.

The column was set up by pouring approximately 20 ml DEAE Sepharose into a clean, dry glass column (8 cm x 3 cm). The resin was allowed to settle and the storage ethanol

separated from it. The resin was then equilibrated with 60 ml (>3 column volumes) 50 mM sodium phosphate (pH 7.5). A maximum of 1 mL was loaded onto the column; larger volume samples were concentrated via reverse osmosis. The sample was loaded in 50 mM sodium phosphate (pH 7.5) and 5 mL fractions were collected immediately. After sample is loading, the column was washed with 20 ml of 50 mM sodium phosphate (pH 7.5), with the fractions collected during this wash being labelled as “*buffer-wash fraction*”. A salt gradient of 0–1 M NaCl was then run, with collected fractions labelled as “*salt-gradient fractions*”. The fractions displaying the most peroxidase and protein activity was determined by the TMB (Section 2.30) and BCA (Section 2.28) assays respectively. The fractions containing the most peroxidase activity were pooled and the final volume noted. An aliquot of post-anion exchange sample was retained for further analysis. The column was cleaned via 2 M NaCl in 50 mM sodium phosphate (pH 7.5) wash (at least 80 mL), and stored in 20% v/v ethanol.

2.26 Preparation of Dialysis Tubing.

Dialysis tubing (1 cm width) was rinsed in dH₂O and placed in a beaker of same. One small spatula of Na₂-EDTA was added to the dH₂O and the solution brought to the boil. The liquid was allowed to cool and then decanted off. The beaker was refilled with dH₂O and reboiled, this time without EDTA. The water was allowed to cool and was poured off. The tubing was rinsed once more with dH₂O and stored in dH₂O at 4 °C until required.

2.27 Protein Gel Electrophoresis.

2.27.1 SDS-PAGE (Sodium DodecylSulfate PolyAcrylamide Gel Electrophoresis)

SDS PAGE was carried out as described by Laemmli (1970). Typically, the glass plates used in the preparation of the gels were washed with detergent, rinsed with dH₂O and wiped with a tissue soaked in 70% v/v ethanol. A gasket was placed about the ridged plate and maintained in position by two clamps. The matrix was prepared as follows:

<u>Resolving Gel</u>		<u>Stacking Gel</u>	
Acrylamide/bis-acrylamide (30/0.8%)	3.3 mL	Acrylamide/bis-acrylamide (30/0.8%)	0.7 mL
Buffer A (Section 2.4)	2.5 mL	Buffer B (Section 2.4)	1.0 mL
dH ₂ O	6.0 ml	dH ₂ O	3.0 ml
APS (NH ₄) ₂ S ₂ O ₈ (10% w/v)	50 µL	APS (NH ₄) ₂ S ₂ O ₈ (10% w/v)	30 µL
TEMED	10 µL	TEMED	10 µL

The resolving gel is poured first to within 2 cm of the plate limit, layered with 70% v/v ethanol and allowed to set. TEMED is added only when ready to pour the respective gel, as it initiates cross-linking of the acrylamide. Next, the stacking gel is poured and a clean comb is inserted into the unpolymerised gel to create wells in which the samples will be loaded. The gels were loaded into the gel box at an angle so as to minimise the production of air bubbles between the electrode and the gel. The gel box chamber was flooded with 1 x Running Buffer (Section 2.4). Samples were prepared by boiling 15 μ L of sample in 5 μ L of 4 X loading buffer for 4 min. The samples were allowed to cool and were then loaded into the gel by deposition into the gel wells. Typically, gels were run at 200 volts, constant ampage for approximately 40 min or until the dye front reached the end of the gel. When the power had been switched off, the plates were removed and separated and the gel immersed in Coomassie Blue (Section 2.4) stain overnight with constant agitation at room temperature. After overnight staining, the gel was placed in destain solution, which was changed constantly as it became saturated with Coomassie Blue. Once destained, the gel was carefully removed, washed with dH₂O, placed onto a sheet of acetate, scanned and saved in a suitable electronic format.

2.27.2 Western Blotting.

An SDS-PAGE gel was run as described in Section 2.27.1. Coloured molecular weight markers (CM_r, Amersham Rainbow MarkersTM, Section 2.4) were included on the gel. Six pieces of 3 mm filter paper (Whatman) and 1 piece of nitrocellulose membrane (Schleicher and Schuell) were cut to the size of the gel. The filter paper sheets and the membrane were soaked in Transfer Buffer for 10 min. Avoiding air bubbles, 3 sheets of filter paper were placed on the cathode of a horizontal semi-dry electro-blotter (Biorad), followed by the membrane, the gel, 3 sheets of filter paper and finally the anode. The protein transfer was allowed to take place at a constant 17 V for 30 min. The membrane was washed three times for 15 min with TBS buffer (Section 2.4). The membrane was then blocked in 30 ml 5% (w/v) Marvel milk powder in TBS buffer for 60 min followed by incubation in 20 ml of murine anti-His antibody solution (prepared in Marvel/TBS buffer) overnight at 4°C, with gentle shaking. The membrane was washed 3 times for 15 min with TBS-T buffer. The secondary antibody, an anti-mouse alkaline phosphatase conjugate prepared in Marvel/TBS buffer, was added to the washed membrane and incubated for 90 min at room temperature, with gentle shaking. Finally the membrane

was incubated briefly with the alkaline phosphatase substrate (Sigma (5-Bromo-4-chloro-3-indolyl phosphate dipotassium/nitrotetrazolium blue chloride; BCIP/NBT) until the signal was clearly visible. Using a flatbed scanner, an image of the blot was saved to a PC.

2.27.3 Native Gel Electrophoresis.

Non-denaturing gels, or native gels, allow the electrophoresed protein to remain active in the gel matrix. This is due mainly to the absence from the gel of denaturing components, such as SDS and β -mercaptoethanol, and also because of the temperature used, 4 °C. Samples are separated based on their size and native charge. The gel plates were cleaned and assembled as per SDS-PAGE procedure above; however, separate running buffer and gel components were utilized, see Section 2.4.

<u>Resolving Gel</u>		<u>Stacking Gel</u>	
Acrylamide/bis-acrylamide (30/0.8%)	5.4 mL	Acrylamide/bis-acrylamide (30/0.8%)	1.4 mL
Buffer A (Section 2.4)	3.8 mL	Buffer B (Section 2.4)	0.6 mL
dH ₂ O	11.0 ml	dH ₂ O	6.0 ml
APS (NH ₄) ₂ S ₂ O ₈ (10% w/v)	100 μ L	APS (NH ₄) ₂ S ₂ O ₈ (10% w/v)	30 μ L
TEMED	10 μ L	TEMED	10 μ L

Once the separating gel had poured, ethanol was layered over the gel until it had set. This layer was then poured off, the stacking gel was poured and the comb inserted to create the protein wells. The gel was allowed to polymerise to completion. Non-denatured molecular weight standards were reconstituted as detailed in the relevant product information. Carbonic anhydrase, 29 kDa, chicken egg albumin, 45 kDa, and bovine serum albumin, 66 kDa, were used in all gels. Combined standard (15 μ L) was applied to each gel, while 20 μ L each of sample mixed with sample buffer were also applied. Samples and standards were loaded whilst the gels were submerged in running buffer. The gel box was then placed at 4 °C, to maintain enzymatic activity, and a constant voltage of 100 V was applied to the gel for 2 hours. The gel was then removed and washed exhaustively in cold distilled water. It was then submerged in TMB (Section 2.30) reagent overnight at 4 °C with gentle agitation. After overnight incubation the gel was rinsed with distilled water to remove any unbound reagent, placed onto a sheet of acetate, scanned and saved in a suitable electronic format.

2.28 Protein Determination using Bicinchoninic Acid Assay (BCA).

This assay was based on the method outlined by Smith and co-workers (1985), and was employed as described by the Pierce kit insert. Briefly, fresh bovine serum albumin (BSA) was diluted from the stock solution of 2 mg.mL⁻¹ using a suitable buffer, to prepare a standard curve in the range of 2000-20 µg.mL⁻¹. The working reagent (WR) of the assay was produced by a 1:50 dilution of kit solutions B to A. sample or control (25 µL) was pipetted into the appropriate microwell. To this, 250 µL of WR was added and the plate gently shaken for 30 s. The plate was then covered with tinfoil and statically incubated at 37 °C for 30 min. The plate was then allowed to cool to room temperature for 1 min and the absorbance was measured at 560 nm. Absorbance readings for unknown protein concentrations were determined from the standard curve previously produced.

2.29 Horseradish Peroxidase UV-Visible spectrum, Reinheitszahl Number and concentration determination.

Broad-scan spectra of native and recombinant HRP were run from 250-800 nm on a UV-VIS spectrophotometer using dedicated PC software (Unicam UV2, with Vision 1.3 software). Smoothing was set to medium. Quartz cuvettes were used throughout and the appropriate buffer was used as the blank. Where required the RZ (Reinheitszahl) value was determined by utilising the following formula:

$$RZ = \frac{A_{403}}{A_{280}}$$

The concentration of HRP could also be determined by measuring the absorbance at 403nm and applying the millimolar extinction coefficient of 100 mM⁻¹.cm⁻¹ (Hiner et al., 1995).

2.30 Quantitative HRP Activity Assay, (TMB).

3,3',5,5'-Tetramethylbenzidine dihydrochloride (TMB; Josephy et al., 1982) was used as the reducing substrate in the catalytic activity assay based on that of Ryan and co-workers (1994). In brief, 1 mg TMB was dissolved in 200 µL DMSO. This TMB solution was added to 9.8 mL of 100 mM citric acid buffer, pH 5.5, and mixed to homogeneity (final DMSO and TMB concentrations 2% v/v and 32 mM respectively). To this solution, immediately prior to assay, 3 µL of H₂O₂ (30% v/v) was added and

mixed to give a final concentration of 0.03% v/v (3mM) H₂O₂ in the reaction solution. Sample or blank (50 µL) was pipetted into an appropriate well of a microplate and 150 µL of reaction solution was added, mixed and allowed to react for 6.5 min. The absorbances of all samples were read at 620 nm.

2.30.1 Optimisation of TMB assay.

The optimum HRP concentration, H₂O₂ concentration and reaction time for the standard TMB reaction were determined using a checkerboard experimental design in a 96 well microplate. HRP concentration was varied horizontally on the plate, whilst simultaneously H₂O₂ concentration was varied vertically. All reactions were carried out in triplicate and the developing colour reaction was measured over time. The sample absorbances were plotted against time to determine the linearity of the reaction and the optimum reaction conditions.

2.31 Determination of free amino groups using the TNBS assay.

Free amino groups, such as those on lysine residues, were determined using the 2,4,6-trinitrobenzenesulphonic acid (TNBS) assay, (Fields, 1971). Briefly, the reaction was carried out in 0.1 M borate buffer at pH 9.5. A standard curve was produced by preparing a 10 mM solution of N- α -acetyl-L-Lysine in distilled water and diluting to create standards in the range 10 mM to 0.5 mM. To 100 µL of enzyme preparation or standard, 500 µL of borate buffer (0.1 M borate buffer in 0.1 M NaOH, pH 9.5) and 400 µL of ultra pure water were added. TNBS (20 µL) was added to the solution and mixed. The reaction tubes were covered in tinfoil and left in the dark for 5 min. The reaction was terminated by the addition of 2 mL of 1.5 M sodium sulphite in 0.1 M NaH₂PO₄. Absorbances were read at 420 nm and unknown samples were determined from the standard curve previously constructed.

2.32 Thermal profile of catalytic activity.

A thermal profile was used to determine the temperature range over which an enzyme begins to lose catalytic activity. In short, HRP solutions were exposed to different temperatures for 10 min, after which a 50 µL aliquot was removed to a microplate, stored on ice to prevent refolding, and assayed for remaining activity (TMB assay). Protein concentration was equalised in all experiments, to allow for the stabilising effect of protein-protein interactions. (Three waterbaths were utilised in the

experimental setup: as one was being utilised at a determined temperature, the other two were being ramped to the next required temperature). Initial temperature was 20 °C; the temperature was then increased in 10 °C increments over the range 20-40 °C and 5 °C increments over the range 40-80 °C. Calculations were carried out on the resulting catalytic data to obtain the T_{50} , the temperature at which 50% catalytic activity was noted. All experiments were carried out in triplicate, with the average value used in T_{50} calculations.

2.33 Thermal Inactivation Assay.

Once the thermal profile was completed, and the T_{50} calculated, a thermal inactivation assay was carried out at the T_{50} (50 °C). Similar to the thermal profile, 50 μ L aliquots were removed to a microplate on ice; however, in this procedure, time is varied whilst temperature remains constant. Aliquots were taken every minute for 10 min. The microplate containing the aliquots was then warmed to room temperature and assayed for catalytic activity (TMB assay). The optical densities obtained were expressed as percent residual activity (where time 0 represented 100% activity) and plotted versus time. All experiments were carried out in triplicate, with the average value used in $t_{1/2}$ calculations. From this graph the half life ($t_{1/2}$) can be calculated via data fitting utilising the *Enzfitter* programme (Biosoft, Cambridge, UK). Only results up to 10 min were utilised in modelling as deviations from the first-order model occurred at longer incubation times.

2.34 Organic Solvent Tolerance Assay.

This procedure was used to determine the % v/v organic solvent range over which an enzyme begins to lose catalytic activity. Recombinant HRP was prepared to a concentration of 100 μ g.mL⁻¹ in 50 mM phosphate buffer, pH 7.0. Reaction mixtures were set up with 10% increasing volumes of the solvent of interest in 50 mM phosphate buffer, pH 7.0, in the range 0% - 90% v/v solvent. HRP samples were exposed to the relevant solvent concentration for 2 hours at 25 °C in a temperature-controlled waterbath. After incubation, 50 μ L aliquots were withdrawn and remaining catalytic activity was assayed using standard TMB conditions (Section 2.30). The results were expressed as a percent residual activity with respect to the recombinant enzyme in aqueous solution. All experiments were carried out in triplicate, with the average value

used in C_{50} calculations. The C_{50} value is the % v/v of organic solvent that reduces catalytic activity to half the initial value in aqueous solution. The solvents used were dimethyl sulfoxide, methanol and dimethylformamide.

2.35 Tolerance of Excess H_2O_2 .

This procedure was used to determine the mM H_2O_2 concentration range over which an enzyme begins to lose catalytic activity. Recombinant HRP was prepared to a concentration of 360 nM in 50 mM phosphate buffer, pH 7.0. Reaction mixtures were set up with increasing concentrations of H_2O_2 in 50 mM phosphate buffer, pH 7.0, in the range 0–50 mM. H_2O_2 concentrations were determined spectrophotometrically at 240 nm using $43.6 \text{ M}^{-1}\text{cm}^{-1}$ as the extinction coefficient (Hernández-Ruiz et al., 2001). HRP samples were exposed to the relevant H_2O_2 concentration for 30 min at 25 °C in a temperature-controlled waterbath. After incubation, 50 μL aliquots were withdrawn and remaining catalytic activity was assayed using standard TMB conditions (Section 2.30). The results were expressed as percent residual activity with respect to recombinant HRP in aqueous solution. All experiments were carried out in triplicate, with the average value used in C_{50} concentrations. The C_{50} value is the mM H_2O_2 that reduces catalytic activity to half the initial value in aqueous solution.

2.36 Recombinant HRP Kinetic Analysis.

2,2'-azino-bis(3-ethyl-benzthiazoline-6-sulphonic acid) (ABTS) was utilised as substrate for steady state kinetic analysis. The present method was adapted from Childs and Bardsley (1975). A 20 mM stock solution of ABTS was prepared in 200 mM Na_2HPO_4 / 100 mM citric acid pH 4.5 buffer. A 100 mM H_2O_2 stock solution was also prepared separately in the same. For Michaelis-Menten kinetic analysis, a range of ABTS from 1.0 mM to 0.05 mM was prepared in buffer by serial dilution of the ABTS stock. Recombinant HRP was prepared to 65 pM in 50 mM phosphate buffer, pH 7.0. This concentration of recombinant HRP yielded absorbance readings within the desired range of 0.1-0.9 at 405 nm. Into a microplate well, 2.5 μL of 100 mM H_2O_2 and 222.5 μL of the desired ABTS substrate dilution were aliquoted, followed by 25 μL of recombinant HRP to initiate the reaction. A blank of zero ABTS was included in all assays. The microplate was shaken as the initiating enzyme was added and the absorbance at 405 nm was recorded every minute for 20 min. The change in absorbance per minute ($\Delta A/\text{min}$) was calculated for each substrate calculation. The *Enzfitter*

programme fitted the data generated to a Michaelis-Menten equation and calculated apparent K'_m values. k_3 (Dunford 1999) was calculated by dividing the mol of ABTS product produced per unit time by the number of mol of rHRP present in the reaction mixture.

2.37 Immobilisation Methods

2.37.1 Cyanogen Bromide-Activated Matrix Immobilisation.

The base form of cyanogen bromide (CNBr) reacts readily with the –OH groups on agarose to form cyanate esters or imidocarbonates. These, in turn react with primary amines under mild conditions, resulting in the covalent coupling of proteins, to the solid phase. HRP (30 pM), plant and recombinant, was immobilised to Sigma CNBr activated Sepharose® 4B, as per manufacturer's instructions. Briefly, the HRP was resuspended in the *coupling buffer*, 0.1 M NaHCO₃ buffer containing 0.5 M NaCl, pH 8.5. The CNBr-activated Sepharose® 4B was washed and swollen in cold 1 mM HCl for at least 30 min. Several washes (>10 column volumes) were required to remove the lactose used for storage stabilisation. The resin was then washed with 10 column volumes of distilled water and, finally, with coupling buffer. Immediately, the resin was transferred to the solution containing HRP and mixed using an end-over-end rotator for at least 2 hours at room temperature. After coupling, any unbound protein was washed away using several washes of coupling buffer. Any unreacted groups were blocked with 0.2 M glycine, pH 8.0, for 2 hours at room temperature. Extensive washing with high (0.1 M NaHCO₃ buffer containing 0.5 M NaCl, pH8.5) and low (0.1 M acetate buffer, pH4) pH buffers removed any remaining glycine and consolidated the HRP-to-resin covalent bonds. The resin, with immobilised protein, could be stored at 4 °C or used immediately.

2.37.2 Pall UltraBind™ Affinity Membrane Immobilisation.

Pall UltraBind™ affinity membranes comprise a polyethersulfone membrane modified with aldehyde surface chemistry, allowing direct protein immobilisation via free amine groups. HRP (30 pM), plant and recombinant, was immobilised onto the activated membrane as outlined in the manufacturer's instructions. The protein was resuspended in 50 mM sodium phosphate buffer, pH 7.5, and directly spotted onto the activated membrane; the latter was allowed to air-dry completely at room temperature for 10 min. The remaining binding sites were then blocked with 1% non-fat dried skim milk

(Marvel) in 50 mM sodium phosphate buffer, pH 7.5, for 1 hour at room temperature. The membrane was again allowed to air-dry completely at room temperature for 10 min. Precipitating chromogens such as TMB and DAB (diaminobenzidine) were utilised to identify immobilised HRP. Membranes were imaged with a Hewlett Packard Scanjet 5590, connected to a Dell Optiplex Computer as follows:

Scanning Variable	Setting
Output Type	True Colour (24 bit)
Selection Area	W: 2.5, H: 1.75
Output Scale	100%
Output Resolution	2400 dpi
Sharpen Level	Extreme
Scan Form	Scanner Glass
Highlights	-100
Shadows	-100
Midtones	-100

2.38 Electrochemical Biosensing Devices.

2.38.1 Screen Printed Electrode.

Screen-printed electrodes (SPE) are small, mass-produced, single-use systems comprising a silver conducting track, a carbon working electrode and an insulation layer. For this study, screen print electrodes were produced in-house (Dr. Aoife Morrin, NCSR, DCU) utilising a semi-automated DEK 247 printing machine (Weymouth, UK). Polyester screens, of varying thickness, were utilised mounted at 45° to the blade stroke. All inks were cured in a conventional oven before to use. The electrode was subjected to an electrochemical pre-treatment by cycling it in 0.2 M H₂SO₄ to remove any impurities on the electrode surface before any electrochemical deposition. Prior to HRP immobilisation, aniline was polymerised onto the SPE surface. In brief, 186 µL of neat aniline, 7.8 mL 1M HCl and 2 mL of PVS (polyvinylsulphonate) was deoxygenated with nitrogen for 10min. Aniline was then polymerised from this solution onto the surface of the working electrode by cyclic voltammetry using a platinum mesh auxiliary and an Ag/AgCl reference electrode. The potential was cycled between -500 and +1100 mV at 100 mV s⁻¹ for the required number of scans, usually 20. All electrochemical protocols were performed on a CH1000 potentiostat with CHI1000 software. Once the aniline had been deposited, the electrode was transferred to a 2 mL

batch cell and the chamber flooded with 1mL phosphate buffered saline (PBS). Electrochemical batch cells were constructed according to Killard and co-workers (1999) and were composed of polycarbonate. The cells were designed specifically for SPE and incorporated internal Ag/AgCl pseudo-reference and platinum wire auxiliary electrodes. The PBS solution in the batch cell was degassed under nitrogen for 10min; afterwards, a layer of nitrogen was maintained over the reaction vessel and the buffer constantly stirred. The polymer surface was then reduced at -500 mV vs Ag/AgCl, with a sample interval of 500 ms over 300 s at a sensitivity of 1×10^{-4} A.V⁻¹. The protein to be immobilised was prepared in PBS also and, immediately upon completion of polymer reduction, the PBS buffer was removed from the cell and replaced with the protein solution, which was neither degassed nor stirred. Oxidation was performed at $+700$ mV vs Ag/AgCl for 1500 s. During the oxidation step, the protein becomes electrostatically attached to the polymer surface. Following oxidation, the protein solution was removed and stored at 4 °C for later use. The batch cell was then washed with PBS to remove any unbound HRP. PBS (1 mL) was then added to the batch cell and the reaction mixture stirred. An amperometric i-t curve was monitored at -100 mV vs Ag/AgCl, with a sample interval of 500 ms over 4000 s at a sensitivity of 1×10^{-4} A.V⁻¹. Once a stable baseline of 0 μ A was achieved, successive additions of 20 mM H₂O₂ (final concentration) were carried out, with the resulting increase in μ A recorded as part of the CHI1000 software. Data points generated were exported and converted to ExcelTM.

2.38.2 Microelectrode Fabrication and Preparation.

Microelectrodes are electrodes with critical dimensions in the micron range. The reduced response time of microelectrodes compared with conventional-sized macroelectrodes (millimetre dimensions) enables electrochemical experiments to be carried out over extremely short timescales (Andriex et al., 1998). For this study, the microelectrode was produced in-house (Dr. Jennifer Brennan, NCSR, DCU) utilising soft glass as the external electrode support. A 0.25 μ m diameter platinum wire was chosen as the conducting material. Platinum is electrochemically inert and compatible with biological buffers. In brief, the microelectrode was fabricated by initial partial closure of a glass tube with heat from a Bunsen burner. The tube was rotated to aid symmetrical closing. A tin-annealed copper wire was used as the starting wire; to this, a hook-up wire was attached by spot soldering. The hook-up wire was kinked to prevent

fracture during electrode polishing. The platinum wire (0.25 μm diameter) was wrapped around the hook-up wire and also carefully spot soldered to ensure correct electrical signal transfer. The platinum wire was then passed through the partially closed glass tube, and the tube completely sealed by rotation in a Bunsen flame. A plastic cap was then glued to the top of the electrode assembly using an epoxy adhesive, both stabilising the hook-up wire and preventing contamination of the electrode interior. To confirm electrical signal transfer throughout the fabricated microelectrode, a cyclic voltamogram (CV) was carried out in MOPS (50 mM, pH 7.5) buffer. The microelectrode tip was then polished to generate a smooth surface, permitting electrochemical analysis of electrode surface area. Initially, the tip was polished with very fine sandpaper to remove any remaining protruding platinum wire. This was followed by sequential polishing with decreasing sizes of silica (0.5-0.3 μm) on moistened emery polishing paper (ten min at each silica size) with the electrode maintained at 90° to the silica. The electrode was rotated in a "figure-of-eight" motion to achieve equal polishing over its entire area. The electrode was rinsed with distilled water after each polishing and sonicated (240 W) for 5 min in Milli-Q water to remove any remaining debris.

Once the electrode was suitably polished, it was placed in a solution of 1.0 M H_2SO_4 , in order to calculate the actual available surface area of the platinum wire. The potential was cycled between limits chosen initially to oxidise and then reduce the surface of the electrode. The area under the reduction peak of the oxide curve can be converted to the actual available surface area by utilising the following equation:

$$A = \frac{A_p}{420 \times 10^{-6} \text{ C.cm}^2} \quad \text{Equation I}$$

Where A = real area of the electrode, A_p = area under the peak and the divisor is the charge in coulombs of the reactive species. The geometric area of the platinum wire, assuming that a perfect disc is formed during smoothing, can be calculated as follows:

$$A = \pi.r^2 \quad \text{Equation II}$$

The ratio of real area, as calculated by equation I, to geometric area, as calculated by equation II, gives an indication of the roughness of the electrode's surface. A roughness ratio between 1.0 and 3.0 is desirable. Continued electrode polishing is required if the roughness ratio falls outside these limits.

The working electrode can also be electrochemically cleaned by cycling in 1.0 M H_2SO_4 between potential limits chosen first to oxidize and then to reduce the surface of

the platinum electrode. A characteristic curve is achieved, which demonstrates the oxidation and reduction peaks of platinum, and also the evolution and adsorption of hydrogen ions at the surface of the electrode. The typical conditions utilised to clean the electrode surface are outlined as follows:

Init E (V):	0.0
High E (V):	1.35
Low E (V):	-0.2
Initial Scan Polarity:	Positive
Scan Rate (V/s):	0.2
Sweep Segments:	10
Sample Interval (V):	0.001
Quiet Time (s):	2
Sensitivity (A/v):	1×10^{-8}

2.38.3 Electrochemical Cell preparation and Electrochemical Analysis.

Voltammetry can be defined as the measurement of the current flowing through the electrode as a function of the applied potential, with the resulting graph referred to as a voltammogram. Amperometry is the measurement of current production when a potential is applied between two electrodes, with the resulting graph referred to as an amperometric *i-t* curve. Both cyclic voltammetry and amperometry were performed using CH Instruments Model 660a Electrochemical workstation and a conventional three-electrode cell. This comprises a working electrode (WE; HRP and Pt wire), a reference electrode (RE) and an auxiliary electrode (AE, Pt flag). The reference electrode was a Bioanalytical Systems (West Lafayette, USA) Ag/AgCl reference electrode, MF2052. A PTFE cap, containing electrode-holding positions, was placed over the glass cell. All solutions were deoxygenated thoroughly by sparging with argon or nitrogen for at least 15 min prior to experimentation; a blanket of argon/nitrogen was maintained over the solution during all experiments. The system potential was maintained by the potentiostat and is quoted with respect to Ag/AgCl reference electrode. All experiments were performed at room temperature (22 ± 3 °C). Before electrochemical measurements were made, the electrodes were rinsed with Milli-Q water and the electrolyte (50 mM MOPS, pH 7.5) to remove unbound material. Subsequent measurements were performed in blank electrolyte.

For cyclic voltammetry the CHI 660a software was set up as follows:

Init E (V):	0.1
High E (V):	0.9
Low E (V):	0.1
Initial Scan Polarity:	Positive
Scan Rate (V/s):	0.2
Sweep Segments:	6
Sample Interval (V):	0.001
Quiet Time (s):	2
Sensitivity (A/V):	1×10^{-8}

For amperometry the CHI 660a software was set up as follows:

Init E (V):	0.1
Sample Interval (s):	0.001
Run Time (s):	1500
Quiet Time (s):	2
Scales During Run:	1
Sensitivity (A/V):	1×10^{-9}

2.38.4 Platinum microelectrode etching.

Aqua regia [a fresh mixture of concentrated nitric acid (specific gravity: 1.42, purity: 70%) and concentrated hydrochloric acid (specific gravity: 1.18, purity: 37%) in a 1:3 ratio] was utilised to etch the platinum electrode to form a cavity between the glass sides and the recessed platinum wire at the tip of the electrode. Aqua regia dissolves platinum, even though neither constituent acid will do so alone. In combination, each acid performs a different task. Nitric acid is a powerful oxidizer, which will dissolve a tiny (virtually undetectable) amount of platinum, forming platinum ions (Pt^{4+}). The hydrochloric acid provides a ready supply of chloride ions (Cl^-), which react with the platinum to produce chloroplatinate ions, also in solution. The reaction with hydrochloric acid is an equilibrium reaction which favors formation of chloroplatinate ions (PtCl_6^{2-}). This results in removal of platinum ions from solution and allows further oxidation of platinum to take place; thus, the platinum is dissolved. (Saito et al., 1995). The tip of the 25 μm diameter platinum electrode was immersed in aqua regia, maintained at 75 °C, and the reaction mixture stirred continuously; etching was allowed to continue for 3 hours. The extent of etching was analysed by SEM image analysis (Section 2.38.5). Upon sufficient etching, the microelectrode was tested for an electrical signal (Section 2.38.3). To determine whether direct electrochemistry was possible, BSA, recombinant wildtype and plant HRP were immobilised in the etched cavity and the electrochemical signals obtained for each protein were compared.

2.38.5 Scanning Electron Microscopy.

Scanning Electron Microscopy (SEM) was performed to ensure correct cavity formation following electrode etching, utilising a Hitachi S 3000N scanning electron microscope. The microelectrode was removed from its storage container and sonicated in dH_2O for 5 min to remove any debris that had collected in the cavity during storage.

The microelectrode was dried under nitrogen gas and mounted onto the SEM stage, held in place by custom SEM contact gel. The stage was retracted into the SEM chamber and the vacuum was applied. Once the vacuum was established, the filament was saturated and the electron gun aligned. Acceleration voltage was set at 20 kV, the working distance was typically 5-8 mm and the spot size was set to 3. The images were obtained from the secondary electron detector. To obtain images of the etched platinum wire, the stage was tilted to an angle between 35 and 45°. The images were downloaded from the Hitachi S 3000N software to the PC and analysed.

2.38.6 Protein immobilisation onto etched platinum microelectrode.

After successful etching and image confirmation, the electrode was sonicated for 5 min and dried under nitrogen. A small hole was introduced into the top of a centrifuge microtube and the etched electrode was placed in a vertical position in this hole. Protein solution (2 nM each of BSA, recombinant wildtype or plant HRP) was introduced to the microtube and allowed to immobilise, via adsorption, overnight at 4 °C. The electrode and protein solution were inverted a number of times to remove from the cavity any air pockets that would hinder protein immobilisation. Once immobilised, amperometry was carried out on the protein (Section 2.38.3) to determine the direct electrochemical properties of the protein.

Chapter Three.

Cloning, Expression and Purification.

3.0 Introduction.

This chapter describes cloning of the HRP gene into a modified pQE60 vector (Qiagen, Figure 3.1), and subsequent development of a recombinant expression system, capable of producing catalytically active recombinant HRP, which could be isolated to a high purity. The QIAGEN pQE-based vectors contain an optimised promoter-operator region, consisting of a strong phage T5 promoter that is recognised by the naturally occurring *E. coli* RNA polymerase. Also contained within the promoter-operator region are two *lac* operator sequences, which bind the *lac* repressor and ensure efficient repression of the powerful T5 promoter. This study utilised *E. coli*, XL10 Gold (Stratagene) which harbours the *lacI^q* mutation and, as such, the strain produces enough *lac* repressor to naturally block transcription.

After cloning, the HRP gene was coupled to a PelB leader sequence, which would promote translocation of the resulting polypeptide to the periplasm of the *E. coli* cell, and a poly histidine tag, that would allow for simple one-step purification via nickel affinity chromatography. A schematic of the cloning process is outlined in Figure 3.2. Recombinant expression studies were carried out in a number of *E. coli* strains. Growth conditions were optimised for maximal production of active HRP; this would also serve other purposes, such as HRP mutant characterisation (Chapters 4, 5 and 6). Purified wildtype recombinant HRP was characterised in terms of thermal, solvent and H₂O₂ stabilities, along with ABTS steady-state kinetics.

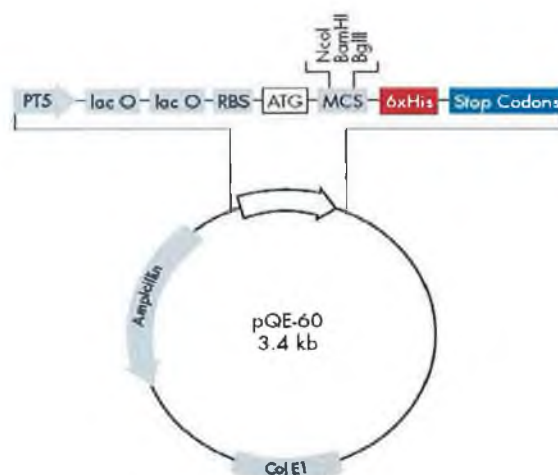


Figure 3.1: Schematic diagram of the pQE60 vector, showing T5 promoter, *lac* operator, synthetic Ribosomal Binding Site (and Shine-Delgarno within), Start codon (ATG), Multiple Cloning Site, Poly His Tag and Stop codons. The ampicillin gene and ColE1 origin of replication are also noted on the vector. The β -lactamase gene confers resistance to the antibiotic ampicillin and, hence, only plasmid containing this gene can be easily selected for. The ColE1 origin of replication also permits this high copy number plasmid to replicate during cell division.

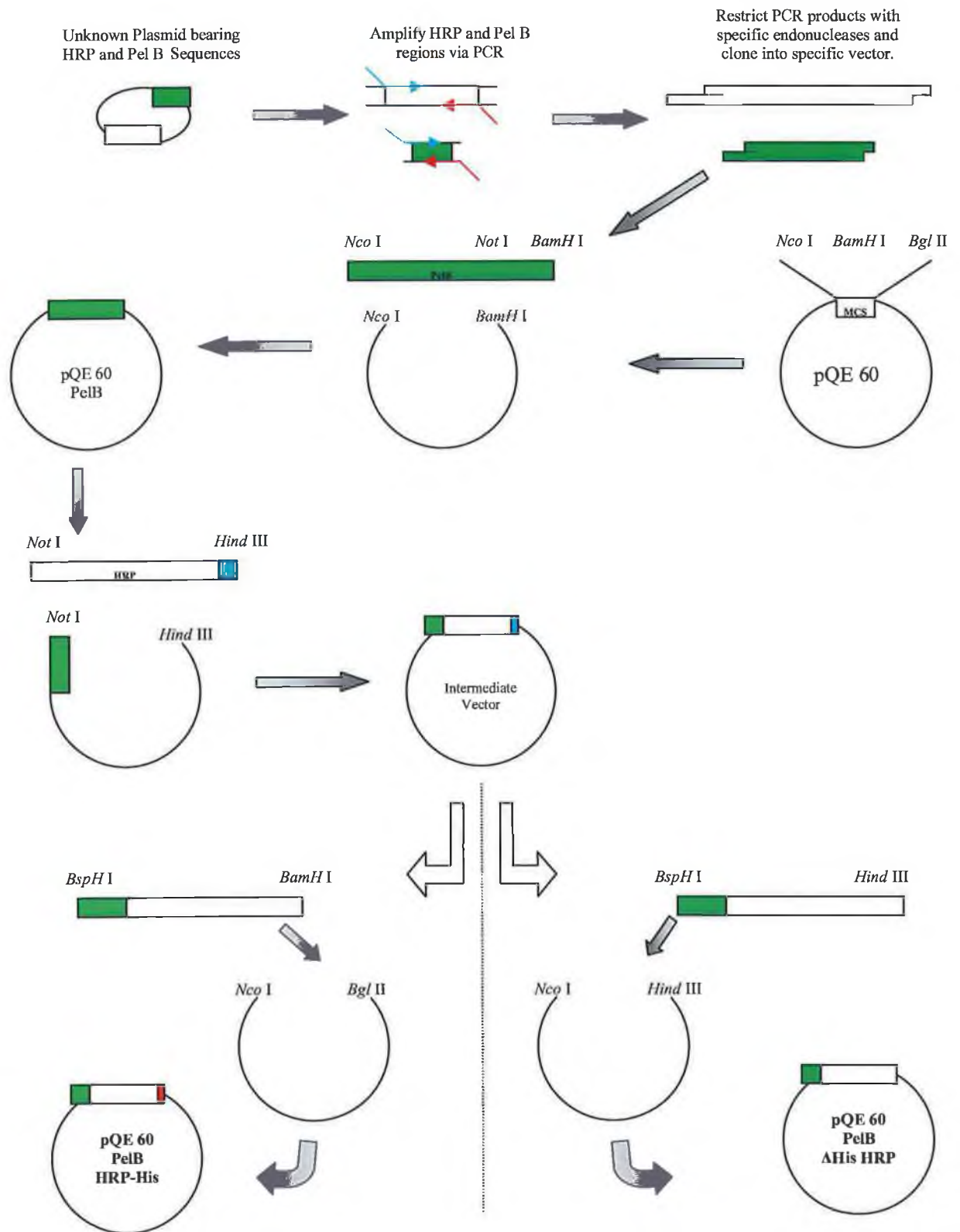


Figure 3.2: Cloning overview of the PelB leader (■) and HRP gene (□). The HRP and PelB sequences were primarily amplified from the unknown donated vector (F. Arnold, Caltech) via PCR. The PCR products were then restricted with the specific endonucleases to allow for directional cloning into the intermediate vector. The primers contained the recognition sequences for the endonucleases. The deleted His Tag (■) intermediate vector (See section 3.6) was used as the template for cloning into the pQE60 vector to form pQE60_PelB_HRP_His (■ denotes correct His Tag incorporation) and pQE60_PelB_HRP Δ His, depending on the restriction sites utilised for directional cloning.

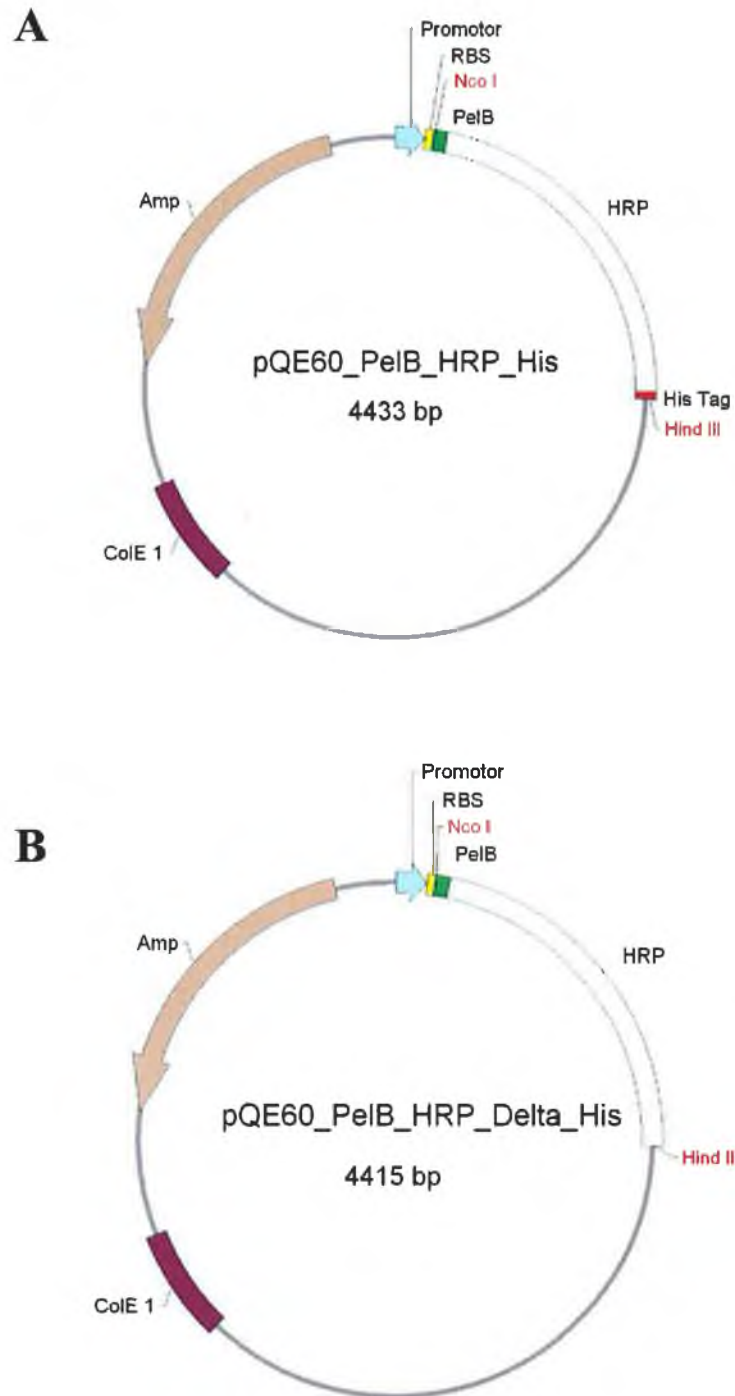


Figure 3.3: Part (A): Schematic representation of pQE60_PelB_HRP_His. The pQE60 vector contains the PelB leader and HRP gene flanked by the initiation codon at the 5' end and the poly His purification tag and stop codon at the 3' end of the multiple cloning site. Part (B): Schematic representation of pQE60_PelB_HRP Δ His. The pQE60 vector contains the PelB leader and HRP gene flanked by the initiation codon at the 5' end and the stop codon at the 3' end of the multiple cloning site. Image generated using Redasoft Visual Cloning 3.2 (www.rebase.neb.com)

3.1 Cloning of HRP gene sequences into an *E. coli* expression vector.

Periplasmic localization of the HRP enzyme is fundamental however, as it is in this region that the cysteine bonds (four in HRP) are formed and correct protein folding is initiated. Thus, the PelB sequence, which aids in protein translocation, was cloned 5' to the HRP gene. Due to the limited nature of the restriction sites, careful consideration of the MCS on the pQE60 vector was required, and cloning of the Pel B leader allowed for the introduction of several unique restriction sites into the pQE60 vector. The HRP sequences and the Pel B leader sequences cloned are identical to those found in the literature (Smith et al., 1990; Welinder, 1979; Lei et al., 1987 and Novagen, 2003).

3.2 Amplification of PelB Leader and HRP gene sequences by PCR.

The presence of the PelB leader and HRP gene on the unknown plasmid donated by Prof F. Arnold (Caltech, USA) was confirmed via di-deoxy sequencing. Primers were designed to amplify these sequences separately. Also located on these primers were the recognition sequences for the endonucleases required for the directional cloning of the sequences into the pQE60 expression vector. A standard PCR methodology was carried out as outlined in Section 2.6. The PCR products and basic cloning strategy are outlined diagrammatically in Figures 3.4 and 3.5 on the following page.

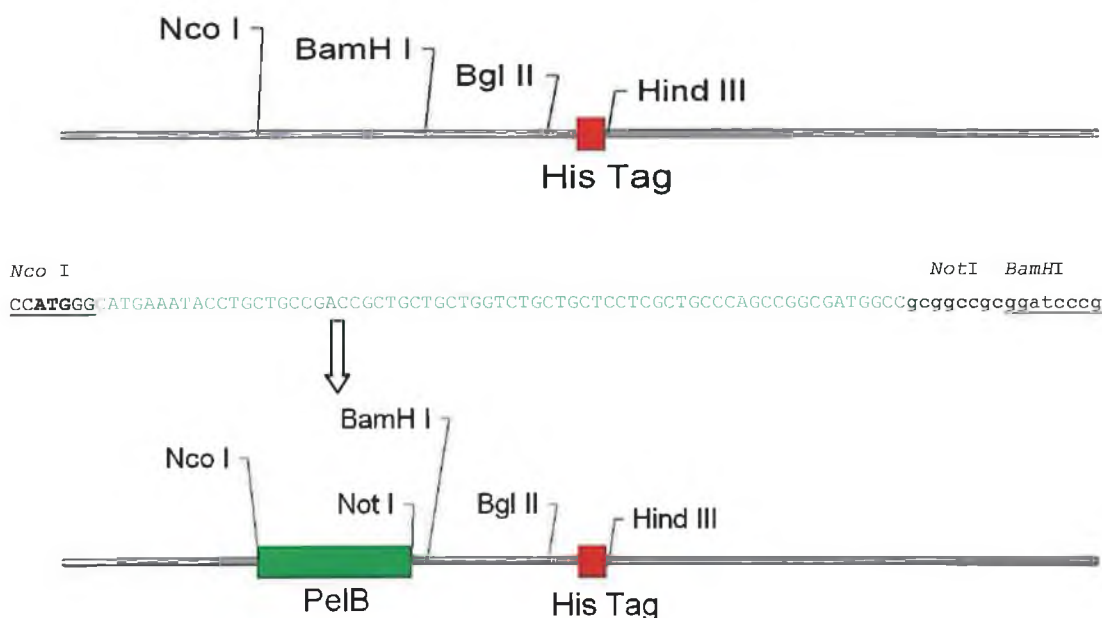


Figure 3.4: Initial amplification of the PelB leader sequence and its inclusion in the pQE60 vector to produce the pQE_60_PelB vector. The region surrounding the MCS in pQE60 vector is outlined first; it has a MCS containing *Nco* I, *Bam*H I and *Bgl* II. The PelB leader sequence was directionally cloned into the MCS utilising the *Nco* I / *Bam*H I cut vector / insert (bottom diagram). Image generated using Redasoft Visual Cloning 3.2 (www.rebase.neb.com).

*Not*I

```
ATGCAGTTAACCCCTACATTCTACGACAATAGCTGTCCCAACGTGTCCAACATCGTTCGCGACACAATCGTCAACGAGCTCAGATCCGATC  
CCAGGATCCCTGCTTCAATATTACGCTTGCACCTCCATGACTGCTTCGTGAATGGTTGCGACGCTAGCATATTACTGGACAACACCACCAGTTTCCGCAC  
TGAAAAGGATGCATTTCGGGAACGCTAACAGCGCCAGGGGCTTCCAGTGATCGATCGCATGAAGGCTGCCGTTGAGTCAGCATGCCACGAAACAGTCAGT  
TGTGACAGCTGCTGACTATAGCTGCGCAACAGAGCGTGACTCTTGCAGGGCGGACCGTCTGGAGAGTGCCGCTCGGTGACGCTGACTCCCTACAGGCAT  
TCCTAGATCTGGCCAACGCCAACTTGCTGCTCCATTCTTCAACCTGCCCCAGCTGAAGGATAGCTTTAGAAAACGTGGGTCTGAATCGCTCGAGTGACCT  
TGTGGCTCTGTCGGGAGGACACACATTTGAAAGAACCAGTGATAGTTTCATCATGGATAGGCTCTACAATTTGAGCAACACTGGGTACCTGACCCACG  
CTGAACACTACGTATCTCCAGACACTGAGAGGCTTGTGCCCACTGAATGGCAACCTCAGTGCACTAGTGGACTTTGATCTGCGGACCCCAACCATCTTCG  
ATAACAAGTACTATGTGAATCTAGAGGAGCAGAAAGGCTGATACAGAGTGATCAAGAAGTGTGTTAGCAGTCCAAACGCCACTGACACCATCCCACTGGT  
GAGAAGTTTTGCTAACTTACTCAAACCTTCTTTAACGCCTTCGTGGAAGCCATGGACCGTATGGGTAACATTACCCCTCTGACGGGTACCCAAGGCCAG  
ATTCGTCTGAAGTGCAGAGTGGTCAACAGCAACTCTCATCACCATCACCATCACAAGCTTGG
```

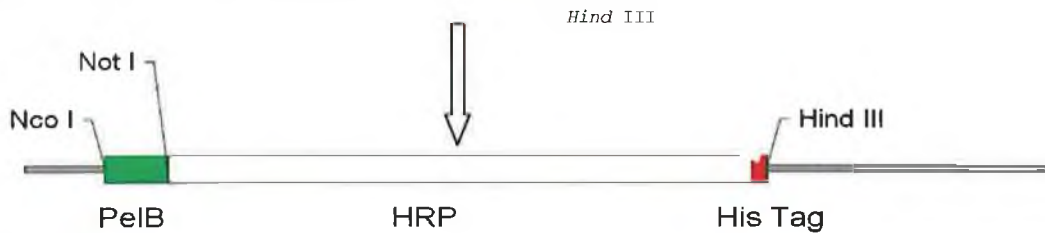


Figure 3.5: Secondary amplification of the HRP gene and its insertion into the pQE 60_PelB vector. The reverse primer of the PelB leader contained a *Not* I site 5' to the *Bam*H I site; this introduced a new unique restriction site which allowed the cloning of the HRP gene between the *Not* I and *Hind* III sites. Introduction of the poly Histidine sequence 5' to the *Hind* III site was accomplished by inclusion of that sequence on the HRP reverse primer. Image generated using Redasoft Visual Cloning 3.2 (www.rebase.neb.com).

3.3 Cloning of Pel B Leader Sequence.

The PCR products generated from Section 3.2 were digested with specific restriction endonucleases to allow for directional cloning into the pQE60 vector. PelB was restricted with *Nco* I and *Bam*H I, whilst HRP was restricted with *Not* I and *Hind* III. Restrictions were carried out as per Section 2.9. The cleaved products were gel purified as per Section 2.10 and the restricted and gel purified vector was ligated with the insert as per Section 2.14.

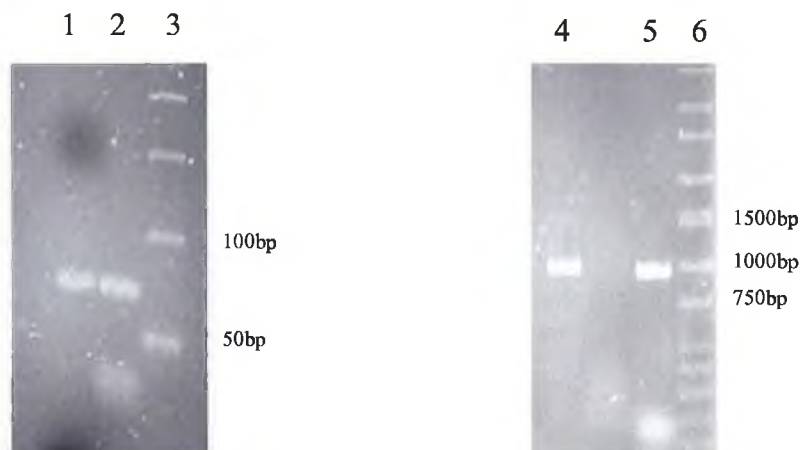


Figure 3.6: PCR products of PelB leader, cleaned and uncleaned, lanes 1 and 2. PCR products of HRP gene, cleaned and uncleaned, lanes 4 and 5. Sigma size markers are in lanes 3 and 6.

This cloning allowed for the introduction of extra unique restriction sites to the MCS to aid the cloning of the HRP gene. To confirm the correct insertion of the PelB leader, the unique, *Not* I, restriction site, introduced by PCR, was used in restriction analysis. If the sequence was correctly introduced, the vector would be linearised by *Not* I restriction. Digests were carried out as per Section 2.9 and visualised as per Section 2.10.

1 2 3 4 5



Figure 3.7: A 1% TAE gel depicting the differences in restriction of the pQE60 vector and the pQE60_PelB vector. Lane one shows the pQE60_PelB vector cut with *Not* I, lane two shows the pQE60_PelB vector undigested. Lane four shows pQE60 digested with *Not* I, and lane five shows pQE60 undigested. As can be clearly seen, the pQE60_PelB vector is linearised by the *Not* I restriction and the pQE60 vector is not. Lane three contains Sigma size marker.

3.4 Cloning of HRP gene.

Due to the nature of the MCS in pQE60 and the presence of all of the pQE60 MCS restriction sites in the HRP gene, judicious introduction of unique restriction sites was required. Primary cloning of the PelB leader allowed for the introduction of the *Not* I restriction site 5' to the *Hind* III site already present in the pQE60 vector. These two unique restriction sites were utilised in cloning the HRP gene. As the *Hind* III site is 3' to the polyHistidine tag in the pQE60 vector, the sequence for the Histidine tag needed to be inserted into the primer for the HRP PCR, as outlined diagrammatically in Section 3.2.

A unique restriction site was again used to screen possible clones. The *Pst* I recognition sequence is located only in the HRP gene and, hence, the pQE60_PelB_HRPHis vector will be linearised only if the HRP gene has been inserted. Restriction analysis was carried out as per Section 2.9 and results were visualised as per Section 2.10. Results are outlined in Figure 3.8.

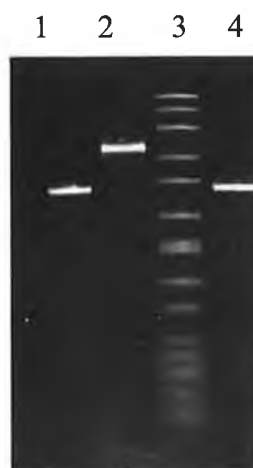


Figure 3.8: A 1% TAE gel depicting the differences in restriction of the pQE 60 vector and the pQE 60_PelHRP. Lane one shows the pQE 60_PelHRP undigested. Lane two shows the pQE 60_PelHRP cut with *Pst* I. Lane four shows pQE 60_PelB digested with *Pst* I. Lane Three is the Sigma molecular size marker

3.5 Sequencing of the cloned PelB and HRP vector construct.

A fresh plasmid preparation of the pQE60_PelB_HRPHis vector construct was sequenced by MWG-Biotech Ltd (Germany). The concentration of vector and sequencing primers utilised are outlined in Section 2.20. Results were obtained in linear nucleotide sequence, and several bioinformatic packages were utilised for data analysis. Due to its size, greater than one kilobase, the cloned construct was sequenced in both 5' to 3' and 3' to 5' directions; it was thus necessary to align both result sets to find the overlapping sequences in the middle of the read. This was done by (i) finding the reverse complement of the 3' to 5' read (www.bioinformatics.vg) and (ii) aligning this reversed sequence to the 5' to 3' read (www.prodes.toulouse.inra.fr). The overlapping sequences were reduced to a single sequence and, hence, a single linear 5' to 3' sequence was produced.

The single linear 5' to 3' sequence was then translated into amino acid code (www.expasy.org), the latter imported into ClustalW multiple alignment program (www.ebi.ac.uk) and the sequence aligned with published amino acid sequences for HRP (Smith et al., 1990 and Welinder, 1979). Aligned sequences were then imported into Genedoc (www.psc.edu), a program utilised for manipulating aligned sequences, and similarities compared.

```

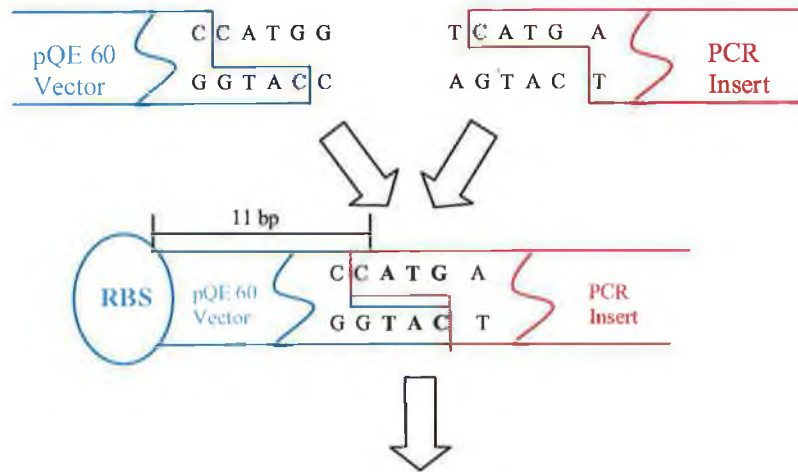
      *      20      *      40      *      60      *      80
PelB_HRP : MKYLLPTAAAGLLLLAAQPAMAAAAMQLTPTFYDNSCPNVSNIVRDTIVNELRSDPRI ASILRLHFHDCFVNGCDASILLDN :
HRP      : --MKYLLPTAAAGLLLLAAQPAMAAAAMQLTPTFYDNSCPNVSNIVRDTIVNELRSDPRI ASILRLHFHDCFVNGCDASILLDN :
      *      100     *      120     *      140     *      160     *
PelB_HRP : TTSFPEEKIAPFNANRARGFVVIDRMKAAVEASACRTVSDADLLTIAAQSVTLAGGPPSWRVPLGRRDSLQAFLLDLANANLEAPF :
HRP      : TTSFPEEKIAPFNANRARGFVVIDRMKAAVEASACRTVSDADLLTIAAQSVTLAGGPPSWRVPLGRRDSLQAFLLDLANANLEAPF :
      *      180     *      200     *      220     *      240     *
PelB_HRP : FTLPQLKDSFRNVGLNRSDDLVALSGGHTFGKNOCRFTMDRLYNESENTGLPDTINTTYLQTLRGLCLPLNGNLSALVDFDLRTPT :
HRP      : FTLPQLKDSFRNVGLNRSDDLVALSGGHTFGKNOCRFTMDRLYNESENTGLPDTINTTYLQTLRGLCLPLNGNLSALVDFDLRTPT :
      *      260     *      280     *      300     *      320     *      340
PelB_HRP : TFDNKYYVNLBEEQKGLIQSDQLFSSPNATDTPLVRSFANSTQTEFNAPVEAMDRMGNITPLTGTQQRINCRVNVNSNS : 3
HRP      : TFDNKYYVNLBEEQKGLIQSDQLFSSPNATDTPLVRSFANSTQTEFNAPVEAMDRMGNITPLTGTQQRINCRVNVNSNS : 3

```

Figure 3.9: Alignment of the pQE60_PelB_HRP cloned construct with the published literature for the Pel B leader (Lei, et al., 1987) and HRP (Welinder, 1979 and Smith et al., 1990). The bioinformatic package Genedoc was used to show the alignment of the sequences, with complete agreement indicated by a black colouration. As can be seen, complete similarity is noted for the entire clone construct with the exception of one mutation at position 34 on the HRP translated protein where an Alanine is replaced by a Proline. This mutation was already present in the gene on the donated plasmid and, hence, no mutations were introduced by the cloning strategy.

3.6 Out of frame cloning and His tag deletion.

Although sequencing of the pQE60_PelB_HRP confirmed that the PelB leader and HRP gene were fused in frame to each other, an extra methionine residue had been incorporated into the PelB forward primer. Thus, HRP expression was erratic due its gene being out of frame with the correct start codon. Sequencing also revealed that the poly His tag, encoded in the reverse primer, was not included in the final construct. To counteract these problems, the PelB-HRP gene fusion was subcloned from pQE60_PelB_HRP back into pQE60 via a *BspH I* / *BamH I* directional cloning strategy, resulting in use of the correct start codon and the encoding His Tag of the vector. A *BspH I* site was included on the forward amplification primer for the gene fusion, as it is an isoschizomer of *Nco I* and thus could be utilised in directional cloning of the product into an *Nco I*-cut pQE60. The correct ATG start codon is located within its recognition site and, hence, correct expression would be achieved. The reverse primer contained a *BamH I* recognition site, and so the gene fusion would be subcloned in frame with the His tag encoded by the pQE60 vector. The vector was cut with *Bgl II*, which allowed the mutually-compatible *BamH I* cut insert to be directionally cloned in-frame to the vector encoded His tag. This cloning mechanism also removed these two restriction sites and would allow future use of a designed *BamH I* site in mutant screening; see Section 4.4.



..ATTCATTAAAGAGGAGAAATTAACCATGAGCAAATACCTGCT..etc

Figure 3.10: Schematic of *NotI* vector digestion and *BspHI* insert digestion and in-frame ligation. Also outlined is the relationship (eleven basepairs) between the RBS (green lettering) and the primary initiation methionine start codon. The reading frame is underlined in the schematic.

The cloning was carried out as per pQE60_PelB_HRP, and similar restriction digest gels were produced as outlined in Figures 3.6, 3.7 and 3.8. The new construct, pQE60_PelB_HRP_His was sent for sequencing as previously outlined, this time the correct reading frame and inclusion of His tag are noted, as outlined in Figure 3.11:

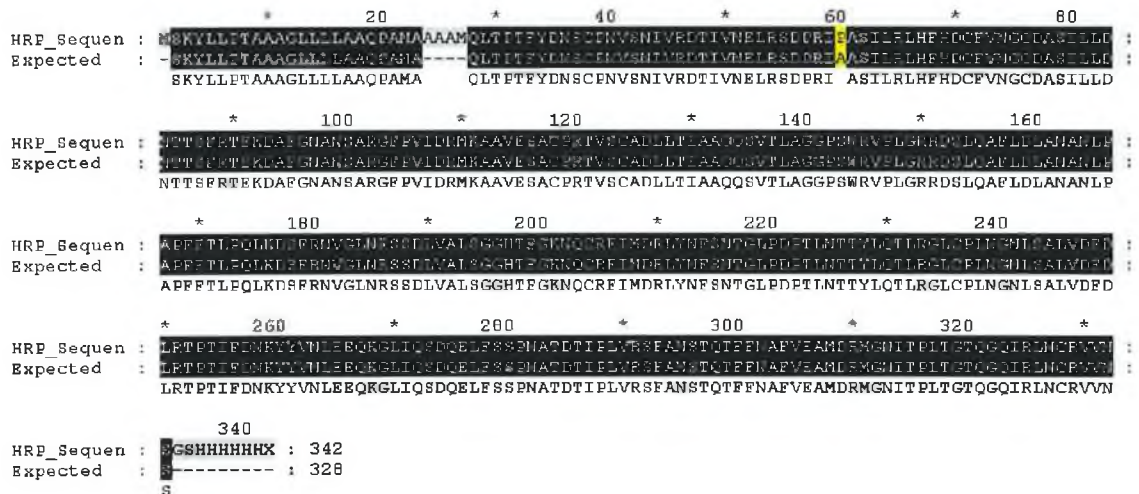


Figure 3.11: Sequencing results aligned against published sequences for PelB leader (Lei, et al., 1987) and HRP (Welinder, 1979 and Smith et al., 1990). Sequencing results are as expected, except for the site mutation at position 34 in the HRP amino acid sequence, as described previously. Positions 1-24 represent the PelB leader, positions 25-28 represent the alanine linker between the leader and the HRP gene, whilst positions 30-342 represent the HRP gene. A single mutation (Ala to Pro) is located at position 34 (position 60 in the numbering system used in this figure).

3.7 Expression of HRP gene in *E. coli*.

Prior to expression studies, the A34P mutation was reverted to wildtype by site-directed mutagenesis as described in Section 4.4. Once reverted expression of the HRP gene was optimised for host *E. coli* strain, induction method, and expression time as outlined in Sections 3.7.1, 3.7.2, and 3.7.3 respectively.

3.7.1 *E. coli* host strain optimisation.

Several commercial *E. coli* host strains, with different genotypes (Section 2.1.1), were examined for optimal expression of HRP under standard expression conditions.

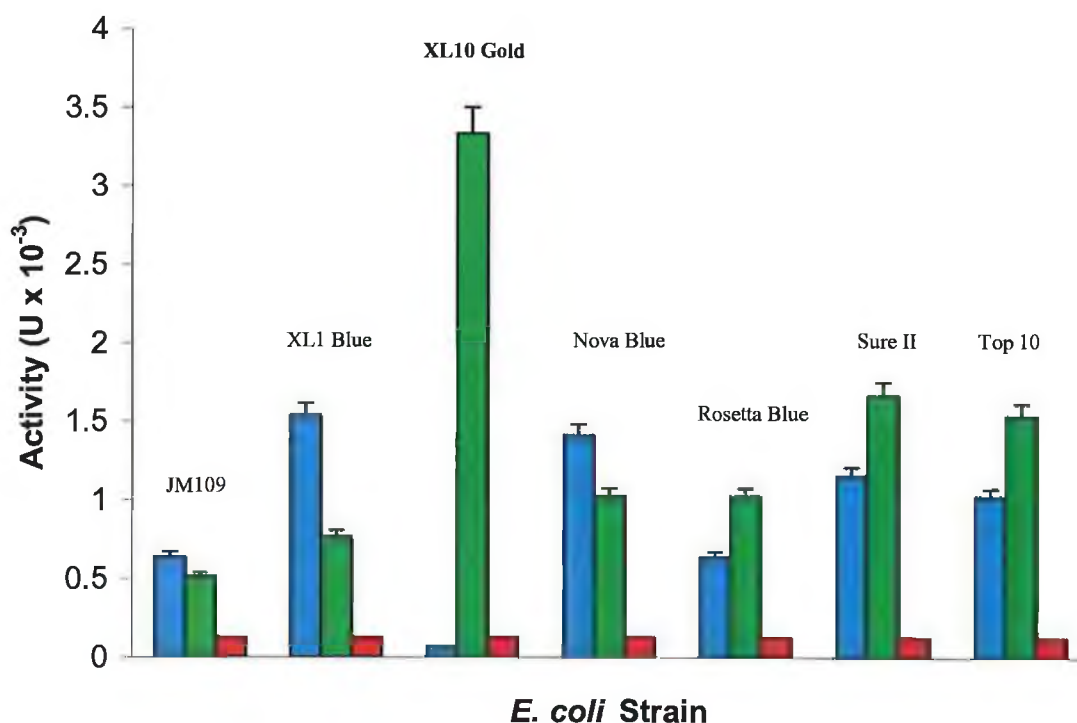


Figure 3.12: The optimal host strain for maximal HRP production was initially investigated: ■ glucose (2% w/v) repressed cells were used as a negative control, cells induced with ■ 50 μM IPTG or grown ■ non-induced overnight, 220 rpm at 30°C.

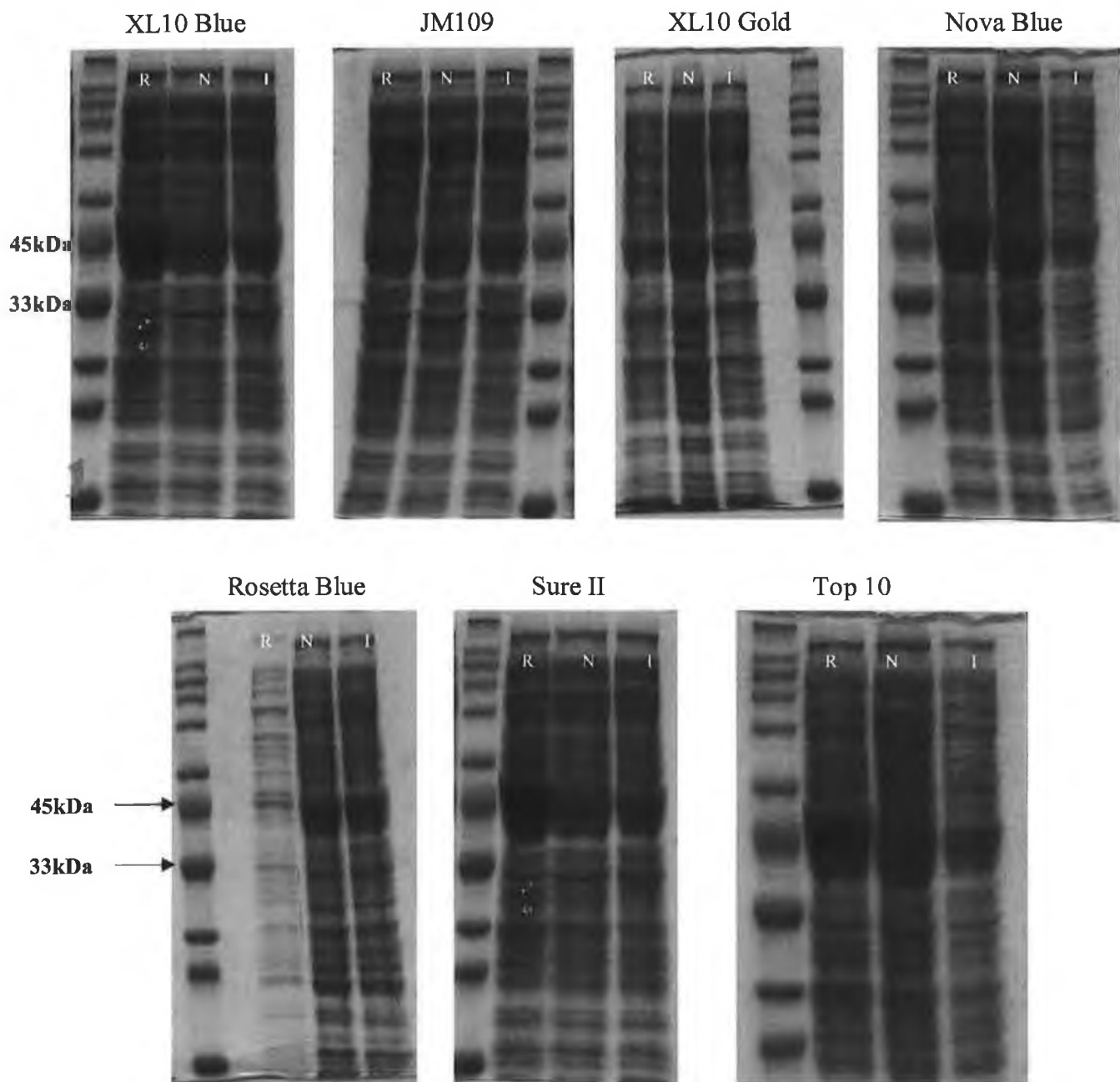


Figure 3.13: Investigation of the optimal host strain for maximal HRP production. (R), glucose (2% w/v) repressed cells were as a negative control; (N), non-induced or induced (I) with $50\mu\text{M}$ IPTG. Cells were grown overnight, 220 rpm, at 30°C . Cell contents were lysed by short sonication. No overexpressed protein bands are visible in any of the strains; however, the TMB activity assay suggests that XL10 Gold cells express functional recombinant protein, although at a low level.

3.7.2 Determination of optimal culture temperature.

The optimal culture temperature for maximal HRP production was also investigated. XL10 Gold cells were grown in the presence of glucose (2% w/v) as a negative control; cells were either induced with 50 μ M IPTG or grown non-induced at both 30°C and 37°C, for 18 hours at 220 rpm.

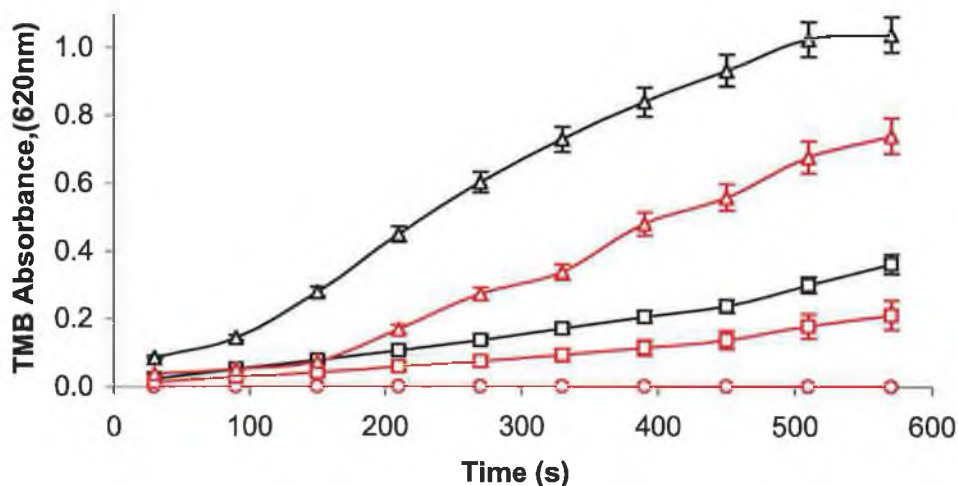


Figure 3.14: TMB assay of HRP catalytic activity for 10mL XL10 Gold lysate, at both 30°C and 37°C. – \circ – Wildtype repressed 30°C, – \circ – Wildtype repressed 37°C, – Δ – Wildtype noninduced 30°C, – Δ – Wildtype noninduced 37°C, – \square – Wildtype Induced 30°C, – \square – Wildtype Induced 37°C. The plots for repressed growth curves overlap exactly.

The optimal culture conditions for maximal HRP production were also investigated. XL10 Gold cells were grown in the presence of glucose (2% w/v) until an OD_{600nm} until expression was to commence, as outlined in Section 2.24.5.

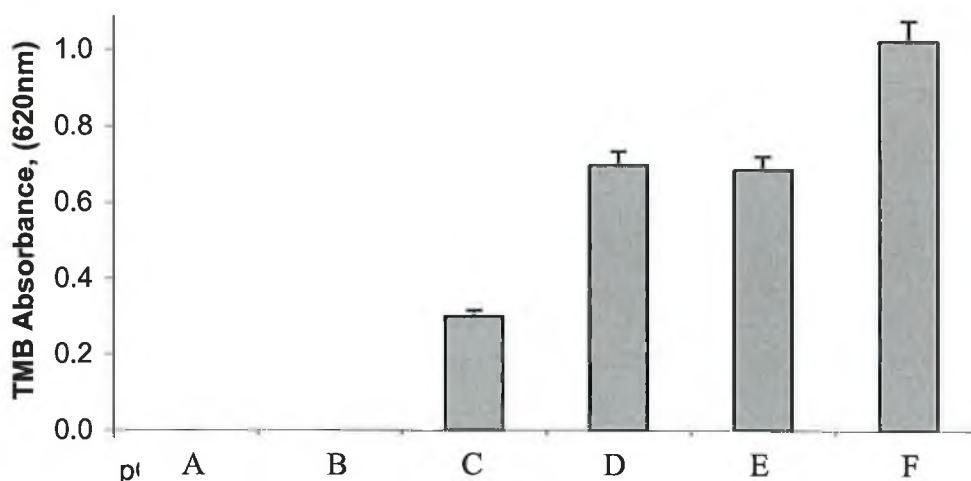


Figure 3.15: Investigation of optimal culture conditions. HRP expression was repressed by use of 2% w/v glucose. Cells were grown in the absence or presence of glucose until the correct OD_{600nm} for expression was reached. Once OD_{600nm} reached 0.5, the glucose was removed by exchange of culture media, and the cells were allowed to grow non-induced (F) or induced with 50 μ M IPTG (C) for 18 hours at 30°C, 220 rpm. The cells grown in the absence of glucose were also induced with 50 μ M IPTG (D) at this OD_{600nm} , or allowed to grow non-induced (E). Negative controls, namely empty pQE60 vector (A) and repressed pBR_I (B), are included.

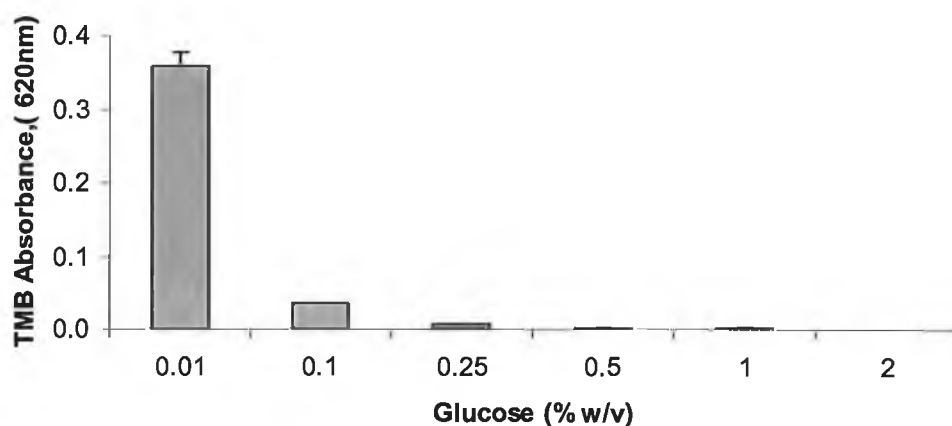


Figure 3.16: Plot of minimal glucose concentration (w/v) to allow cells to reach OD_{600nm} equal to 0.5, prior to production of HRP activity.

3.7.3 Investigation of HRP expression over time.

XL10 Gold cells containing pBR_I were grown in Superbroth medium, supplemented with 50/5 (Section 2.2.3), over an extended period to ascertain the optimal growth time for maximal HRP production.

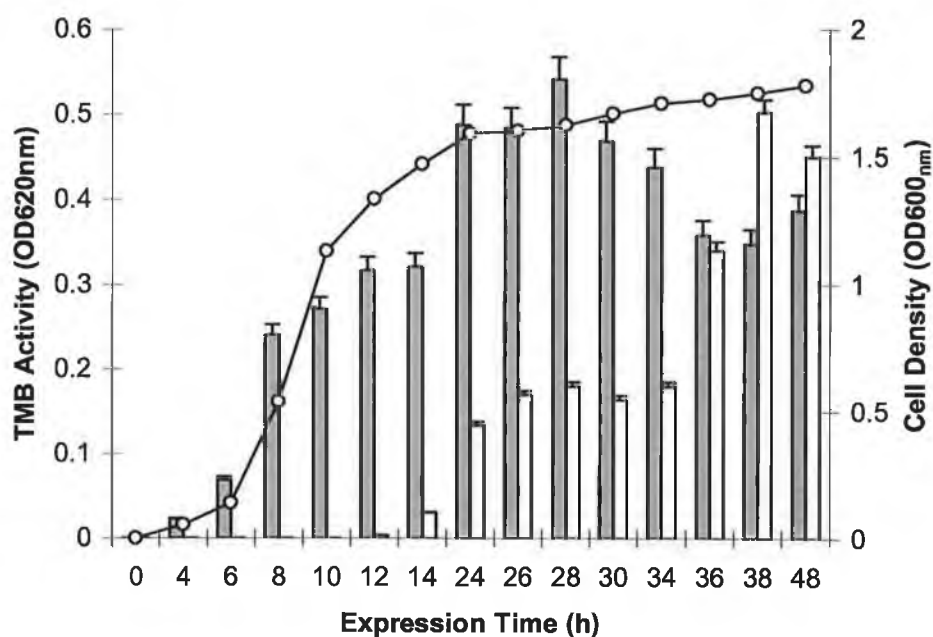


Figure 3.17: Plot of HRP activity versus *E. coli* growth (—○—) at 30°C, 220 rpm. Individual 10mL cultures were taken for each time point to minimise contamination due to extended culturing time. (■) Cell periplasmic fractions, (□) Cell supernatant fraction. Endogenous *E. coli* peroxidase activity has been subtracted from the values noted here.

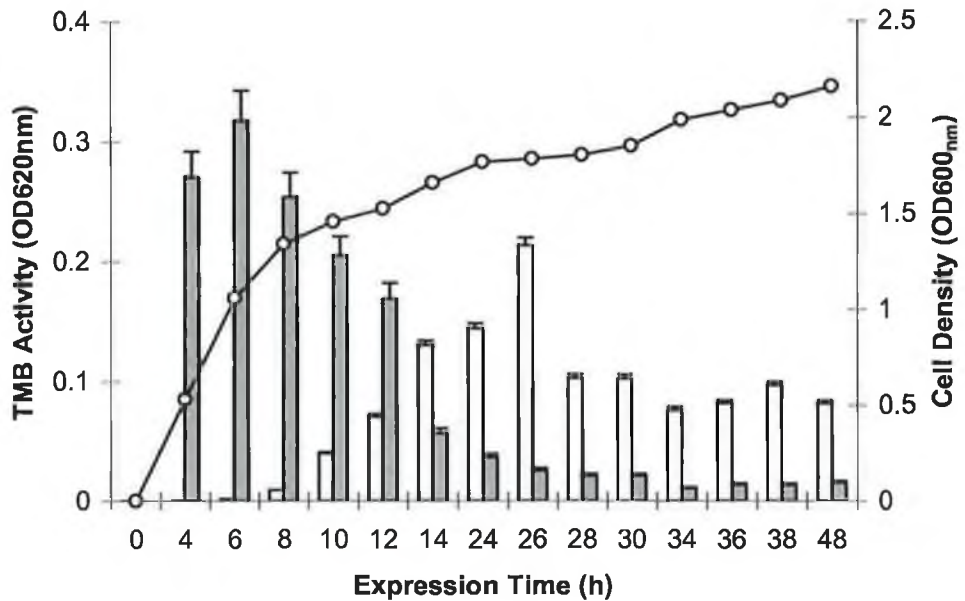


Figure 3.18: Plot of HRP activity versus *E. coli* growth (—○—) at 37°C, 220 rpm. Individual 10mL cultures were taken for each time point to minimise contamination due to extended culturing time. (■) Cell periplasmic fractions, (□) Cell supernatant fraction. Endogenous *E. coli* peroxidase activity has been subtracted from the values noted here.

3.8 Recombinant HRP Purification.

3.8.1 Recombinant HRP Nickel Affinity Purification.

Immobilized nitrilotriacetic acid nickel ion resin was used to purify the expressed recombinant HRP to a high degree.

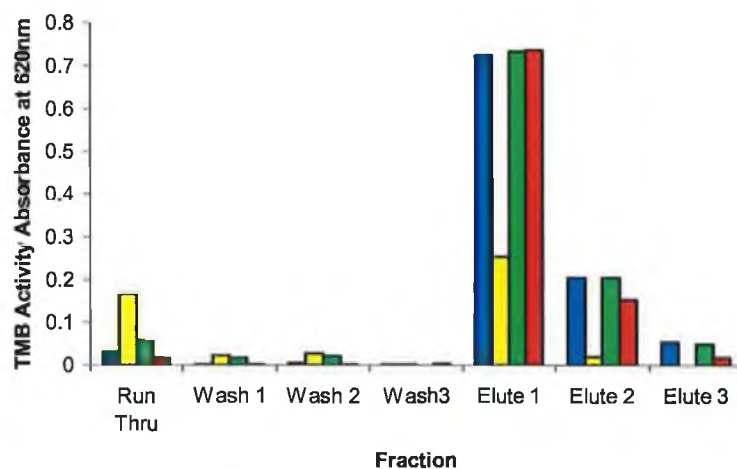


Figure 3.19: Purification of recombinant HRP via nickel affinity chromatography. Equal amounts of enzyme activity were loaded in each case. Various nickel resins were utilised to obtain the optimal purification conditions: Qiagen nickel resin, no salt ■; Sigma nickel resin, no salt ■; Qiagen nickel resin with 1M NaCl ■; Sigma nickel resin with 1M NaCl ■. Total activity for each fraction is noted on Y-axis.

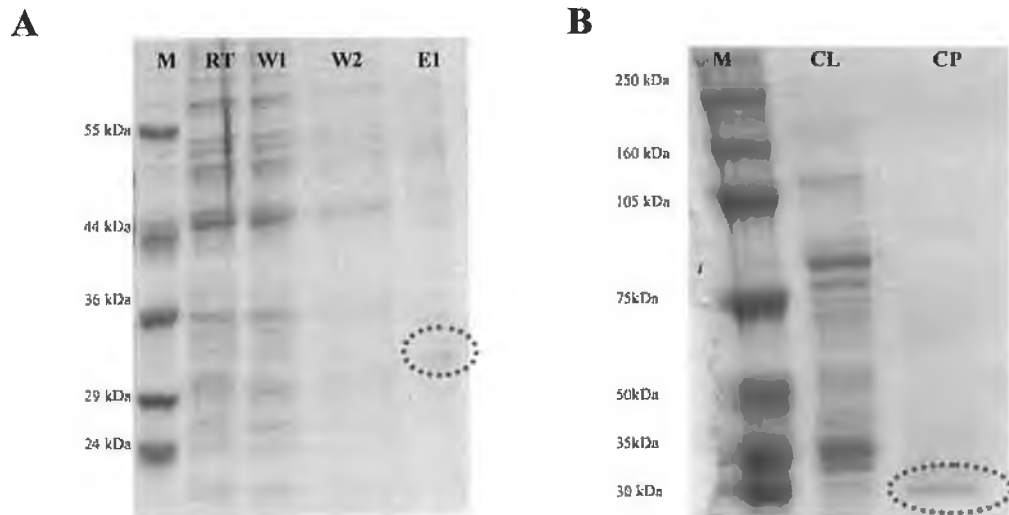


Figure 3.20: Part (A) shows a 12 % SDS PAGE of a typical rHRP purification (RT, Runthrough; W1, wash one; W2, was two; E1 elute one) with purified rHRP band highlighted. Part (B) compares the crude lysate from osmotically lysed cells (CL), XL 10 Gold containing pBR I osmotically shocked, periplasmic contents, to the purified and concentrated rHRP (CP). It should be noted that Sigma WideRangeTM standard markers (M) are utilised in Part (A), whilst Amersham Rainbow MarkersTM (M) are utilised in Part (B).

Initially, this method was difficult to reproduce (see Section 3.9.5 for reasoning), and so conventional purification techniques (hydrophobic interaction chromatography, size exclusion chromatography and anion exchange chromatography) were implemented.

3.8.2 Recombinant HRP Classical Purification.

From continual growth curves (see Section 3.7.3) HRP activity was noted in the bacterial cell culture supernatant, due to the fusion of the periplasmic localisation leader sequence (PelB) to the HRP gene. To minimise contaminating protein, rHRP was precipitated from the cell culture supernatant with 50% w/v ammonium sulphate after removal of cell biomass and conventional protein purification methods were applied to this fraction. The optimal ammonium sulphate concentration required to precipitate the protein was estimated (Figure 3.21) and the precipitated proteins were subjected to sequential hydrophobic interaction, size exclusion and anion exchange purification procedures. This conventional purification strategy was also implemented in the purification of non-His tagged recombinant HRP (Figures 3.22 to 3.24).

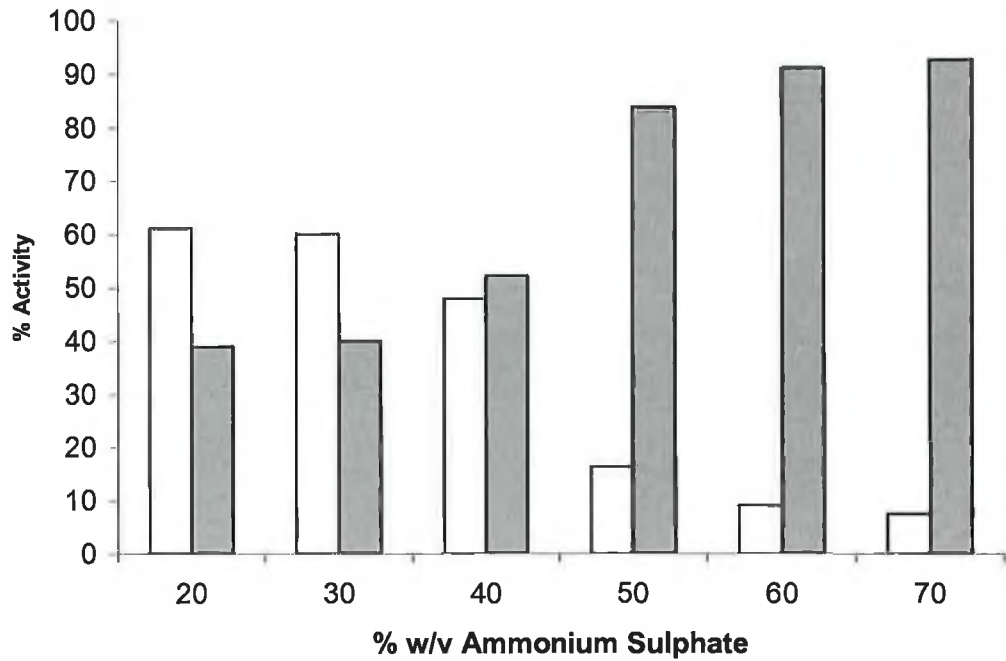


Figure 3.21: Effect of varying concentrations of ammonium sulphate on rHRP precipitation from the bacterial cell culture medium. The TMB assay was used to detect rHRP in the culture supernatant (□) or precipitated protein pellet (■). Approximately 50% ammonium sulphate precipitates rHRP.

Following its precipitation from the bacterial cell culture supernatant, rHRP was dialysed overnight against 50mM sodium phosphate buffer (pH 7.5) to remove the precipitating ammonium sulphate salt.

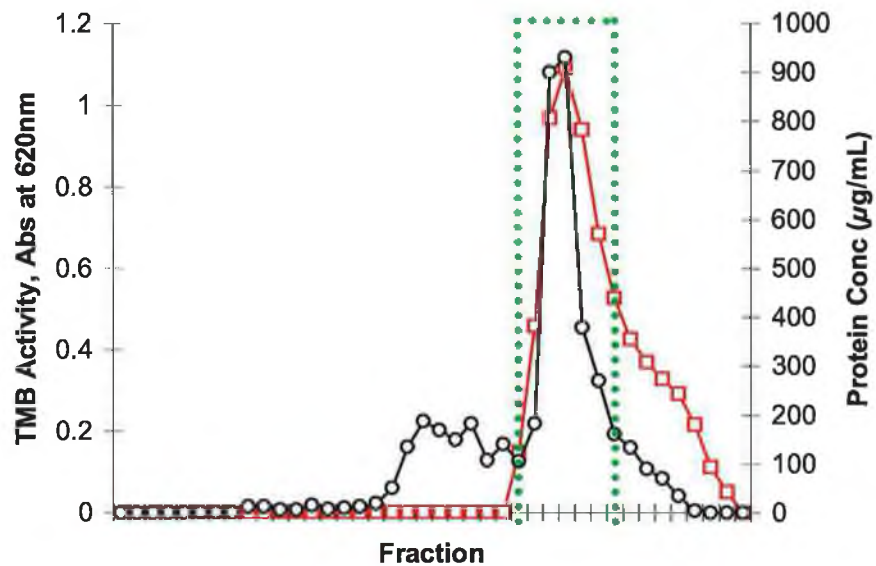


Figure 3.22: Typical plot of hydrophobic interaction purification of wildtype recombinant HRP. Fractions exhibiting the highest peroxidase activity (see boxed area on graph), as denoted by TMB assay (○), and protein concentration, denoted by BCA assay (□), were pooled, dialysed overnight and concentrated (PEG) prior to application onto size exclusion column.

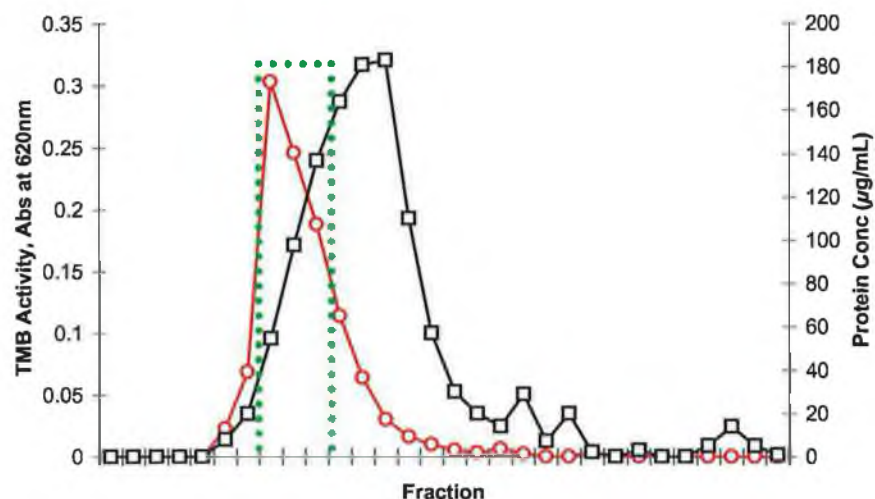


Figure 3.23: Typical plot of size exclusion purification of wildtype recombinant HRP. Fractions exhibiting the highest peroxidase activity (see boxed area on graph), as denoted by TMB assay (○), and protein concentration, denoted by BCA assay (□), were pooled, dialysed overnight and concentrated (PEG) prior to application onto DEAE Sepharose column.

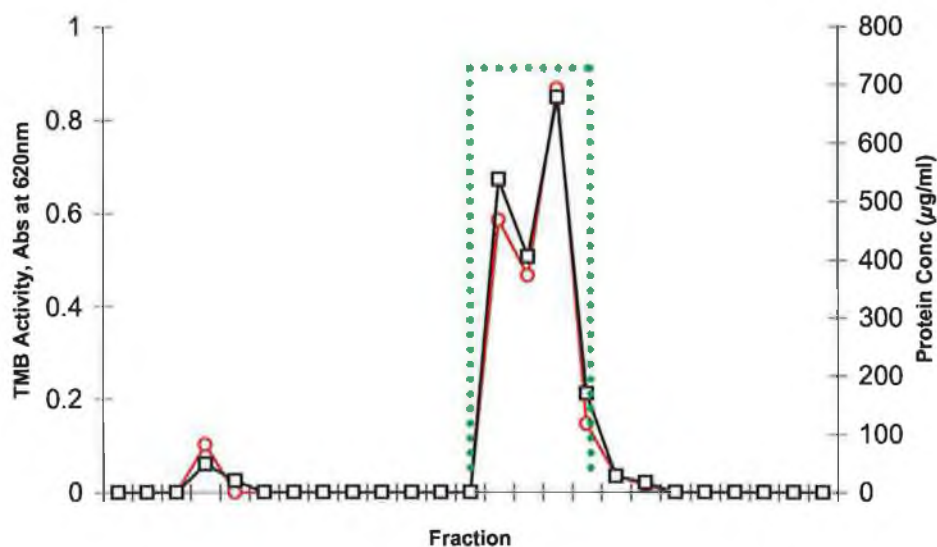


Figure 3.24: Typical plot of anion exchange purification of wildtype recombinant HRP. Fractions exhibiting the highest peroxidase activity (see boxed area on graph), as denoted by TMB assay (○), and protein concentration, denoted by BCA assay (□), were pooled, dialysed overnight and concentrated (PEG) prior to further characterisation.

3.8.3 Optimised Recombinant HRP Nickel Affinity Purification.

Studies of the conventionally purified rHRP (see Figure 3.33) suggested that the rHRP molecule formed dimers, which may have obscured the poly-His purification tag. Use of the combined osmotic/lysozyme treatment, with the inclusion of 200mM guanidine hydrochloride in the purification buffer, dramatically improved IMAC reproducibility and enhanced purification factors and yields (see Table 3.2).

Table 3.1: Typical purification table for lysed cell recombinant Δ His HRP (non-His tagged HRP), purified via conventional chromatography methods.

Purification Method	Fraction Vol (mL)	Protein Con ^c (mg.mL ⁻¹)	Total Protein (mg)	Activity (μ mol.min ⁻¹ .ml)	Total Activity (μ mol.min)	% Recovery	Specific Activity (μ mol.min.mg ⁻¹)	Purification Factor
Crude	15	3.486	52.27	1.02×10^{-2}	1.53×10^{-1}	100	2.9×10^{-3}	1.0
Post HIC	6.0	1.525	9.15	2.6×10^{-3}	1.56×10^{-2}	11	1.7×10^{-3}	.58
Post Cation	0.6	4.805	2.88	4.96×10^{-3}	2.9×10^{-3}	1.32	1.0×10^{-3}	.59
Post Size Ex	9.5	0.189	1.80	4.28×10^{-4}	4.06×10^{-3}	1.85	2.3×10^{-3}	2.3
Post Anion	10.5	0.133	1.40	3.23×10^{-4}	3.39×10^{-3}	1.54	2.4×10^{-3}	1.1

Table 3.2: Typical purification table for osmotically lysed recombinant His HRP, purified via nickel affinity chromatography.

Purification Method	Fraction Vol (mL)	Protein Con ^c (mg.mL ⁻¹)	Total Protein (mg)	Activity (μ mol.min ⁻¹ .ml)	Total Activity (μ mol.min)	% Recovery	Specific Activity (μ mol.min.mg ⁻¹)	Purification Factor
Crude	15	2.24	3.3×10^3	4.13×10^{-2}	6.20×10^{-1}	100	1.8×10^{-2}	1
Post Ni ²⁺	15	0.05	0.75	2.55×10^{-2}	3.81×10^{-1}	62	5.8×10^{-1}	27

3.9 Recombinant HRP Characterisation

3.9.1 Protein Determination

The BCA assay was used to quantify the protein present in a sample. Protein concentrations were measured before and after a purification step and also prior to characterisation of the native recombinant or mutant forms of HRP. Bovine serum albumin (BSA) was used to construct the standard curve.

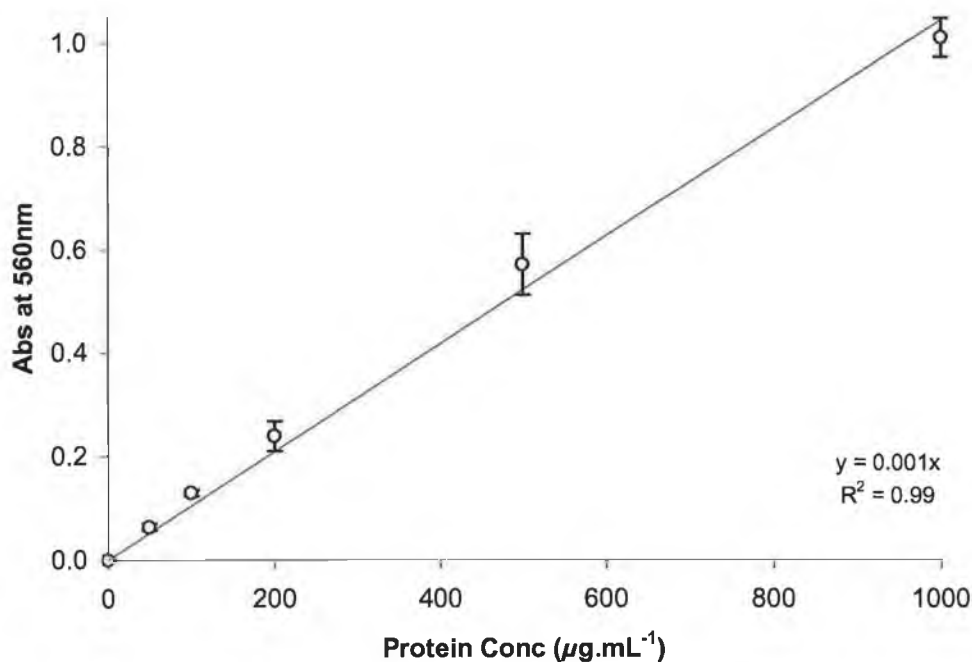


Figure 3.25: Standard curve of bovine serum albumin (BSA) for the determination of protein, as detailed in Section 2.28.

3.9.2 Determination of amine groups and UV-visible spectrum of rHRP.

The TNBS assay (Section 2.31) can be used to determine the number of free amines, and hence the number of lysines, before and after site directed mutagenesis studies. N- α -acetyl-L-Lysine was used to construct the standard curve for this assay: its composition has only one available amine group and, hence, an accurate standard curve could be developed. HRP has three available lysines under normal physiological conditions (O'Brien et al., 2001).

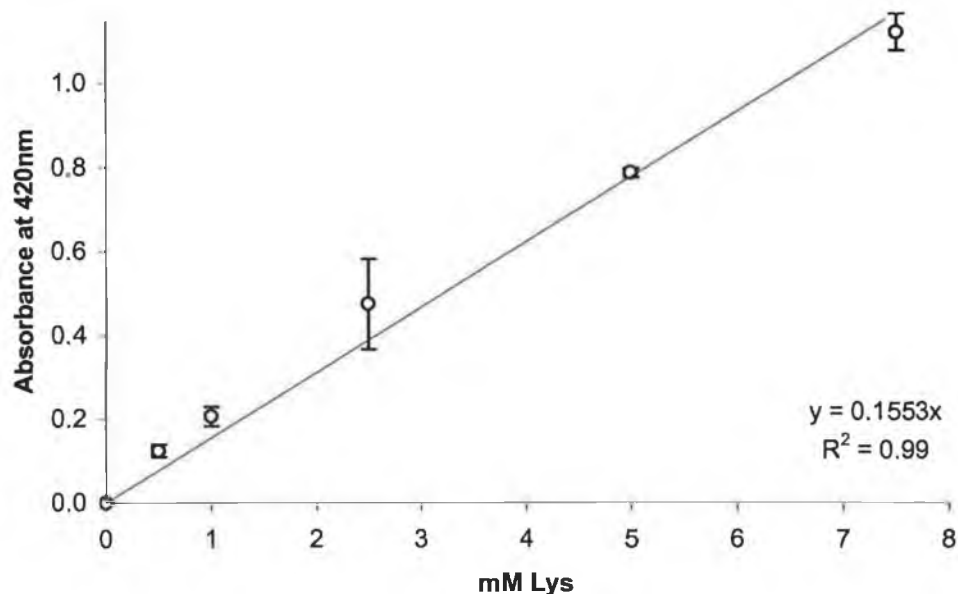


Figure 3.26: Standard curve of N- α -acetyl-L-Lysine for the determination of amines by TNBS method.

The UV-visible spectrum of a concentrated ($5\mu\text{M}$) recombinant HRP sample in 50mM sodium phosphate pH 7.5 was determined. A Soret peak was observed at approximately 403nm and was attributed to the absorbance of the iron in the heme group. The Reinheitszahl (RZ) purity ratio (A_{403}/A_{280}) can be used to determine the purity of a HRP mixture, and is particularly useful after purification procedures. It should be noted that the absorbance peak at 280nm was attributed to the aromatic amino acid residues, with a contribution from the heme moiety (Dunford, 1999). Typical RZ values recorded in this study were circa 1.1; however, these varied between 0.3 and 1.5. Arnold and co-workers also noted poor RZ values for rHRP expression (Arnold and Lin, 2000).

3.9.3 TMB Assay Optimisation.

The HRP in this study was produced via heterologous expression in a prokaryotic cell line, and existing catalytic activity assays designed for plant enzyme had to be optimised for this form of the enzyme. TMB assay optimisation was carried out as per Section 2.30.1, with the assay based on previous work by Ryan (1992, MSc Thesis, DCU). The variables analysed were reaction time, H_2O_2 concentration and HRP concentration (Figs 3.27-3.29). Initially the optimal time was deduced, and the reaction is seen to produce product linearly for 8 min, with an R^2 of 0.98. From this graph, it was concluded that optimal TMB readings should be taken after 6.5 min (Figure 3.27).

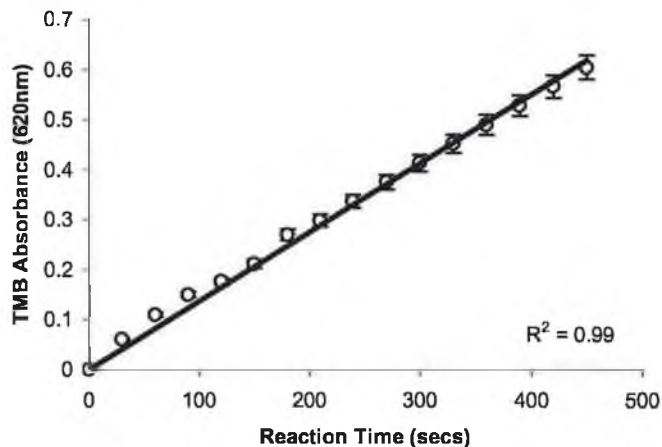


Figure 3.27: Plot of TMB reaction versus time for purified wild type rHRP (10 $\mu\text{g/L}$). The catalytic reaction is linear for 8 min, as indicated by the trend-line and R^2 value of 0.98.

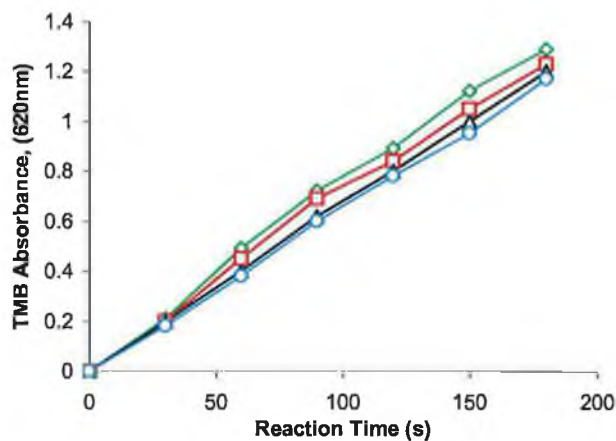


Figure 3.28: Plot of TMB reaction versus time for purified wild type rHRP(10 $\mu\text{g/L}$), with varying concentrations of H_2O_2 . The diagram focuses of the initial phase of activity, with the final concentrations of H_2O_2 being 0.003% (\diamond), 0.004 % (\square), 0.005% (\triangle) and 0.006% (\circ).

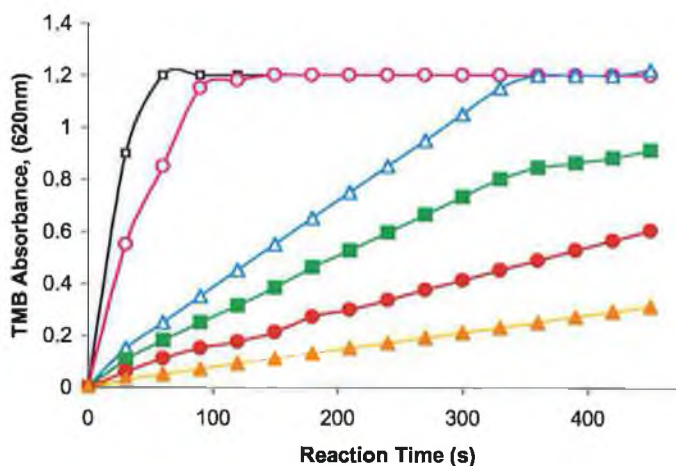


Figure 3.29: Plot of TMB reaction versus time varying concentrations of rHRP: 100 $\mu\text{g/L}$ (\square), 50 $\mu\text{g/L}$ (\circ), 25 $\mu\text{g/L}$ (\triangle), 12.5 $\mu\text{g/L}$ (\square), 10 $\mu\text{g/L}$ (\circ) and 5 $\mu\text{g/L}$ (\triangle)

3.9.4 Thermal Stability of wild type recombinant HRP.

3.9.4.1 Thermal profile.

Characterisation of mutants (Chapters 4, 5 and 6) included thermostability analysis, so the recombinant wildtype was first compared with commercial plant HRP (Type VI, Sigma). This involved constructing a thermal profile of the protein, completing from this a thermal inactivation at constant temperature and, hence, computing the half-life. The thermal profile involves varying temperature at constant incubation time. Residual catalytic activity was plotted versus incubation temperature, and the T_{50} (the temperature at which the enzyme displays 50% of its maximal activity) was calculated.

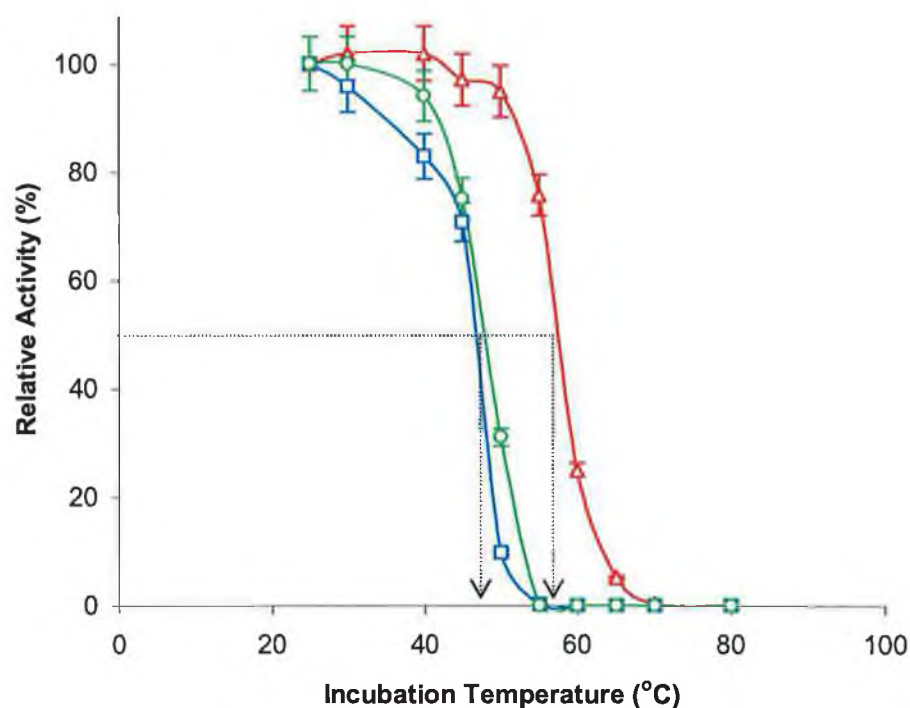


Figure 3.30: Thermal profile of wildtype plant Δ , wildtype recombinant His Tagged \square , wildtype recombinant Non-His Tagged HRP \square . As expected, the recombinant HRP is less stable than plant HRP, probably due to lack of posttranslational modifications such as glycosylation (Tams and Welinder, 1998).

T_{50} of recombinant HRP was estimated, by graphical inspection, to be 50°C , whilst the commercially available (Sigma) plant HRP was seen to have a T_{50} of approximately 55°C . The recombinant HRP T_{50} temperature was used for thermal inactivation. Very little difference can be seen between HRP_{His} and HRP Δ His.

3.9.4.2 Thermal inactivation of wild type recombinant HRP.

A thermal inactivation assay measures activity loss versus time at constant temperature, preferably at the enzyme's T_{50} , which is derived from a thermal profile experiment. The T_{50} suggested by the thermal profile was 50°C; however, at this temperature, complete inactivation of His tagged HRP (conventionally purified from whole cell extract) was not achieved. Hence, the thermal inactivation was repeated at higher temperatures, 55°C and 65°C respectively. Once pure rHRP was obtained, a wildtype k -value of 0.056 min^{-1} was noted.

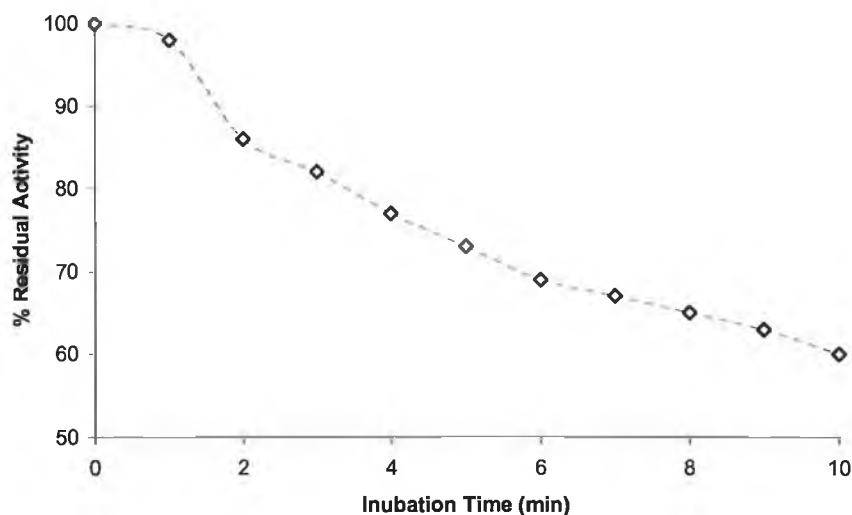


Figure 3.31: Thermal inactivation of wildtype recombinant His tagged HRP at 50°C. Residual activity was measured utilising standard TMB conditions, as outlined in Section 2.30.

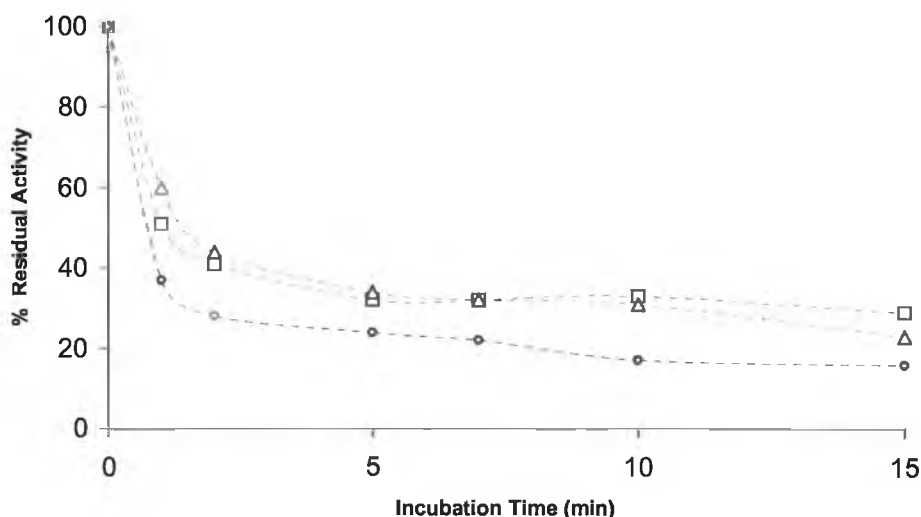


Figure 3.32: Thermal inactivation of wildtype recombinant His tagged, conventionally purified, HRP at 50°C, 55°C, and 65°C. Unlike plant enzyme, the recombinant form does not undergo first order inactivation. Previous reports cited HRP as following pseudo 1.5 order inactivation (Chang et al, 1988); however, pseudo first order inactivation can be achieved by plotting the data from the first 10min of inactivation, as outlined in Figure 3.31.

3.9.5 Native Gel Electrophoresis.

A concentrated wildtype His tagged recombinant sample, conventionally purified from whole cell extract, was electrophoresed through a 12% acrylamide native gel, as outlined in Section 2.27.3. The gel was then developed in various HRP substrates overnight at 4°C, with gentle mixing.

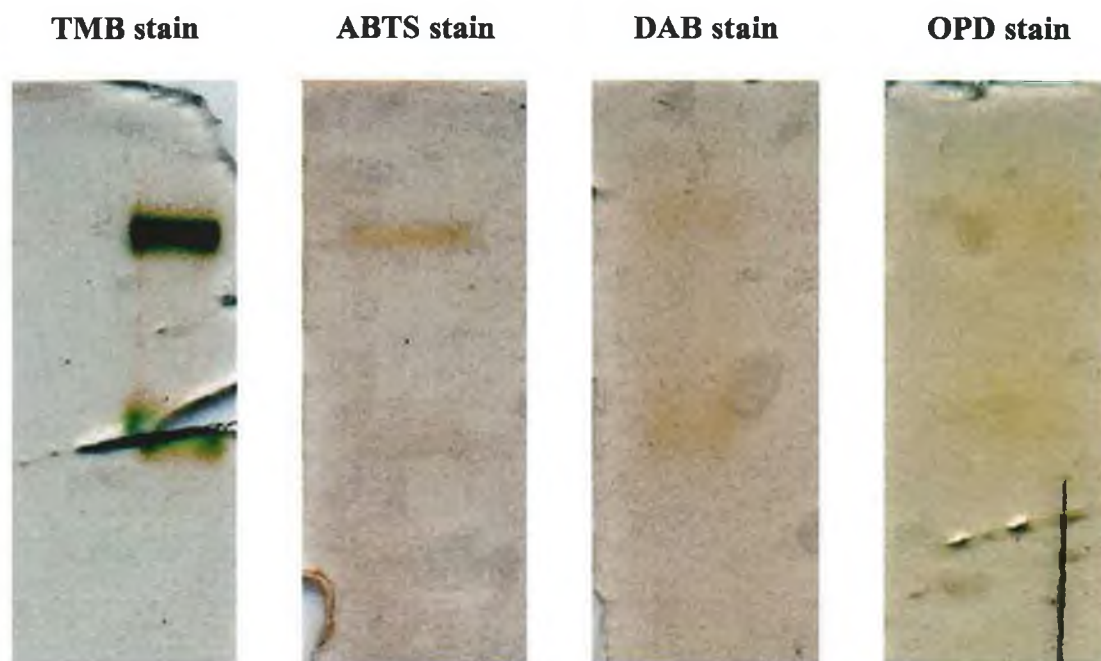


Figure 3.33: Native gel electrophoresis of concentrated wildtype rHRP. Various HRP substrates were utilised to stain the native gel. Each produced two bands of intensity, of approximately 45kDa and 66kDa respectively. TMB and ABTS staining yielded the most visible results.

The formation of two bands of peroxidase activity was unexpected; however, it can be attributed to the native peroxidase activity of the host *E. coli* cell, XL10 Gold (Bakalovic et al., 2006). To elucidate which band the *E. coli* contributes, a native gel containing empty vector and rHRP was stained using TMB substrate.

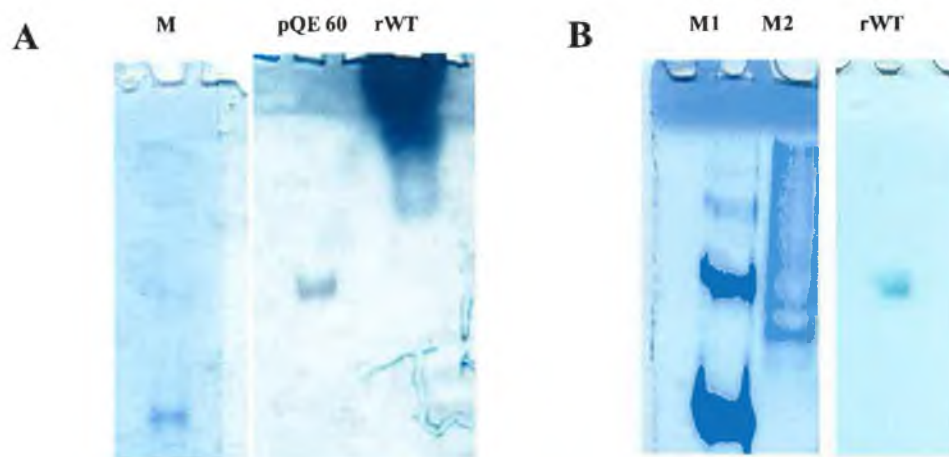


Figure 3.34: Part (A) shows native gel electrophoresis of empty pQE60 vector and wildtype rHRP. The empty pQE60 vector displays a single, weak band at approximately 45kDa. Purified His tagged rHRP, however, yields a strong activity band at approximately 66kDa. However, this gel (A) was overloaded with rWT TMB, as signified by intense staining through resolving section. Gel (B) utilised a lower concentration of WT rHRP, and single, clear band is evident. TMB was utilised to stain the native gel, at 4°C overnight with gentle mixing. Coomassie stain was use for marker staining. Markers are for illustrative purposes only.

A constant residual activity was noted during thermal inactivation assay (see Section 3.9.4.2) with an initial rapid decrease in activity followed by a prolonged period, greater than one hour, of residual activity (results not shown). To investigate if the native *E. coli* peroxidase activity contributed to this, a sample of concentrated rHRP was subjected to 55°C for 15 min prior to loading onto the gel.

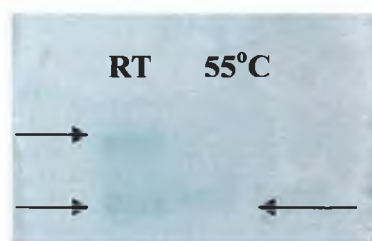


Figure 3.35: Native gel electrophoresis of concentrated wildtype rHRP incubated at room temperature (RT) or 55°C for 15min prior to addition to native gel. TMB was utilised to stain the native gel. Two bands were noted in the RT sample; however, only one band, of approximately 45kDa, was noted in the 55°C treated sample.

rHRP samples utilised in Section 3.9.5 were purified by conventional purification procedures from lysed *E. coli* cells via sonication. This method of cell disruption causes the entire contents of the cell to be ejected into the purification buffer. To reduce the amount of contaminating protein introduced to the purification buffer, cells were lysed via osmotic shock and lysozyme treatment, to release only the proteins secreted to the periplasm of the *E. coli* cell (see Figure 3.36). This, combined with the addition of a mildly chaotropic agent, 200mM guanidine hydrochloride, facilitated optimal His Tag

purification by IMAC (Section 3.8.2). His Tagged purified rHRP was utilised in all characterisation assays (see Sections 3.9.3, 3.9.4.2, 3.9.6, 3.9.7, 3.9.8 and 3.9.9).

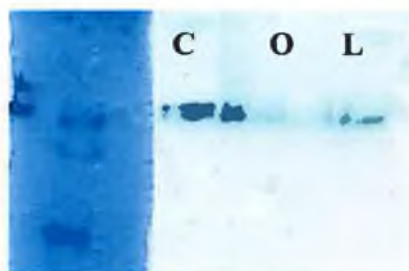


Figure 3.36: Native gel of XL10 Gold HRP-producing cells lysed with osmotic shock (O), lysozyme treatment (L) and combined osmotic/lysozyme treatment (C). TMB was utilised for staining. A single band of TMB activity was noted for all methods utilised. The combined osmotic/lysozyme treatment appears to yield the band with greatest peroxidase activity.

3.9.6 Organic Solvent Tolerance.

Organic solvent tolerance assays were carried out as per Section 2.34, with a final protein concentration of $100 \mu\text{g.mL}^{-1}$ in the reaction solution. Solvent tolerance profiles were produced for wildtype recombinant HRP, in triplicate, for each solvent tested. All standard errors were within $<5\%$ of the triplicate average reading, with the errors bars omitted from the graphs for the sake of clarity.

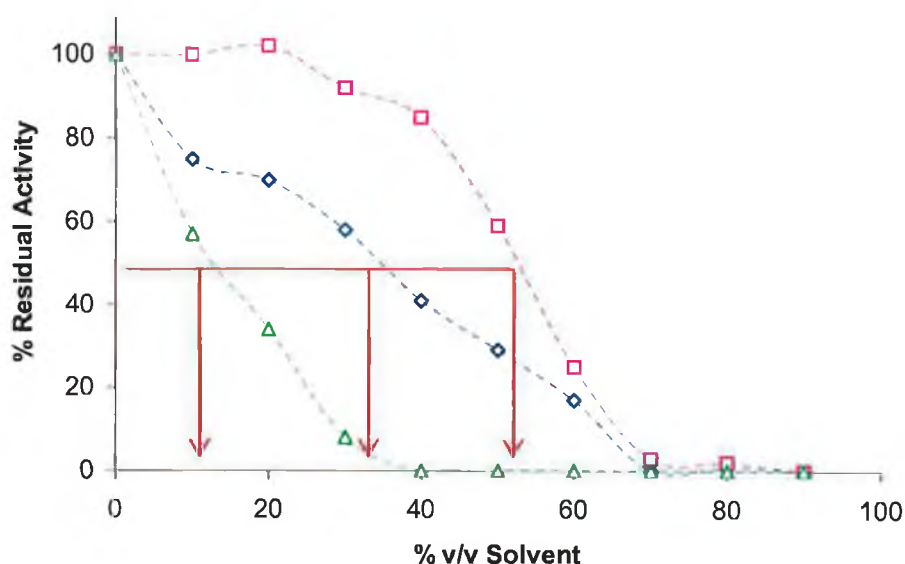


Figure 3.37: Solvent Tolerance Profile of wildtype recombinant His-tagged HRP, \square MeOH, \diamond DMSO, \triangle DMF.

The C_{50} value was utilised as an indicative value for organo-tolerance; this value is the % v/v of organic solvent that causes a 50% decrease in enzymatic activity. DMSO, MeOH and DMF yielded C_{50} values of 35 % v/v, 53 % v/v, 14 % v/v respectively.

3.9.7 H_2O_2 Tolerance.

The stability of recombinant wildtype His tagged HRP to H_2O_2 was measured as per Section 2.35, with a final rHRP concentration of 360 nM in each reaction. In the presence of excess H_2O_2 and in the absence of a suitable reducing substrate, HRP displays suicide inactivation. Profiles were produced in triplicate, and standard errors were noted as less than 10 % for all data points.

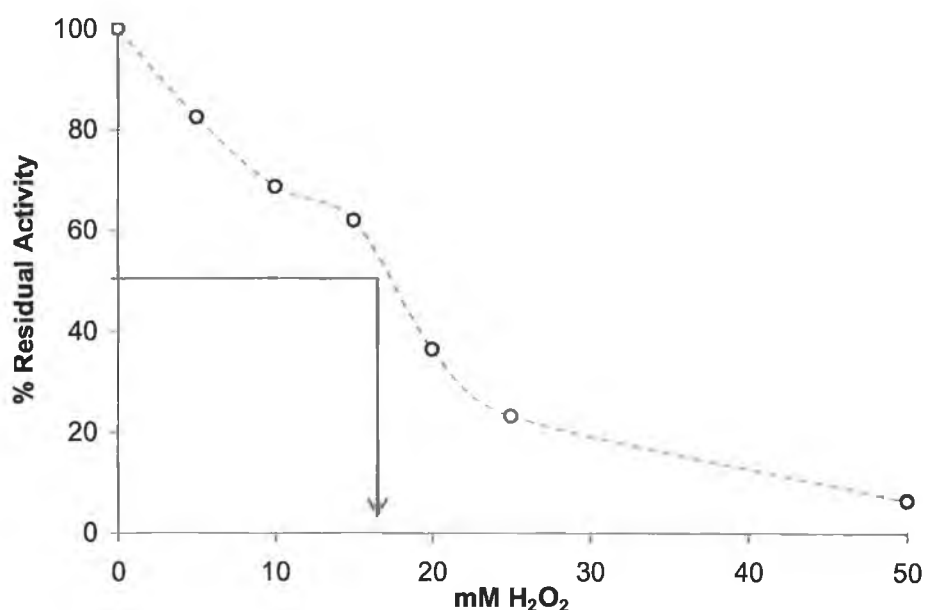


Figure 3.38: H_2O_2 tolerance profile for native recombinant His-tagged HRP.

3.9.8 ABTS Kinetic Analysis.

ABTS was utilised as reducing substrate for steady state kinetic analysis as per Section 2.36, with apparent k_3 and K'_m values calculated by plotting the data generated in the software package *Enzfitter* (see Figure 3.39). Utilising a validated microtitre plate approach, the apparent k_3 for recombinant wildtype was calculated as $333 \text{ s}^{-1} (\pm 25 \text{ s}^{-1})$, whilst the apparent K'_m modelled to be $2.04 \text{ mM} (\pm 0.06 \text{ mM})$.

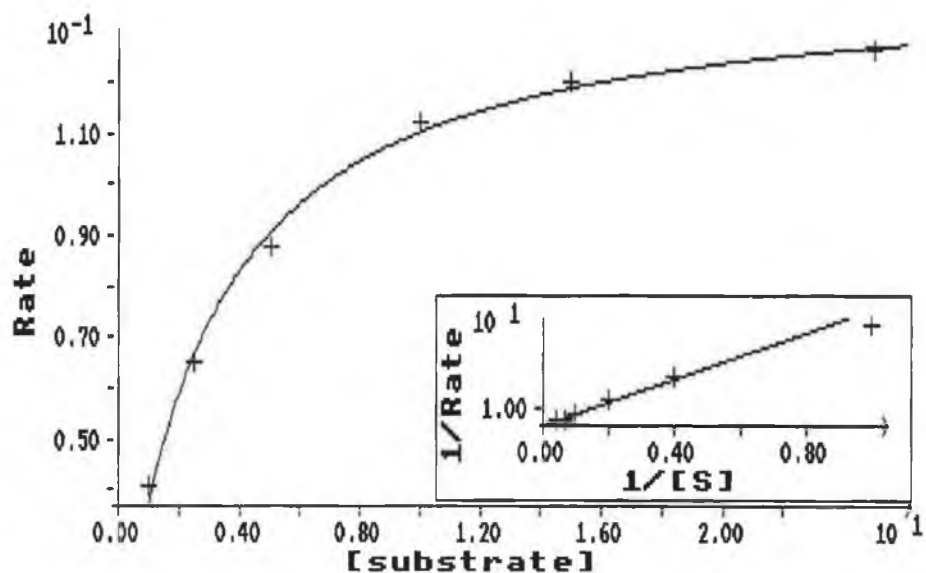


Figure 3.39: Purified native recombinant HRP steady state kinetic data, utilising ABTS as reducing substrate, plotted using the Enzfitter™ programme (Biosoft, Cambridge, UK) modelled to a Michaelis-Menten curve. Rate = $\Delta 405$; $\Delta 405 / \epsilon_{\text{ABTS}} / \text{time} = \mu\text{mol} \cdot \text{min}^{-1}$

3.9.9 Western Blot Analysis.

Western Blot analysis of native recombinant HRP exploited the C-terminal poly Histidine purification tag and was carried out as outlined in Section 2.27.2. The results confirm the expected size of the denatured recombinant rHRP molecule of circa 34,000 Da. This also demonstrates the effect of denaturing the molecule to reveal the buried His-tag, as on a native gel no signal is noted after probing with an anti-(His)₆ antibody.

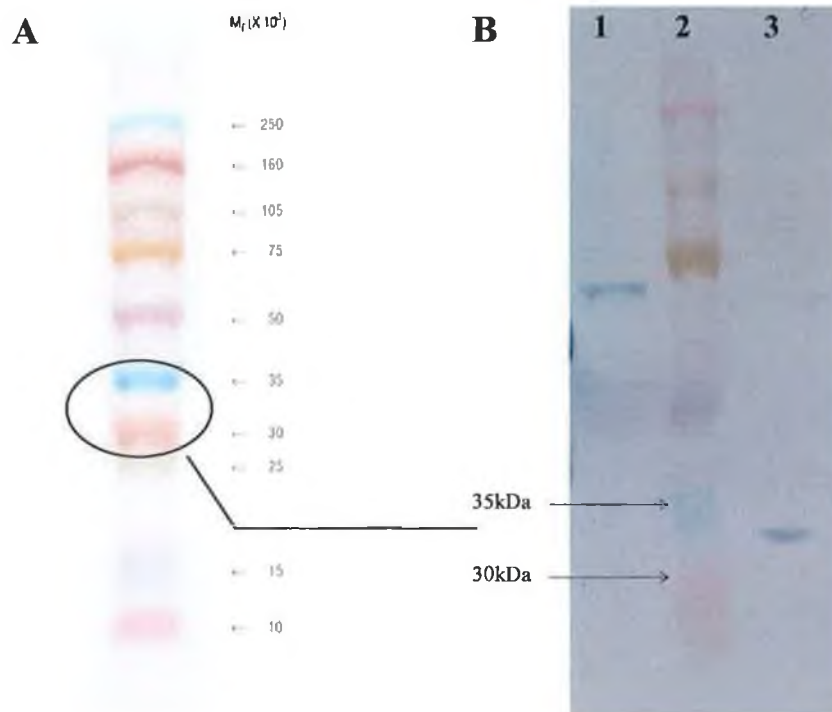


Figure 3.40: Western blot analysis of purified wildtype recombinant HRP. Part (A) represents the relevant sizes of the Rainbow MarkersTM. Lane 1 in Part (B) displays the positive control, lane 2 shows the standard marker and lane 3 illustrates rHRP. The positive control is the Internalin protein, recombinantly expressed as a His-tag fusion protein in *E.coli*, which has a molecular weight of approximately 68kDa (Leonard P, PhD Thesis, DCU). Initially rHRP, standard markers and positive control were electrophoresed through a 12% SDS-PA gel. This was transferred onto a nitrocellulose membrane and probed with an anti-His tag murine antibody, which was in turn probed with an anti-mouse IgG antibody labelled with the reporter protein, alkaline phosphatase. The blot was developed with BCIP/NBT substrate. The blot reveals the size of the rHRP molecule as being circa 34,000 Da, similar to that previously reported (Smith et al., 1990)



Figure 3.41: Western blot analysis of various purified rHRP mutants, to verify correct His tag incorporation into rHRP mutant proteins (see Chapter 4 for more information). The blot is arranged as follows: (1) wildtype rHRP, (2) Rainbow MarkersTM, (3) K174N, (4) K174E, (5) K174N, (6) K232N, (7) K2324E, (8) K232N, (9) K241N, (10) K241E, (11) K241N. All the mutants display a His tag that is recognised by the murine-based anti-His tag antibody, and are of similar size to wildtype rHRP.

3.10 Discussion.

3.10.1 Choice of Expression Vector and Host.

The aim of this section of the project was to clone the HRP gene into an appropriate expression vector and express this gene construct within a suitable bacterial expression host. pQE60 (Qiagen) was chosen as the host vector due to its noted high expression of His tagged proteins. It also has several advantageous features, including an optimised promoter-operator element consisting of the T5 promoter (recognised by *E.coli* RNA polymerase) and the *lac* operator sequence (which binds the *lac* repressor and ensures repression of the powerful T5 promoter). The vector also contains a synthetic bacterial ribosomal binding site (for high translation rates), a β -lactamase gene (*bla*) which confers resistance to ampicillin to $100\mu\text{g.mL}^{-1}$ (to allow for vector selection; used in conjunction with XL 10 Gold's tetracycline and chloramphenicol resistance) and translational stop codons in all reading frames (to prevent read-through transcription and ensure stability of the expression vector). Another key characteristic of the pQE60 vector is the presence of C-terminal poly-His tag, which allows for convenient one-step purification via IMAC (Qiagen, 2003).

The expression host chosen was *E. coli* XL-10 Gold cells (Stratagene), as this strain is capable of high expression of recombinant protein, and is both chloramphenicol and tetracycline resistant (Section 2.1.1). This allows for the use of three antibiotics in the production of the recombinant protein, minimising the chance of non-transformed cells growing in the reaction vessel. It should also be noted that the XL10 Gold strain harbours the *lacI^q* mutation which allows the cell to produce naturally enough *lac* repressor to block transcription until an inducer, e.g. IPTG, is added to the reaction broth. As such, these cells can be seen to work in tandem with the pQE60 vector and, therefore, act as a strong expression system for recombinant proteins (Stratagene, 2004).

The inclusion of a suitable leader sequence in-frame with the gene of interest allows for translocation of the expressed protein to the bacterial envelope and the cell culture medium. Use of the PelB leader has increased in popularity, with many cited reports of successful translocation of expressed proteins noted (Mergulhão et al., 2005 and references within). Inclusion of the PelB leader has allowed for translocation of recombinant proteins to both the periplasmic space (Barth et al., 2000) and the culture supernatant (Zambonelli et al., 2004). Secretion of recombinant proteins to the culture

medium or periplasm of *E. coli* has several advantages over intracellular production, including simplified downstream processing, enhanced biological activity, higher product stability and solubility, and N-terminal authenticity of the expressed peptide; however, the exact mechanism of translocation is not yet fully understood (Cornelis, 2000).

3.10.2 Cloning Difficulties.

As outlined in Section 3.2, the MCS of pQE60 contains the unique restriction sites, *Nco* I, *Bam*H I and *Bgl* II. These restriction sites, however, were also present in the HRP gene sequence (or were proposed as mutagenic screening sites), and so could not be utilised in directional cloning. Hence, the vector was engineered to contain additional unique restriction sites, primarily introduced via the cloning of the PelB leader sequence, as outlined in Section 3.2.

Initially, the PelB leader was cloned *Nco* I - *Bam*H I, with the HRP gene cloned second via the introduced *Not* I site and the *Hind* III site 3' of the poly His tag. This cloning of the HRP gene required the re-introduction of the poly His tag, as the vector His tag had been removed. This was achieved by including exactly the same poly-His sequence in the reverse HRP primer as was on the original vector. Unfortunately, however, this construct was one base pair out of frame with the initiation methionine included in the *Nco* I site, although the PelB leader and the HRP gene were in-frame with each other. This led to erratic HRP production and the requirement to subclone the PelB-HRP construct. Thus, the PelB-HRP construct was amplified utilising the "BspH I For" and "HRP_His_Rev" primers outlined in Section 2.1.3. This PCR introduced a *Bsp*H I site 5' to the PelB sequence and allowed the in-frame PelB-HRP_His to be cloned into the *Bsp*H I - *Hind* III cut vector. The "BspH I For" primer also contained two additional bases between the initiation methionine residue and the first base in the PelB Leader sequence to maintain the correct reading frame. The bases 'GC' were inserted between the start ATG in the *Bsp*H I site and the first base of the PelB Leader sequence. This introduced a small neutral amino acid, serine, between the initiation methionine and the primary alanine of the PelB leader. Also, upon sequencing, it was confirmed that a region of the His tag encoded by the primer had been deleted, resulting in poor purification yields. To circumvent this problem, the PelB-HRP construct was amplified with "BspH I For" and "HRP_Rev" primers that allowed BspHI - BamHI insertion of

the HRP-PelB construct. Sequencing confirmed the presence of the PelB-HRP-His construct, with correct reading frame.

3.10.3 Expression of HRP gene in *E. coli*.

The HRP gene cloned into the pQE60 expression vector contained a point mutation, A34P, which was present prior to cloning. This point mutation was reverted to wildtype before any expression or characterisation work was carried out on the recombinant protein. Once reverted to wildtype (see Section 4.4) the protein was expressed in various cell lines, to select for the optimal host and growth conditions. It was noted that XL10 Gold was a superior host to all other *E.coli* strains investigated. It was also discovered that rHRP activity was highest in cell lines that had not been induced with IPTG, concurrent with previous work with this gene (Arnold and Lin, 2000). Non-induced, “leaky” expression has previously been noted in other pQE-based vector systems (Liu et al., 1999) and hemoproteins (Varnado and Goodwin, 2004). Indeed, if IPTG is added, the cell turbidity begins to drop (data not shown); suggesting that overproduction of HRP is somewhat toxic to the cell. Similarly, Jung and co-workers (2001) again utilising a pQE-based expression vector, noted an increased ratio of holoprotein to apoprotein with decreased addition of IPTG. Jung suggests that slow recombinant hemoprotein production allows for maximal holoprotein production, due to the small concentrations of apoprotein acting as heme sinks, binding all available heme in the system (Jung et al., 2001). Reduced culture temperatures, limited gene induction or utilisation of gentle induction procedures achieves slow recombinant protein production. As such, it was noted that rHRP activity was higher in cell lines cultured at lower temperature, 30°C as opposed to 37°C. The higher activity could be directly attributed to the slower production of the recombinant protein, due to the lower growth temperature. Slower production allows for correct folding of the recombinant protein and minimises inclusion body formation (Hoffmann et al., 2004), a problem that has plagued recombinant HRP production for years (Smith et al., 1990). Use of the periplasmic localisation fusion protein, PelB leader, also helps to minimise inclusion body formation and the non-reducing environment of the periplasm is conducive to formation of disulfide bonds, of which HRP has four. The periplasm is also noted as *E. coli*'s calcium repository, maintaining three times as much free Ca²⁺ as the cytosol (Jones et al., 2002). HRP contains two Ca²⁺ ions per molecule, and Ca²⁺ is critical to HRP folding and stability (Tams and Welinder, 1998). Overexpression of HRP is not seen after SDS-PAGE analysis of the cleared cell lysate, although this is probably due

to the fact that no inducer is utilised in this study. Overexpression of recombinant hemoproteins is notoriously difficult, due mainly to the reduced rate of bacterial heme biosynthesis in comparison to recombinant protein production (Varnado and Goodwin, 2004). Addition of the rate-limiting heme precursor, δ -aminolevulinic acid, may increase the bacterial heme biosynthesis; however, this becomes economically unviable at large production scales. Repression of HRP expression can be achieved by simple addition of 2 % w/v glucose. If the cells are repressed by glucose addition, and subsequently transferred to glucose-free medium, increased expression is noted; see Figure 3.15. This suggests that initial repression of recombinant protein production allows the host cell to grow to a density at which it can later support the production of the recombinant protein. Recently, Studier (2005) reported a simple auto-induction media, which reduces the “hands-on” nature of protein expression. The requirement to physically remove the cells from the glucose-containing medium, via centrifugation, was eliminated by employing the minimal concentration of glucose required to prevent HRP expression prior to attainment of a suitable OD_{600nm} for cell growth. A final glucose concentration between 0.05 and 0.1% w/v resulted in minimal rHRP expression at an *E. coli* cell density (OD_{600nm}) equal to 0.5. At this point the host cell will consume the majority of the glucose, and it will begin utilising other carbon sources, allowing leaky expression of the HRP gene. Utilising these optimal conditions, an extended growth-versus-production study was carried out, which noted maximal HRP activity after 24 hours’ growth at 30°C. As the rHRP located in the periplasmic fraction reached its maximum production point, rHRP activity was also noted in the cell supernatant. With increasing time, the rHRP activity in supernatant fraction began to increase whilst the periplasmic fraction showed decreased activity, suggesting a migration of the rHRP from the periplasmic space to the cell supernatant. When XL10Gold cells containing pBR_I were grown at 37°C, an initial burst of rHRP activity was noted; however, this dropped quickly over eight hours. Similar to cells grown at 30°C, a decrease in periplasmic activity coincided with an increase in supernatant activity. However, the peroxidase activity was much lower for the 37°C production compared with 30°C.

3.10.4 Recombinant HRP Purification.

Immobilized nitrilotriacetic acid was utilised to purify the recombinant HRP. Initially, purification results were difficult to reproduce. Instead, conventional purification techniques were utilised to purify the protein but these met with limited success due to

the large concentrations of contaminating proteins in the sonicated cell fraction. To reduce this problem, HRP was purified from the cell periplasm and the cell supernatant, where it was noted after 24 hours growth. The periplasm is known to contain approximately 100 native *E. coli* proteins, as compared to the 4,000 present within the cytoplasm; hence, considerable purification and concentration of a recombinant protein is achieved by targeting a protein to the former (Blattner et al., 1997). Additionally, simple osmotic/lysozyme treatment allows release of the recombinant protein from the bacterial envelope. Purification from the supernatant is complicated by the dilute nature of the recombinant protein; however, protein precipitation can circumvent this problem. Secretion removes the recombinant protein from the potentially deleterious action of native *E. coli* proteolytic enzymes and may result in increased expression, although many of these strains are protease-deficient anyway. Gene fusions facilitating protein purification, such as His Tags, have developed rapidly in recent years; and can provide up to one hundred-fold purification in optimal conditions. Despite the original promise, however, several reports have noted the poor performance of IMAC chromatography. IMAC can be seen as a cost effective, high-throughput single step purification procedure; however, drawbacks include the poor capture of some proteins (Loughran et al., 2006), interference with crystallographic procedures (Lichty et al., 2005) and effect of the His tag length on protein termini (Mohanty and Wiener, 2004). In this study, poor recombinant protein capture was attributed to protein dimer formation, which in turn blocked His tag – Ni²⁺ interaction. Recombinant HRP is known to form dimers in reverse micelles (Gazaryan et al., 1997) and it is plausible that this also occurred in this study; simple addition of 200mM guanidine hydrochloride (mildly chaotropic) and 1M NaCl (prevents non-specific hydrophobic interaction with the nickel resin) to the purification buffer dispels the putative dimer and allows the His Tagged protein to bind to the resin. It should be noted, however, that recent research has highlighted the inhibitory role of nickel on HRP. Two nickel molecules bind to a single HRP molecule, leading to complete catalytic inactivation (Keyhani et al., 2005). This may cause difficulty in the purification of rHRP utilising nickel affinity chromatography. In this study, rHRP / nickel contact times were minimised to reduce the possible protein inactivation. Typical yields of rHRP were 0.65 $\mu\text{mol.L}^{-1}$ fermentation. Although a low RZ value, approximately 1.1, was routinely noted for this purified fraction, the presence of purified apoprotein can account for increased $A_{280\text{nm}}$ without an equal increase in $A_{403\text{nm}}$.

3.10.5 Recombinant HRP Characterisation.

3.10.5.1 Chromogenic Assay Optimisation.

The TNBS assay can be used to determine the number of free amines, and hence the number of lysines. It was envisaged that this technique would allow quantification of the number of lysines present in the rHRP molecule before and after lysine mutagenesis. However, very high concentrations of rHRP were required to accurately carry out this procedure and, due to the non-induced nature of the expression protocol, these concentrations could not be achieved. This remains a very useful technique for lysine content characterisation for chemical modification of native proteins.

The TMB assay was optimised for use with recombinant HRP, as it had previously been devised for plant HRP (Ryan et al., 1994a). The microplate-based assay was optimised for reaction time, H₂O₂ concentration and HRP concentration. It should be noted that Tween 20, to a final concentration of 0.001% (v/v), was added to the reaction buffer, as HRP can be inactivated by polystyrene microplates in its absence (Berkowitz and Weibert, 1981). By using a suitable hydrogen donor, HRP activity can be measured indirectly by following the transformation of the hydrogen donor, which in the case of TMB is represented by a change in colour of the reaction well, from colourless to blue. The intensity of blue colour formation is proportional to the quantity of HRP present. TMB has an absorbance peak of 650nm; however, this particular narrow-band filter was not available for microplate readings. A broad scan of the spectral region 600nm to 700nm demonstrated that the absorbance peak has a broad shoulder, so readings at 620nm were adequate. To further increase the sensitivity of the TMB assay, the reaction can be terminated with strong acid, at which point the colouration changes from blue to bright yellow due to the loss of two electrons from the substrate (Josephy et al., 1982). The absorbance peak changes to 450nm and a 2-4-fold increase in sensitivity is noted (Bos et al., 1981); however, this latter procedure was not implemented in this study. The HRP concentration that led to continual linear product formation over the experimental timeframe was approximately 12.5 µg/L, with the optimal concentration of 10M H₂O₂ stock being 0.003% (v/v; 3mM final concentration) and the optimal reaction time being 6.5 minutes. This reaction time is longer than that previously reported (Miland, 1996, PhD Thesis, DCU); however, a much smaller concentration of HRP was utilised in this study.

3.10.5.2 Thermal Stability.

Thermal studies formed the basis of initial rHRP characterisation. Wildtype recombinant and plant HRP were both subjected to ramped 10 min incubations at increasing temperatures, to plot the enzyme's thermal profile. It was seen that plant HRP is more stable than recombinant HRP; plant HRP displays a T_{50} of 55°C, while rHRP's is 50°C. The difference could perhaps be attributed to the stabilising effects of the glycan residues on the surface of the plant HRP molecule (Tams and Welinder, 1998) and possibly the pyroglutamyl blocked N-terminus. Posttranslational modifications such as glycosylation cannot be carried out by prokaryotes such as *E. coli*.

The thermal profile suggested that the thermal inactivation assay be carried out at 50°C; however, when the rHRP was incubated at this temperature, an initial rapid decrease in enzymatic activity was followed by a slow steady decline, suggesting a two phase decline in stability. It was attempted to fit the resulting thermal inactivation data to both first- and second-order models of decay; however, the data did not fit. It appeared as though two distinct peroxidase populations existed, the first being extremely heat sensitive, and the other less so.

Continued investigation into the two-peroxidase hypothesis resulted in native gels demonstrating two distinct bands of peroxidase activity. Peroxidase activity was noted utilising TMB, ABTS, DAB and OPD as substrates. The upper band may be a dimer of 66 kDa; the latter figure predicted from the size of monomeric recombinant HRP (Smith et al., 1990). This size was also confirmed by Western blotting (see Section 3.9.9). It was believed that the lower band represents a native *E. coli* peroxidase-like protein. *E. coli* is known to possess at least two bacterial heme containing "catalase-peroxidases", hydroperoxidase I and II. These molecules are larger (84 kDa; Dunford, 1999) than those noted in Figure 3.33; however, it is plausible that smaller bacterial peroxidase-like proteins exist (Bakalovic et al., 2006; Welinder et al., 2002). To confirm this, XL10 Gold cells, containing only empty vector, were lysed, electrophoresed and TMB-stained. The resultant band confirmed the presence of native *E. coli* peroxidase. To verify if the second population of peroxidase activity contributed to the heat-stable portion of the thermal inactivation plot, a rHRP sample was subjected to 55°C for 15 min prior to loading onto the gel. The non heat-treated sample displayed two bands of TMB activity, corresponding to previous results; however, the heat-treated sample exhibited only a single, smaller band. This indicated that two peroxidase populations

exist, and a requirement for further purification to remove this contaminating peroxidase. The rHRP samples utilised in these initial studies were purified by conventional methods; hence, a native *E. coli* protein with similar physio-chemical characteristics could co-purify with the recombinant HRP. To circumvent this problem, different cell lysis protocols were analysed in an attempt to release the rHRP protein from the cell periplasm without releasing the native *E. coli* peroxidase protein. Combined osmotic/lysozyme treatment released maximal rHRP, with minimal contamination. Inclusion of 200mM guanidine hydrochloride in the purification buffer also facilitates purification via the His tag, as it presumably disassociates the rHRP dimer and allows interaction of the buried hexa-His residue with the nickel resin.

Once a purified rHRP population could be produced consistently, further analysis was undertaken. Thermal profiling suggested a T_{50} of 50°C, for the purified His-Tagged rHRP molecule. With further thermal characterisation revealing a k -value of 0.056 min⁻¹ and $t_{1/2}$ of approximately 12.5 min at 50°C. The k -value is the rate constant in the single exponential decay model (Enzfitter, Biosoft, Cambridge, UK). Previous studies of rHRP report lower k -values of 0.032 min⁻¹ but the latter was carried out at 65°C (O'Brien, PhD Thesis, 1997). Plant HRP is known to have a half-life of ~6 min at 65°C (Miland et al., 1996) but the thermal profile (Figure 3.30) demonstrates that recombinant HRP is somewhat less stable than plant HRP. The possible role of glycosylation is highlighted by Morawski and co-workers who noted that rHRP, expressed in *S. cerevisiae* demonstrates a T_{50} of 67°C identical to the plant HRP utilised for comparison (Morawski, et al., 2001).

3.10.5.3 Solvent Stability.

Recombinant HRP's organic solvent tolerance was also investigated in this study. The water miscible solvents investigated were chosen based on their theoretical denaturation capacities, methanol (low) and DMF (medium; Khmel'nitsky et al., 1991a) and also on previous reported peroxidase characterisation (DMSO; Santucci et al., 2003). In all cases rHRP catalytic activity decreased with increasing solvent concentration, while the C_{50} value enabled comparison to previously published tolerances for plant HRP.

Previous solvent stability studies have been carried out on free (non-immobilised) and immobilised plant HRP. Plant HRP was found to retain almost 100% activity in 30% v/v DMSO at 30°C over a two-hour incubation period (Azevedo et al., 2001). Maeda and co-workers (2002) noted that the microenvironment in the distal heme pocket was

altered and activity decreased even in the presence of low concentrations of DMSO. A large loss of secondary structure and the disassociation of the heme moiety from the apoprotein could be attributed to higher concentrations of DMSO. Santucci and co-workers (2002) further investigated the denaturation of plant HRP by DMSO, concluding that below 60% v/v DMSO plant HRP retains a compact tertiary structure and substantial integrity of the active site microenvironment; however, above 80% v/v DMSO, the heme group disassociates from the apoprotein. As noted in this study, recombinant HRP is less stable in DMSO than the plant enzyme, suggesting a role of glycosylation in HRP stability in organic solvents.

The effect of alcohols on plant HRP has also been investigated. It has been reported that ethanol alters the enzyme's heme group by binding to the sixth coordination site (Dunford and Hewson, 1977), although it does not affect the active site or tertiary structure of the protein (Ayyagari et al., 2002). Binding of ethanol reduces the formation of compound I and activity decreases with increasing ethanol concentrations. The effect of ethanol on the heme can be extrapolated to methanol as it is noted that the hydroxy group binds to the heme ligand (Sato et al., 1995). Sato and co-workers (1995) studied the effects of methanol on the rate constants in the HRP catalytic cycle (see Figure 1.3). They noted that k_{1app} was moderately reduced by 50% v/v methanol, k_{2app} was slightly affected, whereas k_{3app} , the rate-limiting step, was greatly affected. As such, assuming that this coordinated ethanol remains bound upon dilution in aqueous buffer, increased methanol concentrations affect the rate at which the enzyme can complete its catalytic cycle and return to its resting state.

The mechanism of DMF denaturation of HRP has not been discussed extensively in the literature; however, it has been stated that this organic solvent can affect an enzyme in a number of ways, including reduced enzyme-substrate binding, alteration of the enzyme conformation, alteration of the reaction rate by changing the dielectric constant and/or the viscosity of the medium, and by reduction of the water content close to the protein backbone (Batra et al., 1997). Previous reports of DMF-induced HRP denaturation conclude that loss of activity is due to water stripping by the solvent (Gorman and Dordick, 1992) and a C_{50} of ~8% v/v for the plant enzyme (Miland, PhD Thesis, DCU, 1996) is similar to the value for rHRP found in this study.

3.10.5.4 H₂O₂ Stability.

H₂O₂, although a primary substrate for HRP catalysis, can also function as a suicide substrate if no secondary reducing substrate (e.g. TMB, ABTS, etc.) is available. Wildtype recombinant HRP yields a H₂O₂ C₅₀ of 17 ±1 mM, which compares with previous published results of 60% activity in 25 mM (Arnold and Lin, 2000) under the same conditions. It should be noted that the H₂O₂ concentrations and incubation times are much smaller for regular rHRP catalytic assays, such as TMB (3 mM, <10 min) and ABTS (1mM, 20min) and where a secondary reducing substrate is present. Hence, no suicide inactivation occurs during these assays.

3.10.5.5 Kinetic Characterisation.

Recombinant wildtype HRP was analysed for kinetic constants using the traditional ABTS chromogenic substrate. ABTS is commonly used to measure steady-state kinetics in peroxidases due to the fact that it is a “poor” substrate and, hence, allows a slow colorimetric kinetic quantification. However, it should be noted that peroxidases do not follow traditional Michaelis-Menten kinetics; instead, apparent k_3 and K'_m values are recorded (Dunford, 1999). Initially, the experimental protocol was validated by comparison of plant HRP values derived from the traditional cuvette-based assay and the microtitre plate approach developed in this study. Previous results for plant HRP estimated apparent k_3 as 321 ± 28 s⁻¹, and an apparent K'_m of 1.92 ± 0.07 mM (D. O'Brien, unpublished). Very similar results were noted with the microtitre plate approach: the apparent k_3 was 333 ± 25 s⁻¹, whilst the apparent K'_m was 2.04 ± 0.06 mM. Using the same microtitre plate method the apparent k_3 for wildtype recombinant His-tagged HRP was calculated as 482 ± 12 s⁻¹, whilst the apparent K'_m was 0.093 ± 0.01 mM. These results compare well with previously reported apparent k_{cat} and apparent K_m values of 670 ± 12 s⁻¹ (Smith et al., 1992) and 0.103 ± 0.01 mM (Grigorenko et al., 1999) respectively. Other reducing substrates were utilised in additional kinetic investigations; however, several problems existed. Non-Michaelis-Menten kinetics occurred with TMB as the reducing substrate; however, this could be attributed to the fact that TMB is a very good peroxidase substrate and is turned over rapidly by the enzyme; thus, steady-state kinetics could not be analysed. Iodine was also assessed for Michaelis-Menten kinetic activity, however, a sigmoidal, as opposed to a Michaelian

curve was achieved (data not shown). The use of the iodine reaction with HRP is known to be proportional to the concentration of H₂O₂ and commonly referred to as enzyme-catalysed clock reaction (Dunford, 1999). The potassium ferrocyanide assay required 1 μM plant HRP per datum point (data not shown). These peroxidase concentrations could not be achieved by recombinant HRP expression, so attempts to measure rHRP ferrocyanide kinetics were abandoned.

3.10.5.6 Western Blot Analysis.

Western blot analysis was carried out on a purified sample of rHRP. Correct fusion of the His tag to the rHRP protein was confirmed by probing the transfer gel with an anti-His antibody. Western blotting also permitted rHRP molecular weight approximation. As outlined in Figure 3.40, the approximate size of rHRP was estimated as 34,000 Da. This mirrors the previously published approximation of 33,000 Da (Smith et al., 1990). A set of mutants (see Chapter 4) was also probed in a similar protocol to verify that mutagenesis does not interfere with His tag incorporation; all mutants tested generated a signal upon anti-His probing. Western blot analysis also verified the non-availability of the rHRP His tag when the protein is suspended a buffer without denaturants. No antibody signal was obtained from a similar experimental procedure utilising a native gel (SDS omitted).

Chapter Four.

Site-Directed Mutagenesis: Proximal Lysine Residues.

4.1 Introduction

The aim of the experiments described in this chapter was to identify, create and characterise site-specific mutants of the cloned HRP gene (see Chapter Three). The cloned HRP gene was also reverted to wildtype by a Pro to Ala mutation at residue 34. Key positions were identified with the aim of increasing the thermal, solvent and H₂O₂ stabilities of the recombinantly expressed HRP protein. The selection procedure was aided by prior knowledge of chemically stabilised plant HRP (O'Brien et al., 2001) and suitable replacement amino acids were determined. A simple, two-step mutagenic PCR strategy was employed to produce the mutants, which in turn were screened for the presence of an indicative altered restriction pattern. Mutants displaying this altered pattern were sequenced to confirm mutation and maintenance of gene integrity.

4.2 Identification of Key Amino Acid Residues.

The initial residues selected for mutation were all lysine residues, located at positions 174, 232 and 241. All lie on the outer proximal region of the HRP structure, and have previously been chemically modified to yield increased thermal and solvent stabilities. O'Brien and co-workers (2001) showed that ethylene-glycol *bis*(succinimidylsuccinate), or EG-NHS, crosslinks Lys 232 and Lys 241. Lys 174 was also modified, but without any crosslinking, possibly due to its increased distance (>16 Å) from another chemically-modifiable lysine. This lysine modification yielded a four-fold increase in stability at 65 °C. Note that stabilisation does not require crosslinking of amino acids: neutralisation of lysine charges (Miland et al., 1996b) or their reversal (O'Brien et al., 2003) also stabilised the HRP molecule. These three Lys residues were mutated to small, hydrophobic, uncharged alanines; medium sized, hydrophilic, uncharged asparagines; medium sized, negatively charged, hydrophilic glutamic acids and bulky aromatic, hydrophobic phenylalanines. Introduction of the alanine residue was anticipated to develop a cavity whilst simultaneously neutralising the lysine's positive charge. Insertion of an asparagine was intended to neutralise the lysine charge whilst approximately maintaining the space-fill characteristic. Charge reversal, whilst maintaining the space-fill, was predicted from a glutamic acid substitution. Another indirect role of charge reversal at positions 232 and 241 could be an increase of calcium ion retention. Based on previous findings, the latter could lead to increased stability (Tams and Welinder, 1998). A second round of mutagenesis focussed on double lysine

and glutamic acid mutations in the same region, as suggested by the outcome of the single lysine replacements.

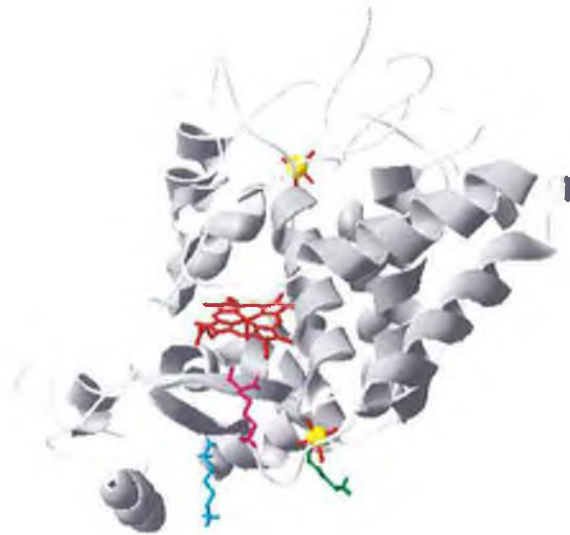


Figure 4.1: Location of key amino acid residues, Lys 174 —, Lys 232 —, Lys 241 —. Also indicated are the heme group — and the two calcium ions —.

4.1 Optimisation of Mutagenic PCR.

Initially, mutagenic PCR was problematic, with low mutagenic efficiencies achieved. This was possibly due to primer-dimer formation between the two highly homologous mutagenic primers. This problem was circumvented by employing a two-stage mutagenic PCR protocol similar to that described by Wang and Malcom (1999). In their approach, the double strands of the wildtype template vector are treated as two separate PCRs (see Figure 4.2).

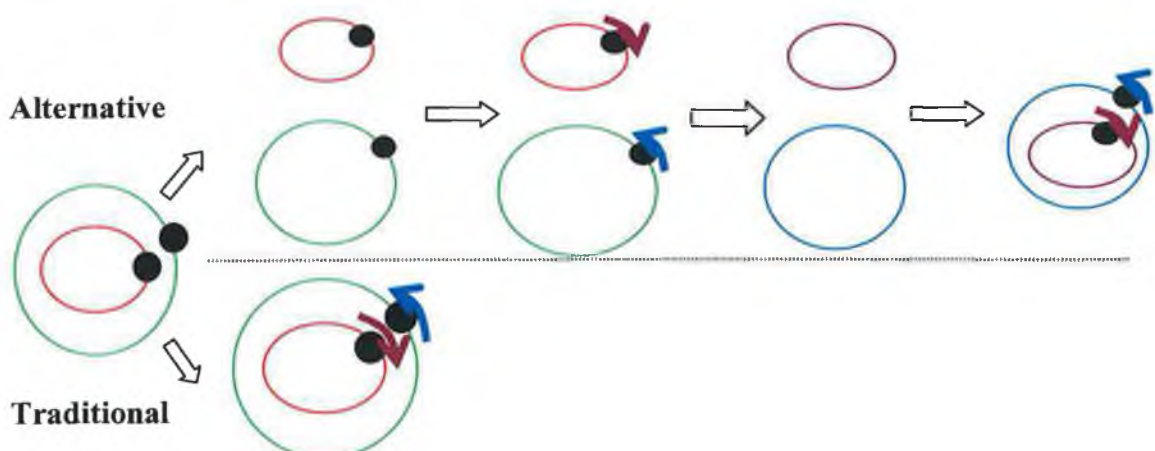


Figure 4.2: Schematic of alternative mutagenesis approach. In the traditional approach, the wildtype vector provides the template for the mutagenic primers, represented by blue and maroon arrows. In the alternative approach, however, the double strands of the wildtype template vector are treated as two separate PCRs. This approach provides more copies of the mutant strands (signified in blue and purple respectively) than the parent wildtype strands. The mutagenic primers will have a higher affinity for the newly-synthesised strands than the parent strands, as the primer is completely homologous with the newly synthesised strands.

4.4 Wildtype reversion mutation.

The cloned HRP gene contained a point mutation, A34P that was present in the gene prior to cloning (see Figure 3.11). This was reverted to wildtype prior to any further mutagenesis studies to allow direct comparison between plant and wildtype recombinant HRP. Mutational primers were designed to alter codon 34 from CCA to GCT; a silent mutation (GATCC) was also incorporated. The latter introduced a *BamH*I recognition site within thirteen basepairs of the reversion and, hence, clones subject to *BamH*I restriction would likely contain the desired P34A back mutation.



Figure 4.3: Diagrammatic representation of wildtype reversion mutation. Mutation is coloured in red, while blue indicates the silent mutation incorporated close to the desired mutants; the latter introduces a new selective restriction site. The reading frame is indicated by the underline.

Mutagenesis was carried out on pQE_PelB_HRP_His as outlined in Section 2.21.1. The primers utilised were pBR_I P34A and the conditions were as per Section 2.22. The reversion was confirmed by commercial sequencing.

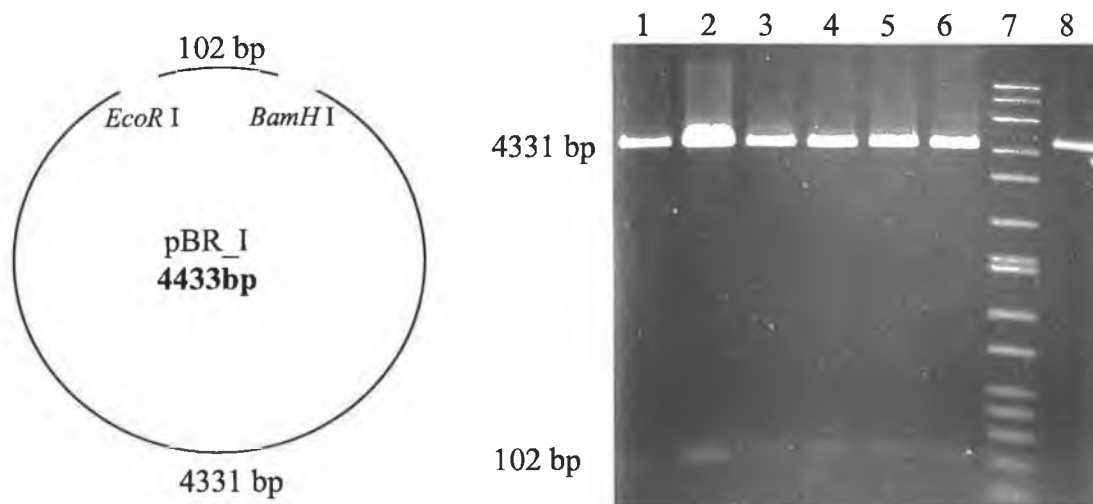


Figure 4.4: Part A represents the expected restriction pattern of pQE_PelB_HRP_His reverted to wildtype by a P34A mutation. *In silico* analysis predicts two bands due to the presence of the mutant *BamH*I site, one band of approximately 100 basepairs and another of 4.3 kilobases. Part B is the mutant plasmid viewed after restriction and electrophoresis through 1% w/v agarose. The approximate band sizes correspond to the predicted pattern. Lanes 1 to 6 contain different clones screened, lane 7 contains Sigma size markers and lane 8 contains template DNA.

4.5 Designed Mutations.

The designed primers (outlined in Section 2.21.1) incorporated the mismatch basepairs that would generate the desired mutation upon translation. The codons were altered from AAG to **GCG, GAG, AAT** for the Lys 174 mutations, from AAG to **GCG, GAG, AAT, TTT** for the Lys 232 mutations, from AAA to **GCA, GAA, AAT, TTT** for the Lys 241 mutations and from **GAG to CAG and GAG to AAC** for Glu 238 and 239 mutations respectively. A silent mutation was also incorporated into each mutagenic primer design: (i) the silent mutation (TGGCCA) introduced a *Msc* I recognition site within fourteen basepairs of the Lys 174 mutations, whilst (ii) the silent mutation (CTCGAG) introduced a *Xho* I recognition site within fifteen basepairs of the Lys 232, 241 and Glu238, 239 mutations respectively. Hence, clones could be screened for these altered restriction sites, which would indicate the presence of the desired mutation.

4.5.1 Lysine 174 Mutations.

Computer-aided modelling was initially utilised to view the mutations *in silico*. The HRP crystal structure co-ordinates (Accession Number 1ATJ) were downloaded from the Protein Data Bank (<http://www.rcsb.org/pdb>). Computer simulations, using *DeepView*TM mutant modelling, suggested that mutations would still allow the protein to fold correctly. Site-directed mutagenesis was carried out on pBR_I as outlined in Section 2.21.1. The primers utilised were pBR_I K174A, pBR_I K174E, pBR_I K174N respectively and the conditions were as per Section 2.22. Mutants were screened with an *Msc* I / *Hind* III double digest as outlined in Figure 4.6. Successful inclusion of the silent mutation would result in a differential cutting pattern (Figure 4.7) that would allow a single clone to be selected for sequence confirmation.

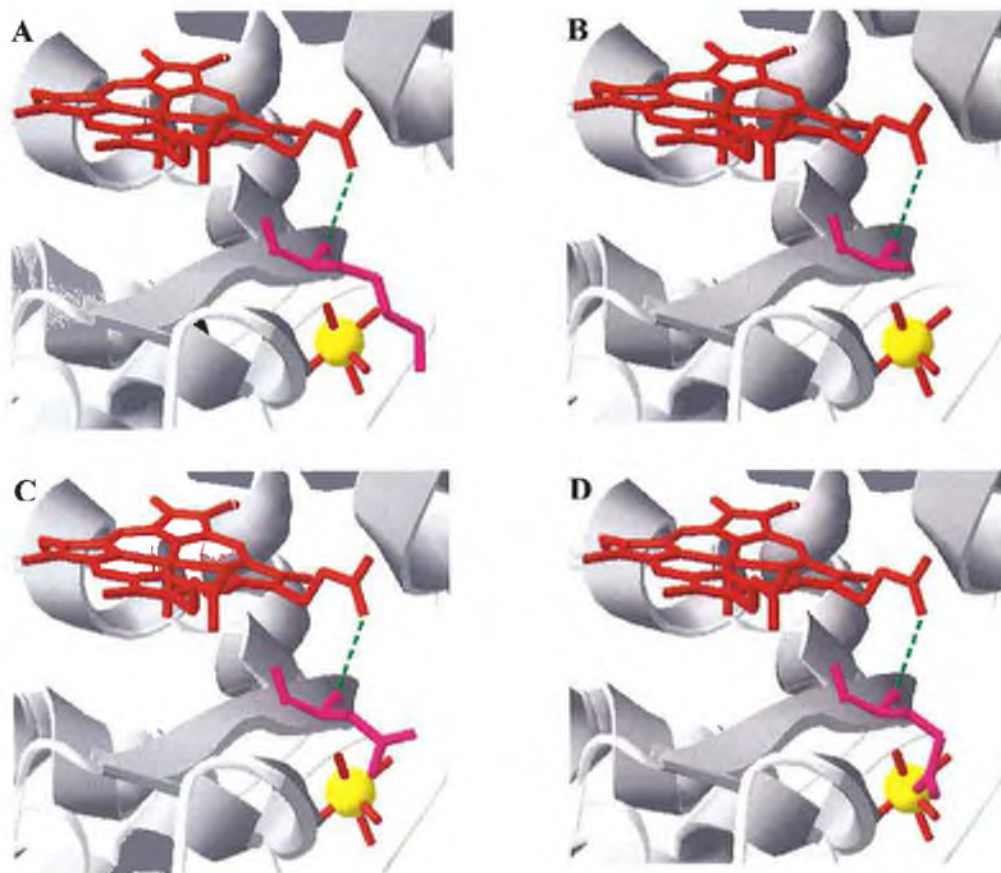


Figure 4.5: DeepView™ modelling of Lysine 174 mutations. Location of native lysine residue (—) in relation to heme group (—) and calcium ion (—) is depicted in picture A, whilst the various mutants are shown in parts B (Ala), C (Asn) and D (Glu). Computer-modelled predicted interactions are shown as dotted lines.

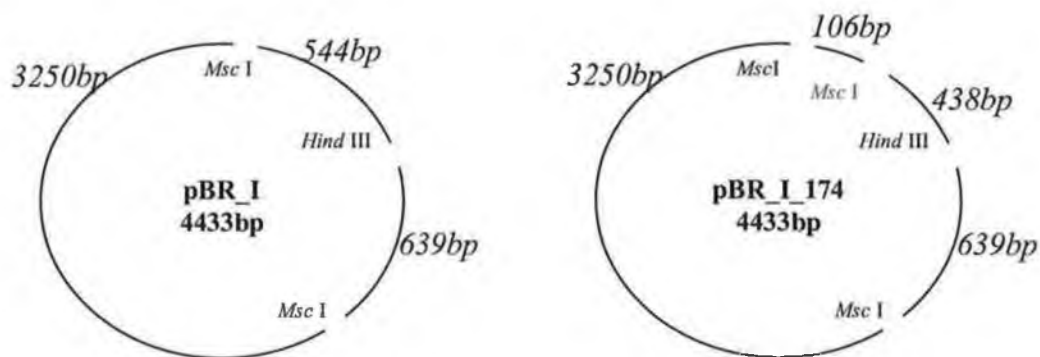


Figure 4.6: Diagrammatic representation of the expected restriction pattern of pBR_I which has been mutated at the 174 lysine residue. *In silico* analysis predicts four bands due to the presence of the silent mutant *Msc* I site. The first band is approximately 3250 basepairs, the second 639 basepairs, the third 438 basepairs and finally the fourth 106 bp.

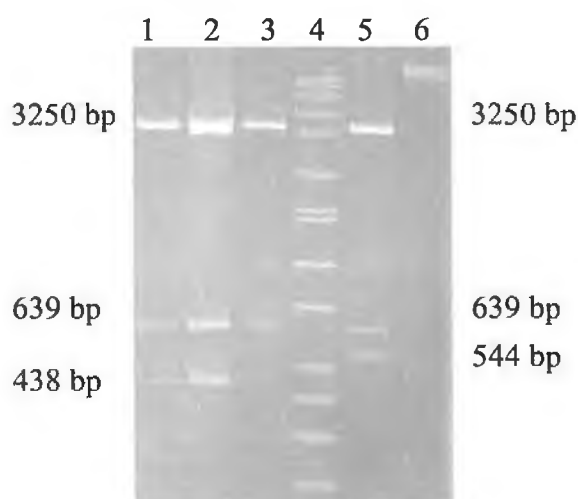


Figure 4.7: The mutant plasmids, pBR_I_174Ala (lane one), pBR_I_174Glu (lane two) and pBR_I_174Asn (lane three), viewed after restriction with *Msc* I and *Hind* III, and electrophoresis through 1% w/v agarose. The approximate band sizes correspond to the predicted pattern, although the 106 bp fragment is not visible, possibly due to poor ethidium bromide staining. Non-mutated wildtype pBR_I, digested with *Msc* I and *Hind* III and non-digested non-mutated pBR_I, are run in lanes five and six respectively as controls. Lane four contains Sigma size markers.

4.5.2 Lysine 232 Mutations.

As previously outlined, computer-generated graphics were used to model the prospective Lysine 232 mutations (Figure 4.8). Mutagenesis was performed as outlined in Section 2.21.1. The primers utilised were pBR_I K232F, pBR_I K232A, pBR_I K232E, pBR_I K232N and the conditions used were as per Section 2.22. Mutants were screened with an *Xho* I single digest as outlined in Figure 4.9. Successful inclusion of the silent mutation results in a differential cutting pattern, permitting a single clone to be selected for sequence confirmation (Figure 4.10).

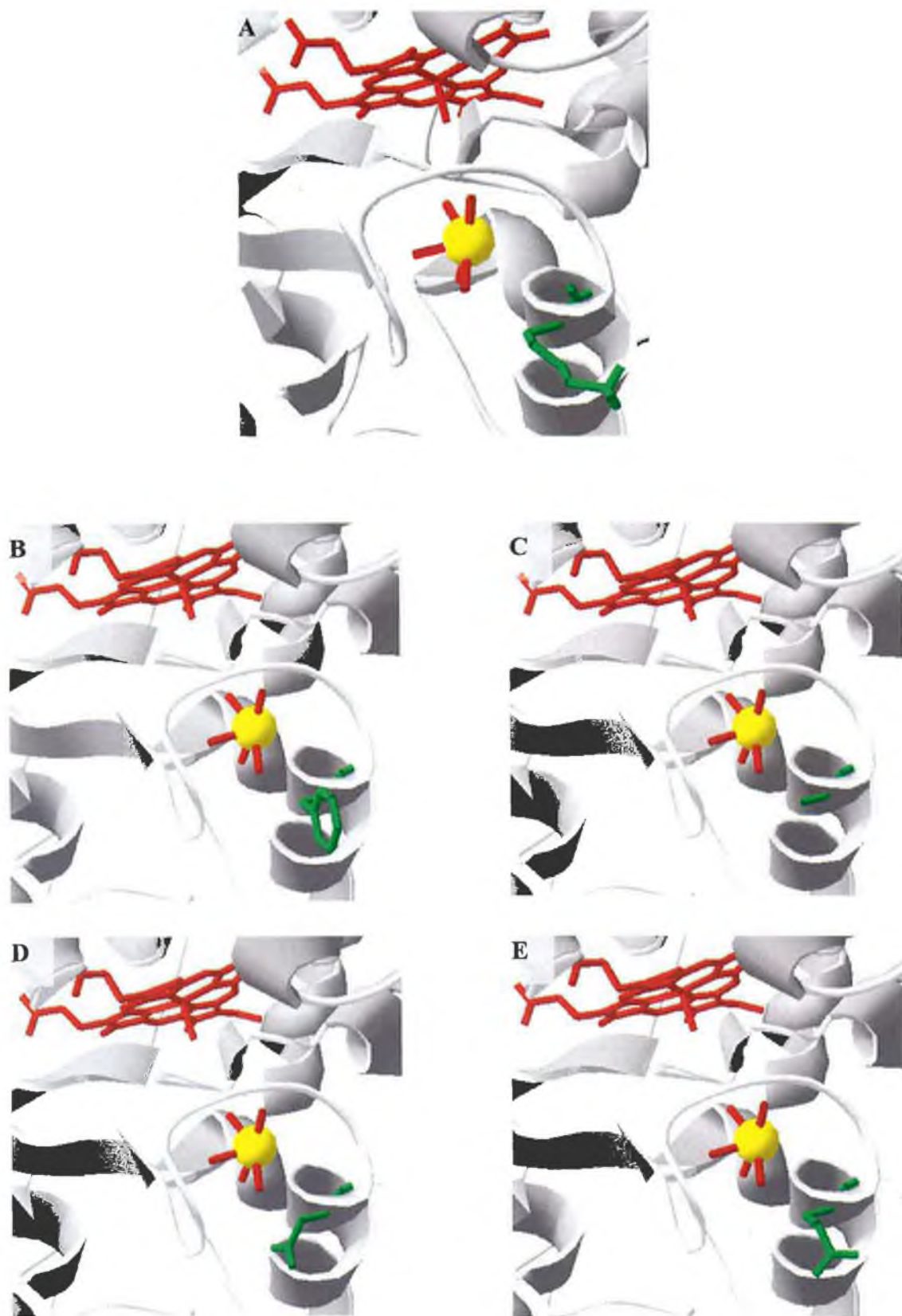


Figure 4.8: DeepView™ modelling of Lysine 232 mutations. Location of native lysine residue (A) and the various lysine mutant residues (—) in relation to heme group (—) and calcium ion (-+ -) are depicted in pictures B (Phe), C (Ala), D (Asn) and E (Glu).

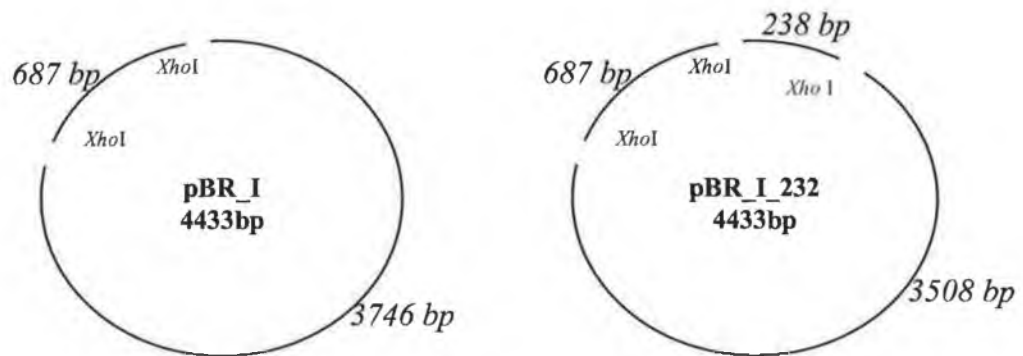


Figure 4.9: Diagrammatical representation of the expected restriction pattern of pBR_I mutated at the 232 lysine residue. *In silico* analysis predicts three bands, due to the presence of the silent mutant's new *Xho* I site. The first band is approximately 3508 basepairs, the second 687 basepairs and the third 238 basepairs.

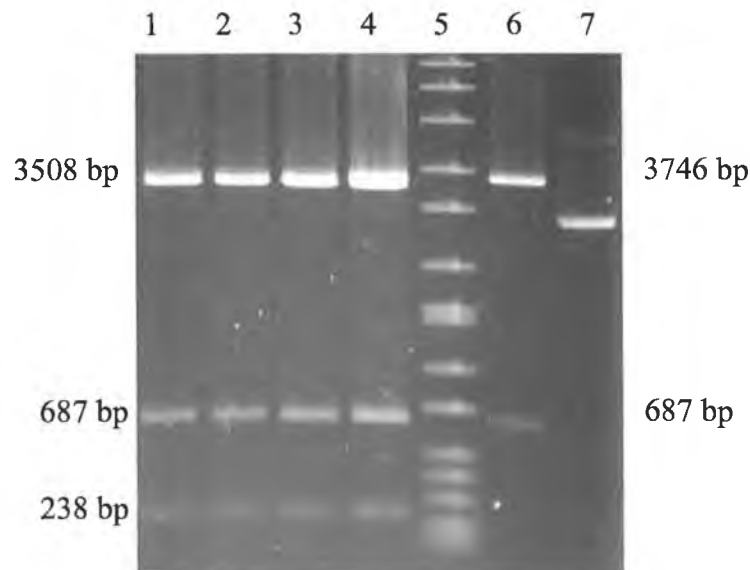


Figure 4.10: Mutant plasmids pBR_I_232Ala (lane one), pBR_I_232Glu (lane two), pBR_I_232Asn (lane three) and pBR_I_232Phe (lane four), viewed after restriction with *Xho* I and electrophoresis through 1% w/v agarose. The approximate band sizes correspond to the predicted pattern. Non-mutated wildtype, pBR_I, digested with *Xho* I, and non-digested non mutated pBR_I, are run in lanes six and seven respectively as controls. Lane five contains Sigma size markers.

4.5.3 Lysine 241 Mutations.

*DeepView*TM-assisted modelling of the Lysine 241 mutants (Figure 4.11) indicated that mutation would still produce a fully functional protein. Mutagenesis was carried out on pBR_I as outlined in Section 2.21.1. The primers utilised were pBR_I K241F, pBR_I K241A, pBR_I K241E and pBR_I K241N respectively and the conditions were as per Section 2.22. Mutants were screened with an *Xho* I single digest as outlined in Figure

4.12. Successful inclusion of the silent mutation results in a differential cutting pattern, permitting selection of a single clone for sequence confirmation (Figure 4.13).

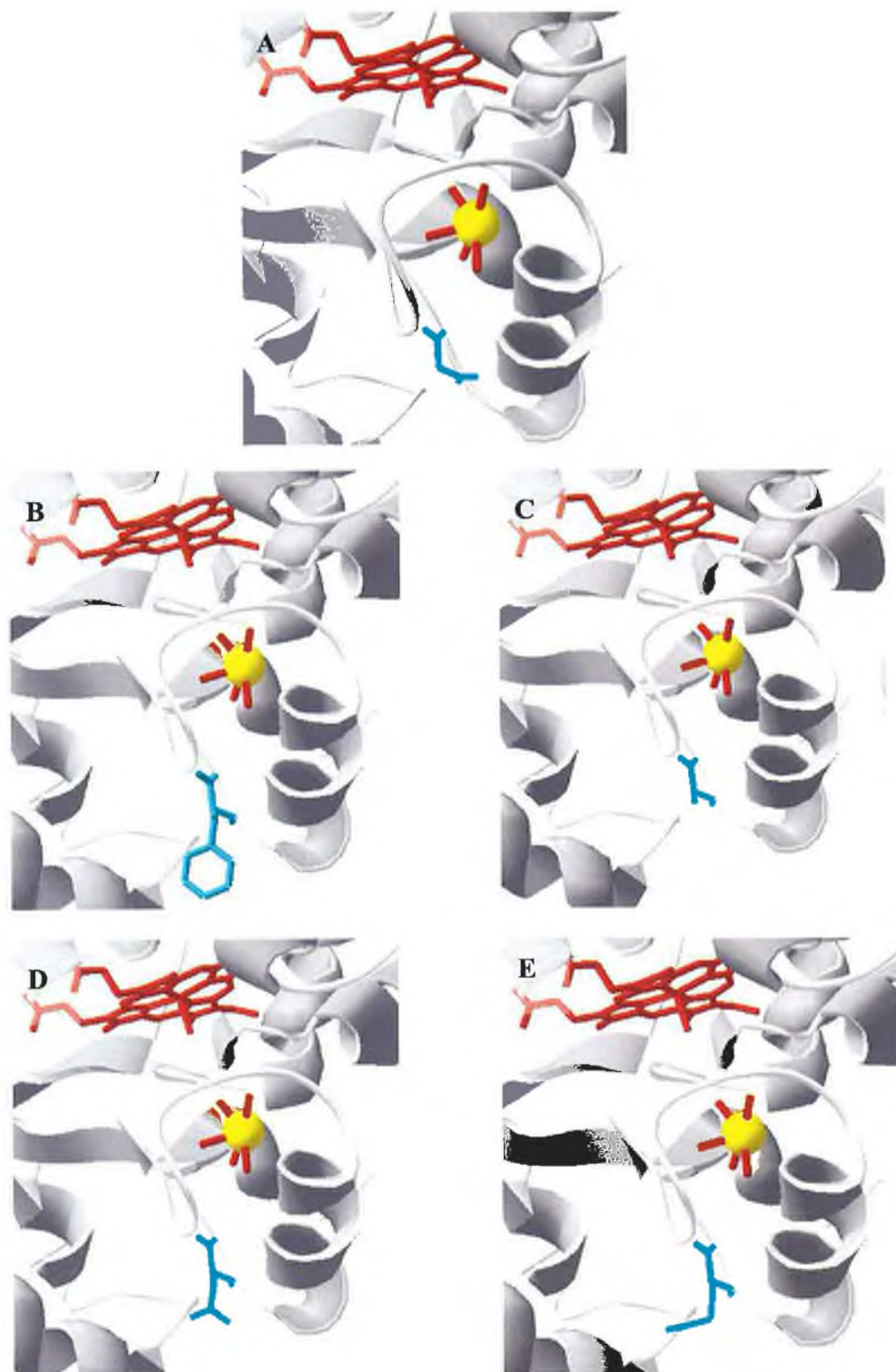


Figure 4.11: DeepView™ modelling of Lysine 241 mutations. Location of native lysine residue (A) and the various lysine mutant residues (—) in relation to heme group (—) and calcium ion (—) are depicted in pictures B (Phe), C (Ala), D (Asn) and E (Glu).

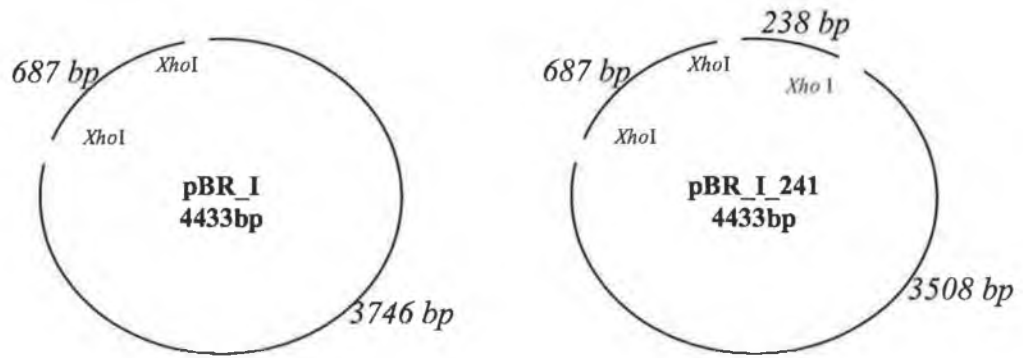


Figure 4.12: Diagrammatical representation of the expected restriction pattern of pBR_I mutated at the 241 lysine residue. *In silico* analysis predicts three bands due to the presence of the silent mutant's new *Xho* I site. The first band is approximately 3508 basepairs, the second 687 basepairs and the third 238 basepairs.

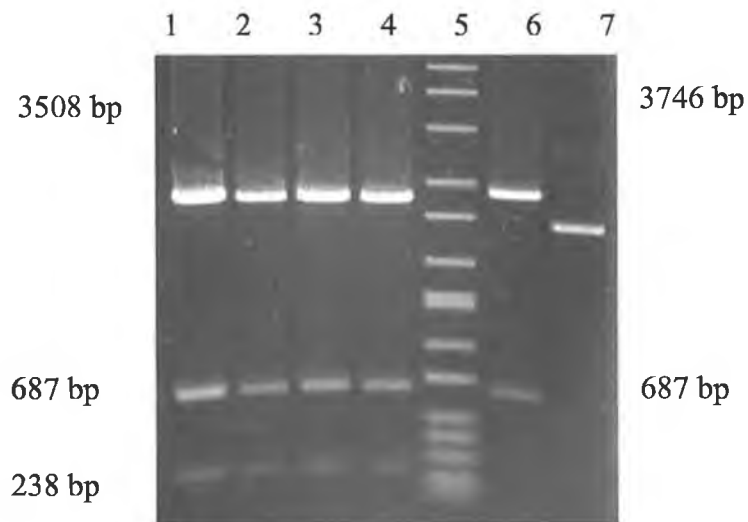


Figure 4.13: Mutant plasmids pBR_I_241Ala (lane one), pBR_I_241Glu (lane two), pBR_I_241Asn (lane three) and pBR_I_241Phe (lane four), viewed after restriction with *Xho* I and electrophoresis through 1% w/v agarose. The approximate band sizes correspond to the predicted pattern. Non-mutated wildtype pBR_I, digested with *Xho* I and non-digested non-mutated pBR_I are run in lanes six and seven respectively as controls. Lane five contains Sigma size markers.

4.5.4 Glutamic Acid (238/239) Mutations.

Three dimensional *in silico* analysis of the glutamic acid (238/239) mutations (Figures 4.14 and 4.15) suggested that mutagenesis would not grossly affect protein tertiary structure. Mutagenesis was carried out on pBR_I and pBR_I_241E as outlined in Section 2.21.1. The primers utilised were pBR_I E238Q and pBR_I E239N and conditions were as per Section 2.22. Mutants were screened with an *Xho* I single digest (Figure 4.16), with successful inclusion of the silent mutation resulting in a differential cutting pattern (Figure 4.17).

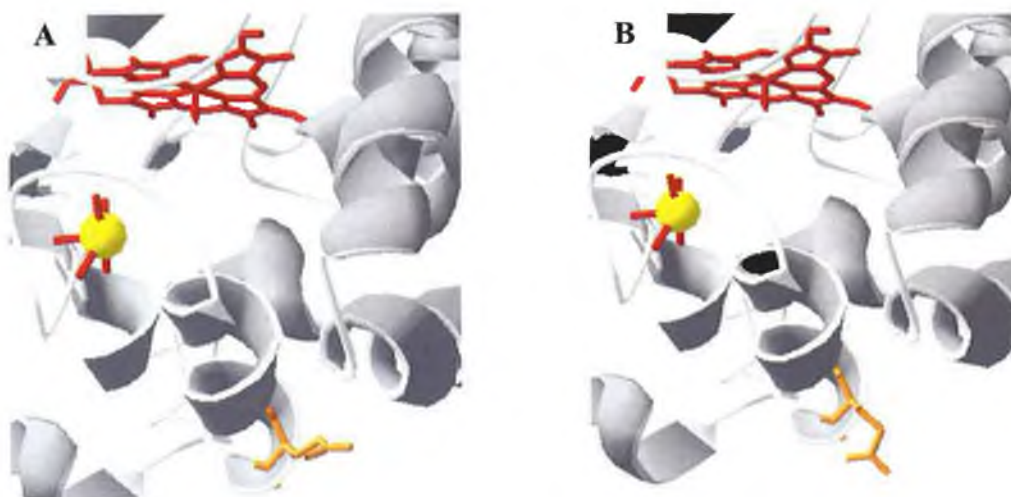


Figure 4.14: DeepView analysis of the Glutamic Acid 238 (A) to Glutamine mutation (B). The mutant is visualised in its most energy stable conformation, as calculated by the DeepView™ software. The heme group is coloured red, the calcium ion is coloured in yellow whilst the mutation is coloured in purple.

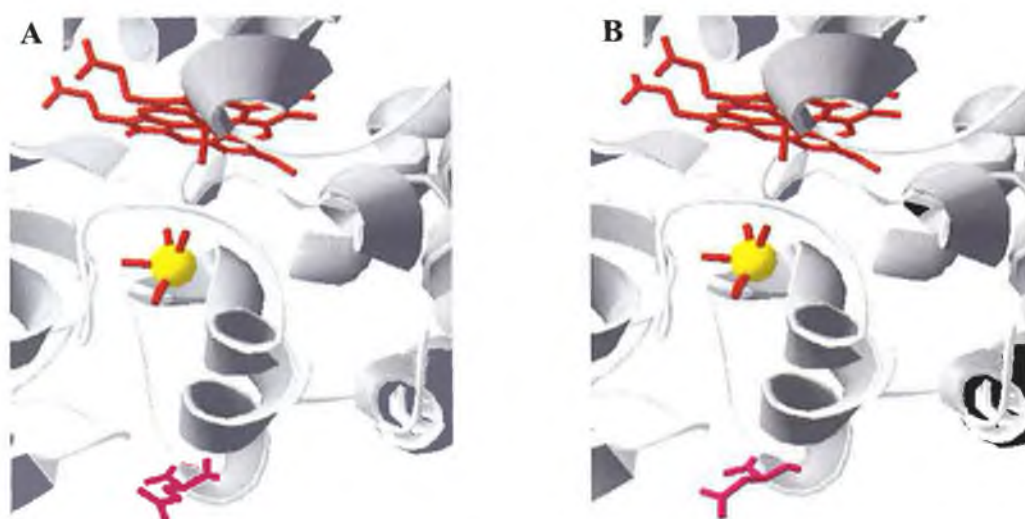


Figure 4.15: DeepView analysis of the Glutamic Acid 239 (A) to Asparagine mutation (B). The mutant is visualised in its most energy stable conformation, as calculated by the DeepView™ software. The heme group is coloured red, the calcium ion is coloured in yellow whilst the mutation is coloured in purple.

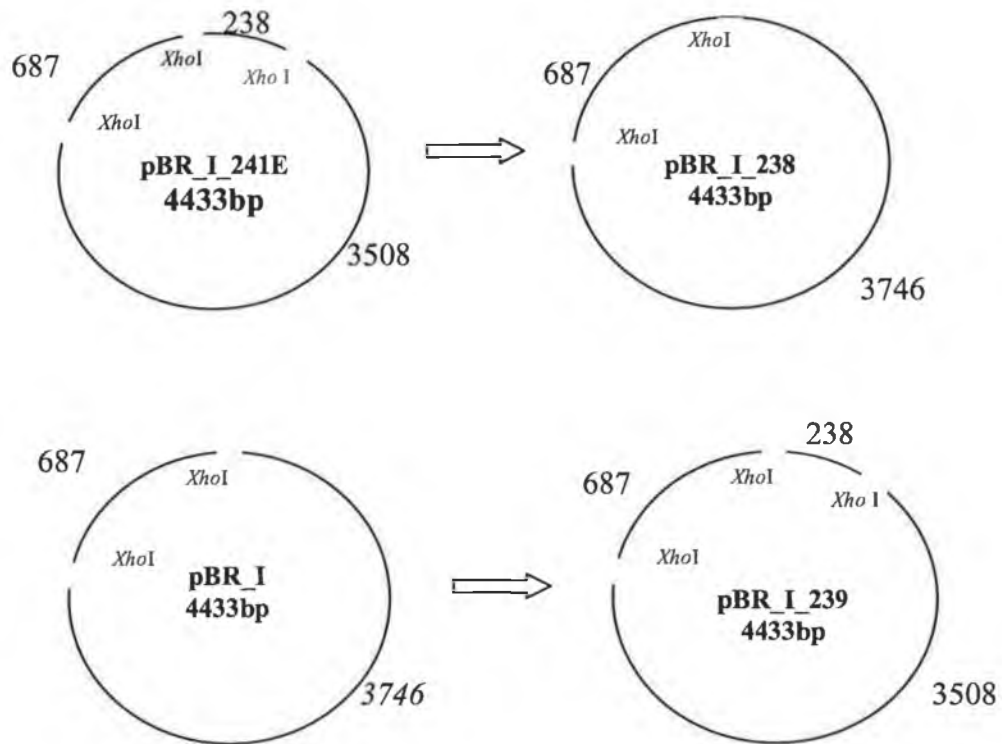


Figure 4.16: A diagrammatical representation of the expected restriction pattern of pBR_I mutated at position 238 or 239. For the pBR_238 mutation, *in silico* analysis predicts two bands due to removal of the third mutant *Xho* I site: one band of approximately 3746 basepairs and another of 687 basepairs. For the pBR_239 mutation, *in silico* analysis predicts three bands due to the introduction of a third *Xho* I site, one band of approximately 3508 basepairs, another of 687 basepairs and a final band of 238 basepairs.

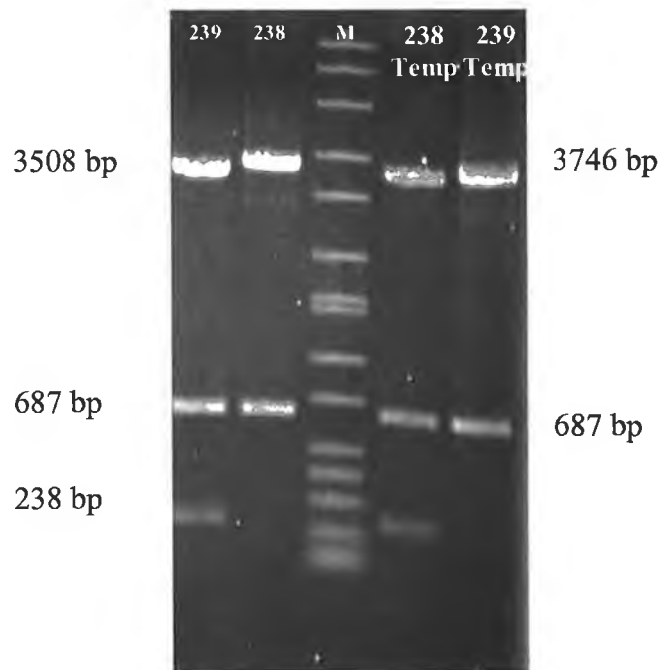


Figure 4.17: The mutant plasmids (E238Q and E239N) viewed after restriction and electrophoresis through 1% w/v agarose. In this mutagenesis approach a different plasmid template was used for each mutant, as indicated by "Temp". The approximate band sizes correspond to the predicted patterns.

4.5.5 Double Lysine (232/241) Mutations.

Double lysine (232/241) mutations were modelled utilising *DeepView*TM (Figure 4.18). Mutagenesis was carried out on pBR_I as outlined in Section 2.21.1. The primers utilised were pBR_I K232/241N, pBR_I K232/241Q and pBR_I K232F/241N and conditions were as per Section 2.22. Mutants were screened with an *Xho* I single digest as outlined in Figure 4.19. Successful inclusion of the silent mutation results in a differential cutting pattern permitting selection of a single clone for sequence confirmation (Figure 4.20).

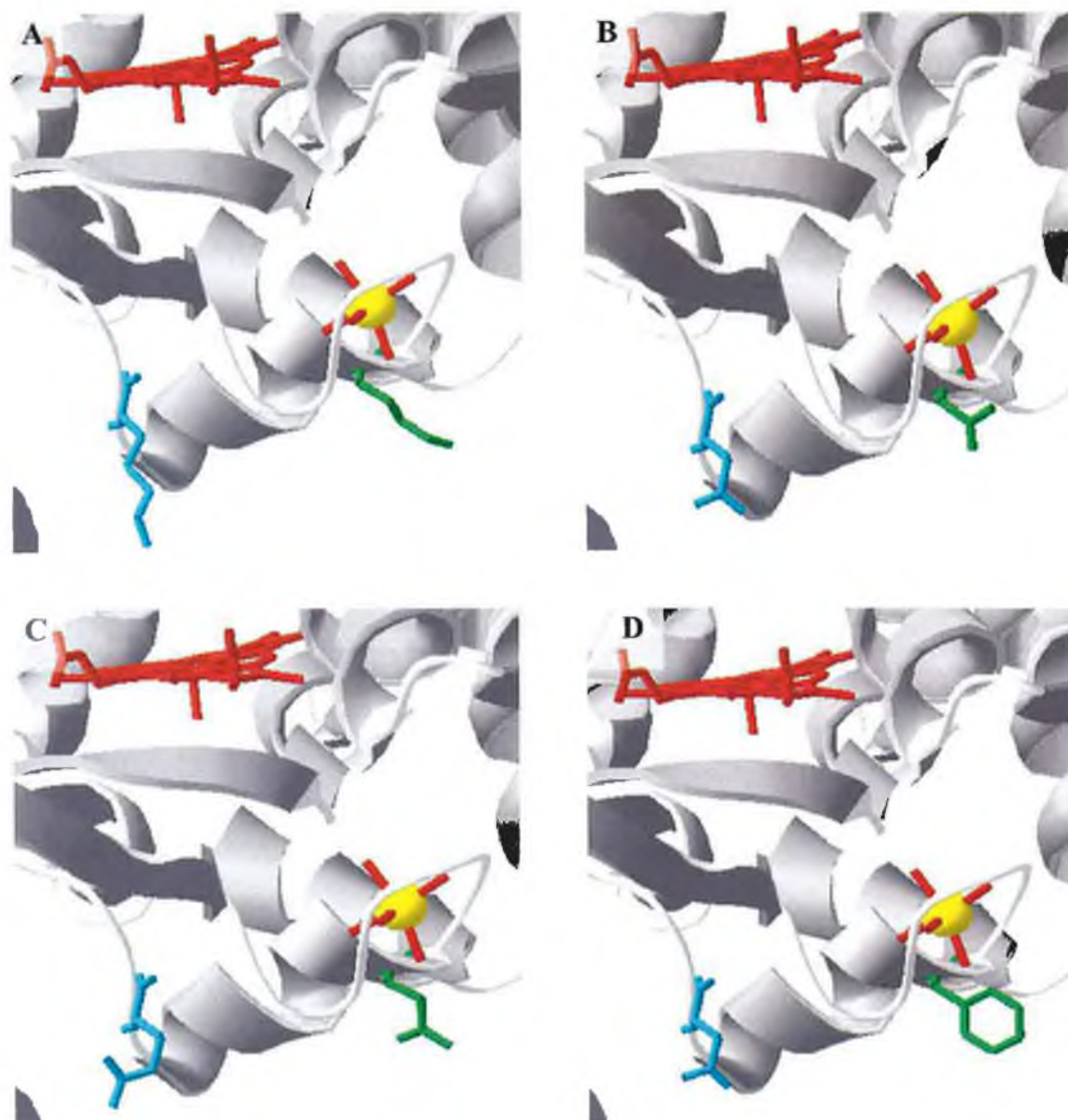


Figure 4.18: *DeepView*TM modelling of Lysine 232/241 double mutations. Location of native lysine residue (232, — and 241, —) in relation to heme group (—) and calcium ion (—) is depicted in picture A, whilst the various mutants are shown in parts B (232/241Asn), C (232/241Gln) and D (232Phe/241Asn).

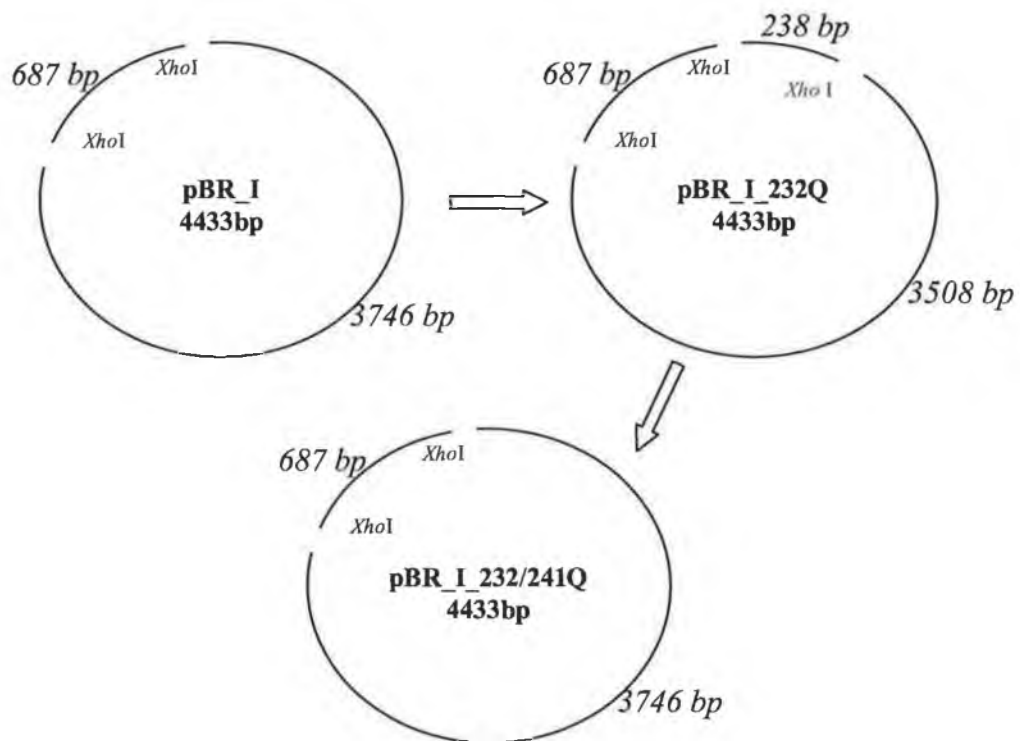


Figure 4.19: Diagrammatic representation of the expected restriction pattern of pBR_I mutated at the 232 and 241 lysine residues. For the intermediate single mutant, *in silico* analysis predicts three bands due to the presence of the silent mutant *Xho* I site. The first band is 3508 basepairs, the second 687 basepairs and the third 238 basepairs. The final double mutant construct removes the third diagnostic *Xho* I site and two bands are predicted, 3746bp and 687bp, similar to pBR_I.

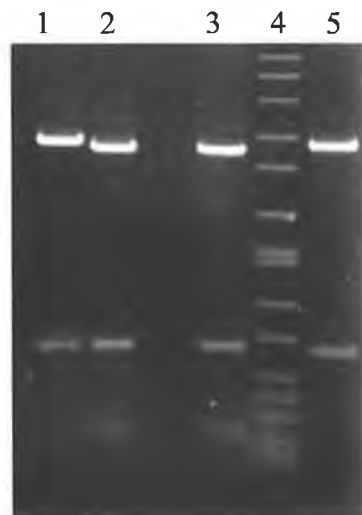


Figure 4.20: The mutant plasmids pBR_I_232/241Gln (lane one), pBR_I_232Gln (lane two) and pBR_I_232/241Asn (lane three) viewed after restriction with *Xho* I and electrophoresis through 1% w/v agarose. The approximate band sizes correspond to the predicted pattern. Non-mutated wildtype pBR_I, digested with *Xho* I was included in lane five as a control. Lane four contains Sigma size markers.

4.5.6 Sequencing of mutants.

Single mutants were selected for sequencing via a restriction digest screening methodology as outlined in Sections 4.5.1 to 4.5.4. Selected plasmids were prepared by the Gene Elute™ method, Section 2.8.3, and sent to MWG Biotech or Fusion Antibodies Ltd for sequencing by the di-deoxy sequencing method. Results were obtained via e-mail and processed through various bioinformatic packages to confirm correct reading frame of clone, suitable mutation and maintenance of gene integrity. The results are outlined in Figure 4.21.

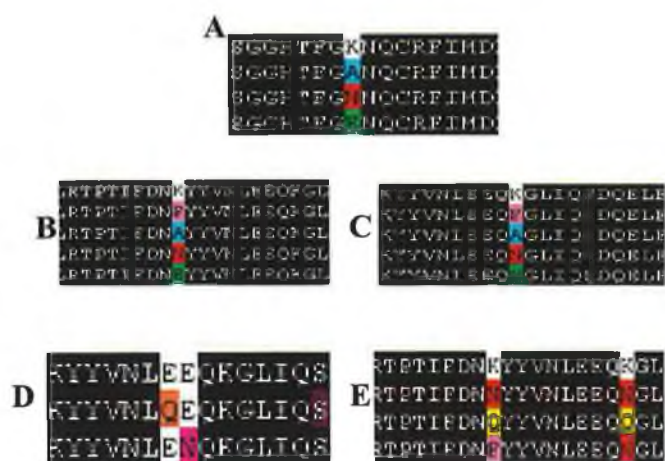


Figure 4.21: Alignment of lysine mutations with wildtype HRP. The sequences show total identity, with the exception of the desired mutation. A depicts K174 mutations; B, K232 mutations; C, K241 mutations; D, E238 and E239 mutations; and E, K232 and K241 double mutations.

4.6 Characterisation of Single Mutants.

4.6.1 Determination of Single Mutants' Concentrations.

Single mutants were individually expressed in 500 mL shake culture flasks (as previously described, see Section 2.24.4) and were purified via optimised nickel affinity chromatography (Section 2.25). Once expressed and purified (typical specific activity of $\sim 7.5 \times 10^{-3} \mu\text{mol}\cdot\text{min}\cdot\text{mg}^{-1}$), the μM concentration of HRP was calculated as per Section 2.29, with the results outlined in Table 4.1.

Table 4.1: Absorbance at 403nm for all lysine mutant forms of rHRP. rHRP concentrations were then calculated using the Beer-Lambert Law, and the rHRP extinction coefficient, $100\text{mM}^{-1}\text{cm}^{-1}$ (Hiner et al., 1995). Protein concentrations were experimentally determined using the BCA assay.

Mutant	Abs 403nm	rHRP (μM)	Protein Conc ($\text{mg}\cdot\text{ml}^{-1}$)	Heme/Protein Ratio
K174N	0.050	1.03	0.645	0.054
K174E	0.026	0.54	0.441	0.042
K174A	0.175	3.62	0.708	0.173
K232N	0.051	1.05	1.182	0.030
K232E	0.182	3.76	1.353	0.094
K232A	0.066	1.36	0.807	0.057
K232F	0.025	0.52	0.165	0.107
E238Q	0.062	1.28	0.320	0.136
E239N	0.013	0.27	0.780	0.012
K241N	0.113	2.33	0.909	0.087
K241E	0.180	3.72	2.163	0.058
K241A	0.089	1.83	1.521	0.041
K241F	0.031	0.64	0.281	0.077

Protein concentrations were equalised for all thermal and organo tolerance assays, whilst concentrations of active rHRP were equalised for all kinetic analysis and H_2O_2 stability studies.

4.6.2 Single Mutant Thermal Tolerance.

All thermal tolerance assays were carried out as per Section 2.31, with a final protein concentration of $100 \mu\text{g.mL}^{-1}$ in the reaction solution. Thermal profiles (Figures 4.22 to 4.25) and thermal inactivations (Figure 4.26) were produced for each of the mutant forms, in triplicate, using recombinant wildtype as a reference. T_{50} values for each mutant are tabulated in Table 4.2

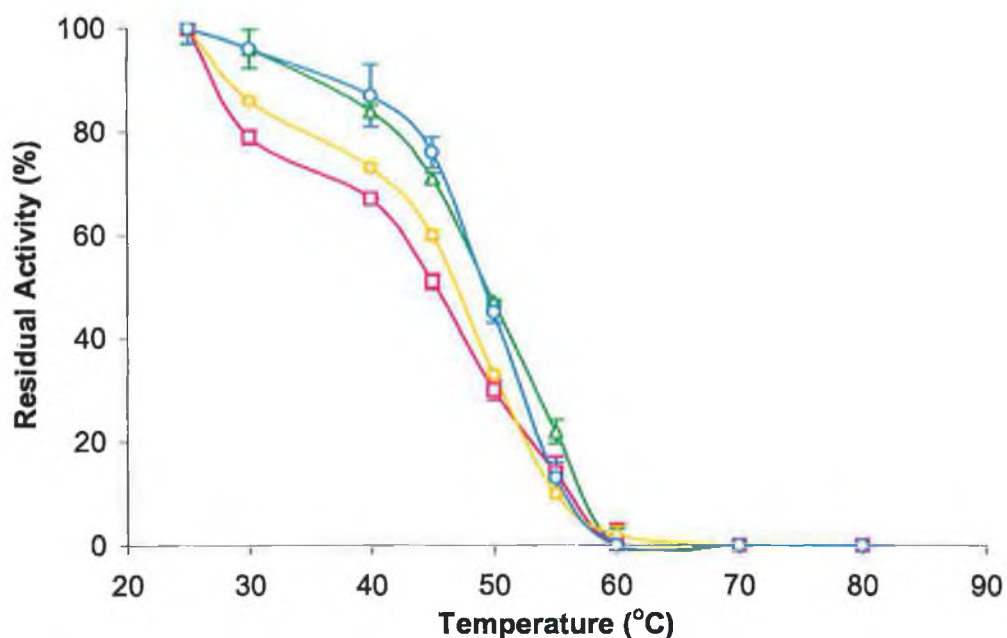


Figure 4.22: Thermal profile of Lysine 174 mutants, Δ K174A, \square K174E, \diamond K174N, \circ WT.

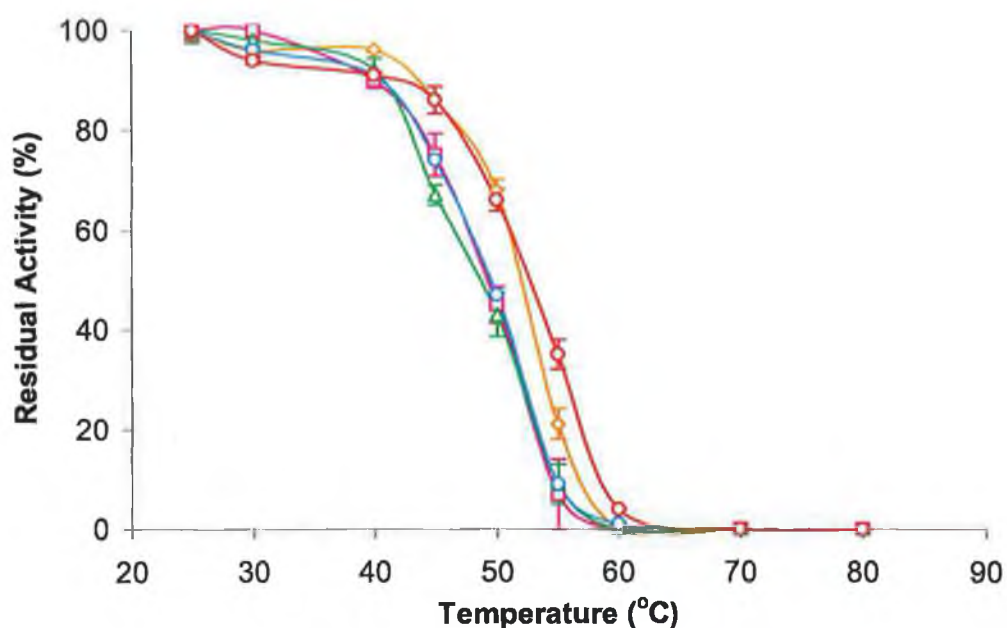


Figure 4.23: Thermal profile of Lysine 232 mutants, Δ K232A, \square K232E, \diamond K232N, \circ K232F, and \circ WT.

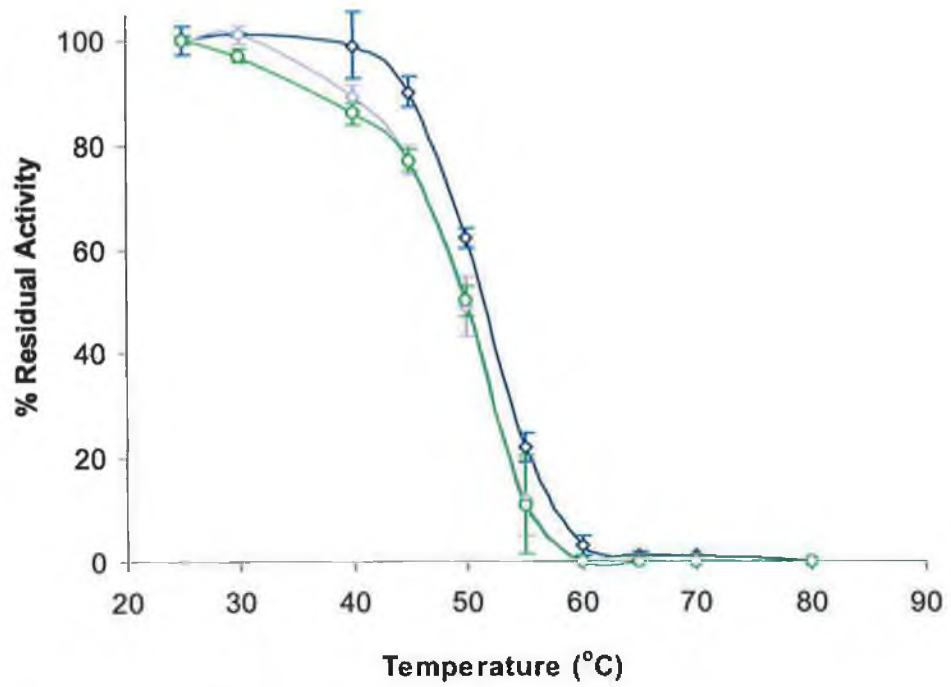


Figure 4.24: Thermal profile of \square E238Q, \triangle E239, \circ -WT.

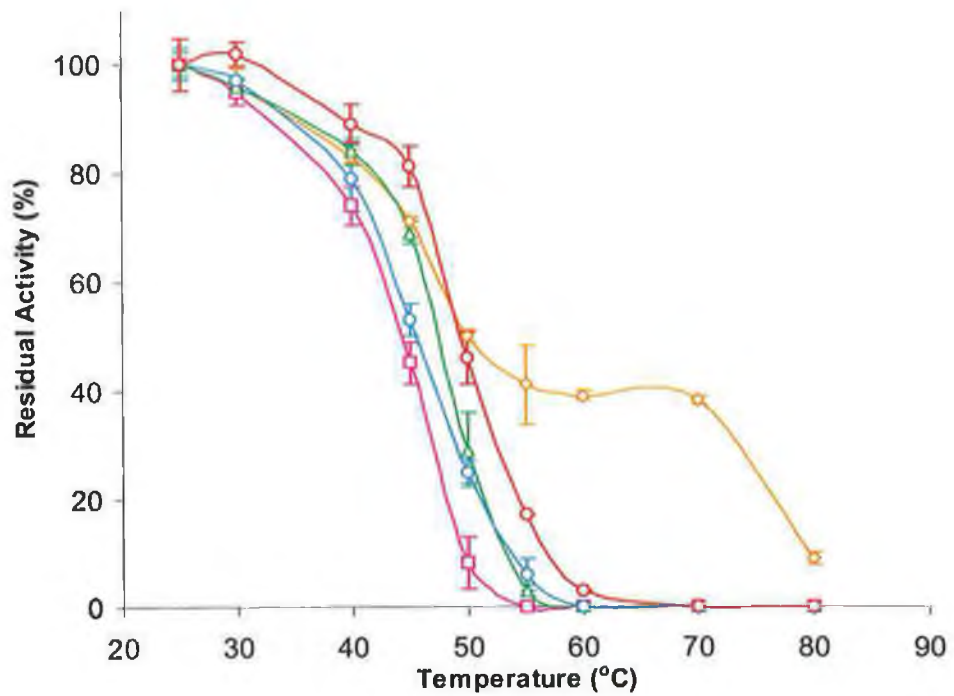


Figure 4.25: Thermal profile of Lysine 241 mutants, \triangle K241A, \square K241E, \diamond K241N, \circ K241F, \circ WT

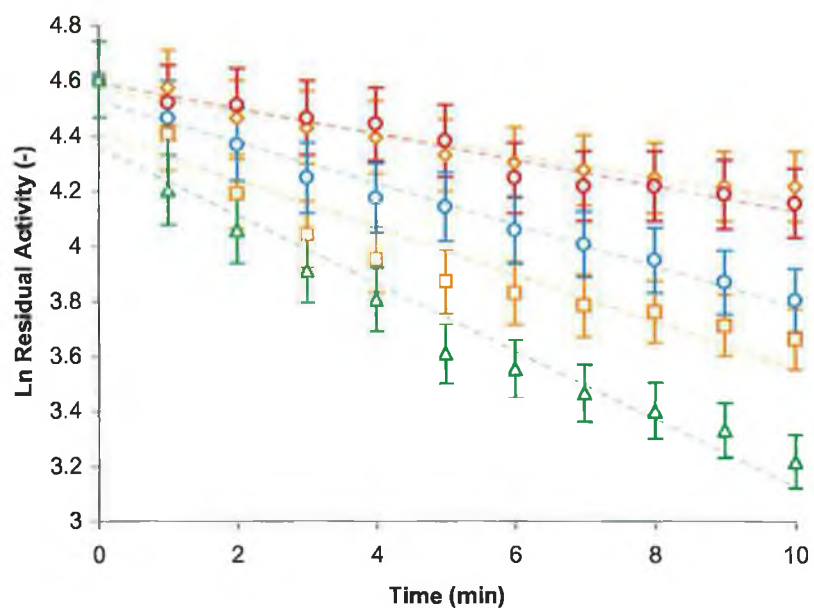


Figure 4.26: Semi-log plot of a selection of single lysine mutants' thermal inactivation at 50°C; Δ K174A, \square K174N, \diamond K232N, \circ K232F, \circ Wildtype.

Apparent half-lives for each of the mutants at 50°C were calculated, as outlined in Section 2.33, with the results tabulated in Table 4.2.

Table 4.2: Rate of inactivation at 50°C and calculated apparent half-life ($t_{1/2}$) for each lysine mutant

Mutant	T_{50} (°C)	Rate Const (min^{-1})	SD (%)	$t_{1/2}$ (min)	r^2 Value
Wildtype	50	5.59×10^{-2}	± 6	12.4	0.98
K174N	47	8.68×10^{-2}	± 10	8.0	0.94
K174E	46	1.02×10^{-1}	± 3	6.8	0.99
K174A	50	6.77×10^{-2}	± 7	10.2	0.98
K232N	52	3.12×10^{-2}	± 7	22.3	0.97
K232E	50	5.95×10^{-2}	± 8	12.0	0.96
K232A	50	9.21×10^{-2}	± 8	7.5	0.96
K232F	52	2.94×10^{-2}	± 8	23.9	0.92
E238Q	51	9.21×10^{-2}	± 11	7.5	0.97
E239N	50	5.74×10^{-2}	± 11	12.1	0.95
K241N	53	Not 1 st Order	-----	-----	-----
K241E	47	Not 1 st Order	-----	-----	-----
K241A	50	1.13×10^{-1}	± 10	6.1	0.93
K241F	53	6.10×10^{-2}	± 9	11.3	0.97

4.6.3 Single Mutant Organic Solvent Tolerance.

All organic solvent tolerance assays were carried out as per Section 2.34, with a final protein concentration of $100 \mu\text{g.mL}^{-1}$ in the reaction solution. Solvent tolerance profiles were produced for each of the mutant forms, in triplicate, using recombinant wildtype as a reference. All standard errors were within $<5\%$ of the triplicate average reading, with the errors bars omitted for the sake of clarity.

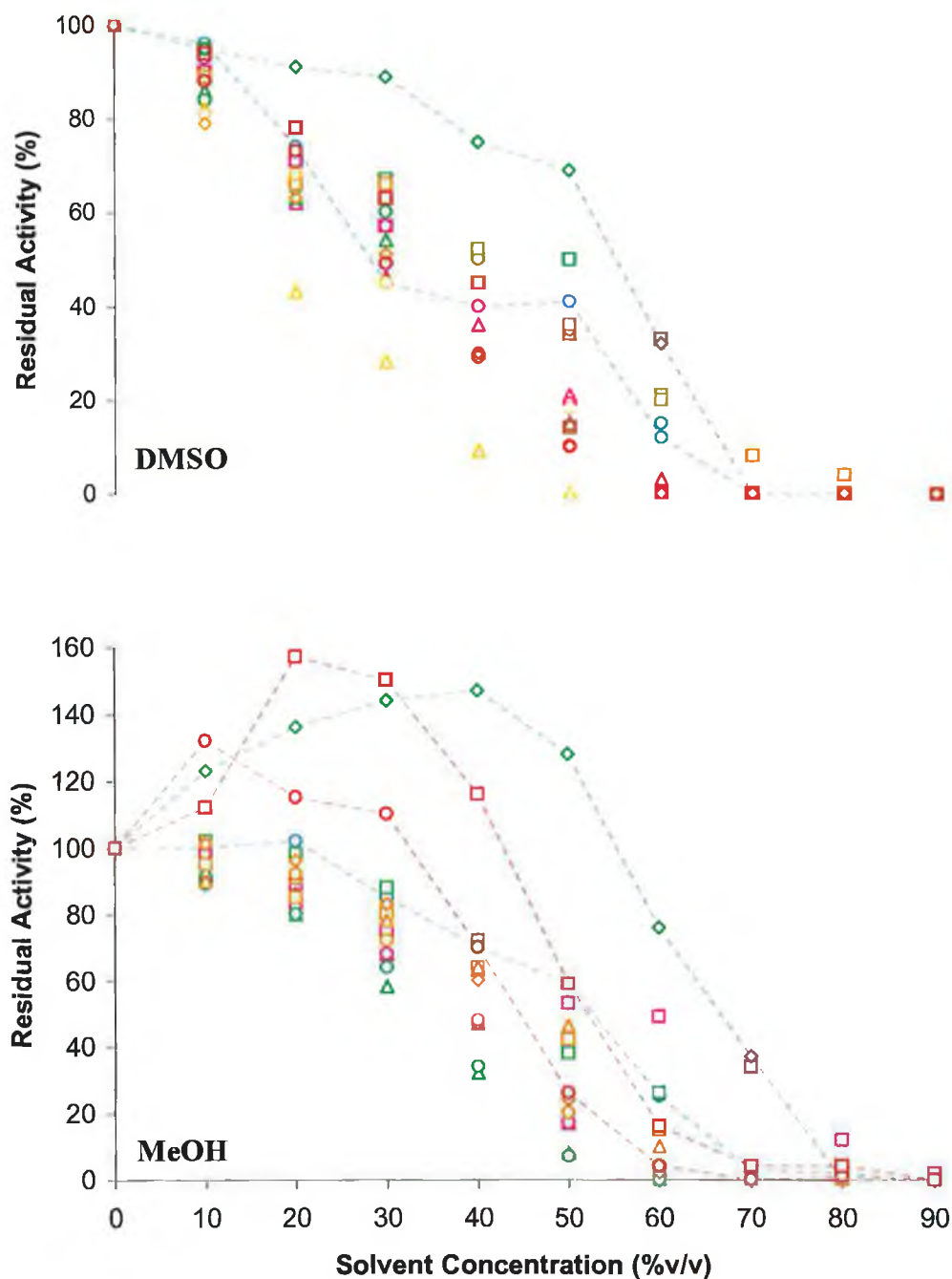


Figure 4.27: Solvent Tolerance Profile of single lysine mutants; \square K174N, \triangle K174E, \circ K174A, \square K232N, \triangle K232E, \circ K232A, \diamond K232F, \circ E238Q, \square E239N, \square K241N, \triangle K241E, \square K241A, \square K232F, \circ Wildtype.

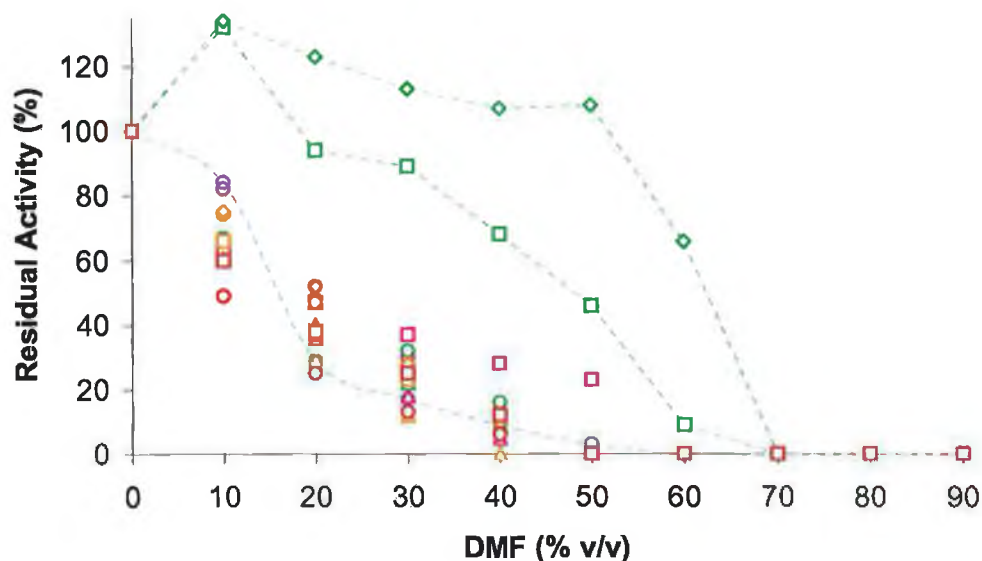


Figure 4.28: DMF Solvent Tolerance Profile of single lysine mutants; \square K174N, \triangle K174E, \circ K174A, \square K232N, \triangle K232E, \circ K232A, \diamond K232F, \square E238Q, \square E239N, \square K241N, \triangle K241E, \circ K241A, \circ Wildtype.

Apparent C_{50} values at 25°C for each of the mutants were calculated (Section 2.34), with the results are tabulated in Table 4.3.

Table 4.3: Calculated apparent inhibitory concentrations (C_{50}) for each lysine mutant. Standard errors are less than 5% in all cases.

Mutant	DMSO C_{50}	MeOH C_{50}	DMF C_{50}
Wildtype	35	53	14
K174N	42	45	15
K174E	20	55	13
K174A	30	35	19
K232N	45	45	48
K232E	38	33	15
K232A	40	35	21
K232F	55	67	60
E238Q	30	45	10
E239N	37	53	13
K241N	38	55	18
K241E	30	38	15
K241A	35	38	18
K241F	34	43	20

4.6.4 Single Mutant H₂O₂ Tolerance.

All H₂O₂ Tolerance assays were carried out as per Section 2.35, with a final rHRP concentration of 360 nM in each reaction. H₂O₂ tolerance profiles were produced for each mutant, in triplicate, using recombinant wildtype as a reference. Standard errors of triplicate assays were less than 15 % in all cases.

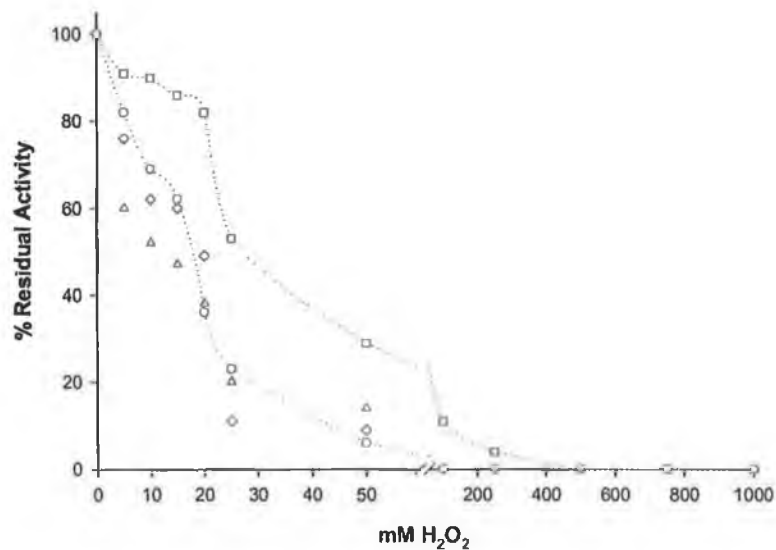


Figure 4.29: H₂O₂ Tolerance profile of Lysine 174 mutants; Δ K174A, \square K174E, \diamond K174N, \circ WT.

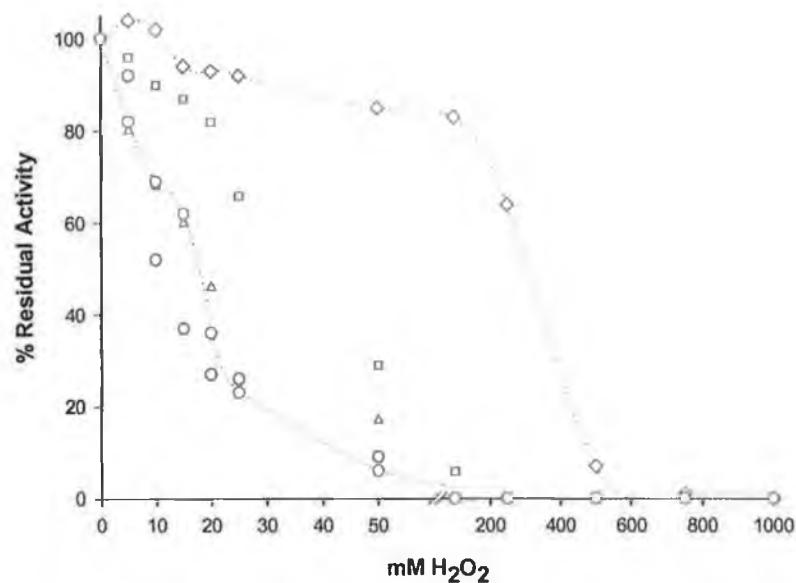


Figure 4.30: H₂O₂ Tolerance profile of Lysine 232 mutants; Δ K232A, \square K232E, \diamond K232N, \circ K232F, and \circ WT.

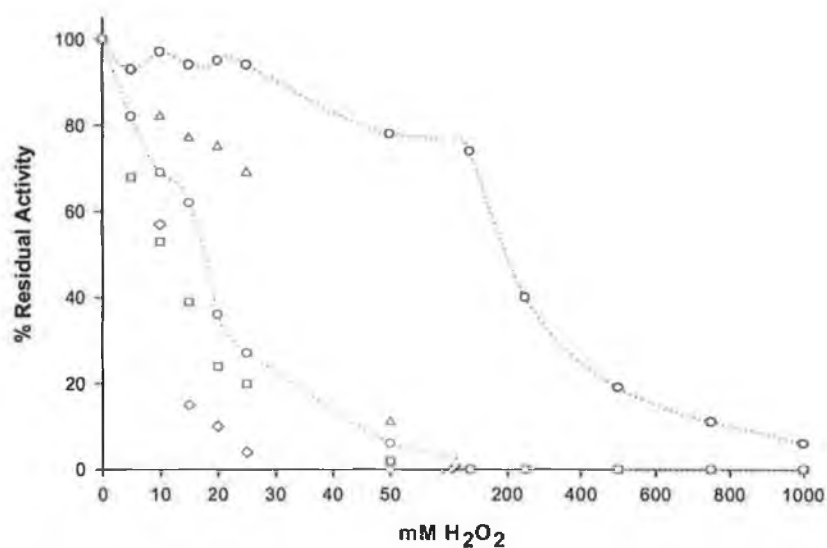


Figure 4.31: H₂O₂ Tolerance profile of Lysine 241 mutants; Δ K241A, \square K241E, \diamond K241N, \circ K241F, \square WT.

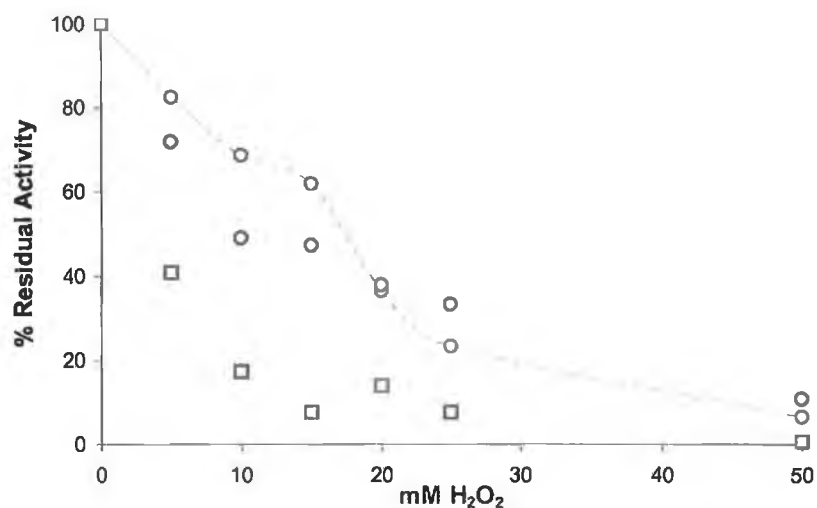


Figure 4.32: H₂O₂ Tolerance profile of Glutamic Acid mutants; \circ - E238Q, \square - E239N and \circ WT.

Table 4.4: Calculated H₂O₂ C₅₀ for each single lysine and glutamic acid mutant.

Mutant	mM H ₂ O ₂ C ₅₀	% Error	Mutant	mM H ₂ O ₂ C ₅₀	% Error
Wildtype	17	± 4	K232F	11	± 4
K174N	20	± 8	E238Q	18	± 15
K174E	27	± 6	E239N	3	± 5
K174A	13	± 3	K241N	11	± 9
K232N	300	± 5	K241E	11	± 4
K232E	36	± 10	K241A	33	± 6
K232A	19	± 6	K241F	200	± 7

4.6.4 Steady-State Kinetics of Single Lysine Mutants.

All kinetic assays were carried out as per Section 2.35, with a final rHRP concentration of 65 pM in each reaction solution. K'_m and k_3 values were calculated by plotting the kinetic data generated in the software package EnzfitterTM. All experiments were determined in triplicate, with the average value being used in the kinetic analysis. Recombinant wildtype HRP was used as reference.

Table 4.5: Kinetic analysis for all lysine mutants, using ABTS as the reducing substrate. K_m and k_3 values, including standard errors, were calculated using the Enzfitter software package.

Mutant	$k_3(\text{s}^{-1})$	SD (s^{-1})	$K'_m(\text{mM})$	SD (mM)
Wildtype	482	± 12	0.093	± 0.013
K174N	624	± 14	0.142	± 0.013
K174E	354	± 19	0.142	± 0.032
K174A	954	± 12	0.096	± 0.007
K232N	1849	± 103	0.168	± 0.038
K232E	467	± 18	0.131	± 0.022
K232A	433	± 10	0.118	± 0.013
K232F	983	± 38	0.126	± 0.034
E238Q	1298	± 63	0.221	± 0.033
E239N	526	± 23	0.134	± 0.026
K241N	1141	± 41	0.092	± 0.017
K241E	978	± 64	0.062	± 0.018
K241A	2410	± 157	0.320	± 0.075
K241F	880	± 20	0.308	± 0.038

4.7 Characterisation of Double Lysine Mutants.

4.7.1 Double Lysine Mutant Concentration Determination.

Double lysine mutants were individually expressed in 500 mL shake culture flasks (Section 2.24.4). The recombinant HRP mutants were purified via optimised nickel affinity chromatography (Section 2.25). Once expressed and purified, the μM concentration of HRP was calculated as per Section 2.29, with the results outlined in Table 4.6.

Table 4.6: Absorbance at 403nm for all double lysine mutant forms of rHRP. rHRP concentrations were calculated using the Beer-Lambert Law and the rHRP extinction coefficient, $100 \text{ mM}^{-1}\text{cm}^{-1}$ (Hiner et al., 1995). Protein concentrations were experimentally determined using the BCA assay.

Mutant	Abs 403nm	rHRP (μM)	Protein Conc (mg.mL^{-1})	Heme/Protein Ratio
K232/241N	0.059	1.2	0.252	0.161
K232/241Q	0.031	0.6	0.194	0.105
K232F/K241N	0.074	1.5	0.187	0.272

Protein concentrations were equalised for all thermal and organo tolerance assays, whilst rHRP concentrations were equalised for all kinetic analysis and H_2O_2 studies.

4.7.2 Double Lysine Mutant Thermal Tolerance.

All thermal tolerance assays were carried out as per Section 2.31, with a final protein concentration of $100 \mu\text{g.mL}^{-1}$ in the reaction solution. Thermal profiles (Figure 4.33) and thermal inactivations (Figure 4.34) were produced for each of the mutant forms, in triplicate, using recombinant wildtype as reference.

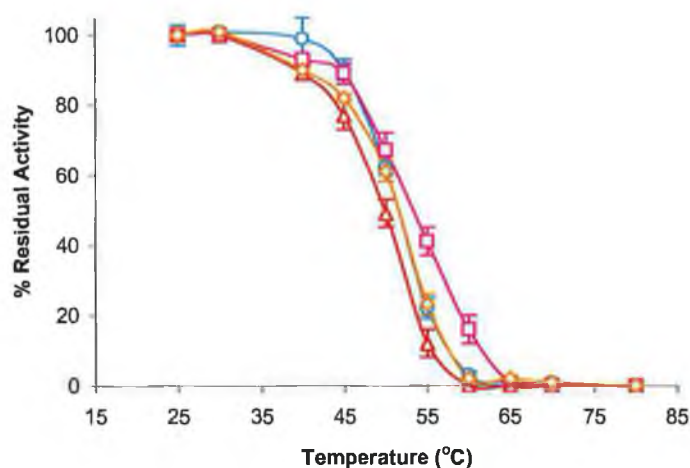


Figure 4.33: Thermal profile of Double Lysine 232/241 mutants; Δ K232/241Q, \square K232/241N, \circ K232F/K241N, \diamond Wildtype.

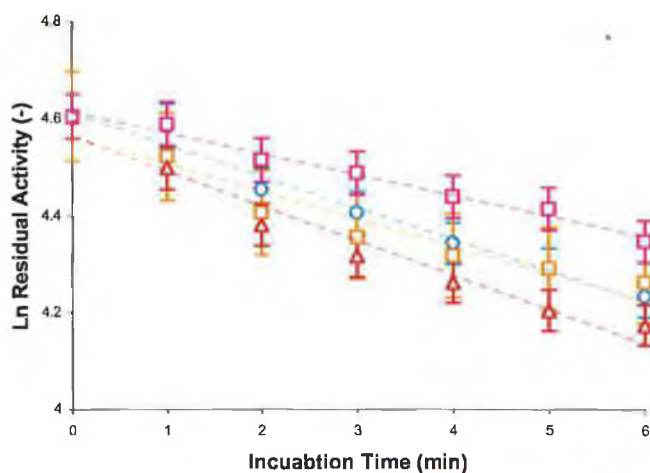


Figure 4.34: Linearisation of Double Lysine 232/241 mutants; Δ K232/241Q, \circ K232/241N, \square K232F/K241N, \circ Wildtype.

Apparent half-lives for each of the mutants at 50°C were calculated (Section 2.33) with the results tabulated in Table 4.7.

Table 4.7: Rate of inactivation at 50°C and calculated apparent half-life ($t_{1/2}$) for lysine double mutants.

Mutant	T_{50} (°C)	Rate Const (min^{-1})	SD (min)	$t_{1/2}$ (min)	r^2 Value
Wildtype	50	5.59×10^{-2}	± 6	12.4	0.98
K232/241N	50	3.61×10^{-2}	± 10	19.3	0.91
K232/241Q	48	4.53×10^{-2}	± 8	15.3	0.94
K232F/K241N	52	2.53×10^{-2}	± 6	27.4	0.95

4.7.3 Double Lysine Mutant Organic Solvent Tolerance.

All solvent tolerance assays were carried out as per Section 2.34, with a final protein concentration of $100 \mu\text{g} \cdot \text{mL}^{-1}$ in the reaction solution. Solvent tolerance profiles were produced for each of the mutant forms, in triplicate, using recombinant wildtype as reference. All standard errors were within <5% of the triplicate average reading, with the errors bars being omitted for the sake of clarity.

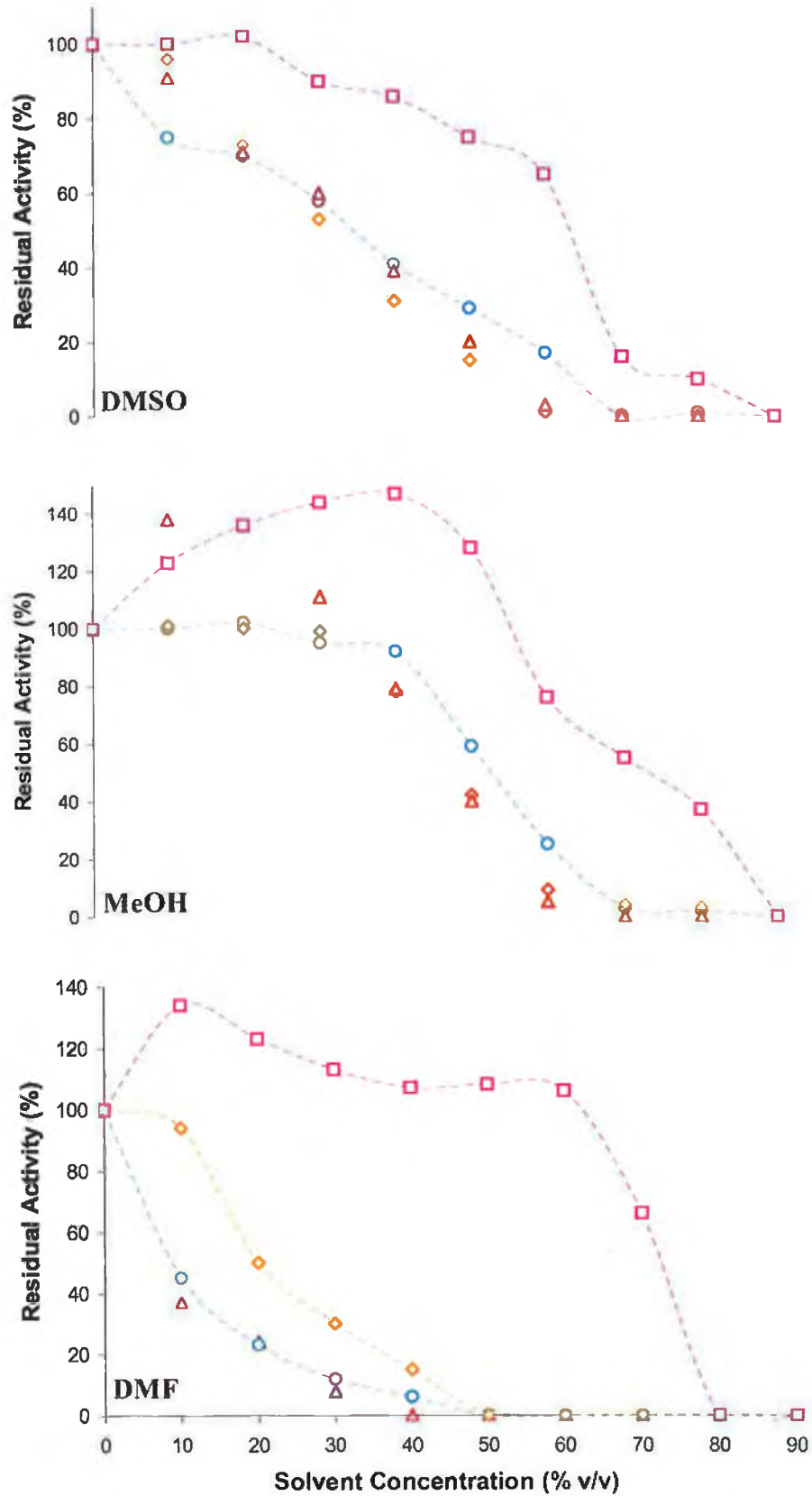


Figure 4.35: Solvent Tolerance profile of Double Lysine 232/241 mutants; Δ K232/241Q, \diamond K232/241N, \square K232F/K241N, \circ Wildtype.

Apparent C_{50} values at 25°C for each of the mutants were estimated (Section 2.34); the results are tabulated in Table 4.8.

Table 4.8: Estimated apparent inhibitory concentrations (C_{50}) for each double lysine mutant

Mutant	DMSO C_{50}	MeOH C_{50}	DMF C_{50}
Wildtype	35	53	14
K232/241N	35	48	20
K232/241Q	32	48	9
K232F/K241N	62	65	62

4.6.4 Double Lysine Mutant H_2O_2 Tolerance.

All H_2O_2 tolerance assays were carried out as per Section 2.35. Triplicate standard errors were less than 10 % in all cases.

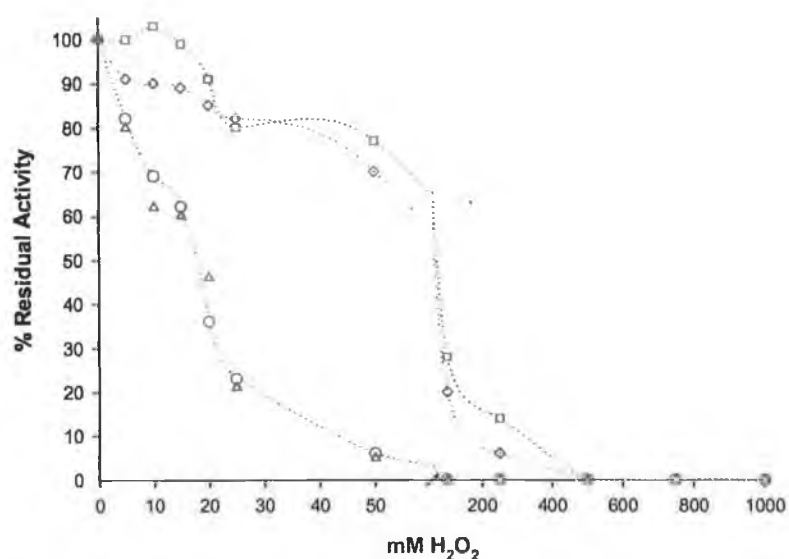


Figure 4.36: H_2O_2 Tolerance Profile of Double Lysine 232/241 mutants; Δ K232/241Q, \diamond K232/241N, \square K232F/K241N, \circ - Wildtype.

Table 4.4: Calculated H₂O₂ C₅₀ for double lysine mutants.

Mutant	mM H ₂ O ₂ C ₅₀	% Error
Wildtype	17	4
K232/241Q	17	3
K232/241N	65	5
K232F/K241N	70	8

4.7.4 Steady-State Kinetics of Double Lysine Mutants.

All kinetic assays were carried out as per Section 2.36, with a final rHRP concentration of 65 pM in each reaction solution. All experiments were repeated in triplicate, with the average value being used in Enzfitter™ analysis to estimate apparent K'_m and k₃. Again, recombinant wildtype HRP was used as a reference.

Table 4.9: Steady-state kinetic analysis for all double lysine mutants, using ABTS as the reducing substrate. K'_m and k₃ values, including standard errors, were calculated using the Enzfitter™ software package.

Mutant	k ₃ (s ⁻¹)	SD (s ⁻¹)	K' _m (mM)	SD (mM)
Wildtype	482	± 12	0.093	± 0.013
K232/241N	378	± 30	0.114	± 0.036
K232/241Q	1549	± 61	0.197	± 0.068
K232F/K241N	1008	± 39	0.114	± 0.018

4.8 Discussion.

4.8.1 Mutation Selection and Generation.

The aim of these experiments was to produce, verify and characterise site-directed mutants of the HRP gene situated in the pBR_I plasmid. A rational design approach was used to select key residues for substitution. Prior knowledge from chemical modifications that stabilised plant HRP suggested that exposed lysine residues play an important role in HRP stability. Ethylene-glycol *bis*(succinimidylsuccinate) modification of three of HRP's six lysines led to an increased thermal stability (O'Brien et al., 2001), whilst neutralisation of lysine's positive charge also afforded increased thermal and solvent stability (Miland et al., 1996b). Charge reversal, via chemical modification with compounds such as phthalic anhydride (O'Brien, et al., 2003) and carboxylic acid anhydrides (Ugarova et al., 1979), has also been shown to affect stability. However, the basis of stabilisation is not known for these latter chemical modifications and, therefore, there is scope for mutational studies to ascertain the effect(s) of simply neutralising and reversing the lysines positive charge without the inclusion of chemical compounds. Phthalic anhydride, for example, contains a benzene ring in its structure: it is not known if the observed stabilisation is due to charge reversal, the spread of electrons around the benzene ring, the hydrophobic interaction between the aromatic benzene ring and a particular hydrophobic patch of the HRP molecule, or some other interaction with the benzene group.

Replacement amino acids were chosen for a variety of reasons. Initially, they were chosen based on size, hydrophilicity and charge. It was attempted to maintain the space-fill and hydrophilicity characteristics of a lysine residue when mutating to another amino acid, but charges were either neutralised (Asn) or reversed (Glu). The effect of a space-creating, hydrophobic, charge-neutralising substitution was investigated by replacing a lysine with an alanine residue and the effect of a bulky aromatic, hydrophobic substitution was examined by the introduction of a phenylalanine.

From initial results, two additional residues, Glu 238 and Glu 239, were also subjected to mutation and analysis. Both residues are negatively charged and mutation of the positively-charged lysines nearby highlighted the important role of charge in this region. An uncharged amino acid was chosen as the substitute residue acid in both cases, glutamine (238) and asparagine (239), mirroring the rationale of the lysine mutagenesis studies.

Initial results of mutagenic PCR were disappointing, with few colonies observed after transformation of the amplified vector into highly competent cells (see traditional method, Figure 4.2). The low yield of amplified mutant vector could possibly have been caused by primer dimer formation, as the two mutagenic primers are 100% homologous to each other. Use of a two-stage mutagenic PCR protocol similar to that described by Wang and Malcom (1999), however, circumvented this problem.

Initially, the mutation present prior to cloning, Ala 34 Pro, was reverted to wildtype. This would allow direct comparison between wildtype and mutant recombinant HRPs and plant HRP. Wildtype and mutant clones were screened via a silent mutation incorporated into the mutagenic primer, which permitted easier identification of positive clones for the desired mutation. By co-introduction of diagnostic restriction sites, using silent mutations, each mutant construct could be verified prior to commercial DNA sequencing. It must be noted, however, that silent mutations may change mRNA conformation, perhaps leading to altered mRNA stability and/or translation efficiency. Although no such problems were noted in this study (due to the use of preferred *E. coli* codons) there are alternative approaches to screening and identifying mutations prior to DNA sequencing, such as a gradient PCR screening strategy (Padmakumar and Varadarajan, 2003). After screening, a single clone was selected; sequencing confirmed the reversion of the gene to wildtype, and henceforth this plasmid was named pBR_I.

Site-directed mutagenesis was then carried out on pBR_I to introduce the desired lysine mutations. Single mutants were made; however, characterisation of these single mutants prompted the development of double lysine and glutamic acid mutants. Again, restriction analysis allowed for economical selection of the desired clones for confirmation sequencing. All clones were synthesised and screened and the mutations confirmed by sequencing. Results were then aligned using GeneDocTM bioinformatic software to demonstrate the precise nature and the location of the mutations.

4.8.2 Thermal Stability.

Initially, single lysine mutants were analysed for thermal tolerance, using a thermal profile as a guide to select a standard temperature for thermal inactivation. Wildtype recombinant displayed 50% activity (T_{50}) at approximately 50°C; most mutants had a similar T_{50} value except for K174E, K174N and K241E, which displayed a slightly lower T_{50} (~8%), and K232F, K232N, K241F, K241A and K241N, which had a slightly

higher T_{50} (~6%). Double mutant K232/241N displayed a similar T_{50} to wildtype, while T_{50} of K232/241Q was slightly decreased T_{50} (~4%). All thermal inactivations were performed at 50°C to allow direct comparison with the reference wildtype recombinant HRP across the mutant matrix. The resulting data were modelled by *Enzfitter*TM (Biosoft, Cambridge, UK) to a first order exponential decay (Mozhaev, 1993) to give the rate constant, k , from the equation:

$$N(t) = N_0 e^{-kt}$$

Where N_0 is the initial activity and $N(t)$ equals activity at time (t). This equation can be rearranged to yield:

$$\ln\left(\frac{N}{N_0}\right) = -kt$$

At 50% activity $\ln(N/N_0)$ becomes $\ln 2$; thus, dividing $\ln 2$ (0.693) by $(-k)$ yields the $t_{1/2}$, or half-life of the enzyme. It has previously been demonstrated that peroxidases do not follow first-order thermal denaturation kinetics; instead, they tend to display 1.5-order (Chang et al., 1998). Therefore, the values described here may not represent true half-lives. First-order decay models were applied to the thermal inactivation data. The majority of the mutants obeyed the model for the first 10 min of inactivation, but some (K174N and K232A for example) gave poor fits, indicated by low correlation coefficients. The $t_{1/2}$ values reported here are for comparison purposes only: increases or decreases over wildtype recombinant are assumed to indicate increased or decreased thermal stability.

Many of the single mutants (6 out of 11) displayed decreased $t_{1/2}$, with the largest decrease (28%) noted for K232A. Although proteins are surprisingly robust to site directed mutations (Taverna and Goldstein, 2002b), this is not apparent in the present study, despite the implementation of a rational mutational approach. All positions mutated led to an altered $t_{1/2}$ compared with wildtype: see Table 4.2. It is clear that certain regions are more important than others for thermostabilisation of the HRP molecule. All lysine 174 mutants display an 18% - 21% decrease in stability (as deduced from the $t_{1/2}$). Hence, it can be seen that lysine 174 is an important contributor to HRP thermostability. *DeepView* analysis of the protein crystal structure, and previous homology modelling, suggests an interaction (possibly hydrogen bond) between Lys174 and the heme group. Therefore, substitution of this residue will disrupt this presumably-stabilising interaction, allowing more freedom for the heme moiety and, ultimately, unfolding of the protein backbone, heme group disassociation and a

decrease in enzyme activity at elevated temperatures. Previous stabilising chemical modifications only changed the properties of this residue, but the residue itself remained. In these earlier reports Lys 174 was not analysed in isolation as a thermostabilising residue; however, this work clearly demonstrates the important thermostabilising role of wildtype Lys 174.

An opposite trend is evident at Lys 232, where most mutations appear to be thermostabilising, with the exception of K232A. Previous chemical modification results suggested that charge neutralisation, charge reversal and crosslinking in this area can effect moderate thermostabilisation of HRP. Charge-neutralising modification of the lysine residues (Miland et al., 1996b) was mimicked by introduction of asparagine, whilst charge reversal (O'Brien et al., 2003) was implemented by the introduction of glutamic acid, and a phenylalanine was introduced to assess the effect of a benzene ring in the region. The rational mutational approach proved successful for position 232, as all mutations yielded increased thermal stability as judged by $t_{1/2}$; Phe, 200%; Asn, 70%; and Glu, 10%. Lys 232 is located in a region of negative electrostatic potential, as determined from crystal structure analysis, and charge neutralisation may help to alleviate some non-optimal charge-charge interactions. Also, Lys 232 is located in a hydrophobic region; so neutralisation of the positive lysine charge may affect thermostability and organo-tolerance, see Sections 4.6.2 and 4.6.3. Substitution by a phenylalanine residue could increase the region's hydrophobicity and aid stabilisation. Mutation of Lys 232 to the neutral, small, alanine yields the largest decrease in thermostability (28%) of all the lysine mutants, from which the importance of the space-fill characteristics of the Asn residue can be inferred. Both Lys to Asn and Lys to Ala mutations neutralise the lysine charge; however, the Asn mutation maintains similar (but not identical) space-fill characteristics to the Lys. Although Lys 232 is situated on the periphery of the enzyme structure, correct protein packing in this outer region is paramount in maintaining enzyme structure, and ultimately function, at elevated temperatures. Thus, at position 232 on the HRP backbone, maintenance of space-fill characteristics is more important than charge in protein thermal stabilisation. *DeepView*TM investigation suggests that the side chain of K232 hydrogen bonds with the side chain of Asp 230 and Asn 236, whilst K241 bonds with Asn236. K232 substitution may improve hydrogen bonding in this region. For example, K232N increases hydrogen bonding (introduction of an additional Asn 231 bond), whilst maintaining pre-existing bonds. Asn 236 bonds directly to the proximal Ca^{2+} whilst Asp

230 forms part of the extended Ca^{2+} binding pocket (Howes et al., 2001a). Consolidation of this pocket may delay proximal calcium ion disassociation which is known to play a pivotal role in HRP stabilisation (Coates et al., 1998). This is reflected in this study, as K232N displays increased thermal (1.8-fold), solvent (DMSO and DMF; see Section 4.8.3) and even H_2O_2 (17.6-fold; although this is probably not Ca^{2+} related, see Section 4.8.4) stabilities. A space-fill substitution (Phe) removes some hydrogen bonds in this region, yet still yields increased thermal (2-fold) and solvent stabilities, probably as part as a result of compensatory packing. Only two mutations at position 241 (K241F and K241A) could be analysed using first order kinetics. A trend similar to K232A is noted, indicated by a 50% (K241A) and a 20% (K241F) decrease in $t_{1/2}$. K241 occurs close to K232, so destabilisation by introduction of a small, neutral amino acid may be due to (i) poor space-fill characteristics afforded by the alanine residue or (ii) increased strain, and/or (iii) electron distribution properties due to incorporation of a phenylalanine. K241A, through *DeepView*TM mutational analysis clearly exemplifies the critical combined role of space-fill and hydrogen bonding. Here all hydrogen bonds are broken and a cavity is created, resulting in dramatic decrease in thermal stability. The other substitutions (K241E and K241N) display differing thermal profiles. K241N shows a significant stabilised plateau between 55°C and 70°C. Thermal inactivation was carried out at temperatures between 50°C and 80°C, with K241N displaying 30% activity after 30 min incubation at 70°C, far superior to wildtype recombinant HRP. The increased thermostability of the K241N mutant may again be attributed to optimised charge interaction and hydrophobic core packing, as noted with K232N. *DeepView*TM predicts increased hydrogen bonding after the introduction of Glu or Asn at position 241 (introduction of a Glu 239 and Gln 240 bond respectively). K241E displays a slightly lower T_{50} than wildtype, and it could be assumed that this mutation would not increase the thermostability of the enzyme.

The single-mutant thermal characterisation and earlier chemical cross-linking suggested the development of glutamic acid (E238 and E239) and double lysine mutant (K232 and K241). Both Glu residues were mutated to non-charged glutamine (238) and asparagine (239). The lysines were mutated to asparagine (K232/241N), glutamine (K232/241Q) or phenylalanine and asparagine (K232F/K241N). Both glutamic acid mutants displayed a decreased thermal stability ($t_{1/2}$), ranging from 3% (E239N) to 60% (E238Q) compared with the wildtype. Surprisingly, neutralisation of residues 238 and 239 close to the important 232/241-stabilisation axis did not improve the thermal

stability. Although neutralisation of Glu 239, the one closer to the important Lys 241, yielded a mutant with only slightly decreased thermal stability, it is clear that a complex charge-transfer mechanism exists in this region, and that careful selection of any potential charge neutralisation mutation is paramount. This is evident from the fact that neutralisation of Glu 238, with the similarly sized glutamine, causes a 60% decrease in thermal stability. It is clear that the Glu 238 plays an important role in HRP thermal stability, possibly by charge-charge interactions, and that mutation of helix-favouring residues within the enzyme core to residues without helical propensities can have detrimental effects on HRP thermal stability (see Chapter 5).

Individually, Lys to Asn mutations at positions 232 and 241, or Lys to Phe at position 232, generated mutant proteins with greater thermostability than wildtype recombinant; however, these mutations appear to be mutually incompatible, i.e. their stabilising effects are not additive. Although an increase in thermostability is noted for the double asparagine mutant, it is not as stable as the individual K232N (21% increase in $t_{1/2}$ for K232/241N as compared with 70% for K232N). Also, the thermostable plateau noted between 50°C and 70°C in K241N is absent from the double mutant. Thus, neutralisation of two lysine charges in this region does not increase protein thermostability further than a single mutation. Because of the importance of space fill characteristics noted above (exemplified by the Lys to Ala mutation), a double glutamine mutation was effected. This would neutralise the positive charges on the wildtype lysine and increase the space fill capacity at this position, compared with Asn. However, K232/K241Q displays an 8% decrease in $t_{1/2}$ compared to the wildtype recombinant HRP. The inclusion of an extra -CH₂- entity in the amino acid's R-group, thus extending its space fill characteristics, appears to be counter productive, and decreases the protein's thermostability, possibly by increased backbone strain.

Understanding the factors underlying protein thermal stability is very complex, due mainly to the numerous parameters that combine to stabilise a protein. For example, plant HRP thermal stability has been shown to be a function of calcium content (Haschke and Friedhoff, 1978), pH (Lemos et al., 2000), solution environment (Machado and Saraiva, 2005) and chaotropic reagents (GnHCl; Huddleston et al., 1995). In this study, thermal stability of glycan-free recombinant HRP and mutants was investigated, and any stabilising effect of protein glycosylation was not evident. Tams and Welinder (1998) demonstrated that deglycosylated plant HRP displays little alteration in thermal stability; however, the deglycosylated form does show a 2-3 fold

decrease in folding stability in guanidium chloride. This contradicted previous reports suggesting that deglycosylation thermally destabilised HRP (Bonnafe et al., 1993). The present study showed a difference in thermal profile between His-tagged recombinant wildtype HRP and plant HRP, which is comparable to previous studies between plant and recombinant forms of HRP (Orlaova et al., 2003). Although the process of HRP thermal denaturation is not yet fully understood, recent experimentation suggests that it is irreversible and under kinetic control (Pina et al., 2001).

Several chemical modification procedures have been used to stabilise HRP in recent years, ranging from attachment of PEG (Garcia et al., 1998), attachment of bis-succinimides to the lysine groups (Ryan et al., 1994 and Miland et al., 1996a), acetylation of the lysine groups (Miland et al., 1996b), phthalic anhydride modification (O'Brien, 1997 and 2003) and glucosamine modification (Liu, et al., 2002). A common trend is evident in all these chemical modification procedures: the overall positive charge of the HRP molecule, which has a pI of 9.0, is reduced and the exposed lysine residues are often the target for charge alteration. As outlined in this study, substitutions of these lysine residues (K241N and K232N) increase the thermostability (although not to the same extent as chemical modification). The present results also suggest an important thermostabilising role for the wildtype Lys K174.

Matthews (1993) noted that *“the process of thermal unfolding disrupts the non-covalent interactions involved in maintaining the native structure and thereby provides a means of detecting changes in this network due to amino acid replacement”*. Traditionally, site-directed mutants probing molecular thermostability focussed on internal regions of the protein structure (the hydrophobic core area) and often highlighted core packing (Gromhina, 2003). Proteins such as lysozyme (Funashashi, et al., 2003) and barnase (Machicado, et al., 2002) were intensely mutated and studied in this way. However, several reports suggest that single amino acid changes, not necessarily located in the protein core, can affect thermostability in recombinant proteins (Kwon et al., 1994; Numata et al., 2001; Krowarsch and Otlewski, 2001; and Hakamada et al., 2001).

4.8.3 Organic Solvent Stability.

The effects of different organic solvents on the lysine / glutamic acid mutants were also analysed. Solvents were chosen based on their theoretical denaturation capacities (Methanol, low and DMF, medium; Khmel'nitsky et al., 1991a), and on previous plant

peroxidase studies (DMSO; Santucci et al., 2003; N. Carolan, PhD Thesis, Dublin City University, 2004). The C_{50} , the % v/v of solvent that causes a 50% decrease in enzymatic activity, was utilised to compare organo-tolerance across the mutant matrix. In all cases, native HRP and single lysine mutants were inactivated as the percentage volume of organic solvent increased. Overall increases in organo-tolerance were noted for DMSO with K174N, K232F, K232N, K232E, K232A and K241N; for DMF with K174A, K232F, K232N, K232A, K241N, and K241A, and for MeOH with K232F, as compared to wildtype recombinant HRP. This indicates that removal of lysines' positive charge benefits solvent stability.

No apparent trend was evident for the K174 mutants: K174E and K174A showed a decrease in C_{50} , whilst K174N showed a 1/5 increase in DMSO. K174E displayed a similar C_{50} to wildtype in MeOH; however, both K174A and K174N showed decreases in C_{50} in the same solvent. No significant change in C_{50} was noted for DMF. All K232 mutants exhibit an increase in C_{50} in DMSO, with K232F displaying the largest increase (3/5). In contrast, however, the majority of 232 mutants displayed decreased MeOH tolerance, with the exception of K232F (1/4). The largest single gain in solvent stability was displayed by K232F in DMF, with a greater than 4-fold increase in C_{50} . K232A and K232N also exhibited increased stability in DMF, whilst K232E showed similar DMF stability to wildtype. It is clear from Figures 4.27 and 4.28 that an activation process occurs in low concentrations of DMF and MeOH. K232N and K232F display a >1/4 increase in activity in 10% v/v DMF compared with aqueous solution, and with K232F in MeOH 1/2 activation is noted at 40% v/v. Many examples of enzyme activation in low-to-moderate concentrations of organic solvents have been reported (Khmelnitsky et al., 1991a), with 1/5 activation of HRP noted in 10% v/v acetonitrile and tetrahydrofuran, accompanied by a notable reduction of K_m for the substrate *o*-dianisidine (Batra et al., 1997). This activation process was attributed to an altered conformational form of HRP structure in the presence of an organic solvent. The HRP mutants may adopt a more active, less stable, form of the enzyme in a mixed organic solvent-aqueous system (Ryu and Dordick, 1989). With the exception of K241E, which showed a slight decrease in stability, the K241 mutations displayed similar DMSO tolerance to wildtype. K241N stability in MeOH was similar to wildtype; however, the Phe, Glu and Ala mutants exhibited decreased in C_{50} s (20% v/v, K241F and 38% v/v, K241E and K241A, compared to a wildtype value of 50% v/v). K241F, K241N and

K241A displayed an increase in DMF stability, (C_{50} of 18-20% v/v compared to a wildtype value 14% v/v) whilst K241E showed a similar stability to wildtype.

Glu 238Q displayed at least a 1/8 decrease in organo-tolerance in all solvents tested. Mutation of Glu 238 may cause minor destabilisation of the protein backbone, which in turn promotes unfolding and loss of activity in non-natural environments. Glu 238 is part of Helix G (Gajhede et al, 1997), and mutations within helical secondary structures can be detrimental to peroxidase stability (see Chapter 5). Glu is the most common residue in helical secondary structure and replacement with a residue with lower helical propensity may reduce overall helical strength (by increased tension) and lower stability (Costantini et al., 2006). Conversely, Glu 239 is not part of Helix G and displays similar stability characteristics as wildtype HRP. The effect of charge neutralisation (E238Q) may also explain drastic loss of thermal and moderate loss of solvent stability for both Glu mutants, possibly due to long-range structural perturbations induced by the single amino acid substitutions (Vendruscolo, 2002). It should be noted that both display an activation in 10% v/v MeOH, with E239N displaying a 1.6-fold increase in activity in 20% v/v MeOH; however, no overall stability gain is afforded by either Glu mutation as all C_{50} values are equal to, or less than, wildtype. No other enzyme activation processes are noted in the two remaining solvents tested. The effects of each individual solvent on HRP and methods of stabilisation have been previously discussed (Section 4.8.2 and 4.8.3) but the present results indicate that certain residues are important for the solvent stability of recombinant HRP. The stabilising interaction that E238 maintains within the recombinant HRP molecule may be space-fill, charge- or secondary structure-related, or a combination of all; however, from the results outlined its presence in the protein backbone is essential to the solvent stability of recombinant HRP. *DeepView*TM analysis shows Glu238 hydrogen bonds with Tyr 234 and Val235, whilst E239 bonds with Arg 224 and Asn236. *DeepView*TM mutational modelling suggests that E238Q may form putative hydrogen bonds with Glu239 or Arg 264 and Phe 251. Stabilising interactions with the proximal Ca^{2+} ion may be improved by introduction of new hydrogen bonding patterns in this region. Additionally, E239 may bond with Lys 241. Bonding to the stabilising K241 residue may explain why E239N displayed similar thermal and solvent stabilities (in all solvents tested) to wildtype.

The double lysine mutants were also analysed for stability in the same solvents, under the same conditions. Again, both double-lysine mutants inactivated as the percentage

volume of organic solvent increased. The double mutants showed similar tolerance in DMSO as wildtype recombinant HRP, although K232/241Q did display a very small decrease in C_{50} , (32% v/v, wildtype 35% v/v). Both double mutants displayed a decreased C_{50} in MeOH (48% v/v, wildtype 53 % v/v) despite the single K241N mutant having similar C_{50} as wildtype. The single K232N mutant displays a 1/8 decrease in C_{50} in MeOH, and so the stabilising effect of K241N in the same solvent may be negated by the presence of the destabilising K232N in this instance. The double glutamine mutant displays a large activation (1.4-fold increase in activity) in low concentrations of MeOH (<20% v/v). As outlined previously, enzyme activation in low concentrations of organic solvent is common; however, the C_{50} value indicates that the mutation does not afford any major stability gains in higher concentrations of organic solvent. The largest increase in solvent stability was noted for single mutant K232N (2.5-fold); however, the double asparagine mutation yields only a 1.4-fold increase in C_{50} . Again, the concerted effect of a small stability gain (K241N, 28%) in conjunction with a large stability gain (K232N, 250%) may result in only a modest stability gain for the double mutant. It is clear from these results that the double mutations are non-synergistic and non-additive in relation to recombinant HRP organo-stability. Although the double glutamine mutant displays a similar solvent tolerance profile to wildtype HRP, it also yields a slightly decreased C_{50} value, indicating that this mutation does not increase organotolerance.

Other enzymes have been subjected to site-directed mutagenesis in order to increase their stability in organic solvents. Yang and co-workers (2000) individually mutated two lysine residues of Pencillin G acylase enzyme, resulting in increased stability in acidic and organic solvent environments. Martinez and Arnold (1991) systematically altered charged surface residues of α -lytic protease to more hydrophobic amino acids; this resulted in a double mutant that displayed increased stability in 84% v/v DMF compared to the wildtype. Arnold's research group have also utilised random mutagenesis techniques in order to increase the stability and activity of various enzymes in organic solvents, including cytochrome P450 BM-3 monooxygenase (Wong et al., 2004), para-nitrobenzyl esterase (Moore and Arnold, 1996) and subtilisin E (Chen and Arnold, 1993). Arnold has reviewed the area of engineering enzymes for organic solvent applications (Arnold, 1990). Several other methods exist for stabilising enzymes for use in organic solvents, including immobilisation, where the enzyme is

immobilised to, or entrapped within, a protective solid support matrix (Batra et al., 1997) and chemical modification (Miland et al., 1996b). Dai and Klibanov (1999) also demonstrated that the phenomenon of “*molecular memory*” is applicable to peroxidases. Here, enzymes are lyophilised in the presence of certain stabilising excipients, which eliminate lyophilization-induced activity losses when the peroxidase is suspended in non-aqueous media. Solvent extraction and reactivation of HRP also utilises the enzyme’s ability to “remember” its solvent-exposed history, and increase its stability once it has been reactivated (Kim et al., 2000). It should also be noted that stabilisation of HRP in water-immiscible solvents, such as toluene and benzene, can be achieved by increasing its hydrophobicity, via attachment of PEG, and this also aids in increasing activity (Vazquez-Duhalt et al., 1992).

As outlined in Section 4.1, previous chemical modifications on the lysine residues both neutralising (Miland et al., 1996b) and charge reversal (O’Brien et al., 2003) exert a stabilising effect on the molecule in organic solvents. In this present study, one of the largest stability gains was exhibited by K232N, which compares well with previous chemical modification results, namely the demonstration that alteration of the charge on lysines 232/241 by succinimides resulted in significant improvement in peroxidase stability in DMF (Miland, 1996c). Khmel'nitsky and co-workers (1991b) also demonstrated that surface hydrophilicity is important for protein stability in organic solvents. It is well known that many enzymes can function in organic solvents (Ogino and Ishikawa, 2001); however, protein denaturation often occurs in water-miscible solvents, by a process referred to as “*water-stripping*” (Gorman and Dordick, 1992). Gorman and Dordick describe how T₂O (tritiated water) is desorbed from HRP by organic solvents such as MeOH and DMF. DMF desorbed significantly less T₂O than MeOH, despite displaying a higher theoretical denaturation capacity. This could be due to the similar structure of MeOH and H₂O, allowing MeOH to strip and replace water molecules close to the protein surface. HRP was also shown to retain less T₂O than other enzymes such as chymotrypsin; however, there is a major requirement for water for HRP activity and, therefore, any water removal will have a detrimental effect on enzyme activity. The mutations carried out in this section removed a positively charged amino acid (Lys) and replaced it with a neutral Asn and negatively charged Glu; thus an increase in solvent stability could be attributed to the ability of the mutant (K232N for example) to retain its bound water molecules in higher concentrations of organic solvent. Although water-stripping may be a cause of protein denaturation, it cannot be

the only reason, as substantial inactivation is noted for all solvents at concentrations less than 50% v/v, i.e. where there is equal volumes of water and solvent, and, hence, adequate water available to the HRP molecule.

4.8.4 H₂O₂ Stability.

The stability of wildtype and mutant HRPs in the presence of excess concentrations of H₂O₂ was also examined. In the absence of a reducing substrate (TMB, ABTS, DAB etc.), and with excess H₂O₂ present, HRP undergoes suicide inactivation. Wildtype recombinant HRP yields a H₂O₂ C₅₀ of 17 ±1 mM, which compares with previous published results of 60% activity in 25 mM H₂O₂ (Arnold and Lin, 2000) under similar conditions. Arnolds and Lin's (2000) HRP was expressed in *Saccharomyces cerevisiae* with glycosylation possibly increasing H₂O₂ stability. H₂O₂ stability of most Lys and Glu mutations is equal to or less than wildtype; however, K232E and K241A display a 2-fold increase in H₂O₂ C₅₀. Surprisingly, K174A displayed the poorest thermal and DMSO stabilities, yet it displays a 1.5-fold increase in H₂O₂ C₅₀. Two mutations, K232N and K241F, yielded a large increase in H₂O₂ C₅₀ (18- and 12-fold respectively) under the conditions used. Both of these mutants also exhibit increased thermal and solvent stabilities. This is also evident in the double lysine mutants' C₅₀ values for H₂O₂, where K232/241N and K232F/K241N retain 75% and 100% activity in 50mM H₂O₂ respectively.

H₂O₂-mediated HRP inactivation has been the subject of much research, with several theories forwarded as to the inactivation pathway. In recent years, however, Hernández-Ruiz and co-workers' (2001) "three-pathway model" has gained support. In this model, catalytic competition exists in the presence of excess H₂O₂, with three possible outcomes. These are: (a) formation of the dead-end Compound III (See Figure 1.3), (b) a catalase-type reaction, and (c) total enzyme inactivation. The first and second outcomes are enzyme survival routes and selection of one over the other depends on several parameters, including pH (Hernández-Ruiz et al., 2001). In following either survival pathway, the strong oxidising power of HRP's Compound I reacts with H₂O₂ as an electron *donor* (i.e. reductant; H₂O₂ normally acts as a oxidant or electron acceptor) in a complex set of reactions. These result in (i) a single electron transfer, leading to Compound II and peroxide anion formation (HO₂⁻) or (ii) a two-electron process forming molecular oxygen (pseudo-catalase activity) (Arnao et al., 1990). Catalases are found in most aerobic systems where they decompose H₂O₂ to water and

oxygen. The major difference between catalase and peroxidase is that the former generates water and oxygen, while the latter generates water and two free radicals (see Figure 1.3; Dunford, 1999). If excess H_2O_2 persists, the survival pathway is abandoned and progressive enzyme inactivation is noted, resulting in the formation of inactive verdohaemochrome P670 (Hiner et al., 2001). The pivotal point of abandonment has been identified as the Compound I - peroxide complex (Hiner et al., 2002). A transient intermediate (P965) has been shown to complex Compound I and the peroxide substrate. Decay of this intermediate, via two competing reactions (survival or inactivation), determines the fate of the enzyme. On a mechanistic level, H_2O_2 inactivation has been shown to effect structural changes, typically affecting the heme moiety, as indicated by an altered Soret band (Schmidt et al., 2002).

Catalase-like activity has been noted for HRP, with possible *in vivo* HRP pseudo-catalase roles involved in plant-pathogen interactions (Baker et al., 2000). Typically, HRP can scavenge H_2O_2 effectively in the presence of a suitable phenolic reducing substrate, e.g. lignin. Indeed, the properties of HRPC (high affinity for H_2O_2 , rapid formation of Compound I and high activity at low substrate concentrations) suggest that it could offer an efficient detoxification mechanism for the plant, a role normally associated with catalases (Yamasaki et al., 1997). Under oxidative stress, however, or during a protective H_2O_2 burst (in response to pathogenic attack), HRP alone can scavenge H_2O_2 with concurrent molecular oxygen production (Hernández-Ruiz et al., 2001).

HRP pseudo-catalase activity, although somewhat weaker than bacterial catalase-peroxidases and chloroperoxidases, is much stronger than that of some Class II peroxidases (e.g. *Arthromyces ramosus* peroxidase; Hiner et al., 2002a). Therefore, HRP is ranked "intermediate" in H_2O_2 protection within the peroxidase superfamily. (Hiner et al., 2001). HRP A2 demonstrates increased H_2O_2 tolerance compared to HRPC. This has been attributed to the presence of a modified Compound III in HRP A2-mediated H_2O_2 catalysis in the absence of a reducing substrate. Normally, a water molecule is weakly bound to Compound III; however, the altered Compound III replaces this H_2O molecule with a tightly bound O_2^\bullet radical, affording increased stability. The alternative Compound III may be kinetically disfavoured during the HRPC catalytic cycle (Hiner et al., 2001).

Hiner and co-workers (2001) defined the 'partition ratio' as a mechanism for comparing H_2O_2 stability of HRP variants. This ratio yields the number of H_2O_2

turnovers occurring prior to enzyme inactivation. Glycosylation was shown to increase HRP's H_2O_2 stability (2-fold), whilst mutations to the active site (Arg 38 and His 42) caused a 10-fold loss. Mutations outside the active site have also reduced susceptibility to H_2O_2 inactivation: F143A, for example, yields in a 15% increase in H_2O_2 stability. Continued mutagenesis studies on other peroxidases highlight the potential for increasing H_2O_2 stability (Valderrama et al., 2002). Miyazaki and Takahashi (2001) engineered a stabilised H_2O_2 binding pocket in a recombinant manganese peroxidase (Class II peroxidase) by Asn81 and multiple Met substitutions. Additionally, a single substitution, H52Q, alters yeast cytochrome *c* peroxidase (Class I peroxidase) H_2O_2 catalysis from reduction to oxidation (Bateman et al., 2001). Arnold and Lin (2000) improved HRP's H_2O_2 stability by directional evolution (65% increase; L131P and L371I mutations). These mutations also resulted in increased thermal and solvent stabilities (although this may be coincidental, as two different phenotypes are in question).

Therefore, the stabilisation of HRP against H_2O_2 inactivation is complex, with many possible outcomes dictating the enzyme's fate. In this study, by altering the charge of the protein (but maintaining the space-fill characteristics in this region) the catalase-type reaction may have been selected over Compound III formation (Hernández-Ruiz et al., 2001). This hypothesis is supported by the stabilising K232N, but not K232A, mutation. This could perhaps lead to a HRP-based catalase-type reaction, which allows HRP to maintain catalytic activity in elevated concentrations of H_2O_2 .

4.8.5 Kinetic Characterisation.

The effect of lysine substitutions on the steady-state kinetics of recombinant HRP was investigated with ABTS as the reducing substrate. Peroxidase kinetics do not follow the traditional Michaelis-Menten model, with the steady state rate constants, k_1 and k_3 (see Figure 1.3), governing the catalytic cycle. k_1 is typically too rapid for accurate measurement by steady state kinetics. k_3 is often referred to as the rate-limiting step in HRP kinetics and is the rate constant described in this study; the use of “*steady state parameters, k_{cat} and K_M , is inappropriate for peroxidase kinetics*” (Dunford, 1999). Hence, experimentally determined steady-state values are often referred to as k_3 *app*, or the apparent catalytic constant.

Six of the nine single lysine mutants display an increase in k_3 , whilst of the remaining three, one shows k_3 value similar to wildtype, while the other two show decreased

values (K232A, 8% and K174E, 25% decrease). The largest increase in k_3 was noted for K241A, which displayed a four-fold increase. Only one mutant (K241E) showed a decreased K'_M (33% reduction in ABTS binding capability). All the other mutants displayed a similar (K174A and K241N) or increased K'_M , (K232A, 27%; K232E, 40%; K174N, 50%; and K174E, 50%; and K232N, 80%). However, similar to the k_3 , the largest increase in K'_M was noted for K241A, which displayed a 240% decrease in binding affinity for ABTS under the experimental conditions used. The explanation for the significantly increased k_3 and K'_M for K241A may be the reorientation of the protein backbone due to the inclusion of a smaller amino acid at this position. This hypothetical molecular rearrangement may affect the overall HRP structure, reducing access to the binding region for the bulky ABTS substrate (K'_M), which may also result in easier product disassociation, thus increasing the k_3 . A similar rationale can be applied to the other mutants displaying increased k_3 or K'_M , with the converse applying to those mutants with decreased kinetic values. However, this hypothesis would have to be confirmed by crystallisation studies and use of additional substrates.

E238Q displayed a 1.7-fold increase in k_3 ; this mirrors previous increases in k_3 following charge neutralisation in that region. A 30% increase in K'_M was noted for E239N; however, only a small increase (<10%) in k_3 was observed.

The kinetic values obtained for the double lysine mutants appear somewhat contradictory to those for the single mutants. The double glutamine mutant, with decreased space fill capacity, displays a 2.3-fold increase in k_3 accompanied by a 1.1-fold increase in K'_M . Although less pronounced an improvement as the single lysine mutant, K241A, it appears that alteration of the protein backbone has occurred, by decreased space fill in this region and that mutant proteins' binding capacity for ABTS has been decreased. Surprisingly, however, use of the other amide, Asn, in a double substitution yields a 1/5 decrease in k_3 , accompanied by a 1/4 increase in K'_M .

4.9 Conclusions.

In this chapter a mutant matrix was generated, focussing on rationally selected lysine and glutamic residues indicated by prior art (O'Brien et al., 2001). The “best” single mutants, those yielding improved thermal, solvent and H₂O₂ stability, were substitutions whereby the positively-charged lysine was neutralised (most notably by asparagine) at positions 232 and 241 in the HRP backbone. Improved space-fill, or hydrogen-bonding, characteristics resulted in improved stability, possibly by delaying proximal calcium ion disassociation. Mutation of lysine 174 and glutamic acid 238 led to decreased thermal and solvent stabilities and suggests important stabilising roles for these residues in wildtype HRP. Double mutations, incorporating the best single mutants, yielded further improvements (K232/K241N, K232/K241Q and K232F/K241N); however, the effects were non-synergistic or additive; also, overpacking resulted in decreased stability. Many of the mutants displayed increased k_3 , although without a concurrent K'_M change, suggesting alteration to catalytic steps rather than substrate binding.

Thermal stability in biocatalysts is a major factor in decreasing process costs, as reactions can be carried out more efficiently, reactants are often more soluble, and microbial contamination is minimised at higher temperatures (van den Burg and Eijsink, 2002). Thermostabilised HRP will find many potential applications, including wastewater treatment, enzymatic synthesis at elevated temperatures, and in “time-temperature integrators” (Lemos et al., 2000). Solvent-stabilised rHRP will similarly find many applications including phenolic polymerisation, as an analytical reagent in monophasic organic media and in organic solvent based biosensors (Dordick, 1991). Improved H₂O₂ stability will increase the applicability of HRP in wastewater treatment, where currently it suffers from intolerance of high concentrations of the primary substrate H₂O₂, low enzymatic reusability, and financial costs (Ryan et al., 2006).

Chapter Five.

Site-Directed Mutagenesis: Consensus Approach.

5.1 Introduction.

Comparison is one of the most basic procedures in biology. Measuring similarities and differences between organisms allows scientists to generate groups and clusters, from which we can infer such things as evolutionary relationships (Levitt and Gerstein, 1998). The alignment of nucleotide or amino acid sequences is an essential tool in molecular biology as it allows rapid detection of “*relatedness*” between seemingly unrelated proteins and can act as an essential prelude to molecular evolutionary analysis. As such, development of bioinformatic software capable of processing vast data sets is paramount (Chenna et al., 2003; Thompson et al., 1994). One application of such alignment procedures is in the identification of key stabilising residues in a protein structure (Lehmann and Wyss, 2001). This methodology is often referred to as the Consensus Approach, or *semi-rational* protein design, with several successful reports of protein stabilisation using this approach available (Miyazaki et al., 2001, Lehmann et al., 2002, Flores and Ellington, 2005). The consensus approach is based on the assumption that conserved residues, as detailed in the sequence alignments of related proteins, contribute more to the protein’s stability than non-conserved residues (van den Burg and Eijsink, 2002). It has been proven that a set of amino acid sequences of homologous, mesophilic enzymes contains sufficient information to allow rapid design of a thermostabilised, fully functional enzyme (Lehmann et al., 2000).

Based on these assumptions, a consensus peroxidase protein was developed “*in silico*”, utilising newly constructed bioinformatic software (Section 5.3) capable of analysing an aligned set of peroxidase sequences. By inspecting the consensus peroxidase protein together with that of the crystal structure of HRP, certain HRP residues were selected and mutated to the corresponding *peroxidase consensus* residue. The mutant protein was expressed and purified and its stability characteristics were measured to ascertain the effects of mutation.

Stability gains for the consensus mutants were disappointing, however. A rigorous bioinformatic approach was implemented which, through the generation of an archetype peroxidase, suggested the importance of the helical secondary structure within the protein backbone. As such, mutation of these residues failed to increase the stability of the protein, and leads to the conclusion that the consensus approach may not be globally applicable.

5.2 Generation of Peroxidase Consensus Gene.

One hundred unique peroxidase sequences were downloaded from the NCBI gene repository (www.ncbi.nlm.nih.gov/entrez/query.fcgi?db=Protein), utilising the following search boolean:

“((((((Peroxidase) AND (plant))) NOT (precursor)) NOT (putative)) NOT (Segment)) NOT (catalase)”

These sequences were then aligned via the Clustal W (Thompson et al., 1994) alignment package, using the default alignment parameters for the Clustal W server (<http://www.ebi.ac.uk/clustalw>). The alignment was saved as a “.aln” file and subsequently processed by the “*ProteinParser*” software (see Section 5.3) to generate the consensus sequence. A baseline level of “50% Frequency” was set with the following amino acids returned as being more frequent within “*peroxidase consensus protein*”.

Table 5.1: Consensus amino acids calculated utilising a 50% tolerance threshold. The first amino acid listed is the residue present in the HRP gene, the number is the position in the sequence, and the second letter is the most frequent amino acid. The % frequency is also reported.

Amino Acid	% Frequency
T102A	58
Q106R	57
Q107D	57
T110V	75
I180F	73

5.3 Generation of the “*ProteinParser*” Bioinformatic Software.

“*ProteinParser*” is a Java based programme that interrogates aligned sequences at individual residue positions and calculates the percentage amino acid at a particular position. A tolerance level can be defined whereby the programme output will contain only residues over a certain consensus level, e.g. the amino acid occurs at that position in > 50% of the aligned sequences. This novel software was generated in conjunction with Ronan Barrett, School of Computing, Dublin City University, and is freely available for download at www.computing.dcu.ie/~rbarrett/software.html.

```

HRP      : MQLTPTFDNSGKENVSNIVRDTIVNELRSDEPIAASILRLRHPHDCQVNGCDASILLNNTTSFRTKFDAPFGNANSARCFPVIDRM : 84
Consensus : MQL---EY---CP---IV-----R---ASLRLRHEHDCFV---GCD---S---LLD-----EK---A---PN---RGE---VID---I : 42

HRP      : KAAVESACRRTVSCADLLTIAAGSVTLAAGGSESRVPLGRRESLQDFLDLANANTKAEFFTLPOIKDSEKRVNVCINRSSDLVALS : 168
Consensus : K---E---CP---VSCADILALAAKRSVLE---G---E---VPIGRREDS---A---AN---LE---E---L---L---E---GL---DLVALS : 92

HRP      : EGHTFEKNOQRFMDRLYNFSNTGLPDPRLNTTYLQTLRGLCPLNENLSALVDFLLRTETIFDNKYVNL EEQKGLIQSDQELF : 252
Consensus : E---HT---E---E---R---LYN-----DP---LN---TY-----G-----LD---TE---FDN---YY---NL-----SDQ---LF : 125

HRP      : SSPNATDTIPLMRSFANSTQTFENAFVEAMDRIKGNITPLTGTQGOIRLNCRVVNSGSHHHHHHX : 316
Consensus : -----T---V---E-----EF---E---AM---KMGNI---LTG---GEIP---C---VN---HHHHHHX : 155

```

Figure 5.1: GeneDoc™ representation of aligned HRP and consensus peroxidase gene sequence. Black shading is representative of conservation, whilst green colouration signifies the consensus amino acids substituted and analysed in this study. It should be noted that at positions 38 and 102 a difference in sequence is present; however, the amino acids in question are leucine and isoleucine, a very conservative replacement, and so this region is shaded in black. Leu is predicted at position 222; however, a baseline (50% frequency) was noted for this substitution, and was not considered for further analysis.

5.4 Mutational Primer Design.

As previously described in Section 2.21, mutational primers were designed to introduce the “*consensus*” desired mutation. The primers incorporated mismatch basepairs that would generate the desired mutation, once translated. A silent mutation was also incorporated into each primer to insert a novel restriction site close to the desired mutation. Hence, screening of clones for the new restriction sites would indicate the presence of the desired mutation.

5.5 Designed Mutations and Computer Simulations.

Initially, computer aided modelling was utilised to view mutations *in silico*. The HRP crystal structure co-ordinates (Accession Number 1ATJ) were downloaded from the Protein Data Bank (<http://www.rcsb.org/pdb>). Computer simulations, using *DeepView*TM modelling (Figure 5.2 to 5.6), suggested that the mutations would still allow the protein to fold correctly. Site directed mutagenesis was carried out on pBR_I as outlined in Section 2.21. The primers utilised were pBR_I T102A, pBR_I Q106R, pBR_I Q107D, pBR_I T110V, and pBR_I I180F respectively, and the conditions were as per Section 2.22. Mutants were screened with a *Bgl* II digest (T102A, Q106R, Q107D), a *Nae* I digest (T110V), and a *Cla* I digest (I180F), as outlined in Figures 5.7 to 5.9. Successful inclusion of the silent mutation would, in turn, result in a differential cutting pattern that would allow a single clone to be selected for sequence confirmation.



Figure 5.2: *DeepView*TM analysis of the Threonine 102 to Alanine mutation. The mutant is visualised in its most energy stable confirmation, as calculated by the *DeepView*TM software. The heme group is red, the calcium ion in yellow and the mutation is in dark purple.

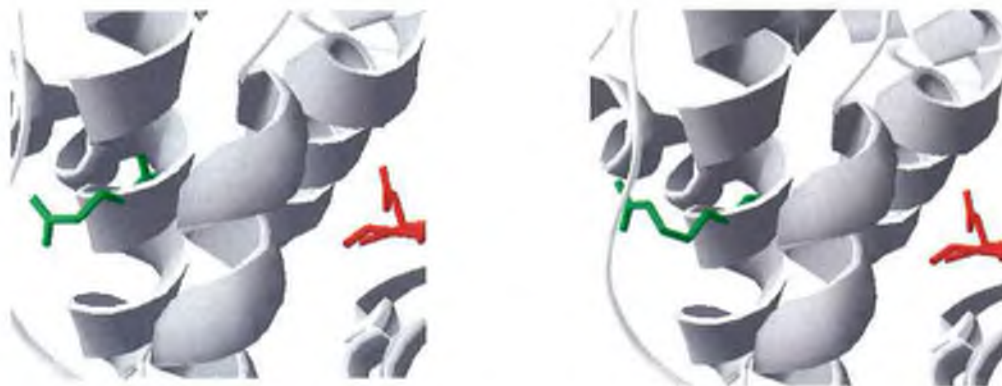


Figure 5.3: *DeepView*TM analysis of the Glutamine 106 to Arginine mutation. The mutant is visualised in its most energy stable conformation, as calculated by the *DeepView*TM software. The heme group is red, whilst the mutation is in green.



Figure 5.4: *DeepView*TM analysis of the Glutamine 107 to Asparagine mutation. The mutant is visualised in its most energy stable conformation, as calculated by the *DeepView*TM software. The heme group is red, whilst the mutation is in light purple.

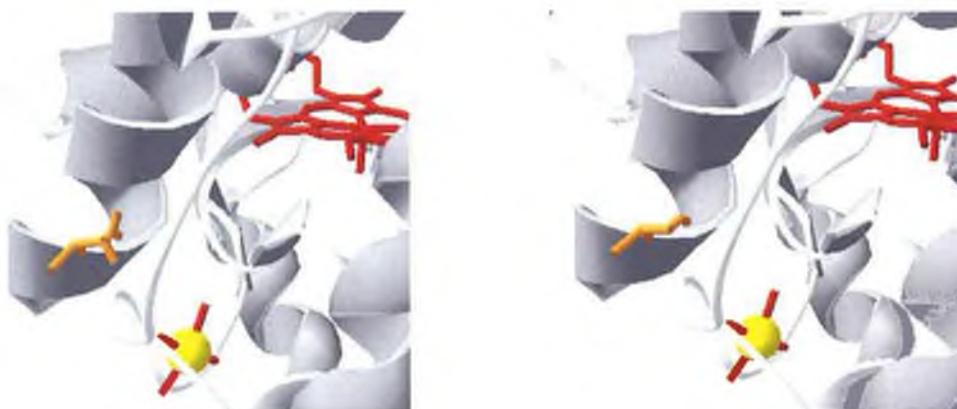


Figure 5.5: *DeepView*TM analysis of the Threonine 110 to Valine mutation. The mutant is visualised in its most energy stable conformation, as calculated by the *DeepView*TM software. The heme group is red, the calcium ion is coloured in yellow, whilst the mutation is in orange.

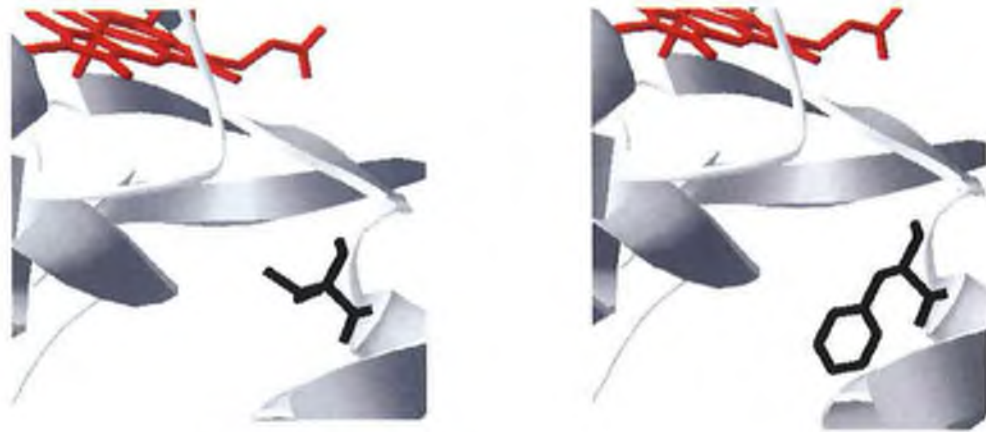


Figure 5.6: *DeepView*[™] analysis of the Isoleucine 180 to Phenylalanine mutation. The mutant is visualised in its most energy stable conformation, as calculated by the *DeepView*[™] software. The heme group is red, whilst the mutation is in black.

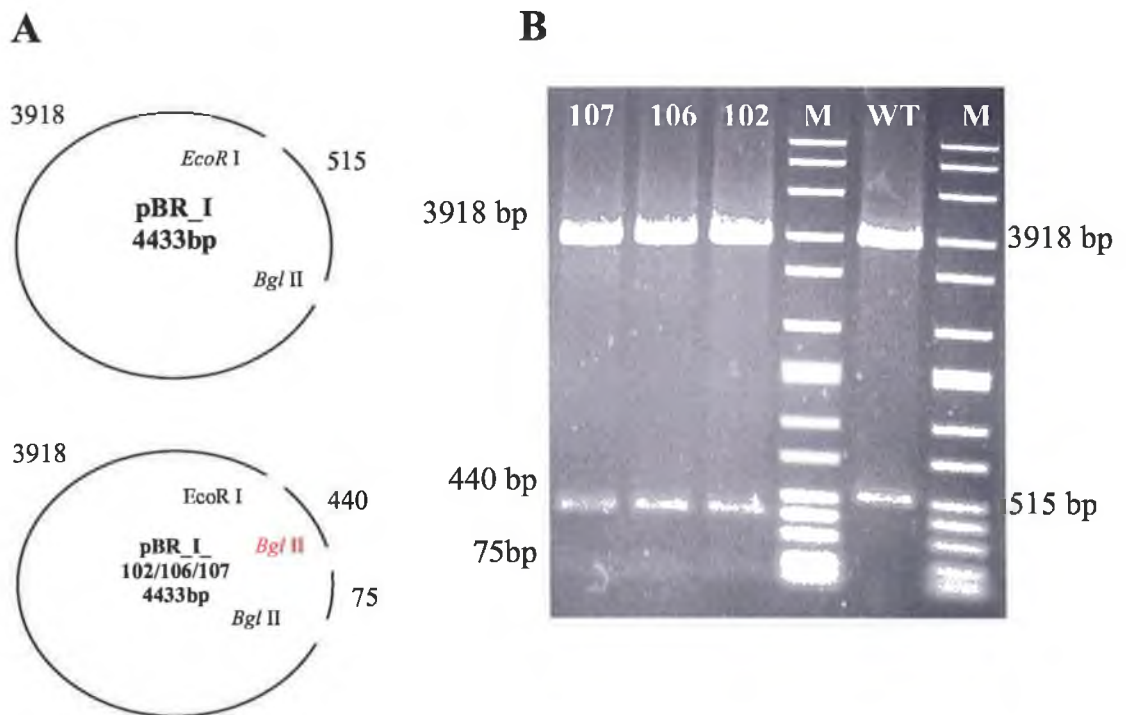


Figure 5.7: Part A represents the expected restriction pattern of pBR_I mutated at either position 102, 106 or 107. *In silico* analysis predicts three bands due to the presence of the mutant *Bgl* II site, one band of approximately 3918 basepairs, another of 440 basepairs, and a final band of 75 basepairs. Part B is the mutant plasmid viewed after restriction and electrophoresis through 1% w/v agarose. The approximate band sizes correspond to the predicted pattern.

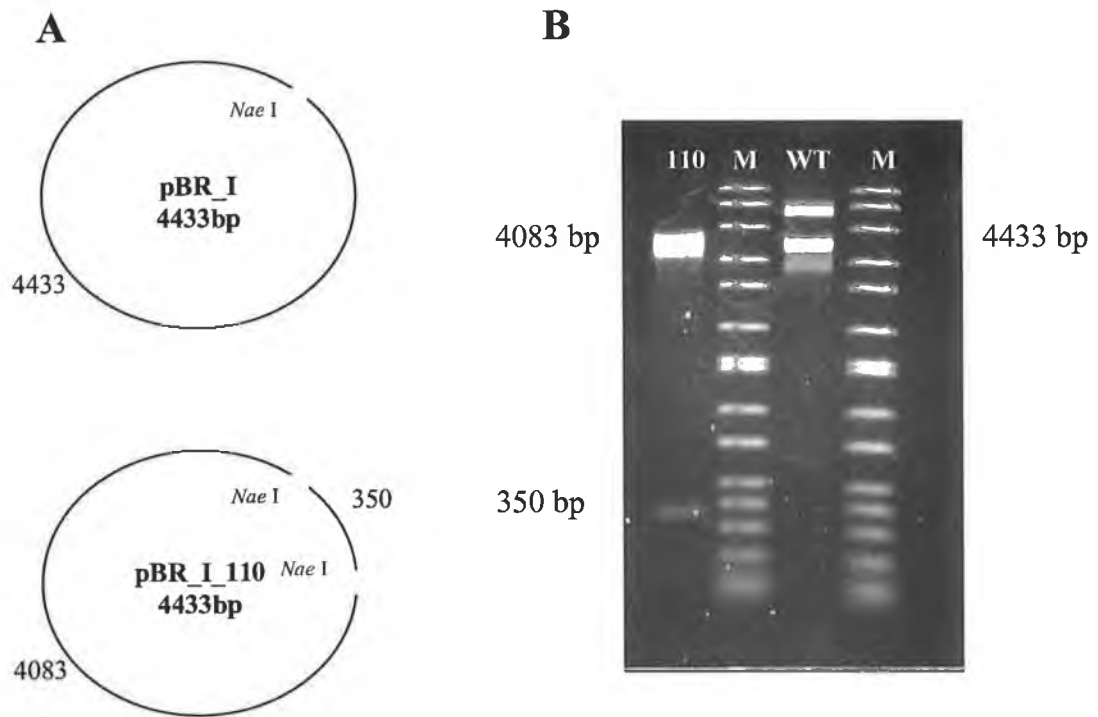


Figure 5.8: Part A represents the expected restriction pattern of pBR_I mutated at position 110. *In silico* analysis predicts two bands due to the presence of the mutant *Nae I* site, one band of approximately 4083 basepairs and another of 350 basepairs. Part B is the mutant plasmid viewed after restriction and electrophoresis through 1% w/v agarose. The approximate band sizes correspond to the predicted pattern.

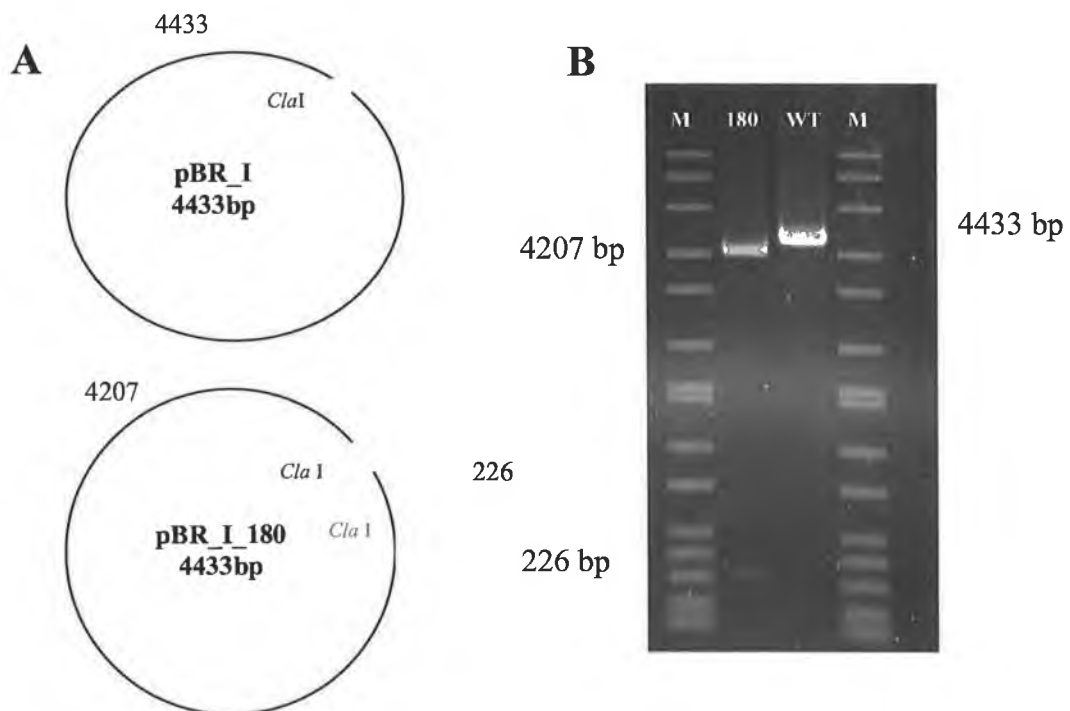


Figure 5.9: Part A represents the expected restriction pattern of pBR_I mutated at position 180. *In silico* analysis predicts two bands due to the presence of the mutant *Cla I* site, one band of approximately 4207 basepairs and another of 226 basepairs. Part B is the mutant plasmid viewed after restriction and electrophoresis through 1% w/v agarose. The approximate band sizes correspond to the predicted pattern. *Cla I* will only restrict Dam- DNA, hence, this plasmid was prepared from a Dam-strain, ER2925 (New England Biolabs, Boston, USA).

5.6 Sequencing of mutants.

Single mutants were selected for sequencing via a restriction digest screening methodology as outlined in Figures 5.7 to 5.9. Selected plasmids were prepared by the Gene Elute™ method, Section 2.8.3, and sent to MWG or Fusion Antibodies Ltd for sequencing using the di-deoxy sequencing method. Results were obtained via e-mail and processed through various bioinformatic packages to confirm correct reading frame of clone, desired mutation and maintenance of gene integrity. The results are outlined in Figure 5.10.



Figure 5.10: Segments of a GeneDoc™ alignment of Consensus Mutants at positions 102, 106, 107, 110 (A), and 180 (B), with wildtype PelB_HRP. The sequences show complete identity, with the exception of the mutated residues, which have been altered to the desired amino acid.

5.7 Characterisation of Consensus Mutants.

5.7.1 Determination of Consensus Mutants Concentration.

Consensus mutants were individually expressed in 500 mL shake culture flasks as previously described, see Section 2.24.4. The recombinant HRP mutants were purified via optimised nickel affinity chromatography, as outlined in Section 2.25. Once expressed and purified (typical specific activity of $\sim 7.5 \times 10^{-3} \mu\text{mol}\cdot\text{min}\cdot\text{mg}^{-1}$), the μM concentration of HRP was calculated as per Section 2.29, with the results outlined in Table 5.2. RZ values of ~ 1.0 were regularly achieved.

Table 5.2: Absorbance at 403nm for all consensus mutant forms of rHRP. rHRP concentrations were calculated using the Beer-Lambert Law, and the rHRP extinction coefficient, $100\text{mM}^{-1}\text{cm}^{-1}$ (Hiner et al., 1995). Protein concentrations were experimentally determined using the BCA assay. “Combination” is a pentuple mutant comprising: T102A, Q106R, Q107N, T110V and I180F.

Mutant	Abs 403nm	rHRP (μM)	Protein Conc ($\text{mg}\cdot\text{mL}^{-1}$)	Heme/Protein Ratio
T102A	0.074	1.52	0.187	0.276
Q1106R	0.074	1.52	0.216	0.239
Q107D	0.110	2.26	0.239	0.320
T110V	0.041	0.85	0.265	0.109
I180F	0.021	0.43	0.157	0.093
Combination	0.130	2.68	903	0.101

Protein concentrations were equalised for all thermal and organo tolerance assays, whilst active rHRP concentrations were equalised for all kinetic studies.

5.7.2 Consensus Mutant Thermal Tolerance.

All thermal tolerance assays were carried out as per Section 2.32 for each of the mutant forms, in triplicate, using recombinant wildtype as a reference, with a final protein concentration of $100 \mu\text{g.mL}^{-1}$ in the reaction solutions.

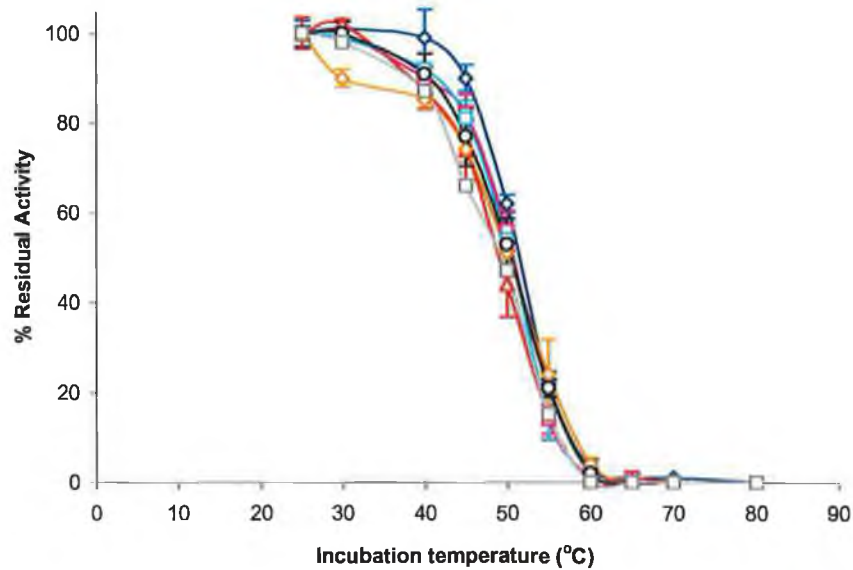


Figure 5.11: Thermal profile of Consensus Mutants \square , T102A; Δ , Q106R; \square , Q107D; \square , T110V; \circ , I80F; \square , Combination; \circ , WT. T_{50} values for each mutant are tabulated in Table 5.3.

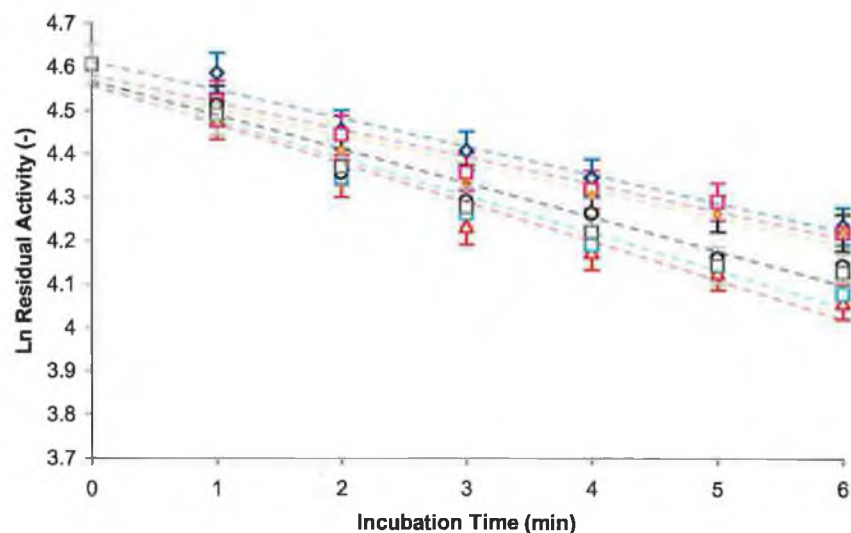


Figure 5.12: Semi-log plot of Consensus Mutants thermal inactivation at 50°C \square , T102A; Δ , Q106R; \square , Q107D; \square , T110V; \circ , I80F; \square , Combination; \circ , WT. $t_{1/2}$ values for each mutant were modelled using *Enzfitter*TM and are tabulated in Table 5.3.

Apparent half-lives for each of the mutants at 50°C were calculated, as outlined in Section 2.33, and are tabulated in Table 5.2.

Table 5.3: T_{50} value, modelled k -value (rate of inactivation) and calculated apparent half-life ($t_{1/2}$) for each consensus mutant at 50°C.

Mutant	T_{50} (°C)	Rate Constant (min^{-1})	%SD	$t_{1/2}$ (mins)	r^2 Value
Wildtype	50	5.59×10^{-2}	± 6.6	12.4	0.98
T102A	51	5.39×10^{-2}	± 7.5	12.9	0.97
Q106R	49	8.52×10^{-2}	± 7.7	8.1	0.96
Q107D	51	6.76×10^{-2}	± 11.0	10.3	0.96
T110V	51	5.07×10^{-2}	± 10.0	13.7	0.93
I180F	50	6.48×10^{-2}	± 10.0	10.7	0.94
Combination	49	7.83×10^{-2}	± 9.4	8.8	0.92

5.7.3 Consensus Mutant Organic Solvent Tolerance.

All solvent tolerances were estimated as per Section 2.34, in triplicate, using recombinant wildtype as a reference at a final protein concentration of $100 \mu\text{g} \cdot \text{mL}^{-1}$. Solvent tolerance profiles were produced for each of the mutant forms. All standard errors were within <5% of the triplicate average reading, so errors bars have been omitted for the sake of clarity.

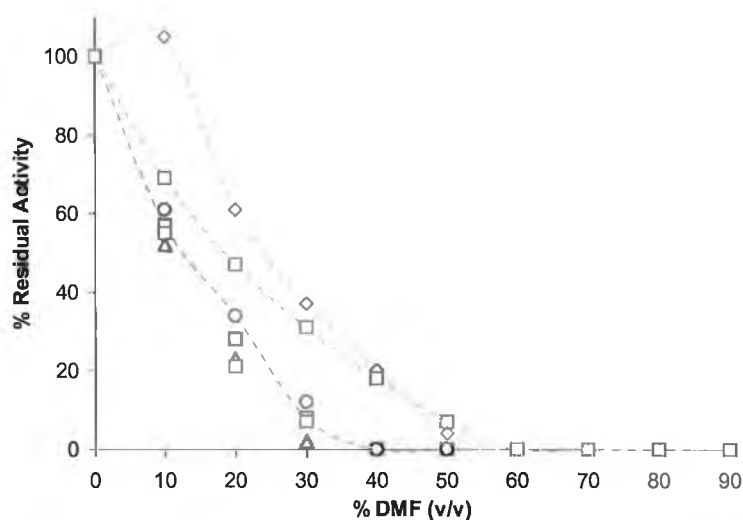


Figure 5.13: DMF Tolerance of Consensus Mutants ◻, T102A; △, Q106R; ◻, Q107D; ◻, T110V; ○, I180F; ◻, Combination; ○, WT.

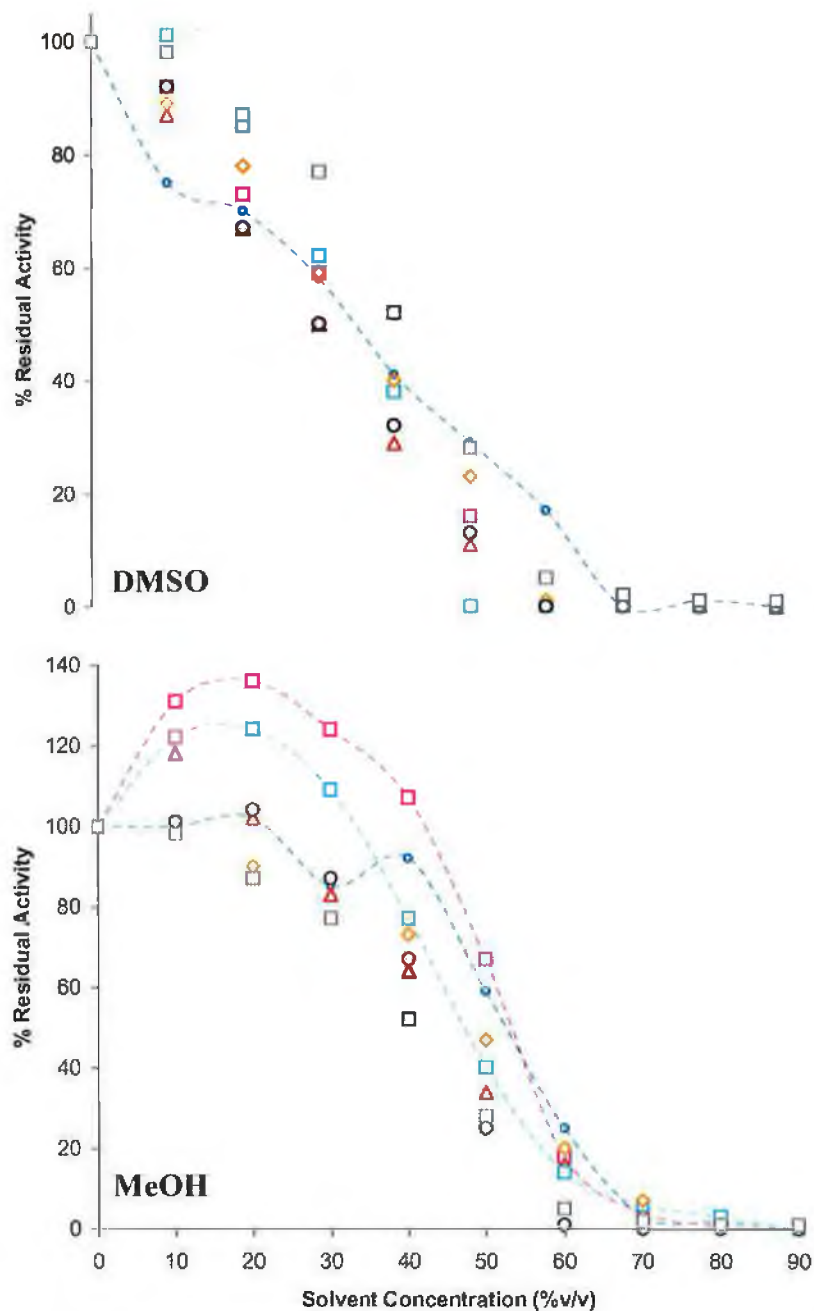


Figure 5.14: Solvent Tolerance (DMSO and MeOH) of Consensus Mutants □, T102A; △, Q106R; □, Q107D; ◆, T110V; ○, I80F; —, Combination; ○, WT.

C_{50} values for each of the mutants at 25°C were calculated, as outlined in Section 2.34, with the results tabulated in Table 5.4.

Table 5.4: Calculated C_{50} for each Consensus Mutant. Standard Errors were less than 5% in all cases.

Mutant	DMSO	MeOH	DMF
	C_{50}	C_{50}	C_{50}
Wildtype	35	53	14
T102A	35	54	12
Q016R	30	45	11
Q107D	35	48	11
T110V	34	45	20
I180F	34	43	14
Combination	35	40	20

5.7.4 Consensus Mutant H_2O_2 Tolerance.

All H_2O_2 tolerance assays were carried out as per Section 2.35 for each mutant in triplicate using recombinant wildtype as a reference. Final rHRP concentration of 360 nM in each reaction. H_2O_2 tolerance profiles were produced for each mutant. Standard errors were less than 15 % in all cases.

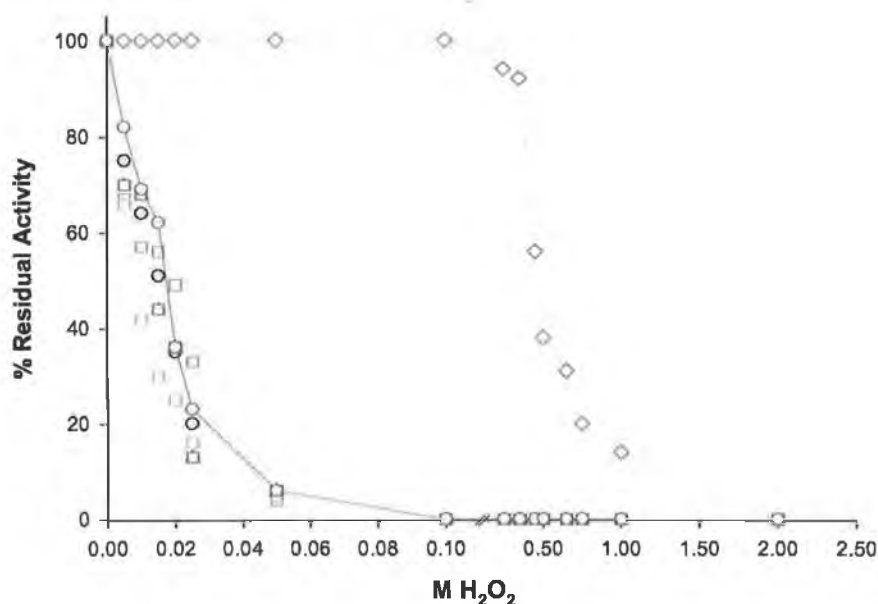


Figure 5.15: H_2O_2 Tolerance Profile of Consensus Mutants \square , T102A; Δ , Q106R; \square , Q107D; \diamond , T110V; \circ , I180F; -, Combination; \circ , WT.

Table 5.5: Calculated H₂O₂ C₅₀ for consensus mutants.

Mutant	mM H₂O₂ C₅₀	% Error
Wildtype	17	± 4
T102A	17	± 13
Q106R	7	± 6
Q107D	18	± 3
T110V	425	± 11
I180F	17	± 4
Combination	8	± 1

5.7.5 Consensus Mutant Steady-State Kinetics.

All kinetic assays were carried out as per Section 2.36, with a final rHRP concentration of 30 pM in each reaction solution. Apparent K'_m and k_3 values were calculated by the software package *Enzfitter*TM. All experiments were performed in triplicate, with the average value being used in the analysis. Again, recombinant wildtype HRP was used as a reference.

Table 5.6: Steady-state kinetic of consensus mutants, with ABTS as reducing substrate. Apparent K'_m and k_3 values, including standard errors, were calculated using *Enzfitter*TM.

Mutant	k_3 (s⁻¹)	SD (s⁻¹)	K'_m (μM)	SD (μM)
Wildtype	482	± 12	0.093	± 0.013
T102A	605	± 37	0.200	± 0.30
Q106R	359	± 7	0.541	± 0.25
Q107D	486	± 33	0.885	± 0.09
T110V	374	± 4	0.170	± 0.02
I180F	497	± 3	0.308	± 0.02
Combination	491	± 10	0.062	± 0.007

5.8 Discussion.

The aim of these experiments was to identify, produce, verify and characterise semi-rational site-directed mutants of the HRP gene situated in the pBR_I plasmid. A semi-rational mutational strategy, based on the consensus approach, was utilised in the identification of key residues for mutation in this study. The consensus approach, in its simplest application, is a comparative methodology. Different relations of a particular protein are aligned against each other and the consensus, or most common, amino acid at a particular position is estimated (Lehmann et al., 2000). In recent years, however, variations of this simple methodology have been implemented to stabilise β -lactamase (Amin et al., 2004) and to alter the cofactor specificity of a lactate dehydrogenase (Flores and Ellington, 2005). *In vivo*, proteins are under no selective pressure to form optimally stable structures; instead, they tend to form structures of adequate stability, i.e. the protein is just stable enough not to limit the host organism's viability (Magliery and Regan, 2004). As such, there is a wide scope for stabilisation of mesophilic proteins, with the substitution of non-consensus amino acids by consensus ones offering a feasible approach to improve the stability of a protein.

5.8.1 Consensus Mutation Selection and Generation.

In this study, 100 peroxidase sequences were downloaded from the freely available gene bank, hosted by the National Centre for Biotechnology (www.ncbi.nlm.nih.gov). The search (carried out on the 5th August, 2005) was restricted to full length, confirmed plant peroxidase proteins, using a variety of limit Booleans in the search. The results yielded 548 protein entries; however, about 1/5 were repeat sequences and were not used as part of the consensus generation. The sequences were aligned utilising the alignment tool, Clustal W (www.ebi.ac.uk/clustalw), employing the programme's default settings. The output ".aln" file was used as the entry data in the novel Java-based "*ProteinParser*" programme. This software interrogated each residue at each position in the peroxidase sequence, and, given a tolerance threshold of 50% identity, generated a consensus amino acid for each position. The "*Consensus Plant Peroxidase Protein*" was then aligned with the HRP protein sequence and similarities and differences were noted. The HRP protein demonstrates a 49% similarity the Consensus Protein. More significant for this study, however, the HRP protein differs from the Consensus Protein at five positions, four of which are within a

conserved region, residues 94-111, and these residues were therefore selected for mutation to the consensus residue.

As previously outlined in Section 4.8.1, the consensus mutants were synthesised using the optimised two-stage mutagenic PCR strategy (Wang and Malcom, 1999). Also, a silent diagnostic restriction site was included in the mutagenic primer to allow for rapid, economical screening of several potential clones. Once all clones were synthesised, screened and the mutations confirmed by commercial sequencing, the results were aligned using GeneDocTM bioinformatic software to demonstrate the identity and the location of the mutations. One of the key results from this chapter is the generation of a suite of site-specific, semi-rationally designed, HRP mutants based in the modified pQE60 expression vector (see Chapter 3). These clones permitted the expression, purification and characterisation of the desired mutant proteins with the aims of (i) generating a stabilised form of recombinant HRP, and also of (ii) ascertaining the applicability of the consensus approach to stabilising rHRP.

5.8.2 Thermal Stability.

Initial characterisation of the consensus mutants comprised thermal profiles and thermal inactivation. As stated previously, all thermal studies were carried out at a constant protein concentration, in order to normalise any possible effects of protein concentration on stability. Thermal profiles of the consensus mutants suggested that 50°C was a suitable standard temperature at which to carry out thermal inactivation. Although the consensus mutants did not display any increase in T_{50} in comparison over wildtype, the lowest T_{50} noted (Q106R and Combination Consensus; this latter pentuple mutant comprises T102A, Q106R, Q107N, T110V and I180F) was within 4% of the wildtype value. This corresponds closely to previous results (see Table 4.2). *Enzfitter*TM modelling of thermal inactivation data permitted the calculation of the apparent half-life, $t_{1/2}$, of the mutant enzymes at 50°C and direct comparison with the recombinant wildtype form of HRP. Only two mutants displayed increased thermal stability as judged by the $t_{1/2}$ value, namely T102A and T110V. These displayed a marginal 4% and 11% increase in $t_{1/2}$ respectively, whilst the remaining mutants all showed decreased thermal stability, ranging from a 17% (Q107D) to 35% (Q106R) decrease in $t_{1/2}$ versus wildtype. T102A is located in Helix D (Gajhede et al., 1997) at the back of the substrate-binding site and, as such, incorporation of an alanine residue in the helical secondary structure is acceptable. Ala, a small non-charged amino acid,

may lead to improved helical structure (Fersht and Serrano, 1993, and Nosoh and Sekiguchi, 1990) resulting in decreased protein entropy and, hence, improved thermostability. Rojkova and co-workers (1999) recently described a 24% increase in thermal stability by a single serine-to-alanine helical substitution. They utilised a consensus-based approach together with rational stabilisation logic (hydrophobization of the α -helix structure) to select the helical residues for mutation, and thus confirmed the important role of alanine residues in helical structure stabilisation. T110V is located on the last turn of the same helix, (D; Gajhede et al, 1997) as T102A. Recent reports suggest that incorporation of valine into helices can be destabilising (Brosnan and Brosnan, 2006), although several studies concluded that helical valines may instead stabilise proteins (Gregoret and Sauer, 1998): Val's conformational rigidity lowers the entropic cost of forming favourable side-chain van der Waals interactions (Cornish et al., 1994).

In comparison, substitution of the glutamine residues at positions 106 and 107, with aspartic acid and bulky arginine could place increased torque on the helix, leading to destabilisation and, hence, to the observed decrease in thermal stability. Recently, however, arginine residues have been demonstrated to occur at high frequency in α -helical structures in thermophilic enzymes, with the propensity towards a central location within the helix structure (Kumar et al., 2000). Conversely, in this study, the introduction of an arginine residue at the centre of a helix results in the least thermal stable HRP mutant. Additionally, the H-bonding side chain of aspartic acid is known to compete directly with backbone H-bonds of the helix structure; this disrupts the secondary structure and leads to protein destabilisation (Chou and Fasman, 1978). Also, due to the buried nature of these mutations, re-orientation of the core packing may cause decreased thermal stability. Previous studies have demonstrated that, in most proteins, the core is exquisitely packed and stabilisation by mutation is generally difficult to achieve; as a result, any mutation will probably result in suboptimal packing (Lee and Vasmatzis, 1997). Another possible reason for destabilisation resulting from the substitution of Gln 106 and 107 with charged amino acids, Arg (106) and Asp (107), is the introduction of an unpaired charge in the protein core. Ladbury and co-workers (1995) demonstrated that an unpaired charge in the core of an *E. coli* thioredoxin protein results in reduced heat stability and unfolding of the protein. The I180F mutation, located close to a helix, gave no significant alteration in thermal stability over wildtype. Although not noted for helical propensity, Phe can

serve as a helical amino acid, as the helix-forming tendency of a particular amino acid depends on the sequence context in which it occurs (Padmanabhan et al., 1990). The combined mutant, (T102A/Q106R/Q107D/T110V/I80F), displayed a 30% decrease in thermal stability, indicating that thermally stabilising mutants cannot offset the negative effects of destabilising substitutions (in HRP at least). Indeed, the mutations could be seen to be *'subtractive'*, as the decreased stability for the combination mutant matches the least thermostable mutant, Q106R.

As outlined previously, thermal stabilisation of proteins is both complex and challenging. The exact mechanisms of protein stability remain unclear, with several phenomena playing important roles, often in a concerted fashion. Hence, slight adjustment of one of these factors may have a knock-on effect onto other stabilising interactions, as discussed for amino acid charge interactions (Vendruscolo, 2002). Although previous consensus-based approaches have yielded proteins with increased thermal stability (Lehmann et al. 2000, and references within, Lehmann et al 2002, and Lett et al., 1999), it has also allowed for identification of particular residues that influence thermal stability (Hakamada et al., 2001, Clemente and Marquez, 2000). From the present data, it is clear that mutation of helix-favouring residues to residues within the enzyme core without helical propensities can have detrimental effects on HRP thermal stability.

5.8.3 Organic Solvent Stability.

The effects of different organic solvents on the consensus mutants were also analysed. As before, solvents were chosen based on their denaturation capacities (Methanol, low; and DMF, medium; Khmelnsky et al 1991a), and from previous heme plant peroxidase solvent studies (DMSO, Santucci et al., 2003; and N. Carolan, PhD Thesis, Dublin City University, 2004). In all cases, consensus mutants were inactivated as the percentage volume of organic solvent increased. Overall, no increases in organo-tolerance were noted for any of the solvents tested compared with wildtype. As previously described, solvents can effect protein denaturation in a number of ways, including removal of the hydration shell close to the protein backbone. In an aqueous environment, an enzyme can be visualised as comprising two regions. The first, of high polarity, is in contact with the aqueous solution, while the second region is concealed from the aqueous environment. When, however, the polarity of the hydration shell is decreased by sequential removal of aqueous solvent and

replacement by non-aqueous solvent, the previously-sequestered hydrophobic region begins to disperse, resulting in disorganisation and destabilisation of the protein (Butler, 1979). The C_{50} value (Section 2.34) was again utilised to compare organo-tolerance across the mutant matrix. The largest decrease in C_{50} was 25%, for the combination mutant in MeOH. Q106R displayed at least a 12% decrease in organo-tolerance in all solvents tested. Versus wildtype, T110V and the combined mutant showed increased stability in DMF, decreased stability in MeOH and comparable stability in DMSO. I180F displayed similar stability to wildtype in DMSO and DMF, but lower stability MeOH. T102A and Q107D displayed similar stabilities to wildtype in all solvents tested.

Previous computational analysis of protein mutation suggests that most mutations within the protein backbone will have neutral effects on protein stability, due to the flexibility of the protein structure (Palma and Curmi, 1999). Also, conservative substitutions that maintain protein polarity do not cause a notable loss of solvent tolerance compared to wildtype. Mutation of the Gln 106 may cause minor destabilisation of the protein backbone, which in turn promotes unfolding and loss of activity in non-natural environments, although this would have to be confirmed by crystallisation studies. The effect of charge introduction (e.g. Q106R) may explain the drastic loss of thermal and medium loss of organo-stability for both Gln mutants, possibly due to long-range structural perturbations induced by single amino acid substitutions (Vendruscolo, 2002). Interactions between closely situated amino acids are known to influence secondary structure, which in turn contributes to overall protein stability (Munoz et al., 1996). Note that all mutants display an activation in 10% v/v MeOH, with T102A displaying a 35% increase in activity in 20% v/v MeOH; however, no overall stability gain is afforded by any mutation, as all C_{50} values are equal to, or less than, wildtype's. Peroxidase activation in MeOH has previously been reported, with the activation process being attributed to an altered form of the peroxidase conformational structure in the presence of an organic solvent (Carolan N, PhD Thesis, Dublin City University, 2004). No activations are noted in the other two solvents tested. The effects of each solvent on HRP and methods of stabilisation have been previously discussed (Section 4.8.3). The present results do indicate, however, that certain residues are important for the organo-stability of recombinant HRP. Q106 clearly maintains a stabilising interaction within the HRP molecule. This maybe charge- or space-fill related, or a combination of both;

however, from the results outlined in this chapter, its presence is essential to the solvent-stability of the recombinant HRP molecule.

5.8.4 H₂O₂ Stability.

The H₂O₂ tolerance of consensus mutants was also investigated, with the results mirroring the thermal stability characterisation. Three mutants (T102A, Q107D and I180F) displayed almost identical C₅₀ values to wildtype. Q106R, the least stable mutant under all conditions tested, demonstrated a 58% decrease in H₂O₂ tolerance, compared to wildtype. Interestingly, T110V stabilises the protein against high H₂O₂ concentrations; this may be due to the removal of the –OH moiety of Threonine, which could oxidise to an aldehyde or acid carboxyl in the presence of the reactive oxygen species generated during H₂O₂ catalysis. Valine, although a similar amino acid, contains only an aliphatic side chain (Creighton, 1993). The ‘*subtractive*’ nature of this set of mutations is again noted as, similar to the thermal characterisation, a significantly destabilising mutation (Q106R) cannot be “*rescued*” by inclusion of a stabilising mutation (T110V).

5.8.5 Kinetic Characterisation.

The effect of consensus mutations on the kinetics of recombinant HRP was investigated under steady-state conditions with ABTS as reducing substrate. As discussed previously (Section 4.8.5), peroxidase kinetics do not follow the traditional Michaelis Menten model; instead k_3 and K'_M , or the apparent catalytic constants, are routinely used to describe peroxidase reaction rates. Two of the consensus mutants, Q106R and T110V, displayed a decrease (~25%) in k_3 , with the remaining mutants all displaying a value equal to or greater than wildtype. The largest increase in k_3 , 25%, was noted for T102A; typically however, k_3 varies between 0% to 25% of the wildtype value. The importance of charge and suitable space-fill characteristics are noted for mutations in this region: those located at the back of the substrate-binding site (T102A, Q106R, Q107D) display a similar $k_{3\text{ app}}$ to wildtype. In contrast, these mutations notably affect the K'_M for ABTS, with increases of 9.5-fold noted for Q107D, almost six-fold for Q106R, and over two-fold for T102A. These increases in K'_M can be attributed to mutation-induced alterations within the substrate-binding domain.

5.8.6 Failure of Consensus Approach: Bioinformatic Analysis.

As outlined, only two mutants (T102A and T110V) registered marginal stability gains over wild type, in sharp contrast to previous consensus studies with other enzymes (Miyazaki et al., 2001, Lehmann et al., 2000 and 2002, Amin et al., 2004; Flores and Ellington, 2005). This unexpected outcome prompted further investigation, utilising bioinformatic analysis of the Class III peroxidases and comparison of wildtype rHRP to a novel hypothetical archetypal peroxidase sequence, as a means to explain the apparent failure of this approach to stabilise rHRP. This section of the study was undertaken in conjunction with Dr. Mary J. O'Connell, School of Biotechnology, Dublin City University. All of the following bioinformatic analysis was carried out by Dr. O'Connell at "The Bioinformatics and Pharmacogenomics Laboratory", NUI Maynooth, Ireland.

5.8.6.1 Consensus Methodology Validation.

The Consensus Approach outlined in Section 5.2 ignores phylogenetic relationships among the sequences and so may be biased towards those clades (sub-groups) where there are more sequences available, due to redundancy of GenBank. For this reason, and to validate the consensus sequence generated in this study, a phylogenetic approach based on a recently published phylogenetic tree for the Class III plant peroxidases (Duroux and Welinder, 2003) was applied to produce a second consensus sequence. This tree was "*pruned*" by selecting a single representative from each clade. The resulting sequences were aligned and a phylogenetic consensus peroxidase was generated, as previously outlined in Section 5.2. Comparison of the original consensus sequence, based on a frequency counting algorithm, with the phylogenetic one revealed 90% identity, validating the original consensus methodology.

Further investigation of Class III peroxidases resulted in the generation of a hypothetical archetypal peroxidase sequence. Reconstructed ancestral protein sequences have rapidly developed as an important way to infer information about a protein's evolutionary history (Hall, 2006). The ancient peroxidase sequence was formulated utilising powerful bioinformatic software in which a model-based statistical algorithm for maximum likelihood (ML) reconstructs the complete set of all ancestral nodes on the phylogenetic tree. This algorithm for marginal reconstruction applies Bayesian statistics to define the most probable character state for each ancestral character, given a set of extant sequences and their phylogenetic

relationships. This statistical approach has previously been shown to yield very high confidence intervals (91-99% accuracy for Lysozyme c sequences; Yang et al., 1995) and was recently validated by Hall (2006), see Figure 5.16.

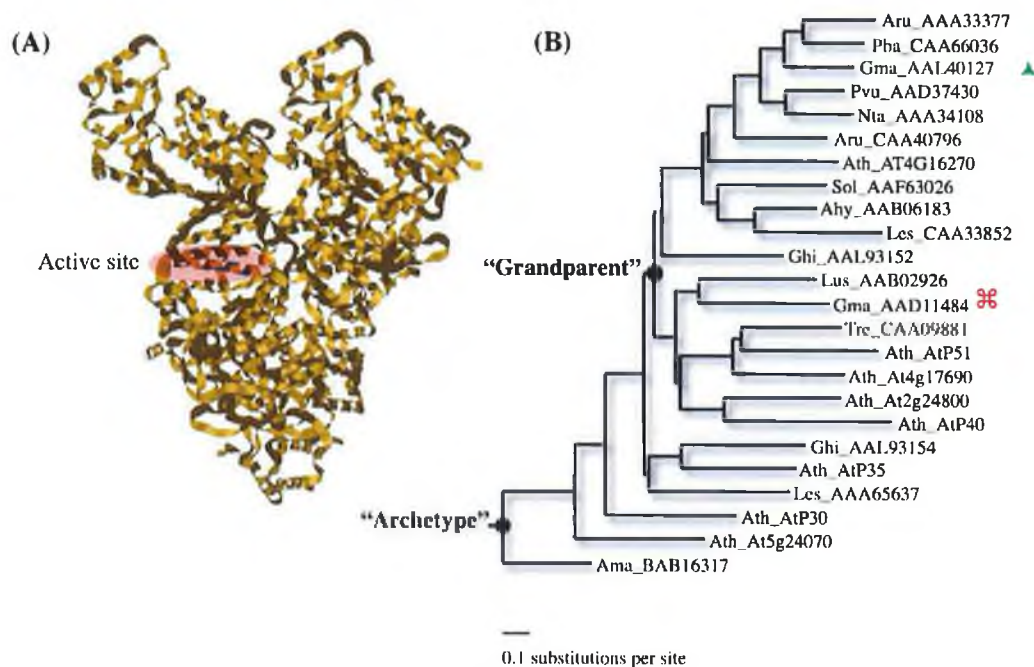


Figure 5.16: Part (A) depicts a ribbon 3-D structure of modern day HRP, as deposited in PDB (*IATJ*). The active site residues conserved throughout the evolution of the peroxidase phylogeny are highlighted in red. Part (B) is the Reduced Phylogenetic tree adapted from Duroux and Welinder (2003). A sequence representing each of the 24 clades identified for the peroxidase family (one unavailable due to sequence mis-annotation) were taken at random from the published and fully resolved peroxidase phylogenetic tree (Duroux and Welinder 2003). The phylogenetic tree above was generated using a Maximum likelihood method implemented in PAML (Yang, 1997). Branch lengths represent the degree of sequence divergence, the scale in number of substitutions per site is given below the tree. The leaves of the phylogeny represent the following species names before the “_”: Aru, *Armoracia rusticana*; Pba, *Populus balsamifera*; Gma, *Glycine max*; Pvu, *Phaseolus vulgaris*; Nta, *Nicotiana tabacum*; Ath, *Arabidopsis thaliana*; Sol, *Spinacia oleracea*; Les, *Lycopersicon esculentum*; Ghi, *Gossypium hirsutum*; Lus, *Linum usitatissimum*; Tre, *Trifolium repens*; and Ama, *Avicennia marina*. The number following the “_” is the Genbank Accession number. The clade representing HRP and HRP_A2 is denoted by (▲), whilst the SBP representative is depicted by (⌘). The closest branchpoint between HRP and SBP is denoted by “Grandparent”, whilst the hypothetical archetypal peroxidase sequence is defined as “Archetype”. Image generated by Dr. M.J. O’Connell.

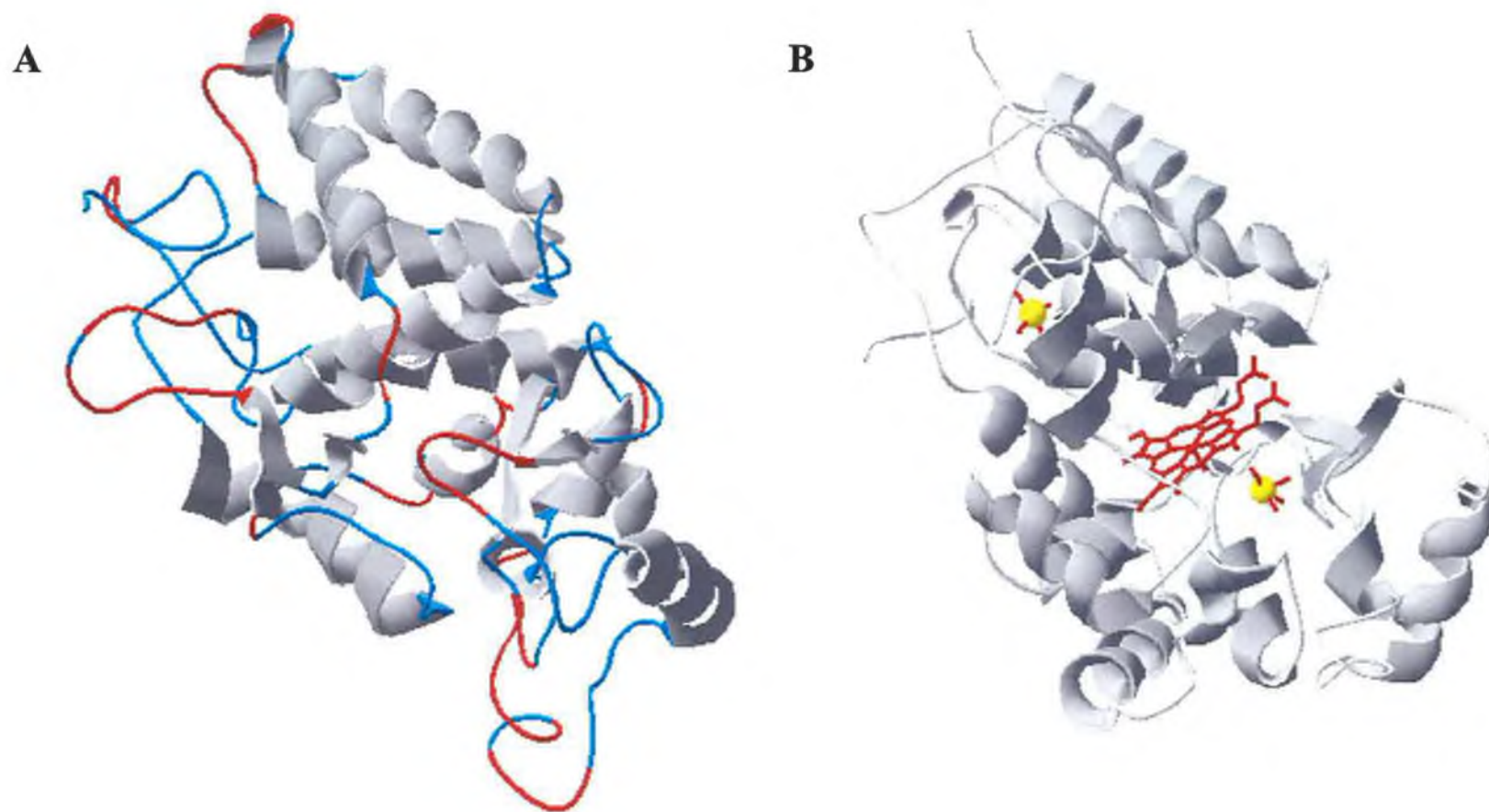


Figure 5.17: *DeepView*[™] modelling of the hypothetical archetypal peroxidase (A) compared to the modern day HRP (B). Archetypal sequence was submitted to the SWISS-MODEL web server, which provides an automated protein homology-modelling service (Guex and Peitsch, 1997; Schwede *et al.*, 2003). The heme group is highlighted in red and the calcium ions are highlighted in yellow in part (B).

The most ancient reconstructed peroxidase pre-dates all other peroxidases and represents the first or “archetype” peroxidase. The second peroxidase used in the comparison represents the most recent common ancestor (MRCA) of the SBP and HRP enzymes, the “grandparent”. SBP is known to be a more stable plant peroxidase than HRP (McEldoon and Dordick, 1996) and, hence, elucidation of key stabilising differences between SBP and HRP would be advantageous. The “archetype” and “grandparent” full-length sequences should agree closely with the consensus sequences generated by *Protein Parser*. Comparison of these ancestral sequences with the consensus sequences generated from both the frequency counting and phylogenetic approaches reveals agreement across most of the alignment (grandparent 97%, archetype 85%). All three approaches identified T102A, Q106R and Q107D. Furthermore, two of the three methods (frequency counting and ancestral protein generation) revealed T110V and I180F. Again, these correspondences confirm that the initial consensus-identification approach was valid.

5.8.6.2 Class III peroxidase Bioinformatic Analysis.

Only one mutation, T102A (4% increase in thermal stability, Table 5.3), was predicted by all three consensus methods applied. This substitution is also present in the notably more stable SBP, and was generated (together with other mutations) in Morawski and co-worker’s (2001) directed evolution study of HRP; however, T102A was not studied alone and was included among mutants with enhanced activity rather than increased stability. It is also interesting to note that only one other of Morawski and co-workers mutations (2001), at position F221L, was predicted by consensus methodology (specifically, by the *ProteinParser* programme and the “Archetype” sequence), although previous reports have shown that this position can influence HRP stability (Morimoto et al., 1998; and Howes et al., 2001b). Alignment of the relevant sequences reveals that HRPC consensus substitution T110V actually occurs in the more stable SBP but, curiously, the T102A and I180F substitutions occur in both SBP and in the less stable HRP_A2. These coincidences suggest that the consensus approach is not a fruitful one for plant peroxidases, irrespective of its success with other proteins. Further, four of the five consensus positions lie within a very short, nine-residue cluster spanning T102 - T110 in helix D (Figures 5.2 – 5.5), with only I180 occurring outside this region (between helices F and F’). This narrow focus of the peroxidase consensus positions may explain the lack of stability gains in the

present instance. No such clustering is apparent in previous reports of consensus protein stabilization, where the various consensus positions are distributed more evenly throughout the entire sequence (Lehmann et al., 2000). In contrast, this study indicates that the peroxidases are not a suitable case for consensus building. Figure 5.18 displays the clusters of consecutive columns in the constructed consensus sequence. From previous studies on peroxidases within *A. thaliana*, these enzymes share on average 75% identity in their primary structure (Welinder, 2002). This indicates that within the *A. thaliana* clade there is strong selective pressure to retain the structural confirmation. It is known that there is close similarity between Horseradish Peroxidases and their equivalent *A. thaliana* peroxidase, for example HRP A2 is 95% similar to *A. thaliana* A2 peroxidase (Nielsen et al., 2001).

The ancestral peroxidase generated in this study (Dr. M.J. O'Connell) permits the peroxidase structural form to be traced. It appears that the Class III peroxidases have evolved to retain their structural helices and active site, suggesting that structure and function are tightly associated in this family (see Figure 5.18). There is some slight sliding of helices throughout evolution but this is acceptable over longer periods of time (Lesk, 2004). Alternatively, peripheral regions of a protein outside the helices are free to change their folding pattern entirely (Lesk, 2004). Retention of such structures suggests that these enzymes have a very ancient function consistent with their modern day one. From this study it is clear that identification of the key residues giving rise to HRP stability must rely on some methodology other than the consensus approach.

Finally, several researchers have noted that stability differences between homologous proteins may be due to a very few naturally occurring sequence variations (Eijsink et al., 2004 and references within). Previous published reports of consensus mutations have also noted low, 33%, success rates (i.e. mutants with increased stability as a percentage of the total mutants generated; Lehmann et al., 2000). Magliery and Regan (2004) have recently developed a more advanced consensus model, which accounts for some of the inadequacies of the basic consensus approach (Lehmann et al 2000), including: accounting for (i) regions of poor consensus and (ii) regions of high homology that mask subfamilies. A collection of subfamilies may also negatively affect the basic consensus result, and this is rationally integrated into the statistical free energy model (Magliery and Regan, 2004). This present study, however, aimed to refine a simple, easy to implement, frequency-counting methodology, as opposed to the more complex simulation of the covariation of amino acid residues.

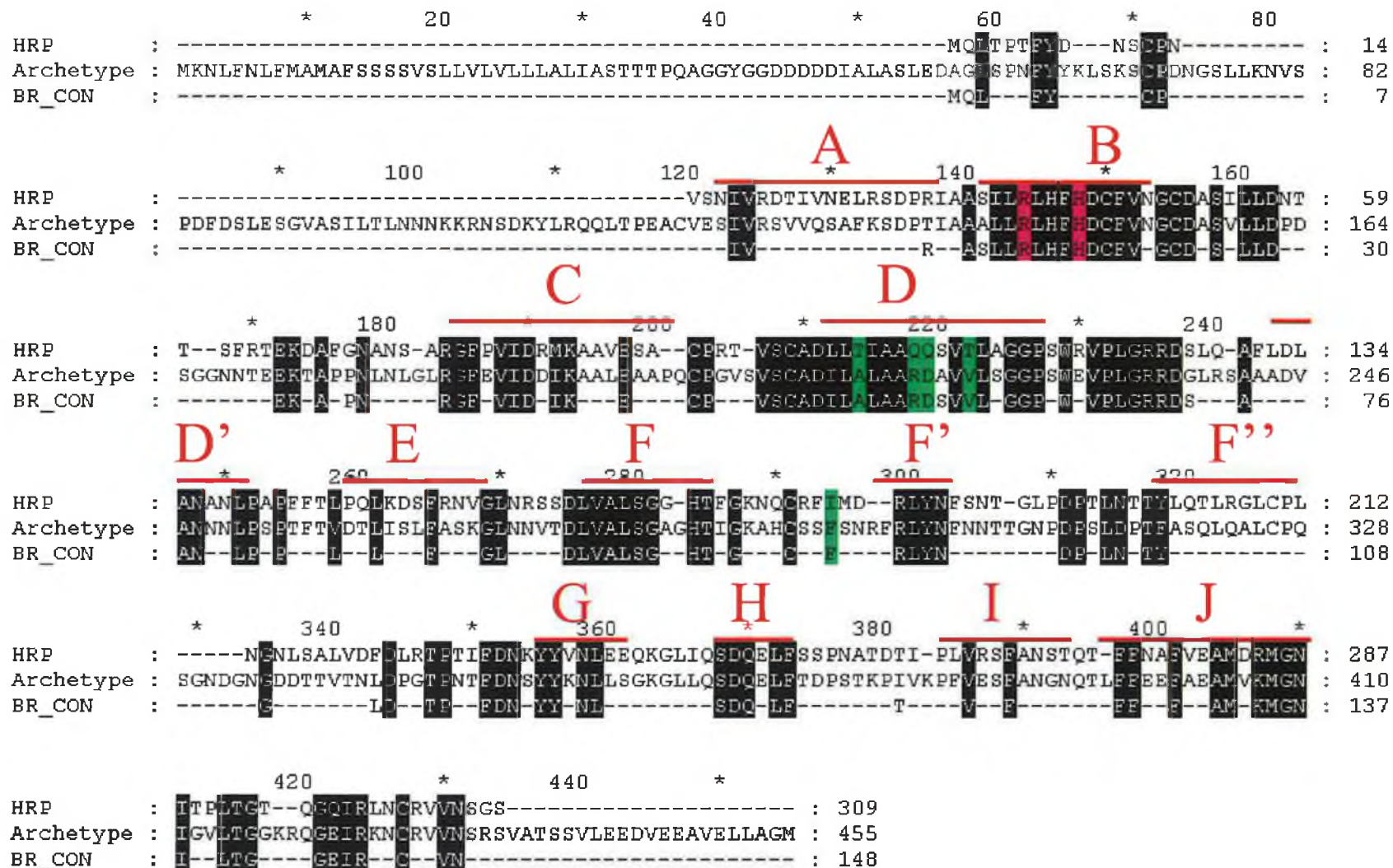


Figure 5.18: Location of helices within HRP, the hypothetical archetypal peroxidase and *Protein Parser*-generated consensus protein (BR_Con). The defined “block” nature of the consensus residues is also clear. Residues selected for mutation as part of this study are highlighted in green, whilst the catalytic residues are coloured in red. Numbering above the sequences is based on the larger hypothetical archetypal peroxidase. Image generated in GeneDoc™ as outlined in Section 2.20

5.9 Conclusion

This chapter describes the application of a semi-rational consensus approach to protein stabilisation. Residues were selected for substitution based on direct comparison with the *ProteinParser* “*Consensus Peroxidase Protein*”. The *ProteinParser* frequency counting algorithm is valid, as confirmed by two separate approaches (phylogenetic and archetype generation procedures). It was noted that certain residues were important for rHRP stability. Mutation of Gln 106 results in decreased thermal and solvent stabilities. Saturation mutagenesis, however, is required to confirm the potentially important role of Gln 106 in HRP stability. Disappointingly, many of the mutants displayed similar (or inferior) thermal and solvent stabilities as wildtype rHRP. Surprisingly, T110V displayed dramatic H₂O₂ stability, and requires further study to elucidate the key interactions causing this stabilisation. A possible *pseudo-catalase* activity may be attributed to this mutant’s ability to function at high concentrations of H₂O₂. Major differences are noted, however, between the mutants and wildtype in apparent binding coefficient, K'_M , the opposite of what was observed for the Lys-Glu substitutions (Chapter4). This is possibly due to the location of the mutations, close to the binding site, and not the mutation itself. A subtractive, destabilising affect was noted upon combination of all the individual mutations.

Sequence comparison of the modern-day HRP with the hypothetical archetypal peroxidase sequence generated in this study suggested the important role of conserved helices within the Class III peroxidases. The determinants of the different thermal stabilities seen among plant peroxidases (e.g. HRP A2, HRP C and SBP) evidently lie in the unstructured loops linking the conserved helices. Unfortunately, these loops show a low incidence of consensus amino acids, so rational or semi-rational design of stabilizing mutations within these loops remains a challenging task.

Chapter Six.

Immobilisation and Sensor Development.

6.0 Introduction.

Protein immobilisation has been studied for many years, mainly focussing on the simplest immobilisation technique, adsorption. This methodology, although simple to implement, suffers from several drawbacks, including the removal of adsorbed protein by stringent washing, high contamination (due to non-specific protein binding) and denaturation of proteins adsorbed onto hydrophobic surfaces (Cretich et al., 2006). Covalent immobilisation of proteins offers a more robust approach and, in recent years, this technology has developed rapidly, primarily due to the increase in number and range of activated solid supports, and the ability to engineer or chemically modify biomolecules to allow for easier covalent attachment. Protein chemistry is now commonly utilised to covalently bind biomolecules to an activated solid phase via reactive amino acid side groups. In recent years, several protein-engineering strategies have introduced reactive amino acids to promote directed protein immobilisation. Lysine is the most commonly utilised amino acid in this instance, due to the fact that it can be incorporated into most secondary structures with minimal distortion of the protein backbone. This compares to the more reactive cysteine, which can cause misfolded proteins due to unpaired disulphide bridges (Allard et al., 2002). While site-directed thiol-based immobilisation has been achieved (Zhen et al., 2004), employing a cysteine-free wildtype protein reduces the risk of protein misfolding (Huang et al., 1997). Although generic approaches to orientated protein immobilisation are rapidly developing (His tags, Leucine zippers, etc.), there still remains a need for the development of site-directed, directionally immobilised proteins.

Peroxidase application spans the bioscience and biotechnology spectra, ranging from bioremediation (Wanger and Nicell, 2002) and biocatalysis (van de Velde, et al., 2001) through diagnostics (Dotsikas and Loukas, 2004) to recombinant protein expression (Jung et al., 2001), transgenics (Veitch, 2004), bioinformatics (Duroux and Welinder, 2003), protein engineering (Morawski. et al., 2000) and even to therapeutics (Tupper et al., 2004). However, one of the most common uses of HRP is in biosensors. A biosensor is *“an analytical device that brings together an immobilised biological sensing material [often HRP] and a transducer to produce an electronic signal that is proportional to the concentration of the target chemical substance”* (Luong et al., 1995). HRP dominates peroxidase-based sensor research and has continued to develop through many forms, from the

traditional voltammetric- and amperometric-based methods of detection, to nano-sized devices. Real-time quantification of hydrogen peroxide continues to be one of the main reasons for sensor development (Tønning et al., 2005), although other diverse applications include the detection of glucose (Alonso Lomillo et al., 2005), ethanol (Azevedo et al., 2005) and tumour markers *in vivo* (Lin and Ju, 2005). Enzyme-based biosensors require rapid and uniform transfer of electrons generated at the enzyme active site to the transducer. The distance between the active site and the transducer can hinder electron transfer; often, posttranslational modifications such as glycosylation increase this distance. Recombinant HRP, devoid of glycans, offers a shorter path for electron transfer and numerous reports of rHRP-based sensors have appeared (Ferapontova, 2004a). The typical bioelectrocatalytic reduction of H_2O_2 at the surface of the electrode configurations utilised in this study, screen-printed and etched electrodes, is outlined in Figure 6.1.

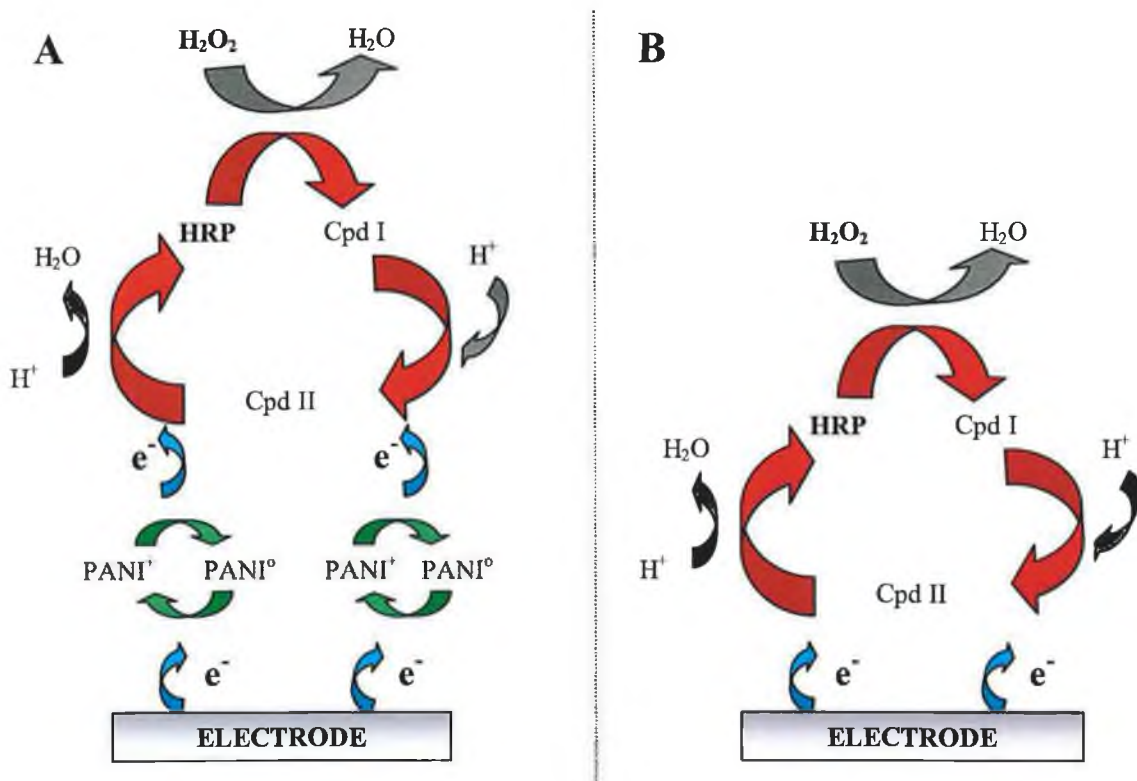


Figure 6.1: Schematic representation of bioelectrocatalytic reduction of H_2O_2 at a peroxidase-modified electrode. Part A depicts a screen-printed electrode configuration, with a polyaniline mediator (PANI) shuttling electrons from the active site to the electrode surface. Part B illustrates a non-mediated etched electrode configuration, in which the electrons ‘jump’ between the active site and the electrode surface.

6.1 Identification of Key Amino Acid Residues for Immobilisation.

This study focussed on the introduction of extra lysine residues to allow for orientated rHRP multipoint attachment to a cyanate ester activated solid phase, e.g. cyanogen bromide activated matrix. Previous reports of this methodology selected asparagine, glutamic acid or arginine residues for replacement by lysine (Abian et al., 2004); however, only arginine residues were considered in this study, as Arg to Lys is a conservative mutation: both size and charge are similar, and should result in minimal secondary structure rearrangement. There are twenty-one arginine residues in the HRP protein; these were viewed via *Deep View*TM (see Figure 6.2) and analysed based on secondary structure and location. Residues located in β -sheets were preferred over helical residues, and surface-exposed residues were selected in preference to buried ones. Only residues on the opposite side to the active site entrance were considered, as attachment via the “back” of the molecule would allow an orientated “molecular velcro” approach to rHRP immobilisation. This resulted in a selection of Arg118, Arg159 and Arg283 for mutation as outlined in the flow diagram (Figure 6.3).

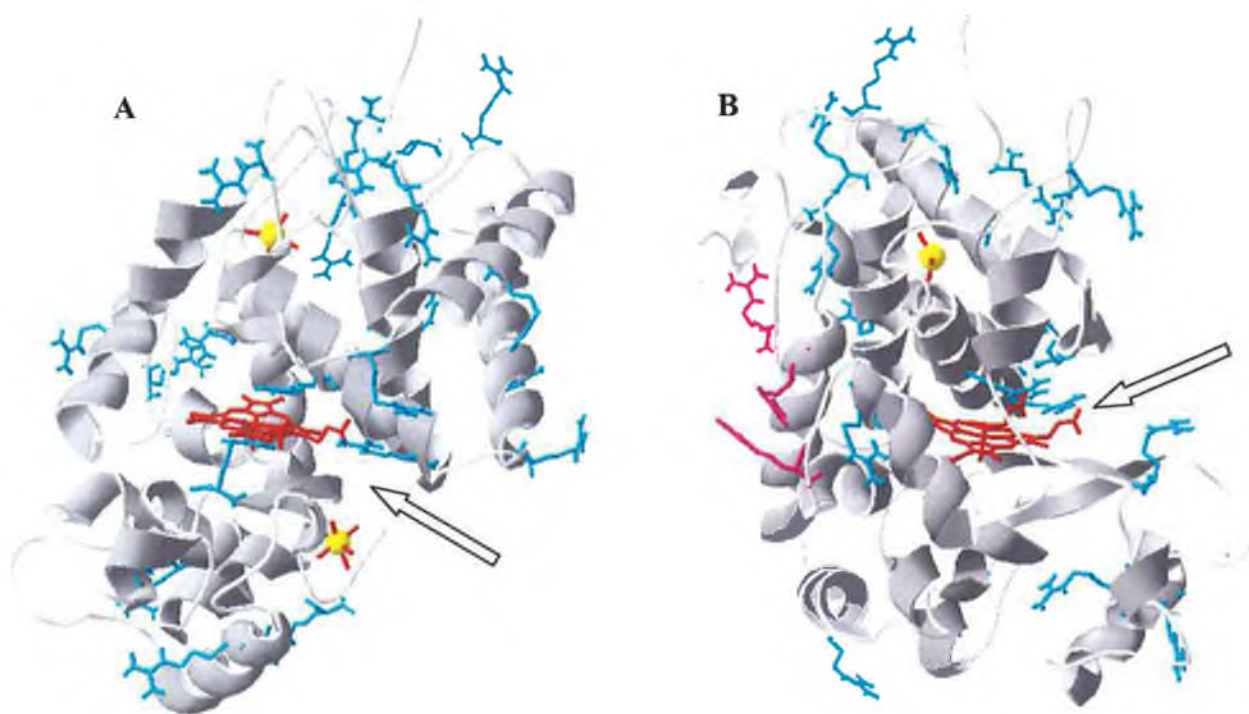


Figure 6.2: Part A displays the location of the arginine residues (●) in HRP. The arrow highlights the active site entrance in both cases. The purple residues (●) highlighted in Part B show the location of the three arginine residues (R118, R159, R283) selected for mutation to lysine, to allow for orientated rHRP immobilisation.

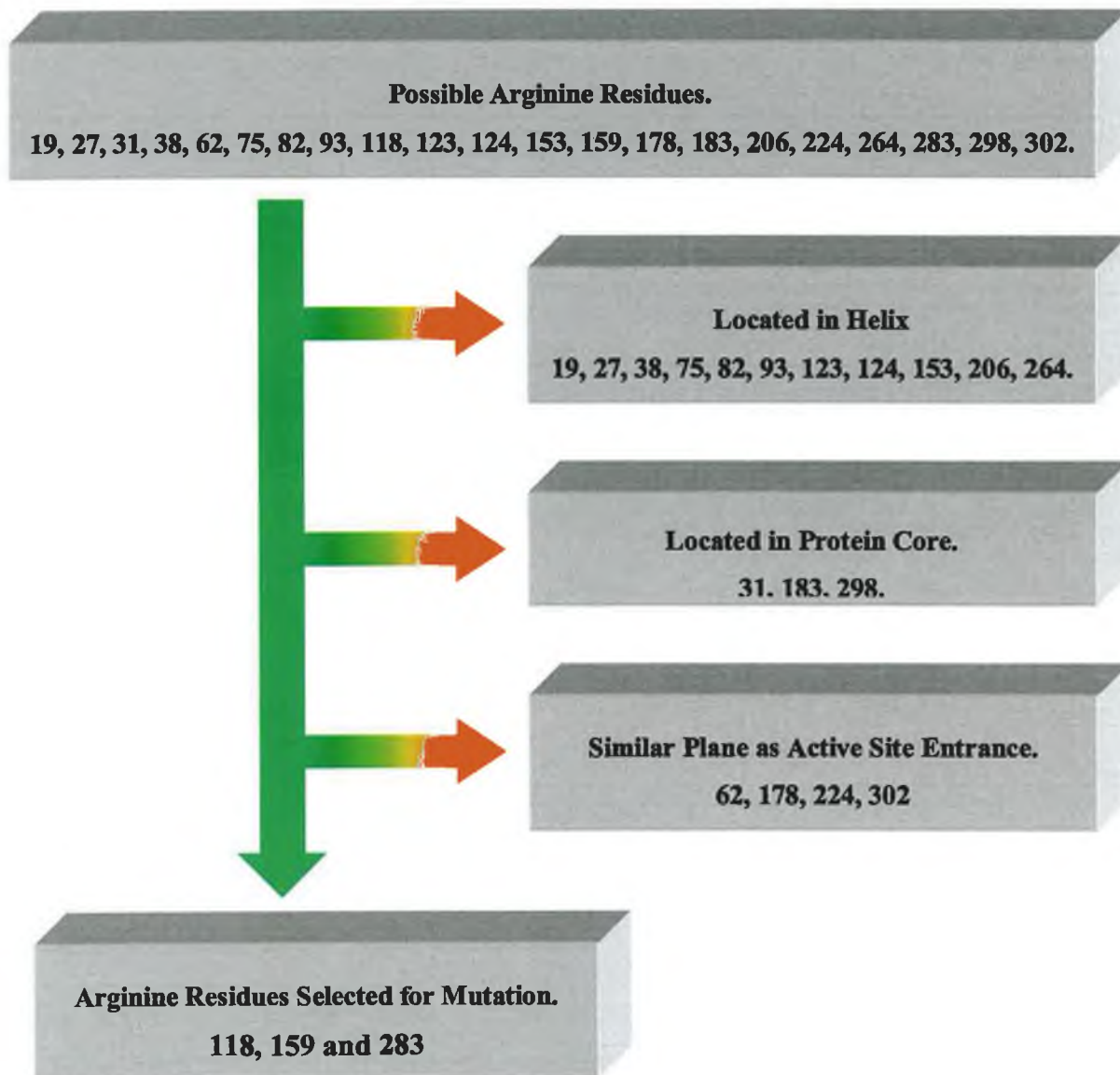


Figure 6.3: Rationale and selection flowchart for arginine to lysine mutations. Initially, arginine residues were analysed based on secondary structure, helix, beta sheet or turn. Those residues that were not part of a helix (or first amino acid of a helix) were then evaluated based on location. Residues buried within the protein core were eliminated, as immobilisation would not be possible with these residues. Any residue close to the active site entrance was also eliminated, as immobilisation with such residues would not allow *orientated* immobilisation.

6.1.1 Visualisation and Generation of Immobilisation Amino Acids.

Any alterations to the tertiary protein structure were predicted by the “*mutation*” function in the *DeepView*TM software; these were subsequently analysed and visualised (Guex and Peitsch, 1997). The individual mutagenic PCR was carried out as described in Section 2.22, and the primers utilised were pBR_I R118K, pBR_I R159K and pBR_I R283K. R118K was synthesised initially, followed by R159K and, finally, R283K. The existing, chemically-modifiable lysine residues (232 and 241) were substituted, by Phe (K232) and Asn (K241) as outlined in Sections 4.5.2 and 4.5.3.

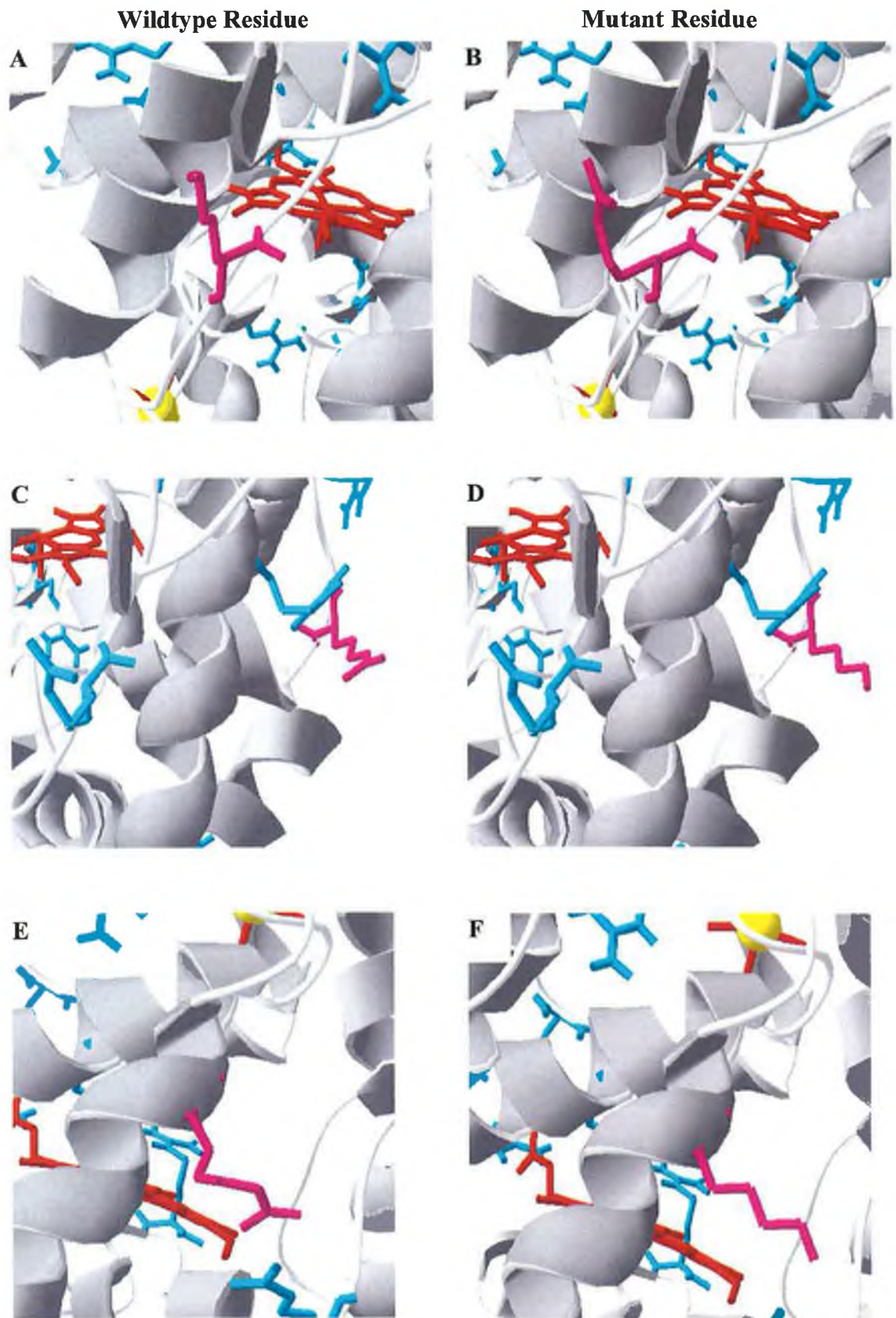


Figure 6.4: Location of arginine to lysine mutations (→) and predicted tertiary structure alterations. R118K is depicted in pictures A and B, R159K in C and D and R283K in E and F. The heme group (→) and calcium ions (●) are also highlighted.

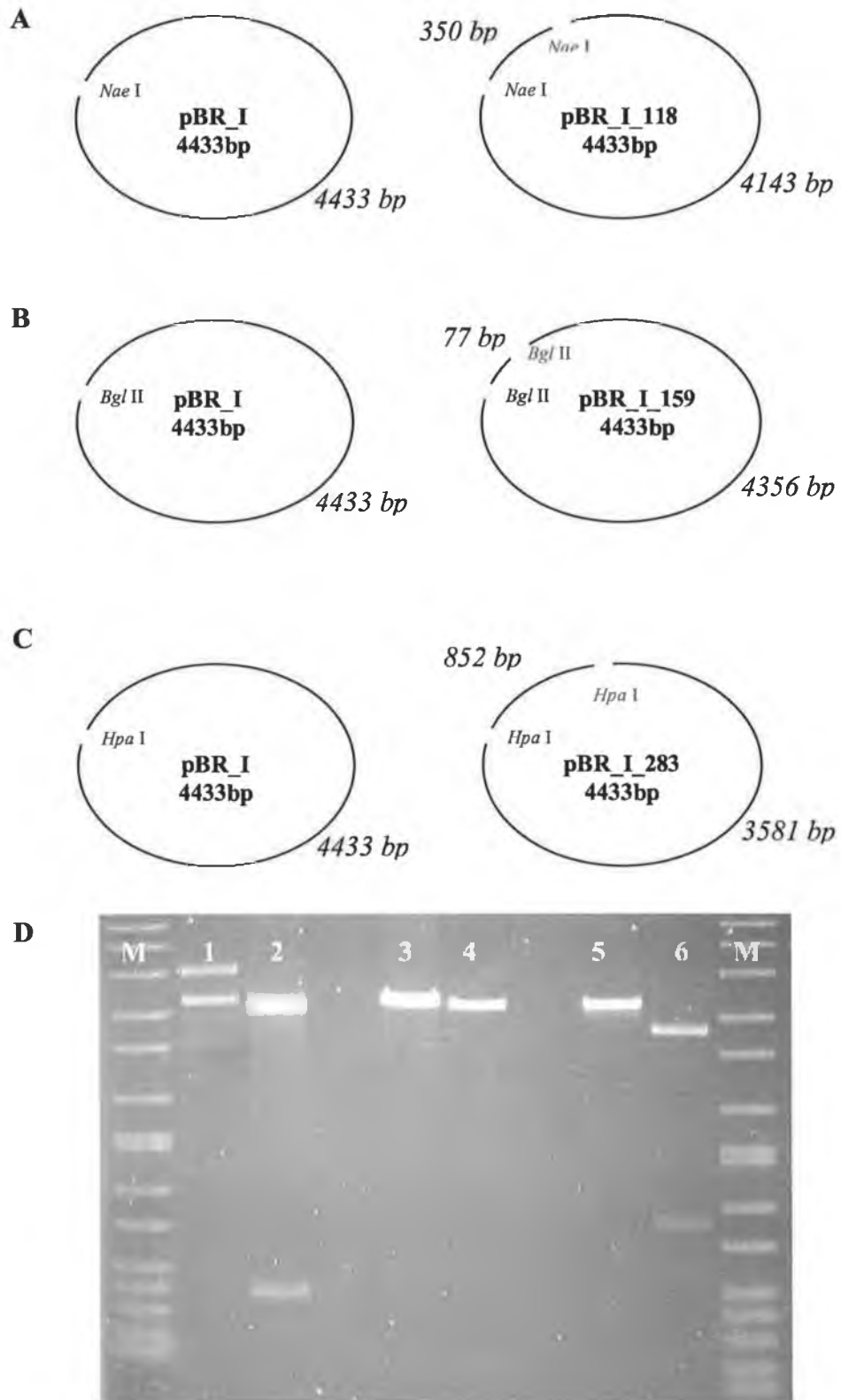


Figure 6.5: Parts A, B, and C are, respectively, diagrammatical representations of the expected restriction pattern for the mutant plasmids, pBR_I_118Lys, pBR_I_159Lys and pBR_I_283Lys. Part D shows these mutants viewed after restriction with the relevant restriction enzyme and electrophoresed through 1% w/v agarose. The approximate band sizes correspond to the predicted pattern, pBR_I_118Lys (lane two), pBR_I_159Lys (lane four) and pBR_I_283Lys (lane six). Non mutated wildtype, pBR_I, digested with the relevant restriction enzyme (WT) is run as comparison in each case (Lanes 1, 3 and 5). Lanes "M" contain Sigma size markers. The additional bands observed in lane one are the different forms of a plasmid: open circular, covalently closed-circular and nicked.

6.1.2 Sequencing of mutants.

Individual immobilisation mutant clones, “*Velcro Plus*” (R118K, R159K, R283K) and “*Velcro Minus*” (R118K, R159K, K232F, K241N, R283K), were selected for sequencing via a restriction digest screening methodology as outlined in Figure 6.5. Selected plasmids were prepared by the Gene Elute™ method, Section 2.8.3, and sent to Fusion Antibodies Ltd (Belfast) for sequencing using the di-deoxy sequencing method. Results were obtained via e-mail and processed through various bioinformatic packages (Section 2.20) to confirm correct reading frame of clone, suitable mutation and maintenance of gene integrity. The results are outlined in Figure 6.6.

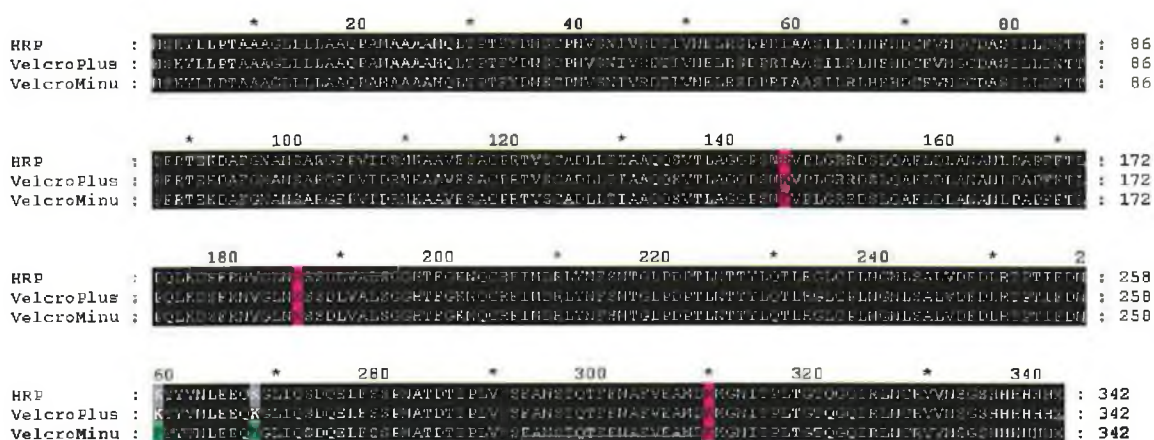


Figure 6.6: Alignment “*Velcro Plus*” and “*Velcro Minus*” sequencing results with wildtype PelB_HRP. The sequences show total identity, with the exception of the 118, 159, 283 residues in “*Velcro Plus*” and the 118, 159, 232, 241, 283 in “*Velcro Minus*”, which have been mutated to the desired amino acid.

6.2 Expression, Purification and Immobilisation of “*Velcro*” Mutants.

Immobilisation mutants were individually expressed in 500 mL shake culture flasks and purified via optimised nickel affinity chromatography as previously described; see Section 2.24.4 and Section 2.25. Once expressed and purified, the μM concentration of rHRP mutants were calculated as per Section 2.29, with the results outlined in Table 6.1.

Table 6.1: Absorbance at 403nm for immobilisation mutants. rHRP concentrations were calculated using the Beer-Lambert Law, and the rHRP extinction coefficient, $100\text{mM}^{-1}\text{cm}^{-1}$ (Hiner et al., 1995). Protein concentrations were experimentally determined using the BCA assay. K283R revertant *Velcro* is indicated by “‡”.

Mutant	Abs 403nm	rHRP (μM)	Protein Conc (mg/ml)	Heme/Protein Ratio
<i>Velcro Plus</i>	0.015	0.3	0.258	0.039
‡ <i>Velcro Plus</i>	0.045	0.9	0.538	0.057
<i>Velcro Minus</i>	0.159	3.2	1.418	0.077
‡ <i>Velcro Minus</i>	0.047	0.9	0.521	0.059

6.2.1 Immobilisation on Cyanogen Bromide Activated Matrix.

Initially, all immobilisation mutants and wildtype rHRP were immobilised to CNBr-activated Sepharose, see Section 2.37.1. The % immobilisation was calculated as outlined in Table 6.2.

Table 6.2: Immobilisation rate for wildtype, *Velcro Plus* and *Velcro Minus* mutants. Calculation is based on activity before and after immobilisation, assuming that no protein inactivation occurs during the immobilisation process. K283R revertant *Velcro* is indicated by “‡”.

Mutant Name	Pre Immobilisation Units of Activity ($\mu\text{mol}\cdot\text{min}^{-1}$)	Post Immobilisation Units of Activity ($\mu\text{mol}\cdot\text{min}^{-1}$)	Immobilisation (%)
Wildtype	5.25	2.67	50 %
<i>Velcro Plus</i>	1.54	1.32	86 %
‡ <i>Velcro Plus</i>	0.43	0.33	69 %
<i>Velcro Minus</i>	2.14	1.22	57 %
‡ <i>Velcro Minus</i>	1.02	0.49	42 %

Each form of immobilised rHRP was then characterised as to its thermal, solvent and H_2O_2 stabilities, as outlined in Section 6.3.

6.3 Characterisation of Free and Immobilised Immobilisation Mutants.

6.3.1 CNBr-Immobilised HRP Thermal Tolerance.

Thermal inactivation was carried out as per Section 2.32. Preliminary assays suggested 50°C as the T_{50} for free *Velcro Plus*, *Velcro Plus(K283R)*, *Velcro Minus*, *Velcro Minus(K283R)* and wildtype rHRP, and this was the temperature used for both free and immobilised rHRP forms. Thermal inactivation curves were produced for each mutant triplicate (i) in free solution and (ii) CNBr-immobilised, using recombinant wildtype as a reference.

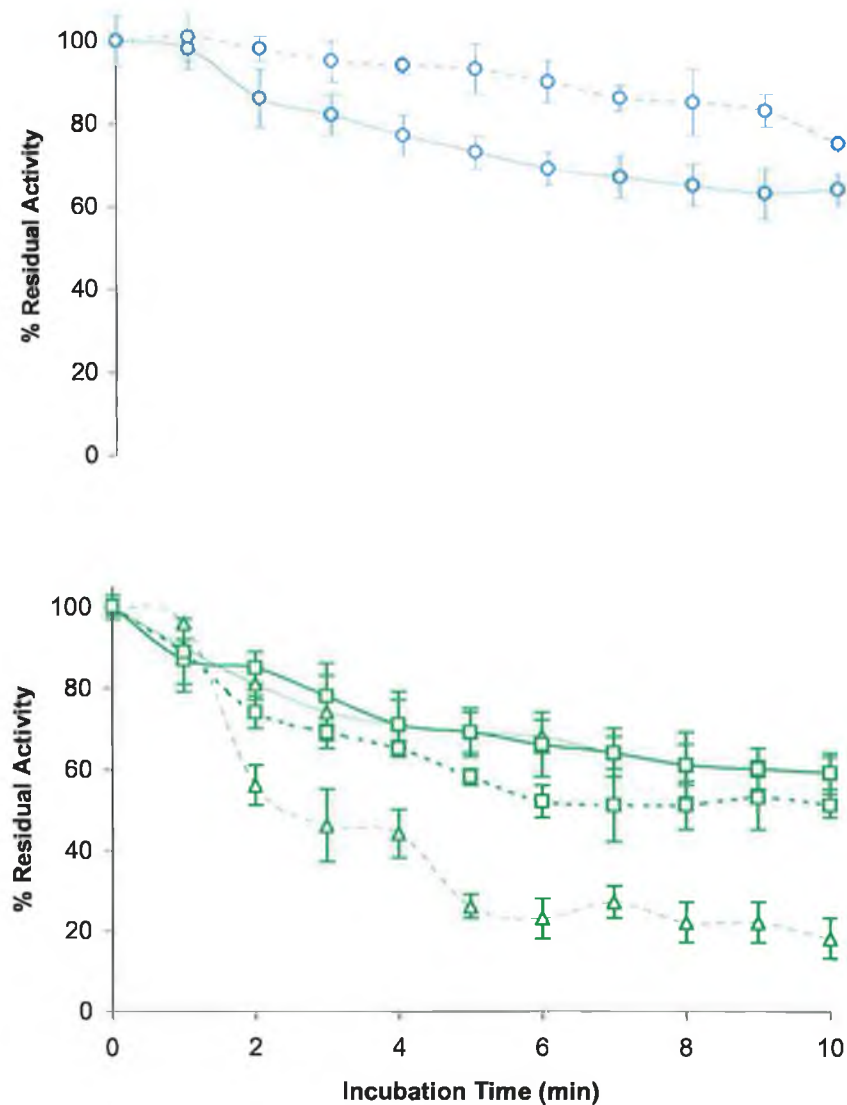


Figure 6.7: Thermal inactivation curve of Wildtype rHRP (○) *Velcro Plus* (△) and *Velcro Plus(K283R)* (□) rHRP carried out at 50°C. The solid lines indicate the free solution activities; the dashed lines, immobilised activities.

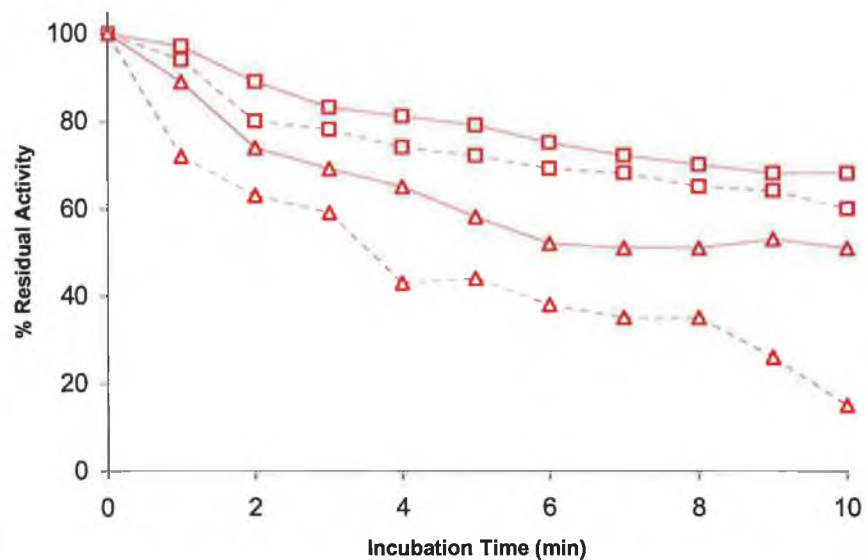


Figure 6.8 Thermal inactivation curve of *Velcro Minus* (Δ) and *Velcro Minus(K283R)* (\square) rHRP carried out at 50°C. The solid lines indicate the free solution activities; the dashed lines, immobilised activities.

Table 6.3: Rate of inactivation at 50°C and calculated apparent half-life ($t_{1/2}$) for immobilisation mutants in both free and immobilised (*) forms. K283R revertant Velcro is indicated by “‡”.

Mutant	T_{50} (°C)	k-value (-)	SD (%)	$t_{1/2}$ (min)	r^2 Value
Wildtype	50	5.59×10^{-2}	± 6	12.4	0.98
Wildtype*	-	2.55×10^{-2}	± 9	27.2	0.91
<i>Velcro Plus</i>	50	5.35×10^{-2}	± 9	12.5	0.91
<i>Velcro Plus</i> *	-	2.23×10^{-1}	± 9	3.1	0.90
‡ <i>Velcro Plus</i>	50	5.68×10^{-2}	± 10	12.2	0.91
‡ <i>Velcro Plus</i> *	-	5.44×10^{-2}	± 8	12.8	0.92
<i>Velcro Minus</i>	50	1.09×10^{-1}	± 7	6.3	0.93
<i>Velcro Minus</i> *	-	1.52×10^{-1}	± 11	4.6	0.90
‡ <i>Velcro Minus</i>	50	4.45×10^{-2}	± 6	16.5	0.98
‡ <i>Velcro Minus</i> *	-	4.91×10^{-2}	± 10	14.2	0.91

6.3.2 CNBr-Immobilised Organic Solvent Tolerance.

All organic solvent tolerance assays were carried out as per Section 2.33, with a final protein concentration of 100 $\mu\text{g}/\text{mL}$ in the reaction solution. Solvent tolerance profiles were produced for each mutant form, in triplicate, using recombinant wildtype as a reference. All standard errors were within $<5\%$ of the triplicate average reading. These results were then compared to the CNBr-immobilised forms of the enzyme under the same conditions. Larger standard errors (5-15%) were noted for the immobilised forms; however, this could be attributed to the non-homogenous suspensions generated during individual triplicate sampling.

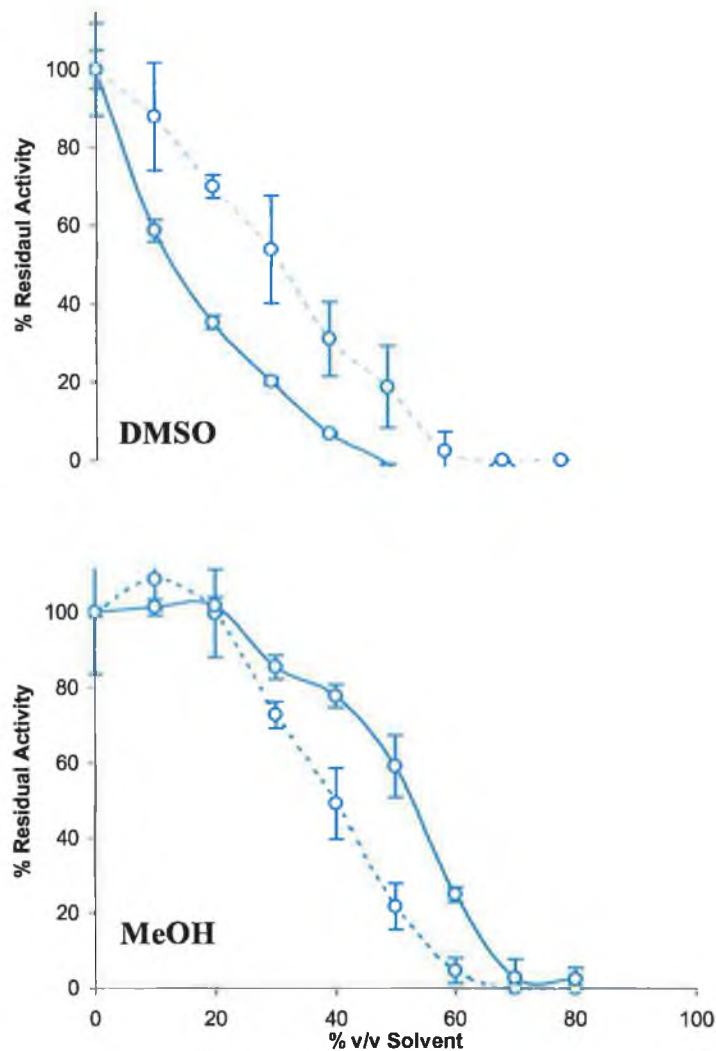


Figure 6.9: Solvent Tolerance Profile of (○) rWT HRP in DMSO and MeOH. The solid lines indicate the free solution activities; the dashed lines, immobilised activities.

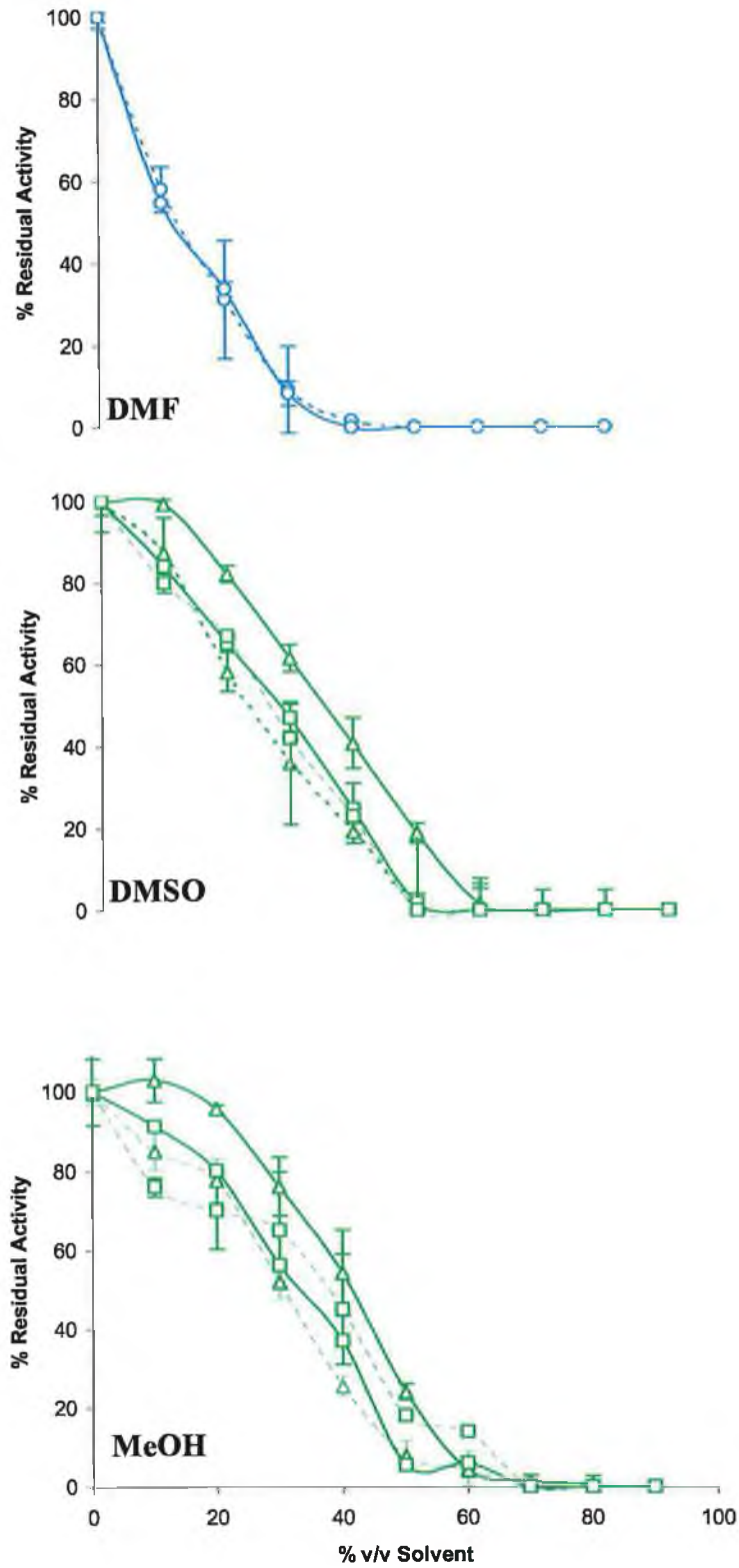


Figure 6.10: Solvent Tolerance Profile of (○) rWT HRP (in DMF), *Velcro Plus* (△) and *Velcro Plus(K283R)* (□) rHRP in DMSO and MeOH. The solid lines indicate the free solution activities; the dashed lines, immobilised activities.

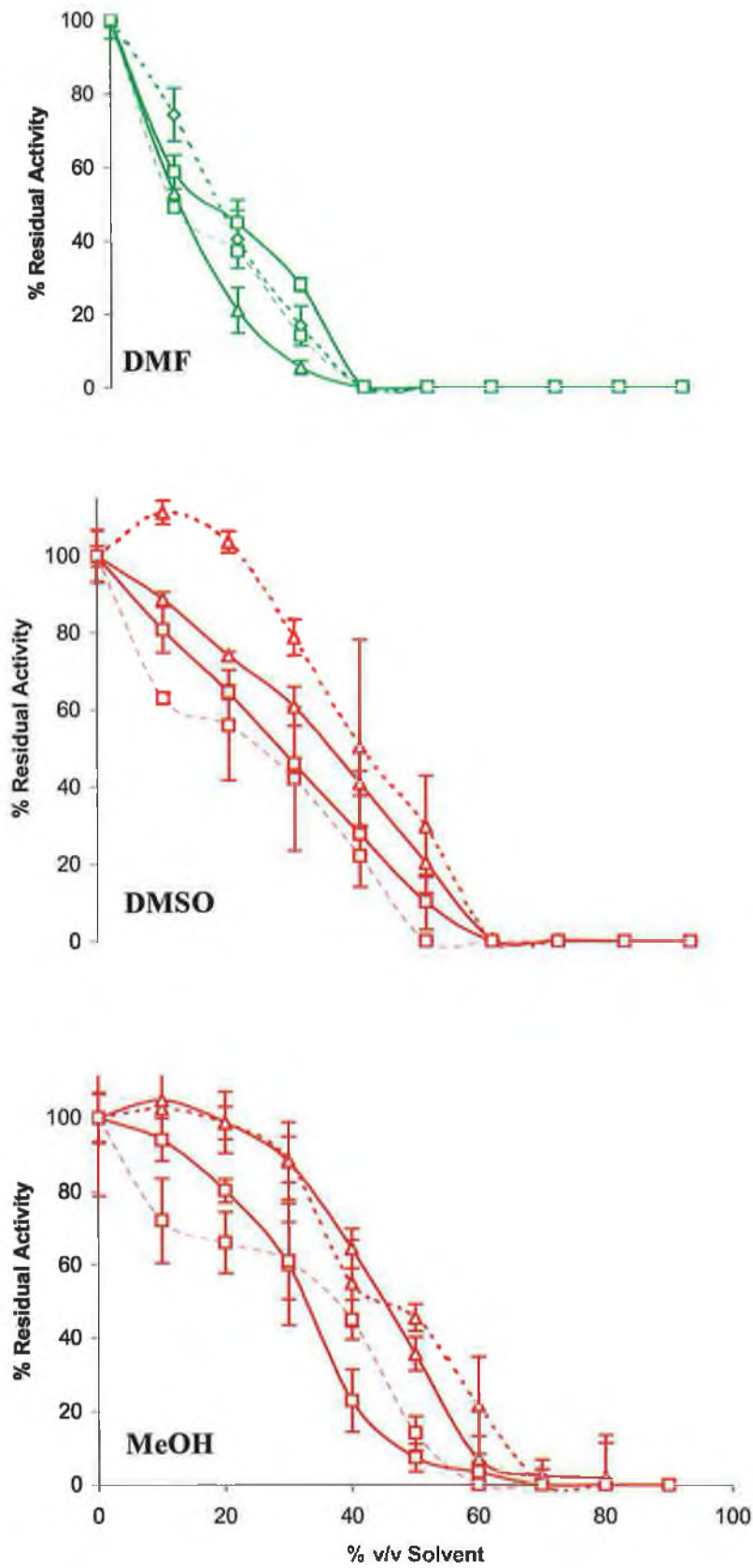


Figure 6.11 Solvent Tolerance Profile of *Velcro Plus* (Δ) and *Velcro Plus(K283R)* (\square) rHRP in DMF and *Velcro Minus* (Δ) and *Velcro Minus(K283R)* (\square) rHRP in DMSO and MeOH. The solid lines indicate the free solution activities; the dashed lines, immobilised activities.

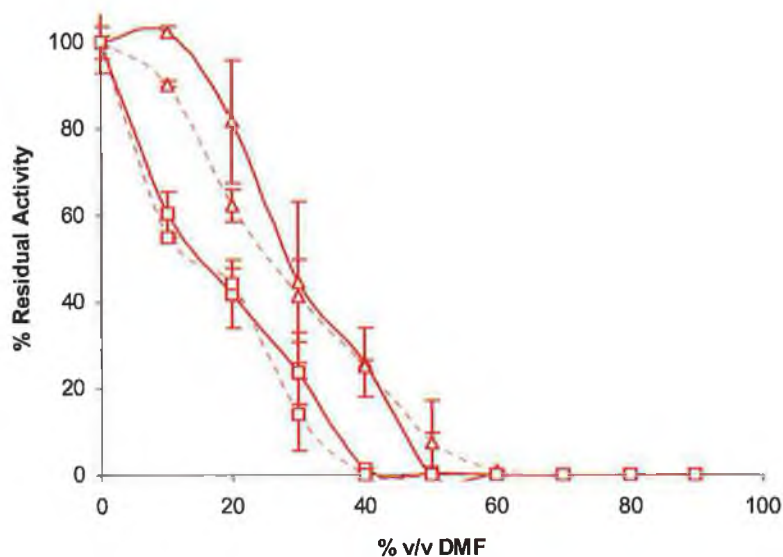


Figure 6.12: DMF Solvent Tolerance Profile of *Velcro Minus* (Δ) and *Velcro Minus(K283R)* (\square) rHRP. The solid lines indicate the free solution activities, whilst the dashed lines represent immobilised activities

Apparent C_{50} (% v/v solvent that causes half inactivation) concentrations for each of the mutants at 25°C were calculated, as outlined in Section 2.33, with the results tabulated in Table 4.3.

Table 6.4: Half-inactivation concentrations (C_{50}) for each *Velcro* mutant. K283R revertant *Velcro* is indicated by “ \ddagger ”.

Mutant	DMSO		MeOH		DMF	
	Free	Immob	Free	Immob	Free	Immob
Wildtype	35	32	53	40	14	14
<i>Velcro Plus</i>	35	24	44	32	12	17
\ddagger <i>Velcro Plus</i>	30	28	35	38	16	10
<i>Velcro Minus</i>	35	42	45	43	25	29
\ddagger <i>Velcro Minus</i>	30	28	35	38	16	15

6.3.3 H₂O₂ Tolerance of CNBr Immobilised HRP mutants.

H₂O₂ Tolerance assays were carried out as per Sections 2.34. H₂O₂ tolerance profiles were produced for each mutant, in triplicate, using recombinant wildtype as a reference. These results were then compared to the CNBr-immobilised forms of the enzyme under the same conditions. Triplicate standard errors were less than 12 % in all cases.

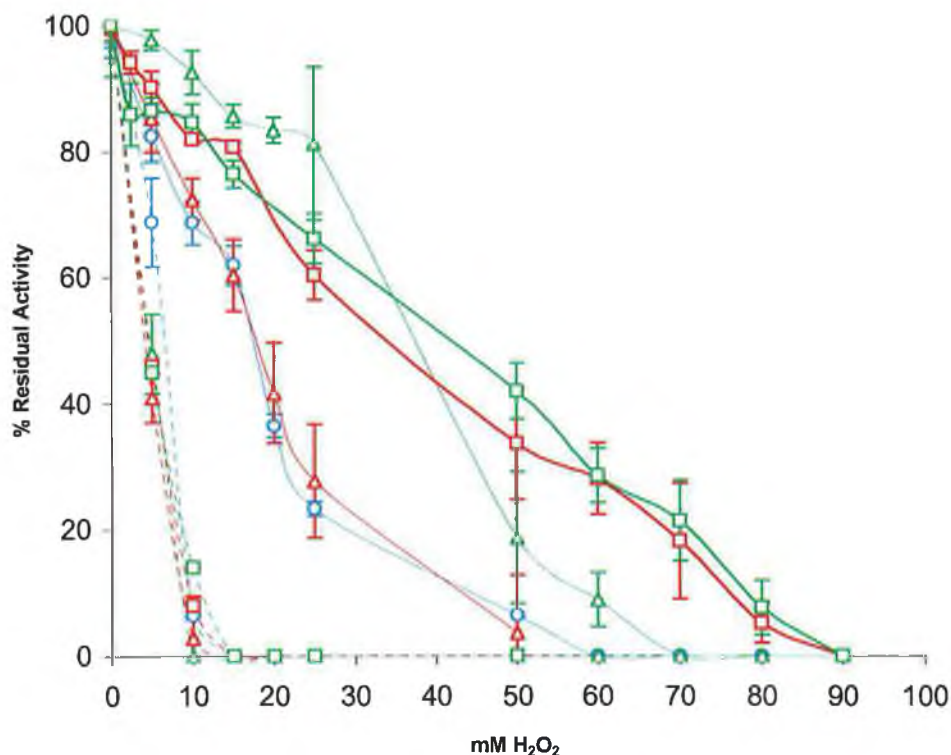


Figure 6.13: H₂O₂ inactivation curves of Wildtype (○), *Velcro Plus* (△), *Velcro PlusK283R* (□), *Velcro Minus* (◇) and *Velcro Minus K283R* (▽) rHRP carried out at 25°C. The solid lines indicate the free solution activities; the dashed lines, immobilised activities.

Table 6.5: Calculated half inactivation concentrations (C₅₀) for each free and CNBr-immobilised mutant. K283R revertant *Velcro* is indicated by “‡”. Immobilised forms are highlighted with ‘*’.

Mutant	C ₅₀ H ₂ O ₂ (mM)	% Error	Mutant	C ₅₀ H ₂ O ₂ (mM)	% Error
Wildtype	17	± 4	* <i>Velcro Plus</i> *	5	± 9
Wildtype*	6	± 7	<i>Velcro Minus</i>	17	± 9
<i>Velcro Plus</i>	38	± 12	<i>Velcro Minus</i> *	5	± 7
<i>Velcro Plus</i> *	5	± 8	‡ <i>Velcro Minus</i>	33	± 9
‡ <i>Velcro Plus</i>	44	± 4	‡ <i>Velcro Minus</i> *	5	± 5

6.3.4 UltraBind™ Affinity Membrane Immobilised Activity.

Velcro Plus, *Velcro Plus(K283R)*, *Velcro Minus*, *Velcro Minus(K283R)* and wildtype rHRP were also immobilised to an activated, modified polyethersulfone (PES) membrane to demonstrate proof of the principle of an orientated immobilised rHRP molecule on a planar surface.

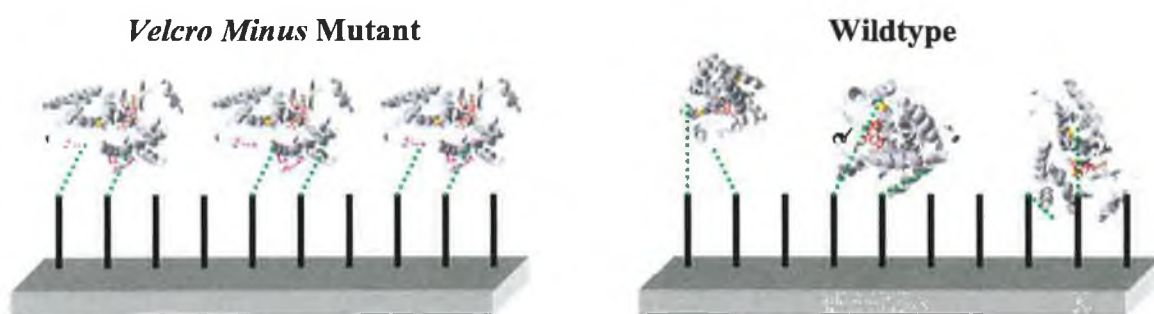


Figure 6.14: Diagrammatical representation of proposed UltraBind™ Affinity Membrane Immobilisation strategy. The *Velcro Minus* mutant should immobilise in an orientated fashion, with the active site facing away from the membrane. The Wildtype rHRP can immobilise with only K232, K241 and K174, and many do so in a random mode; thus, the active site entrance may be blocked or sterically hindered, leading to reduced catalytic activity.

Equimolar concentrations of rHRP, *Velcro Plus* and *Velcro Minus* mutants were spotted onto the UltraBind™ Affinity Membrane, as outlined in Section 2.37.2.

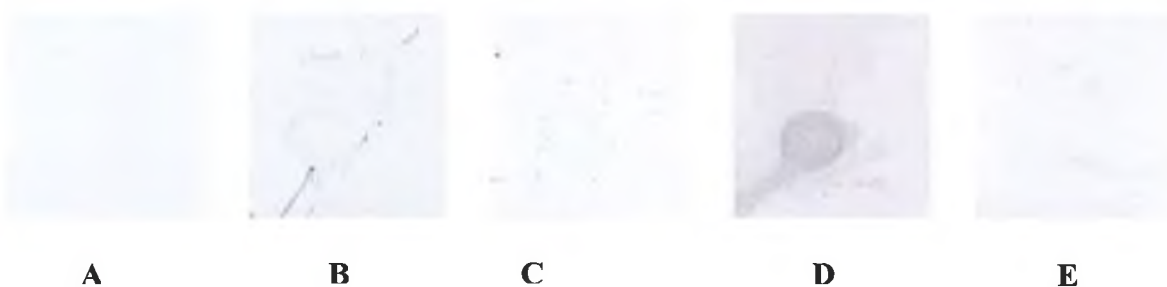


Figure 6.15: Scanned images of spotted immobilised overnight (24 hours) DAB stained rHRP activity. Image A represents BSA blank, image B wildtype rHRP, image C *Velcro Plus*, image D *Velcro Minus* and image E the reverse membrane side of image D.

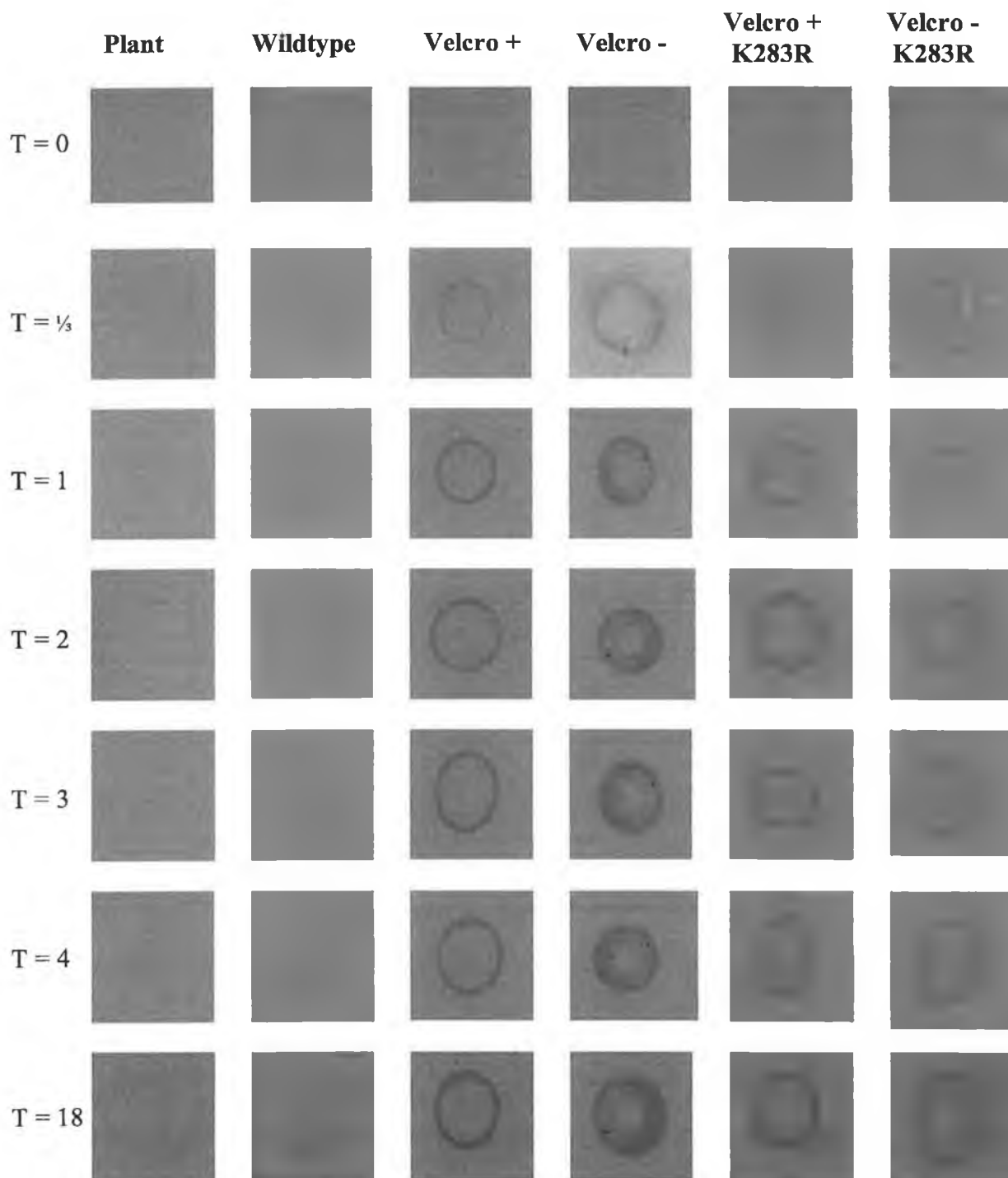


Figure 6.16: Scanned images of DAB stained, spotted immobilised rHRP activity. Images were scanned as outlined in 2.37.2, and converted to greyscale utilising Hewlett Packard Scanjet 5590 image software. Time points indicated on the left are in hours. Increased DAB colouration was indicative of peroxidase activity; this was noted within minutes for the Velcro mutants, whereas wildtype and plant HRP required a longer time period to develop any colouration.

6.4 Electrochemical Biosensors.

6.4.1 Plotting convention for this study.

The American convention for electrochemical data is used throughout this study. A typical current-potential plot is outlined in Figure 6.17, with cathodic currents related to reduction processes plotted in an upward direction and anodic currents related to oxidation processes plotted in downward direction.

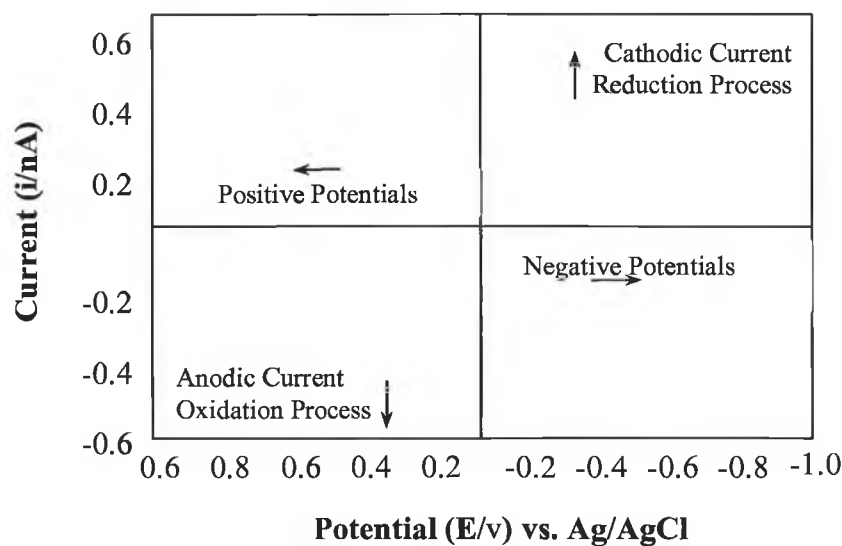


Figure 6.17: Current-potential plotting convention utilised in this study.

6.4.2 Screen Printed Electrode.

Recombinant HRP offers the possibility of direct electron transfer from the active site to the sensing device, since it lacks the bulky sugar chains of the plant enzyme. This is currently a vibrant area of research. In this study, the electron transfer rate of recombinant wildtype and plant HRP were investigated on screen-printed electrodes. Screen-printed electrodes are small, mass-produced, single use devices comprising a silver-conducting track, a carbon working electrode and an insulation layer (see Figure 6.18). Initially, a conducting layer of aniline was deposited onto the carbon working electrode via cyclic voltammetry. BSA, recombinant and plant HRP were then electrochemically immobilised onto the polyaniline surface via “time-based” Amperometry (Section 2.38.1). The CHI1000 software then recorded the response of each protein to the addition of H_2O_2 .

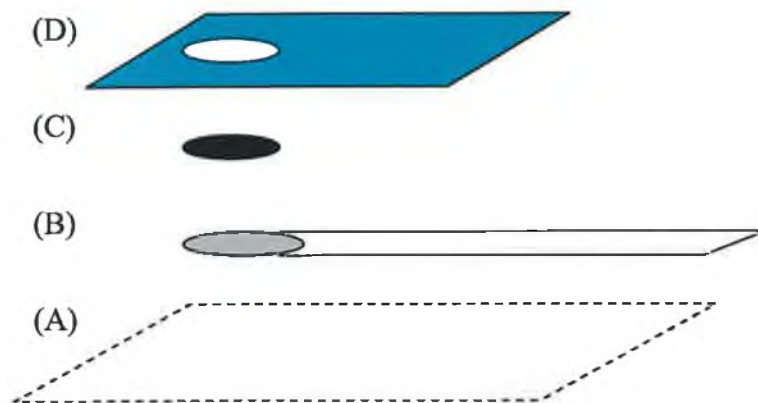


Figure 6.18: Components of the in-house screen-printed electrode: (A) Plastic electrode backing, (B) Ag/AgCl conducting path, (C) carbon working electrode, (D) Insulation layer. Working area: 7.07mm^2 , (A Morrin, PhD Thesis, Dublin City University, 2003).

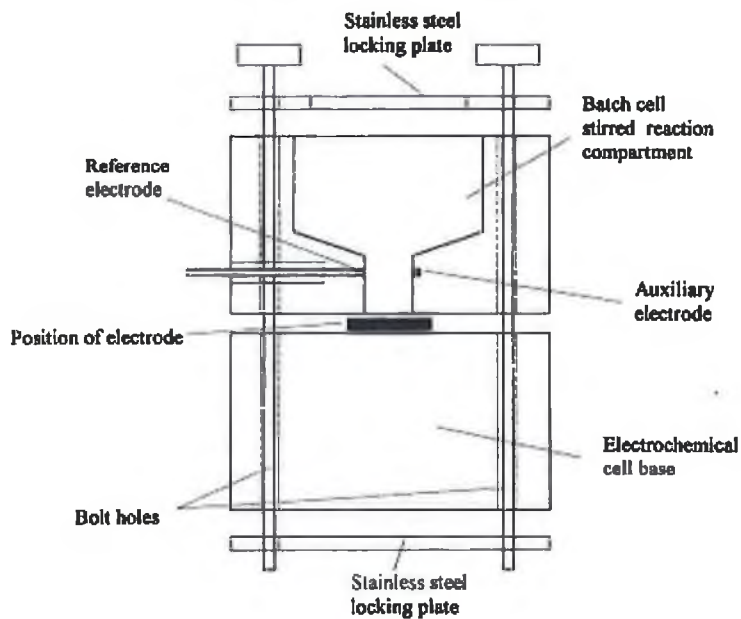


Figure 6.19: Batch Cell configuration. The polycarbonate batch cell comprised an upper reaction vessel and a lower base, between which the screen print electrode was clamped. Platinum wire auxiliary and pseudo silver/silver chloride wire reference electrodes were incorporated into the reaction vessel with external connections, as shown in diagram (Adapted from Killard et al., 1999)

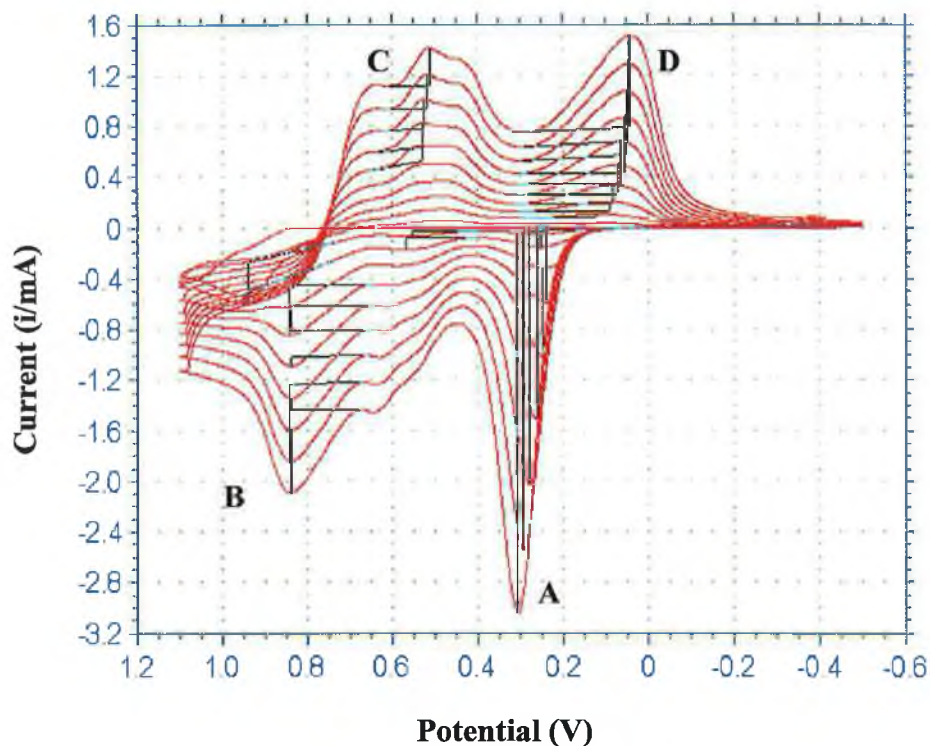


Figure 6.20: Electro-deposition of polyaniline in 1M HCl onto the surface of the screen printed electrode. Successive polymerisation cycles are shown which correspond to increase in thickness of the film during aniline deposition. The oxidation peaks were assigned to the [A] oxidation of leucoemeraldine (LM) to leucoemeraldine radical cation ($LM^{\bullet+}$), and the [B] oxidation of $LM^{\bullet+}$ to emeraldine (EM). The reduction peaks are assigned to the [C] reduction of EM to emeraldine radical cation ($EM^{\bullet+}$) and [D] $EM^{\bullet+}$ back to LM (Wallace et al., 2003).

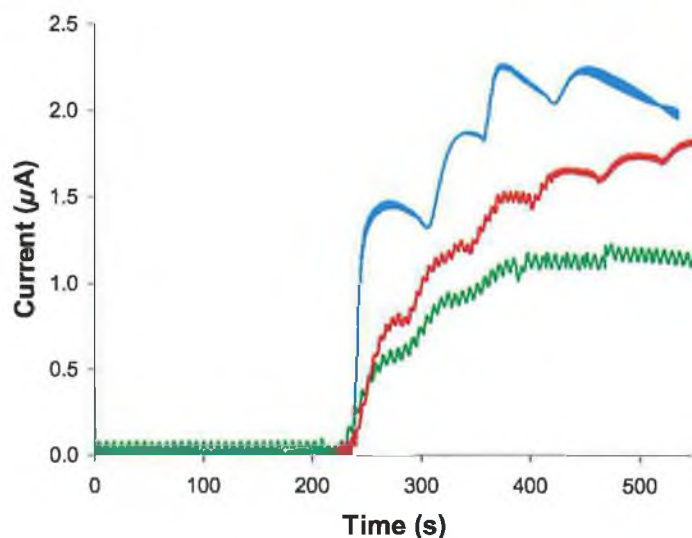


Figure 6.21: Current response plot of immobilised rHRP (—), plant HRP (—) and immobilised Bovine Serum Albumin (—). BSA was used as a blocking, non-reactive protein to account for any background noise. After 1 hour equilibration and 200 seconds constant current, $0.025 \text{ mol.L}^{-1} \text{ H}_2\text{O}_2$ (final concentration) was added at 50 second intervals to a 1 mL mixing reaction vessel containing the screen-printed electrode with immobilised HRP; the electrode was connected to a CHI 600A Potentiostat.

6.4.3 Etched Micro-Electrode.

6.4.3.1 Schematic of a microelectrode.

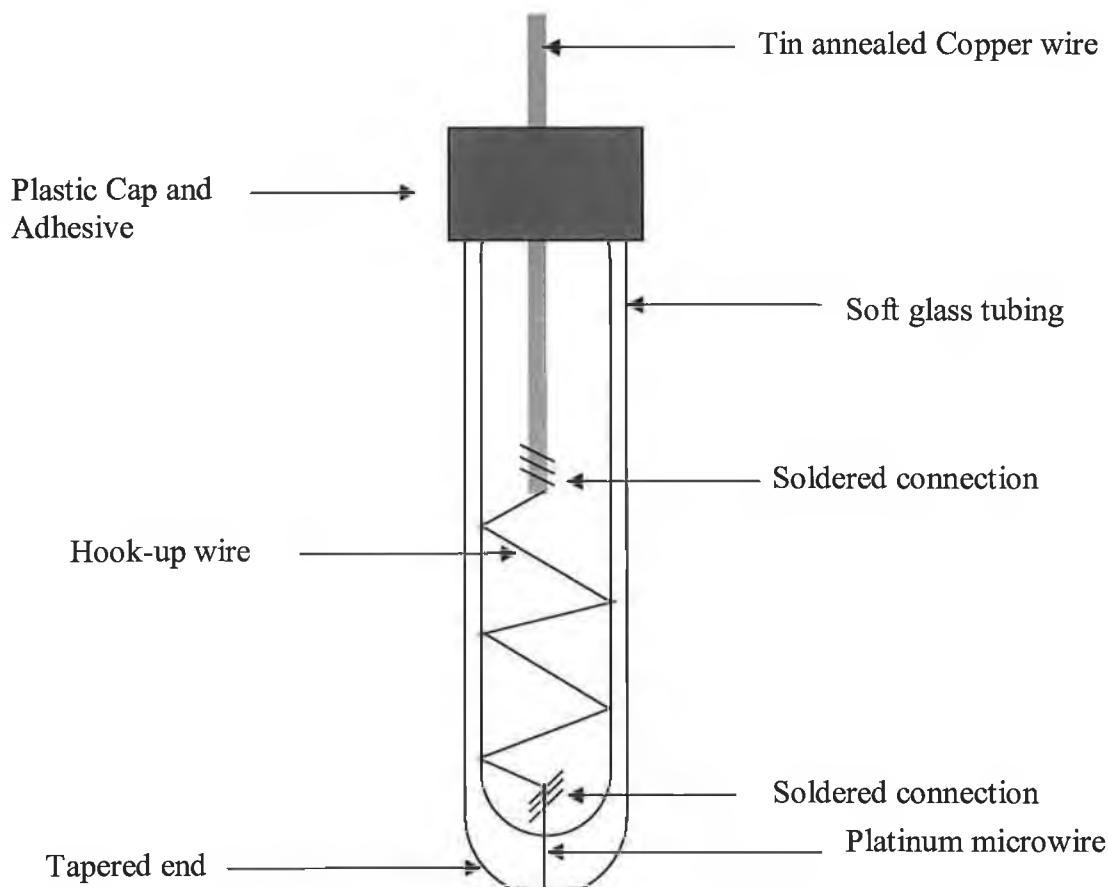


Figure 6.22: Schematic cross-section of an in-house fabricated microelectrode. Typical tip diameter: 2mm

6.4.3.2 Characterisation of fabricated platinum microelectrode in H_2SO_4 .

When a platinum electrode is cycled over a certain potential range in 1.0 M H_2SO_4 , a characteristic curve is noted. This curve consists of several peaks, which can be attributed to various forms of platinum, oxygen and hydrogen at the surface of the electrode. In Figure 6.23 these forms are labelled as: O_a – formation of adsorbed oxygen and platinum oxide layers, O_c – reduction of oxide layers, H_a - oxidation of adsorbed hydrogen, H_c – reduction of adsorbed hydrogen. The voltammogram displays two distinct peaks for adsorbed and desorbed hydrogen; these have been attributed to strongly and weakly adsorbed (or desorbed) hydrogen. The strongly adsorbed hydrogen is more positive, due to the fact that a higher free energy of adsorption is needed for a larger shift in potential (Lambrechts and Sansen, 1999).

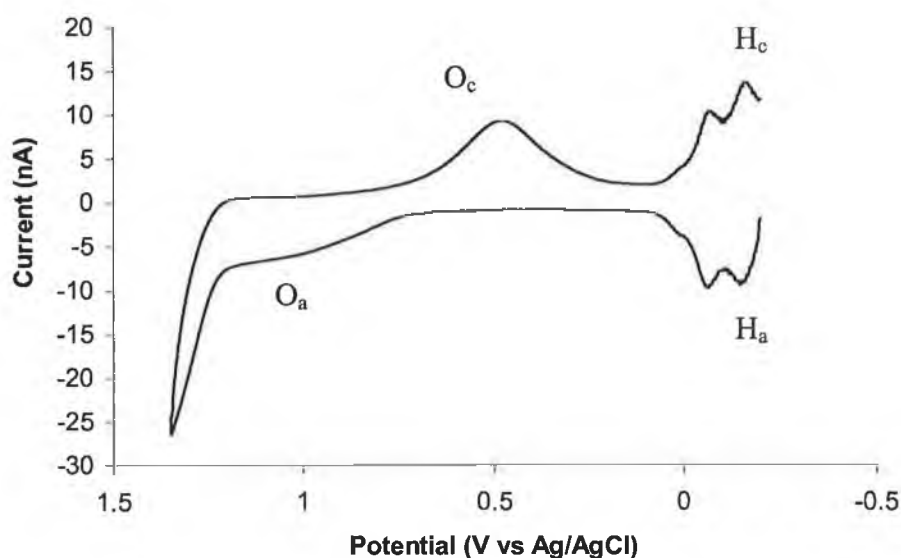


Figure 6.23: Cyclic voltammogram of a platinum microelectrode ($25\mu\text{M}$ radius) in $1.0\text{ M H}_2\text{SO}_4$, at a scan rate of 0.2 V/s . O_a – formation of adsorbed oxygen and platinum oxide layers, O_c – reduction of oxide layers, H_a – oxidation of adsorbed hydrogen, H_c – reduction of adsorbed hydrogen.

Due to the well-characterised formation of oxide monolayers on platinum, the charge passed in removal of these adsorbed layers (labelled O_c in Figure 6.23) is routinely used to determine the real or microscopic surface area of these electrodes. In the case of platinum, hydrogen adsorption or desorption on its surface may also be used to determine the microscopic area. The method of oxide reduction for the determination of the real surface areas of platinum microelectrodes assumes that oxygen is adsorbed at the surface in a monomolecular layer and also that one oxygen atom is attached to one metal atom (Carolan N, PhD Thesis, DCU, 2004). The surface roughness of the microelectrodes was calculated by dividing the microscopic surface area by the geometric area. The surface roughness value for the microelectrode was calculated as 1.25 (see Table 6.6).

Table 6.6: Calculation of geometric area, electrochemical surface area and surface roughness factor for in-house fabricated $25\mu\text{m}$ radius platinum electrode.

Microelectrode Type	Radius (μm)	Geometric Area (cm^2)	Actual surface Area (cm^2)	Surface Roughness
Platinum	25	1.96×10^{-5}	2.46×10^{-5}	1.25

6.4.3.3 Cyclic Voltammetry of a bare platinum electrode.

Cyclic voltammetry was carried out initially in phosphate buffer (50 mM Sodium Phosphate, pH 7.0) and subsequently in MOPS buffer (50 mM MOPS, pH 7.0), to verify that no oxidation or reduction events took place over the given potential window of +0.1 to +0.9 Volts. This indicates that the electrode is clean and was polished sufficiently. Biological buffer interference was assessed and measures taken to eliminate it over the potential window studied. The buffers were deoxygenated thoroughly prior to, and an inert gas atmosphere maintained over the buffer during, any electrochemical analysis. Lithium perchlorate was used as a standard, non-electrochemically active solution.

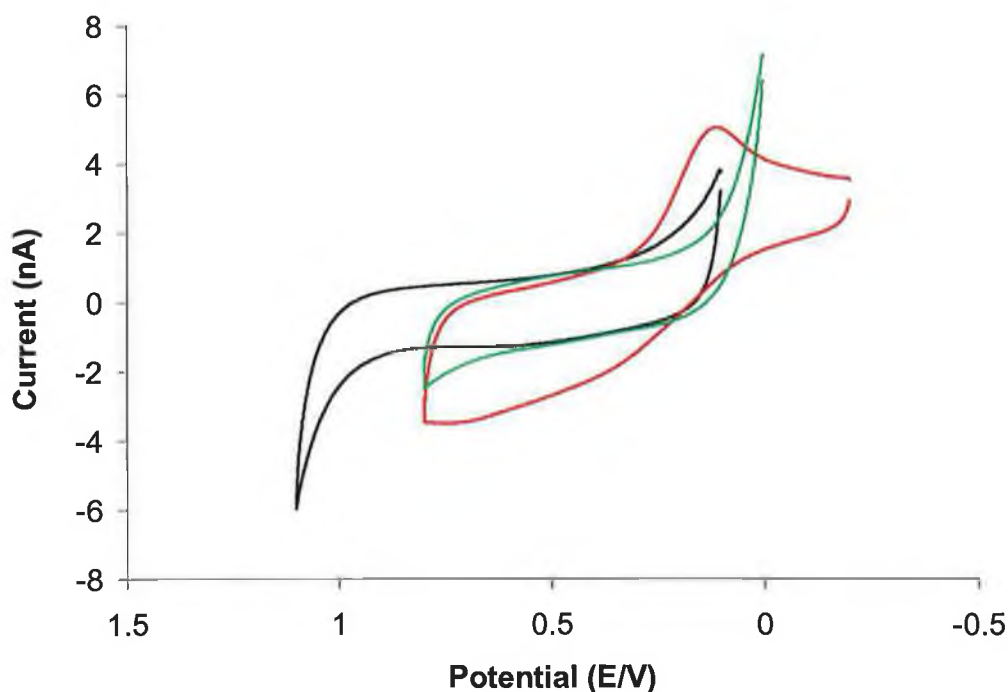


Figure 6.24: Cyclic voltammogram depicting the electrochemical response of a 25 μ m platinum microelectrode in (—) 50mM Sodium Phosphate Buffer pH 7.0, (—) 50mM MOPS Buffer pH 7.0. and (—) 50mM lithium perchlorate standard. The scan rate was 0.2 V/s.

6.4.3.4 Direct Electrooxidation of H_2O_2 at the platinum microelectrode.

It is known that direct electro-oxidation of H_2O_2 can occur in the vicinity of a platinum electrode at high potentials, e.g close +0.80V (N. Carolan, PhD Thesis, DCU, 2004). As the aim of these experiments was to demonstrate direct electron transfer from the HRP active site to the surface of the electrode, via H_2O_2 catalysis; it was imperative that spontaneous H_2O_2 breakdown was characterised and taken into consideration.

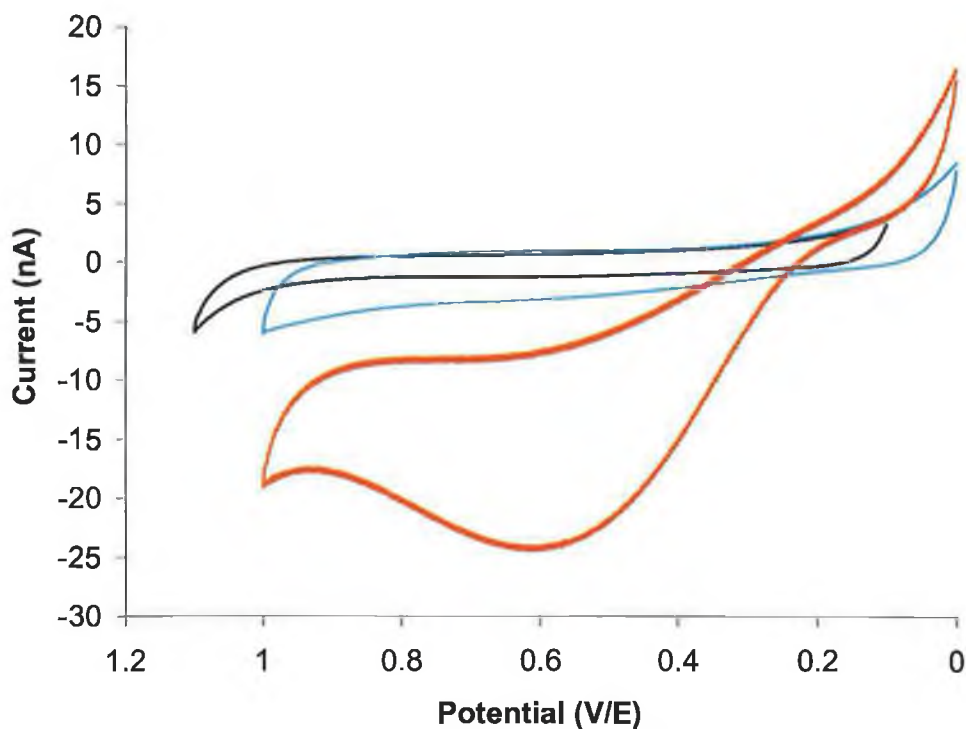


Figure 6.25: Cyclic voltammogram depicting the electrochemical response of a $25\mu\text{m}$ platinum microelectrode in the presence of (—) $0\mu\text{M}$ H_2O_2 in 50mM MOPS buffer, $\text{pH } 7.0\text{pH}$, (—) 2.5×10^{-4} mol.L^{-1} H_2O_2 in 50mM MOPS Buffer and (—) 1×10^{-3} mol.L^{-1} H_2O_2 in 50mM MOPS buffer. The scan rate was 0.2 V/s.

6.4.3.5 Etching of the platinum microwire in the microelectrode.

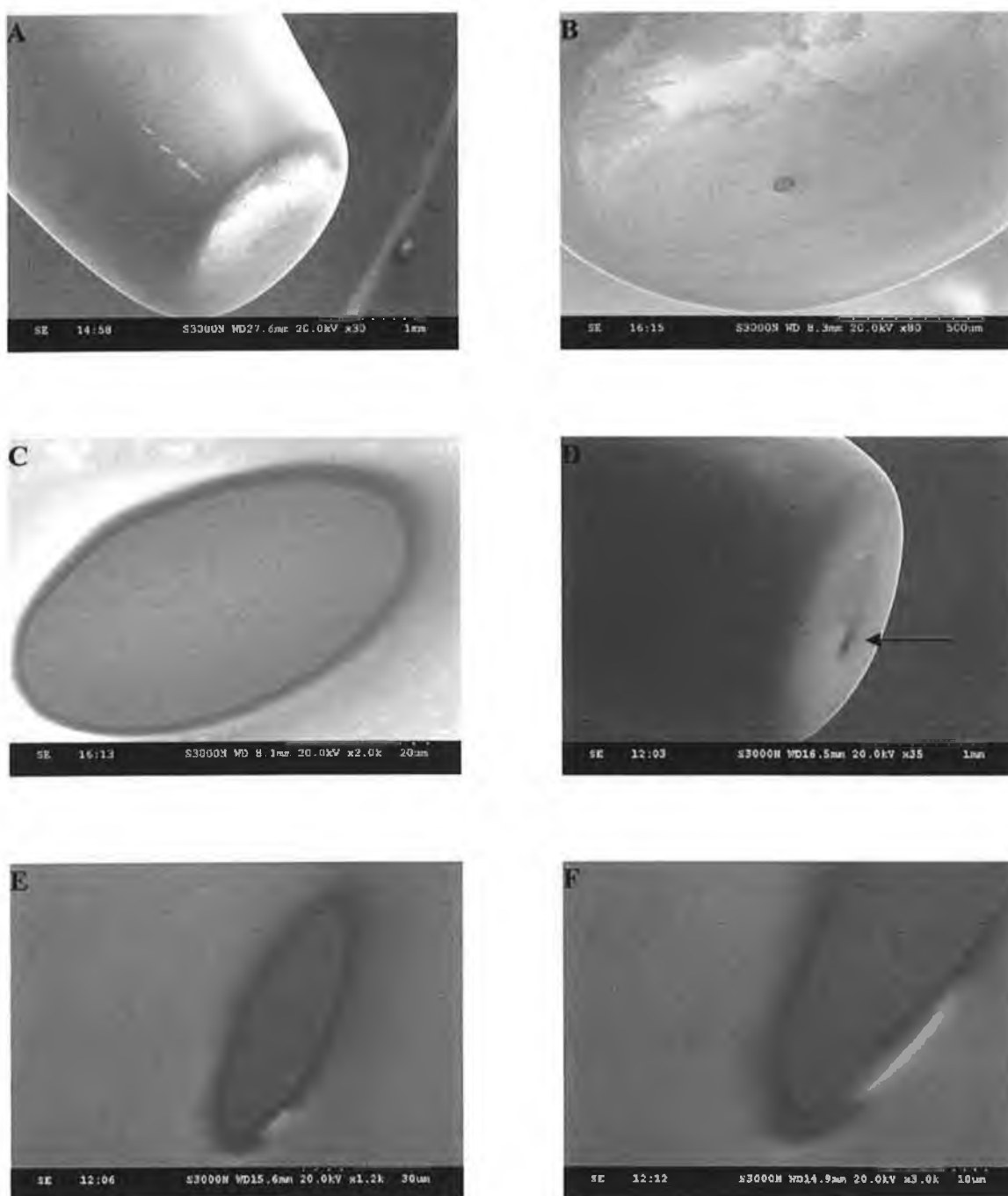


Figure 6.26: Scanning Electron Microscope (SEM) images of non-etched and etched microelectrodes. A and B depict low magnification (30x and 80x respectively) images of the platinum microwire at the tip of the electrode. C shows a high magnification (2,000x) image of the polished, non-etched electrode. The black ellipse surrounding the platinum wire is due to electron charge build-up. Image D is a low magnification (30x) of the etched microelectrode. A hollow is present (darkened shadowed area indicated by the arrow) where the microwire was present in Images A and B. Picture E is a high magnification (1,200x) image of the etched depression in the electrode, whilst picture F is a high magnification (3,000x) illustration of the lower region of the etched microwire, depicting the recessed nature of the platinum in relation to the glass surround.

6.4.3.6 Time-current response following addition of H₂O₂.

Upon addition of H₂O₂ substrate to the electrochemical cell, as outlined in Section 2.38.3, electrons are generated at the active site of the HRP molecule, immobilised within the etched cavity of the platinum microelectrode. These electrons can be shuttled from the active site to the platinum microwire, which in turn causes a change in the potential of the system, resulting in an increase in charge. Sequential additions of H₂O₂ substrate will result in a 'staircase' like graph as outlined in Figure 6.27.

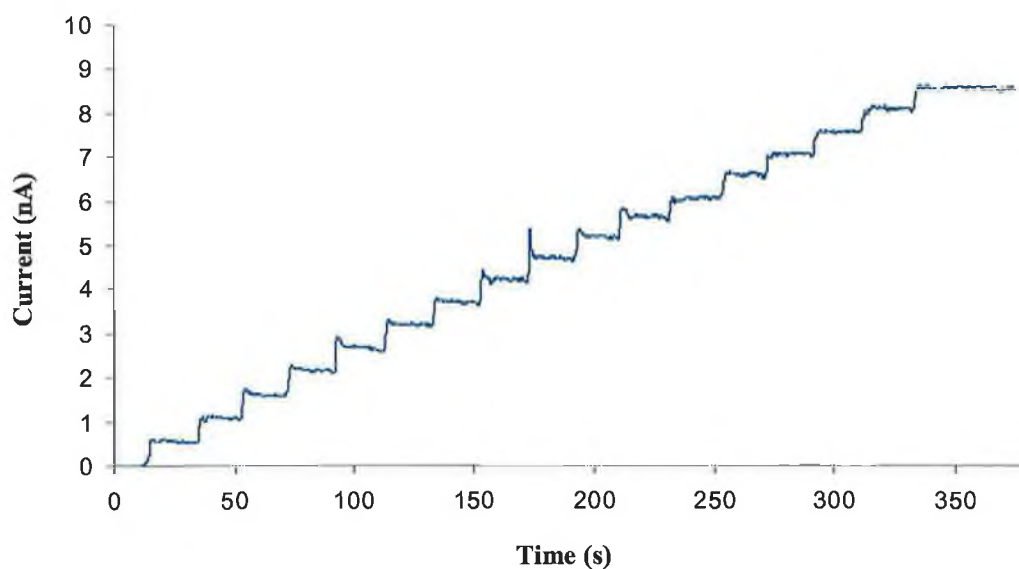


Figure 6.27: Typical amperometric time course curve depicting the electrochemical response of an etched platinum microelectrode with recombinant HRP immobilised within the cavity. $2.5 \times 10^{-4} \text{ mol.L}^{-1}$ H₂O₂ (final concentration) was injected sequentially every 20 s to the rapidly mixed, degassed, electrochemical cell.

The amperometric time course can be linearised by plotting the plateau current value after each substrate injection versus substrate concentration. Any potential plant HRP direct electrochemistry was also investigated by carrying out the same experimental procedure as outlined for recombinant HRP, with an equal initial peroxidase activity available for immobilisation. As adsorption is a non-specific method of enzyme immobilisation, each enzyme was immobilised in triplicate and the average amperometric response recorded for each H₂O₂ concentration. BSA was utilised as a negative control: this provides an immobilised protein surface but one lacking in peroxidase activity. This procedure took any direct, non-enzymatic, electro-oxidation of H₂O₂ at the platinum microelectrode into consideration.

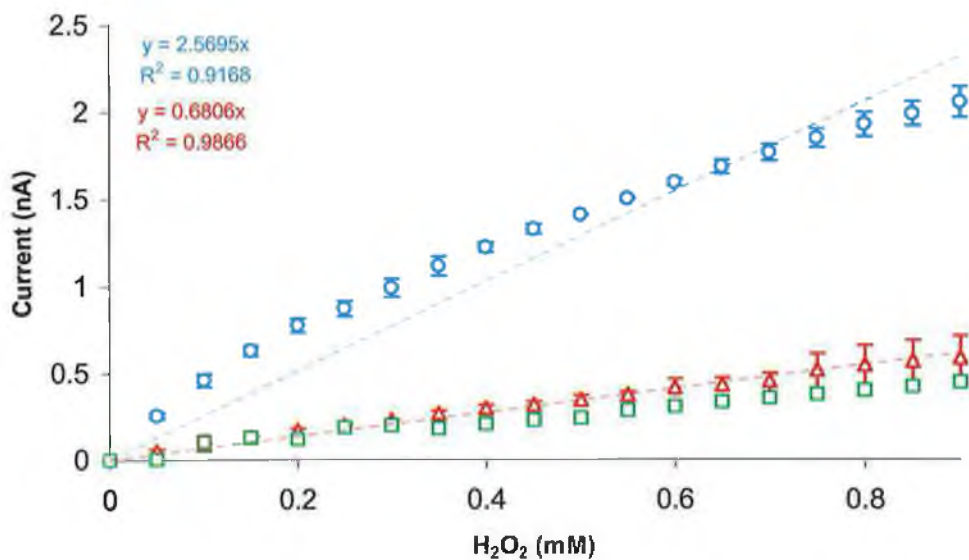


Figure 6.28: Linearised amperometric time curve, with sequential additions of $5.0 \times 10^{-5} \text{ mol.L}^{-1} \text{ H}_2\text{O}_2$ at 20 s intervals. Recombinant HRP (\circ), Plant HRP (\triangle) and BSA (\square) (2nM final concentration) were immobilised within the etched cavity, via adsorption, overnight at 4°C .

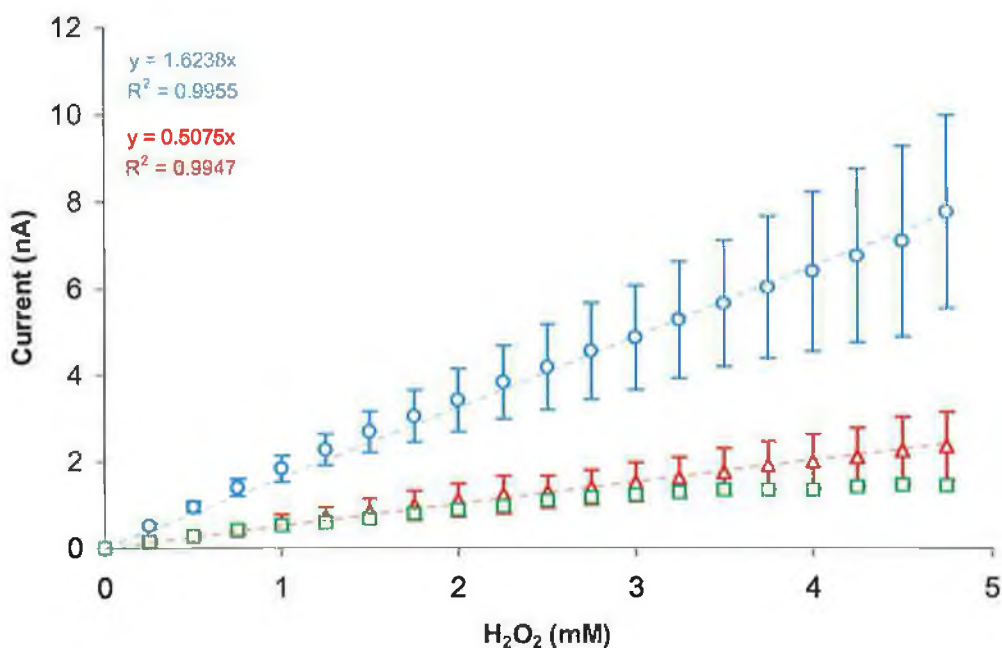


Figure 6.29: Linearised amperometric time curve, with sequential additions of $2.5 \times 10^{-4} \text{ mol.L}^{-1} \text{ H}_2\text{O}_2$ at 20 s intervals. Recombinant HRP (\circ), Plant HRP (\triangle) and BSA (\square) (2nM final concentration) were immobilised within the etched cavity, via adsorption, overnight at 4°C .

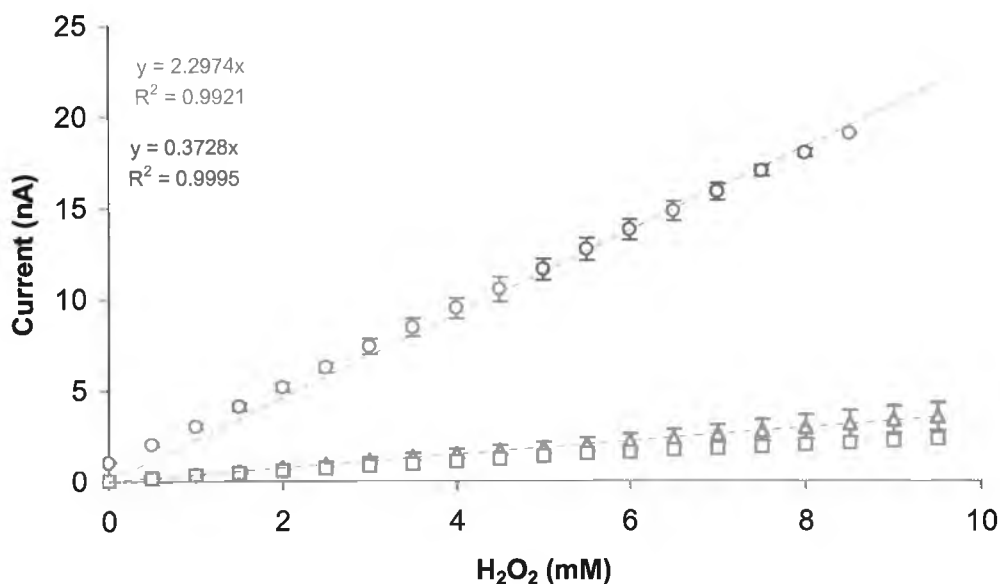


Figure 6.30: Linearised amperometric time curve, with sequential additions of $5.0 \times 10^{-4} \text{ mol.L}^{-1} \text{ H}_2\text{O}_2$ at 20 s intervals. Recombinant HRP (\circ), Plant HRP (\triangle) and BSA (\square) (2nM final concentration) were immobilised within the etched cavity, via adsorption, overnight at 4°C .

6.4.3.7 Electrochemical kinetic analysis, Eadie-Hofstee Plot.

The data generated for the amperometric response to H_2O_2 catalysis by recombinant HRP can also be utilised to calculate apparent K'_m value for HRP towards H_2O_2 . The Eadie-Hofstee plot is a commonly utilised method to determine the kinetic parameters of biosensors (Kamin and Wilson, 1980).

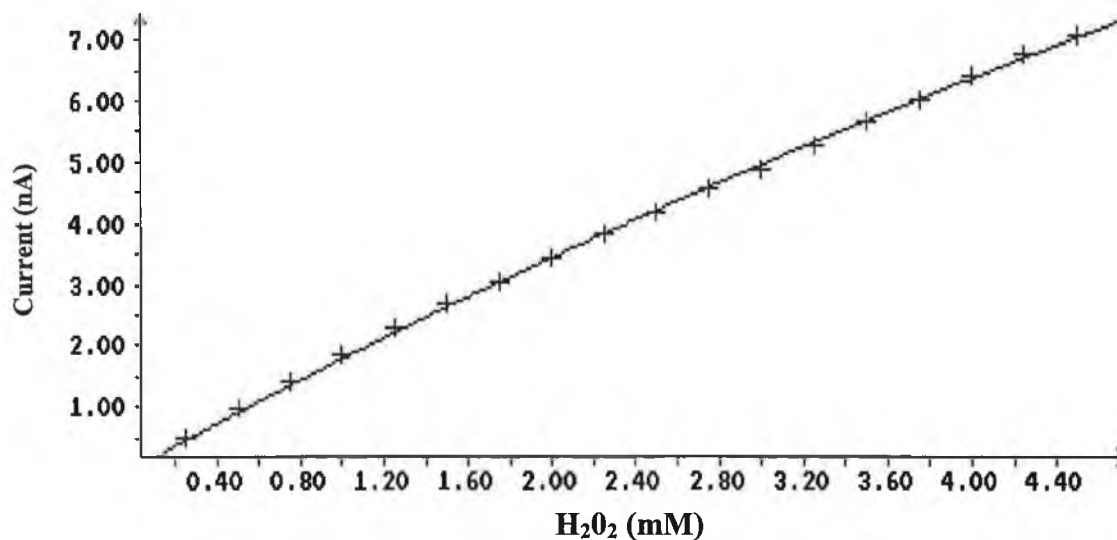


Figure 6.31: *Enzfitter*TM MichaelisMenten kinetic modelling of the linearised recombinant HRP H_2O_2 catalysis data in Figure 6.30.

When the rHRP electrochemical data from Figure 6.29 was plotted with the Eadie-Hofstee methodology an pseudo-sigmoidal curve was noted. The upward curvature was attributed to H_2O_2 diffusional limitations. However, when a higher H_2O_2 concentration was utilised ($2.5 \times 10^{-4} \text{ mol.L}^{-1}$), the data fitted very well to a Michaelis-Menten kinetic model (see Figure 6.31), and an Eadie-Hofstee plot resulted in an apparent K'_m calculation of $17.2 \times 10^{-3} \text{ M}$ for H_2O_2 . This apparent K'_m was calculated in the absence of a reducing substrate (e.g. ABTS), with the electrode providing the electron source/sink.

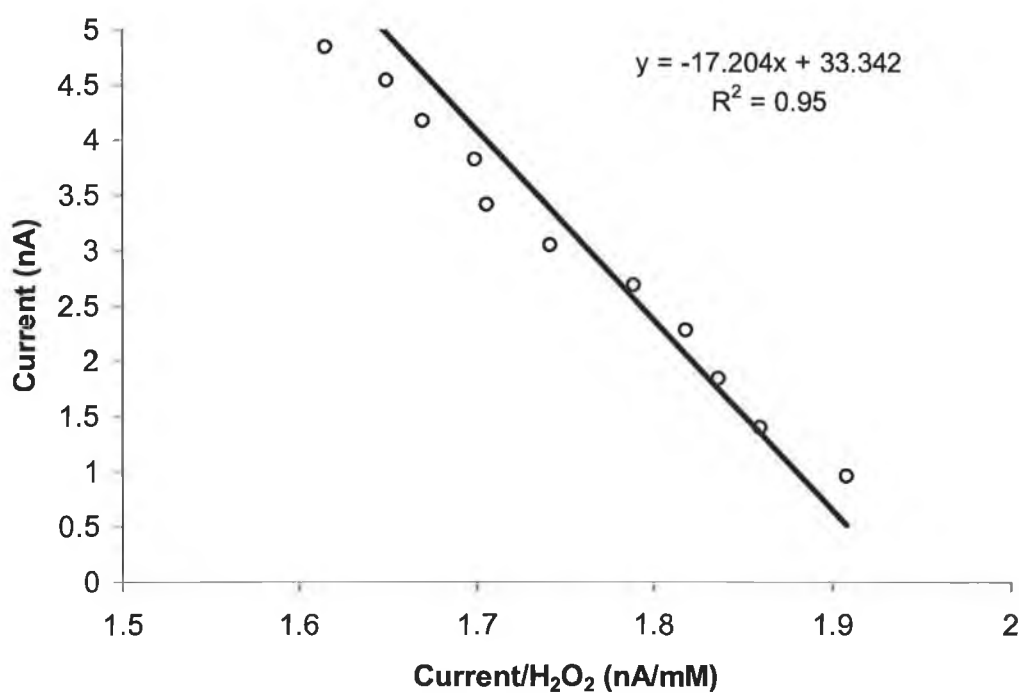


Figure 6.32: The electrochemical Eadie-Hofstee plot for a recombinant HRP etched electrode biosensor. The slope of the line was used to calculate the apparent K'_m of recombinant HRP for H_2O_2 .

6.5 Discussion.

Protein immobilisation can be simply defined as the limitation of protein molecule mobility in space, or relative to another molecule (Martinek and Mozhaev, 1985). Four basic immobilisation techniques exist: physical adsorption, covalent attachment, copolymerisation, and microencapsulation. “Immobilisation can result in increased protein stability; however, this may not be the primary reason for immobilisation. Enzymes are often immobilised because of the economic costs involved in their isolation and purification, to allow their reuse, or use in bioreactors, and to prevent contamination of the end product” (Ó’Fágáin, 1997).

6.5.1 Immobilisation Mutants’ Free Solution Stability.

In this study, arginine residues were selected for substitution to lysine residues, to allow directed immobilisation of rHRP to an activated matrix. Of the twenty-one arginine residues in rHRP, only three were deemed suitable for the proposed mutagenesis: Arg118, Arg159 and Arg283. Lysines are often chosen as the amino acid of choice for covalent immobilisation as they occur frequently in proteins and are active nucleophiles when unprotonated, i.e. at alkaline pH. They are also routinely located on surface-exposed regions of proteins, due to their charged/polar nature. This characteristic also allows for simple immobilisation reactions, as lysine residues do not require activation prior to immobilisation (Ó’Fágáin, 1997). Arg to Lys is a conservative mutation and should result in minimal disruption to the protein tertiary structure (Betts and Russell, 2003). Important hydrogen bonds between an arginine and a phosphate moiety have previously been noted, however, and replacement of such an Arg with a Lys can be disastrous. This is due to lysine possessing only a single amino group and, hence, hydrogen bonding is limited (Betts and Russell, 2003). This problem is not evident here, however, as *Velcro Plus* (where the Arg residues are replaced by Lys), displayed almost identical thermal and solvent stabilities (with the exception of MeOH) to wildtype rHRP in free solution studies. It should be noted that additional mutagenesis of *Velcro Plus* to *Velcro Minus* (by removal of the chemically modifiable Lys 232 and Lys241) results in a dramatic decrease in stability. This is somewhat surprising, as the modifiable residues were mutated to the most stabilising residues, K232F and K241N, described in Chapter 4. Addition of the bulky aromatic Phe residue may have combined with the impaired hydrogen bonding introduced by additional Lys residues, resulting in a destabilised molecule. In free solution studies, *Velcro Minus* displays a 50% decrease

in thermal stability and a 20% decrease in MeOH stability. However, *Velcro Minus* also displays equal H₂O₂ stability and two-fold greater stability to DMF at room temperature, although these latter stabilities do not match those of K232F/K241N double mutation in free solution (see Section 4.6.3 and 4.6.4). As such, free solution analysis indicates that inclusion of K232/K241N is not advantageous to the *Velcro* molecule in terms of stability, but is necessary to ensure directed immobilisation. One of the Arg residues (283) is located on the last turn of Helix J (Gajadhe et al., 1997). Previous results (see Chapter Five) demonstrated the key role of the helix within the HRP structure scaffold. As such, both *Velcro Plus* and *Velcro Minus* were back-mutated at this position to yield *Velcro Plus(K283R)* and *Velcro Minus(K283R)* revertants respectively. Although this reduced the number of potential immobilisation sites, it was noted to have an effect on free solution stability. For example, *Velcro Minus(K283R)* displayed a 2.6-fold increase in thermal stability over *Velcro Minus* as judged by $t_{1/2}$ at 50°C. This mutant also showed a 1.3-fold increase in thermal stability over wildtype. However, *Velcro Plus* and *Velcro Plus(K283R)* displayed very similar thermal stabilities. Solvent stability was also affected by re-introduction of the Arg residue at position 283, with *Velcro Plus(K283R)* exhibiting a decrease in DMSO (1/6) and MeOH (1/5) tolerance compared to *Velcro Plus*, although *Velcro Plus(K283R)* did show a 1/3 increase in C₅₀ in DMF. *Velcro Minus(K283R)* displayed decreased solvent stabilities in all solvents tested (DMSO: 1/7, MeOH: 1/5 and DMF: 1/3, respectively) in free solution studies. Interestingly, both reversion mutants displayed an increased H₂O₂ stability in free solution, (14% for *Velcro Plus(K283R)* and 94% for *Velcro Minus(K283R)*). As such, the thermal and H₂O₂-stabilising effect of the Lys232 and 241 mutations (Phe and Asn respectively) are only noticeable when the helical properties are maintained within the protein backbone.

6.5.2 Immobilisation on CNBr-Activated Sepharose.

Another disadvantage of K232 and K241 removal is evident during immobilisation to CNBr-Activated Sepharose. Wildtype rHRP, with three potential immobilisation sites (Lys 174, 232, 241), displays 50% immobilisation. *Velcro Minus(K283R)* with three potential immobilisation sites (K174, K118 and K159), yields only 42% immobilisation. *Velcro Minus*, with four potential immobilisation residues (K174, 118, 159, 283), achieves 57% immobilisation. However, *Velcro Plus(K283R)* with five potential immobilisation sites (K118, 174, 159, 232, and 241), yields 69%

immobilisation. *Velcro Plus*, with six possible immobilisation sites (K118, 174, 159, 232, 241, 283) yields 86% immobilisation. These calculations were based on units of activity available for immobilisation and units of activity immobilised, making the assumption that no inactivation occurred during the immobilisation process. rHRP has previously demonstrated its stability in all conditions utilised during immobilisation, e.g. low pH during the elution step of nickel affinity protein purification. The total duration of low pH conditions for rHRP coupling was minimised and was much shorter than that used in protein purification. Cyanide inactivation of HRP is known to occur (Dunford, 1999); however, cyanide release would be minimal and quickly diluted and removed due to the high number of washes during the immobilisation procedure. Fuentes and colleagues (2006) noted that the rate of HRP immobilisation depended exponentially on the concentration of reactive groups on the protein and the support. Therefore, protein immobilisation occurs at regions exhibiting the highest density of reactive groups.

Wilcheck and Miron (2002) noted that lysine is the key amino acid responsible for protein immobilisation onto CNBr-Activated Sepharose. However, they noted that random immobilisation of the proteins examined did not cause any loss of activity, and they argue that random immobilisation is similar to orientated, as immobilisation occurs through one to two bonds. It should be noted that all proteins investigated in that publication were native, glycosylated proteins, with no indication given as to the total number or location of available lysine residues. Conversely, Cha and co-workers (2005) demonstrated that orientated immobilisation of enzymes is critical, particularly as applied to protein chips. Ultimately, the future of immobilised protein chips in biomedical diagnostics is orientation dependent. Cha and co-workers (2005) noted that random immobilisation on an activated silicon chip is seen to drastically alter protein function, as compared to free solution activity.

6.5.3 Cyanogen Bromide Activated Matrix Immobilised Enzyme Characteristics.

6.5.3.1 Thermal Stability.

Following successful immobilisation onto activated CNBr, the four *Velcro* mutants were characterised as to their thermal, solvent and H₂O₂ stabilities, utilising immobilised wildtype rHRP as a reference. Free-solution thermal profiling suggested 50°C as standard temperature to carry out thermal inactivation analysis on the immobilised forms. At this temperature, immobilised wildtype rHRP demonstrated

more than two-fold stabilisation, as indicated by $t_{1/2}$. However, the only Velcro mutant to display an increase in immobilised thermal stability was *Velcro Plus(K283R)*, with a marginal 5% increase in $t_{1/2}$ at 50°C. *Velcro Plus* (4-fold), *Velcro Minus* (1.25-fold) and *Velcro Minus(K283R)* (1.25-fold) all displayed a notable decrease in thermal stability. It appears that multipoint attachment, most evident in the case of *Velcro Plus*, increases strain on the rHRP molecule. This, in conjunction with restricted movement, causes a dramatic decrease in thermal stability. Previous reports of destabilising multipoint immobilisation of glucoamylase also point to increased protein strain as reason for decreased thermal stability (Gerasimas et al., 1980), while the type of immobilisation resin can also destabilise the immobilised protein (Nys et al., 1977). These results contradict previous reports of increased thermal stability, due to multipoint attachment (Abian et al., 2004). However, Abian and co-workers (2004) focused their mutations on a lysine-rich area of Penicillin G Acylase, which previous chemical modification studies had proven not to be critical for protein stability, and so minimised the chance of a deleterious mutation (or interaction from other mutations) in this area. This group also utilised a glyoxyl-agarose activated solid phase for protein immobilisation. Plant HRP has previously been immobilised onto a variety of solid phases, by a range of different techniques, to increase thermal stability. For example, Lai and Lin (2005) covalently immobilised plant HRP onto porous aminopropyl glass beads. Upon immobilisation, the operational pH range was broadened in the acidic range by one pH unit and optimal operating temperature was increased by 10%, with the thermal stability of the immobilised molecule increased by 20% compared to free solution plant HRP. The immobilised HRP was utilised in the removal of *p*-chlorophenol from wastewater; however, the removal efficiency did not match that of free HRP due to substrate diffusion limitations (Lai and Lin, 2005). Rojas-Melgarejo and co-workers (2004) also noted increased thermal stability (30%) for plant HRP absorbed onto cinnamic carbohydrate esters, similar to that noted in this present study for wildtype rHRP (27%), covalently immobilised onto CNBr.

6.5.3.2 Solvent Stability.

Immobilised wildtype rHRP shows no alteration in DMSO and DMF stability; however, it displays decreased (25%) MeOH tolerance. *Velcro Plus* displays a 40% decrease in DMSO, 30% decrease in MeOH, but a 40% increase in DMF stabilities. CNBr-immobilised *Velcro Plus(K283R)* displays similar solvent stabilities to the non-

immobilised form; however, DMF incubation results in a 38% stability decrease. Surprisingly, *Velcro Minus* CNBr immobilisation yields increased (20% in DMSO, 16% in DMF) or equal stability (MeOH) in all solvents tested. CNBr-immobilised *Velcro Minus(K283R)* displays almost identical solvent stabilities to free solution *Velcro Minus(K283R)*. The reduced tolerance of *Velcro Plus* can again be ascribed to increased strain and lack of protein flexibility. Organic solvent molecules, that have stripped and replaced water molecules, are maintained in close proximity to the protein surface due to the confined nature of the immobilised protein, leading to protein denaturation. Increased catalytic stability, as demonstrated by *Velcro Minus*, can be attributed to orientated immobilisation. The immobilisation is not as rigid as *Velcro Plus*, as demonstrated by the smaller thermal stability loss, yet it maintains the molecule's active site correctly orientated for optimal catalytic activity.

Protein immobilisation for use in organic solvents is a rapidly developing area of research; recently Temino and co-workers (2005) demonstrated that encapsulation of an alcohol dehydrogenase and its NADPH cofactor within a polyvinyl alcohol hydrogel protected the enzyme from organic solvents and thermal denaturation. This allowed the enzyme to effectively catalyse the conversion of prochiral ketones to chiral alcohols in the presence of organic solvents. Encapsulation is one of the simplest immobilisation strategies to execute; however, it is critical that there is rapid diffusion of substrates and products in and out of the encapsulating material (Hudson et al., 2005). The possible role of HRP in organic solvent catalysis has been previously outlined (Section 1.1.6) and so any increase in stability in this area will be of great benefit.

6.5.3.3 H₂O₂ Stability.

An unexpected result was noted for Wildtype and *Velcro* mutants' stability in H₂O₂. Despite a large variation in H₂O₂ stability (*Velcro Plus(K283R)*, *Velcro Plus* and *Velcro Minus(K283R)* display a 2.6, 2.2 and 2-fold increase in stability respectively compared to wildtype and *Velcro Minus*), all four mutants and wildtype show a dramatically decreased H₂O₂ stability after CNBr immobilisation. For example, *Velcro Plus* exhibits a 7-fold decrease, whilst wildtype and *Velcro Minus* displays a 3.4-fold reduction. All immobilised forms demonstrate an apparent basal C₅₀ value of 5 mM H₂O₂. A possible reason for this may be the immobilised rHRP favouring the Compound III or inactivation pathways of the peroxidase H₂O₂ catalytic cycle (Hernández-Ruiz et al., 2001). Immobilisation-induced strain may interfere with the

necessary enzyme flexibility, leading to inappropriate H₂O₂ turnover and, ultimately, enzyme inactivation. Previous immobilised HRP H₂O₂ tolerance results appear to depend on the type and reactivity of the activated solid phase. Rojas-Melgarejo and co-workers (2004) report increased H₂O₂ tolerance with HRP adsorbed onto cinnamic carbohydrate esters when the stability analysis was carried out at pH 7.0; however, when the experiment was repeated at pH 4.5, there was a dramatic loss of H₂O₂ stability. The authors believe that reactive oxygen species such as superoxide, generated during H₂O₂ catalysis, may have been absorbed by the cinnamic support instead of attacking the essential enzyme residues. Alternatively, at lower pH, carbonyl groups are oxidised and do not provide a sink for oxidising reactive oxygen species, leading to dramatic enzyme destabilisation (Rojas-Melgarejo et al., 2004).

Although covalent immobilisation was utilised in this study, many methods of immobilisation exist; however, the selection of the optimal procedure is critical to maximising immobilisation efficiency and potential stability gains. Azevedo and co-workers (2004), for example, utilised immobilised plant HRP in a mini-packed bed reactor flow-injection analysis system. HRP was immobilised onto alkylamine controlled pore glass by two methods: adsorption and covalent linkage (using glutaraldehyde and EDC coupling methodologies). High operational stabilities were noted for glutaraldehyde-immobilised HRP; whilst EDC coupled HRP demonstrated poor stability. Adsorbed HRP simply desorbed upon reactor washing, and required cross-linking after adsorption to promote correct immobilisation. The immobilised HRP permitted the monitoring and quantification of H₂O₂ (up to 1.1×10^{-2} mol.L⁻¹) in a continuous on-line bioprocess set-up.

Nahar and Bora (2004) recently outlined an interesting immobilisation method utilising microwaves to covalently immobilise HRP to light-activated inert polymers. This technique is rapid, simple and maintains enzyme catalytic activity. Non-specific protein absorption is minimised due to short reaction time (less than 60 s) and this technique may prove useful in protein micro-array production.

There are very few reports of either direct or random immobilisation of recombinant HRP in the literature. Rojas-Melgarejo and colleagues (2006) noted the difficulty in immobilising recombinant HRP to traditional adsorbent solid phases, as the recombinant protein lacks the carbohydrate residues commonly used for this type of immobilisation. Instead, cinnamic esters were successfully employed (63% immobilisation rate) as an immobilisation platform. This platform utilises physical

adsorption in conjunction with glycosylation-independent hydrophobic interaction. Wildtype recombinant HRP immobilised in such a fashion yielded an 8% increase in thermal stability. Abad and co-workers (2005) recently described directed recombinant HRP immobilisation via an N-terminal His tag–cobalt (II)-terminated gold nanoparticle interaction. Although no stability data were available for this method, its potential application in orientated immobilised rHRP onto gold electrodes for biosensing is obvious. Allard and colleagues (2002) utilised a poly-His/poly-Lys double-tagged recombinant protein expression procedure, which permitted the inclusion of various combinations of the His/Lys tags for directed immobilisation. Similar methods for directed immobilisation include the use of a poly-Arginine tag, as demonstrated by Stempfner and colleagues (1996). In this case an (Arg)₆ tag was genetically engineered as a C-terminal fusion peptide, permitting orientated adsorption onto polyanionic adsorbents under low-salt conditions. The mutant's stability closely resembled the wildtype's under heat and urea denaturing conditions; however, there was a slight alkaline shift in pH optimum.

6.5.4 UltraBind™ Orientated *Proof of Principle*.

Lopez-Gallego and co-workers (2005) recently illustrated an alternative to traditional protein chemical modification for stabilisation. In their communication, chemical modification of an enzyme was proposed, not to increase stability, but to enrich the protein surface with reactive groups. This should facilitate multipoint covalent attachment during protein immobilisation. The present work has further advanced this idea by alteration of the amino acid composition of rHRP to increase the number of lysine residues, and also to focus these lysines to a specific region of the 3-dimensional structure. This study proposes directed, multipoint immobilisation of rHRP onto a commercially available, modified polyethersulfone (PES) membrane. The additional lysine residues are located on the opposite side of the molecule to the active site (*Velcro Minus*); hence, immobilisation via these lysines forces the protein to orientate its active site away from the membrane and towards the bulk solution phase. Figure 6.16 demonstrates increased catalytic activity for the *Velcro Minus* immobilised rHRP compared with Wildtype, over a five-hour period. Equal concentrations of *Velcro Minus*, *Velcro Plus* and wildtype rHRP were applied; however, increased catalytic activity towards DAB substrate is directly attributed to optimal orientation of the rHRP molecule (*Velcro Minus*), as compared to the random orientation of wildtype rHRP,

(see Figure 6.16). *Velcro Plus* mutants displayed a similar trend to wildtype rHRP; however, poor coloration was noted over the four-hour initial incubation period. If the catalytic reaction is allowed to proceed overnight at room temperature (Figure 6.15), it is clear that the colour development is more intense for the *Velcro Minus*, compared to Wildtype and *Velcro Plus*. The initial poor colouration of *Velcro Plus* is augmented by increased reaction time, and reaches a threshold similar to wildtype. As outlined previously, conformational changes due to multipoint attachment may have caused the suboptimal catalytic activity of *Velcro Plus*. No simple adsorption is noted in the immobilisation procedure, as the reverse side of the membrane displays no catalytic colouration (see Figure 6.15, part E). Activated membranes are typically single-side activation; hence, if correct covalent immobilisation is achieved, as demonstrated here, only one side will capture enzyme. Furthermore, this experimental setup also demonstrated reusability. Immobilised *Velcro Minus*, was stained repeatedly (up to three times, data not shown) with TMB, non-precipitating substrate, over a period of several hours, with appreciable catalytic activity noted each time.

The immobilisation of enzymes can increase protein stability (Mateo et al., 2000); however, by implementing orientation-dependent protein immobilisation, researchers may not only stabilise a protein, but may also promote superior performance in applications such as biosensors. Recent developments in this area focus on the type of bio-recognition involved in immobilisation. Traditionally, lysines (as in this study) or cysteines can be engineered into a protein backbone to allow for immobilisation. However, as the field of proteomics enlarges, protein microarrays require vast concentrations of immobilised protein, which cannot be easily achieved by site-specific immobilisation. More generic methods of immobilisation have developed in recent years, from His-tag chelation to biotin-avidin interaction. Polypeptide scaffolds comprise a topical generic immobilisation method, employing a hydrophobic anchor attached to a leucine-zipper protein capture domain utilised to directionally immobilise several different proteins to a hydrophobic solid phase (Zhang et al., 2005).

6.5.5 Electrochemical Biosensing Devices.

6.5.5.1 Screen Print Electrode.

Screen-printed electrodes are commonly utilised in the mass production of disposable electrochemical sensors. The practical utility of screen-printed electrodes has long been exploited, despite the limited knowledge on the actual electrode reactions (Wang et al., 1998). In this study the different electrochemical properties of wildtype and plant HRP were investigated, utilising an in-house produced screen-printed electrode. Prior to any enzyme immobilisation, the screen-print electrode was electrochemically cleaned by the pre-treatment method of Killard and co-workers (1999). In this method, cycling of the screen-printed electrode in sulphuric acid is believed to strip the carbon electrode surface, removing any insulating materials present on that surface. Once the pre-treatment was completed, a polyaniline:polyvinylsulphonate (PANI/PVS) layer was deposited on the bare screen-print electrode, via cyclic voltammetry. The voltage was cycled until the leucoemeraldine radical cation peak reached an anodic current of approximately 2.8mA (see peak A, Figure 6.20). This typically required 10 cyclic sweeps, and mirrors well previous work in this area (Iwuoha et al., 1997). However, this was difficult to reproduce accurately and, as such, the layer depth demonstrates some variability. PANI can fulfil many roles in biosensor configuration, including extension of the linear range of the sensor, as an immobilisation platform for biocomponents and as the electron mediator (Grennan et al., 2005). The inclusion of PVS in the polymer synthesis maintains electrical neutrality once the polymer is oxidised and results in increased polymer structural stability and conductivity over a broader range of pH values (A. Morrin, PhD Thesis, DCU, 2003). The conducting polymer is capable of penetrating the insulating exterior of proteins and can provide a direct electrochemical communication between the redox centre of the protein and the electrode surface. This is achieved by delocalisation of redox charges over a series of conducting polymer groups, thereby acting as self-contained electron-transfer mediators (Grennan et al., 2006). Once the PANI/PVS conducting layer had been deposited, the protein of choice; in this study BSA, recombinant or plant HRP, was immobilised onto the surface of the PANI/PVP layer via time-based amperometry. A long (~1 hr) equilibration period was required to allow the electrode to reach steady state prior to amperometric analysis. This extended equilibration period was required to allow the polymer charge, built up during PANI/PVP oxidation in previous preparatory steps, to dissipate. This charging current is common in polymer-modified screen-printed

electrodes (Iwuoha et al., 1997). Previous non-biosensor PANI-based HRP immobilisation studies have demonstrated increased thermal and solvent stabilities, in conjunction with improved kinetic values (Fernandes et al., 2004). Steady-state amperometric analysis of BSA, recombinant and plant HRP was then carried out. Protein molecules are too large to permeate the polyaniline layer and, as such, catalytic activities occur on the surface of the polymer (A. Morrin, PhD Thesis, DCU). There are very few reports of recombinant HRP utilised in screen print electrodes, with none incorporating polyaniline. Schumacher and co-workers (2001) employed a graphite electrode with adsorption and entrapment used as the immobilisation techniques.

In the present study, equimolar concentrations of each protein (2 nm) were individually electrostatically immobilised onto the polyaniline layer. Once immobilised and a steady state condition achieved, successive additions of $2.0 \times 10^{-2} \text{ mol.L}^{-1} \text{ H}_2\text{O}_2$ were carried out, with the resulting increase in μA recorded. Figure 6.21 demonstrates the increased μA output for recombinant HRP as compared to plant HRP. This can be attributed to rHRP's lack of glycosylation, allowing a more rapid transfer of electrons from the enzyme's active site to the sensing electrode surface. Plant HRP displays 20% glycosylation (Ryan et al., 2006), which is known to hinder efficient electron transfer (Presnova et al., 2000). BSA was utilised as a non-reactive blocking protein, to account for any direct electro-oxidation of H_2O_2 at the polymer surface. Figure 6.21 demonstrates that there is some direct electro-oxidation of H_2O_2 ; however, both forms of the peroxidase yield results above this basal value. When lower concentrations of H_2O_2 were employed, very small $\Delta\mu\text{A}$ were observed (data not shown), possibly due to H_2O_2 diffusion problems. However, use of high concentrations of H_2O_2 led to rapid peroxidase denaturation. Wildtype recombinant HRP has a free-solution H_2O_2 C_{50} of $\sim 1.7 \times 10^{-2} \text{ mol.L}^{-1}$, during a 30 min incubation (see Chapter 3); the value is just 5mM for CNBr-immobilised rHRP (see Chapter 6). As such, $2.0 \times 10^{-2} \text{ mol.L}^{-1}$ injections would rapidly denature the enzyme. This is observed by the initial rise, followed by a drop in $\Delta\mu\text{A}$ as H_2O_2 concentration increases within the electrochemical cell. Previous SEM and AFM image analysis of screen-printed electrodes with HRP immobilised suggested that the protein is immobilised in a non-orientated fashion, and often in aggregates (Grennan et al., 2006). This may have resulted in steric hindrance for H_2O_2 access to the active site of the protein. A possible method to overcome aggregate formation was recently suggested by Lori and co-workers (2006), in which N-nitrilotriacetic acid (NTA) was co-doped into the electropolymerised PANI/PVS

polymer. The NTA could efficiently chelate recombinant proteins incorporating a His-tag to the electrode surface. Further to this, incorporation of HRP into the screen print “ink” prior to deposition may provide an alternative approach. Direct electron transfer is achieved by plant HRP inclusion in this “biocomposite ink”. However, several difficulties exist in mass production of such screen print electrodes, mainly involving the optimisation of the “biocomposite ink” (Ledru et al., 2006). Morrin and co-workers (2002) previously demonstrated that the optimum plant HRP concentration was 0.75 mg.mL^{-1} for polyaniline-modified screen-printed electrodes. This concentration achieved a theoretical monolayer distribution on the electrode surface. However, a similar concentration of active recombinant HRP could not be achieved, as detailed previously (Section 3.10.4). The maximal production of rHRP dictated the working concentration of peroxidase within this arrangement, which was typically $0.65 \mu\text{M.L}^{-1}$. To overcome this problem, a more sensitive method of amperometric analysis was investigated, namely etched microelectrodes.

6.5.5.2 Etched Microelectrode.

Microelectrodes are defined as electrodes of critical dimensions in the micron range. Microelectrodes possess many advantages over the traditional macro electrode (millimetre dimensions) including a reduced response time, which enables electrochemical experiments to be carried out over extremely short timescales (Andriex et al., 1998). Also, current measurement can be carried out in the pico- and nano-Amp range, which permits more sensitive analysis. The microelectrode utilised in this study was produced in-house in collaboration with Dr. Jennifer Brennan, NCSR, DCU, and is outlined diagrammatically in Figure 6.22. The microelectrode was polished, to achieve a smooth surface, and then electrochemically characterised.

Cyclic voltammetry on a platinum electrode, in $1.0 \text{ M H}_2\text{SO}_4$, yields a characteristic curve. The oxide monolayer peak was utilised to calculate the “*electrochemical area*” which, in conjunction with the geometric area, allowed an estimation of the surface roughness. Typical values for the microelectrode surface roughness ratio are between 1.0 and 3.0, with the microelectrode generated in this study achieving 1.25. A cyclic voltammogram over the potential window of +0.1 to +0.9 Volts illustrated the importance of biological buffer choice. Sodium phosphate (50 mM, pH 7.0) buffer demonstrated a curve similar to that of H_2SO_4 cycling. This was attributed to the HCl

utilised to adjust the buffer solution's pH acting like the H_2SO_4 , and electrochemically cleaning the electrode. As such, MOPS (50 mM, pH7.0) buffer was utilised as the biological buffer of choice. This buffer was pH-adjusted only with NaOH, and had previously demonstrated its electrochemical compatibility (N. Carolan, PhD Thesis, DCU, 2004). The cyclic voltammetry curve generated in MOPS (50 mM, pH 7.0) was very similar to that of a non-electrochemically active solution, lithium perchlorate. The potential window was extended for MOPS (50 mM, pH7.0) to ensure that no peaks were observed at more positive potentials, as noted in Figure 6.24.

Possible direct electro-oxidation of H_2O_2 in the vicinity of a platinum electrode was investigated by injection of various concentrations (0, 2.5, and $10 \times 10^{-4} \text{ mol.L}^{-1}$) of H_2O_2 into rapidly-mixing MOPS (50 mM, pH7.0) buffer solution. A small curve-shift was recorded for $2.5 \times 10^{-4} \text{ mol.L}^{-1} \text{ H}_2\text{O}_2$ injection; however, upon the addition of $1.0 \times 10^{-3} \text{ mol.L}^{-1} \text{ H}_2\text{O}_2$, an anodic peak at 0.6 Volts was noted. This was ascribed to the direct electro-oxidation of H_2O_2 in the electrolyte solution, MOPS (50 mM, pH 7.0). Therefore, a negative control was critical for all subsequent amperometric electrochemical analysis.

The platinum wire of the electrode was then etched, via submersion into hot (75°C) aqua regia, for 3 hours. The microwire was imaged using scanning electron microscopy before and after etching. Prior to etching, the wire was clearly visible at the tip of the electrode; however, after 3 hours etching, it was no longer visible and a recess was noted, as indicated by shadowing, upon visualisation of the microwire region at high magnification. The dark ellipse surrounding the platinum wire in some of the images is due to electron charge build-up. Platinum conducts electrons, glass does not: where the two meet, there is a difference in electron concentration, resulting in a darkened ring around the platinum wire. The roughness of the etched electrode was not calculated, as the exact depth of the etched cavity could not be determined.

Equimolar concentrations (2 nM) of recombinant HRP, plant HRP and BSA were immobilised into the cavity generated and a current-time assay was performed to analyse the response of the etched electrode to successive additions of H_2O_2 . All experiments were carried out in triplicate, as protein immobilisation via adsorption is difficult to reproduce. The average values were plotted in Figures 6.28 to 6.30, with error bars noted for each. Upon successive additions of H_2O_2 , a sharp increase in the reduction current was recorded for recombinant HRP; which reached steady state within 20 s of H_2O_2 injection, resulting in the typical "staircase" shape curve. A

shallower curve was noted for plant HRP, which was very similar to the negative control, BSA. Various concentrations of H₂O₂ were investigated, with increasing substrate concentration resulting in increased reduction currents. A linearised calibration curve was constructed from the current–time response assay data, utilising the current value at the steady-state region for each H₂O₂ addition. The correlation coefficients for the linearised graphs were all ≥ 0.99 , with the exception of 5.0×10^{-5} mol.L⁻¹ H₂O₂ injection curve (correlation coefficient = 0.92, Figure 6.28); the latter was possibly caused by substrate diffusional limitations. A common trend was noted throughout: steeper curves were recorded for recombinant HRP as compared to plant HRP, indicating that a recombinant HRP-based etched electrode sensor is more responsive to successive additions of H₂O₂. The electrochemical Eadie-Hofstee plot can be utilised to demonstrate the effect of internal diffusion as well as approximate K'_m value. A sigmoidal curve was obtained for 5.0×10^{-5} mol.L⁻¹ H₂O₂ injection data, indicating diffusional limitations within the system. This reinstates previous assumptions on diffusional problems at low H₂O₂ concentrations indicated by the poor correlation coefficient of the calibration curves for this data set. However, with increased substrate concentration, data were obtained that fitted the Michaelis-Menten kinetic model, resulting in the calculation of 17.2×10^{-3} M as K'_m for H₂O₂. This compares with the published K'_m of 12.8×10^{-3} M for the closely related, but glycosylated, soybean peroxidase (SBP; Wang et al., 2001). Other, recently published, peroxidase H₂O₂ K'_m values include: 1.27 mM (Korean radish peroxidase; Kim and Lee, 2005) and 1.77 mM respectively (Marula fruit; Mdluli, 2005).

6.6 Conclusion.

In this study, extra lysines were utilised to directionally immobilise rHRP onto both a CNBr-Activated Sepharose solid phase and an activated, modified polyethersulfone (PES) membrane. The key element to achieve controlled enzyme orientation is to selectively attach the biomolecule at a predetermined site(s) on the protein surface (Zhen et al., 2004). Therefore, additional lysine residues were genetically introduced to the wildtype HRP molecule (*Velcro Plus*) and those chemically modifiable lysines present in rHRP (K232 and K241) were removed (*Velcro Minus*). Subsequent bioinformatic analysis indicated that restoration of one of the arginine residues (R283) to both *Velcro Plus* and *Velcro Minus* would be beneficial. These substitutions generated a suite of rHRP mutants tailored for immobilisation. Mutants showed decreased CNBr-immobilisation rates with decreasing lysine content. Following CNBr-immobilisation, only wildtype rHRP displayed an increased thermal stability (approximately 2.2-fold). Frustratingly, the *Velcro* mutants displayed a notable decrease in thermal stability. *Velcro Minus* yielded the best solvent stabilities of the immobilised rHRP forms. All the immobilised rHRP forms exhibited very poor H₂O₂ stabilities, with an apparent common basal C₅₀ noted. Directional immobilisation onto an activated, modified polyethersulfone (PES) membrane permitting maximal catalytic activity was achieved.

Recombinant and plant HRP immobilised onto screen-printed electrodes resulted in μA differences in reduction current upon H₂O₂ addition. However, the concentration of substrate required to produce this $\Delta\mu\text{A}$ caused rapid enzyme inactivation. Additionally, the optimal peroxidase concentration required could not be achieved by the current prokaryotic host organism. To overcome this effect, a more sensitive sensor, namely the etched microelectrode, was utilised. This configuration confirmed that rHRP could achieve direct electron transfer, generating a series of calibration curves ranging from 0 to 10 mM. An Eadie-Hofstee replot of the data allowed for an estimation of the K'_m 17.2 x 10⁻³ M of recombinant HRP towards H₂O₂, similar to other plant peroxidases. Diffusional limitations were noted at lower concentrations of H₂O₂, attributed to the external and internal diffusional resistance (Limoges and Savéant, 2003). This preliminary work provides much scope for mutants to be applied in these and other biosensor configurations.

Chapter Seven.

Overall Conclusions.

7.0 Overall Conclusions.

This work has shown that a N-terminal PelB leader and C-terminal (His)₆ is compatible with functional HRP. Culture optimisation permitted expression of functional HRP as a fusion protein with PelB leader sequence to 0.65 $\mu\text{M.L}^{-1}$, without the need for protein refolding. Attempts to use conventional purification methodologies (HIC, Size Exclusion and Anion Exchange chromatography) resulted in the co-purification of a native *E. coli* peroxidase; however, nickel affinity chromatography achieved 30-fold increase in purification values and 70% recovery rates once the protocol had been optimised.

Stability characterisation of purified rHRP demonstrated that catalytic activity was maintained up to 55°C, with a graphically determined T_{50} value of 50°C. The apparent half-life ($t_{1/2}$) at 50°C ($k=0.0559$) was subsequently calculated as 12.4 min. Organotolerance studies indicated that rHRP was most stable in MeOH (C₅₀ 53 % v/v), followed by DMSO (C₅₀ 35 % v/v). DMF was the most deleterious solvent, exhibiting a C₅₀ of 14 % v/v. No activation was noted in any solvent tested. rHRP yielded a C₅₀ of 17 mM H₂O₂, after 30 min static incubation. Characterisation also revealed the apparent k_3 for recombinant wildtype to be $333 \pm 25\text{s}^{-1}$, whilst the K'_m was 2.04 ± 0.06 mM.

Initially, solvent-exposed lysine residues (K174, K232 and K241) were selected for substitution to increase overall stability. Single mutations (Ala, Glu, Asn and Phe) were introduced by an adapted mutagenic PCR strategy. A similar characterisation protocol to wildtype rHRP followed protein expression and purification, which concluded that mutations to Lysines 232 and 241 can positively influence stability, whilst Lys 174 substitutions have a negative effect. The outcome of these single mutations suggested the development of additional single and double mutations. The double mutations combined the two best individual lysine mutations. All double mutations yielded increased thermal tolerance as judged by $t_{1/2}$. K232F/K241N was the most stabilising mutation; however, stabilising single mutations were not additive. The important stabilising role of Glu238 was noted. All lysine mutants displayed altered kinetic constants, k_3 in particular.

Five potentially stabilising mutations (T102A, Q106R, Q107D, T110V and I180F) were predicted by novel validated bioinformatic software (*ProteinParser*) and developed in

the third section of this study. Overall, the stability characteristics of these mutants were disappointing. Marginal gains in thermal stability were noted, whilst only one mutant displayed increased solvent or H₂O₂ stability, the latter significantly so; however, this unexpected outcome prompted further investigation. The original frequency-counting algorithm was independently validated, which suggested the pivotal stabilising role played by the helical structures in HRP. The location of the mutations analysed in this study (in or close to a helix) highlighted the fact that the *Consensus Concept* is not globally applicable. This study does suggest, however, the important stabilising role of Q106 and, that a single residue substitution can significantly alter the stability of HRP to H₂O₂.

Judicious introduction of modifiable groups (lysine residues) to the outer surface of rHRP permitted simple orientated immobilisation, although at a cost to stability in the case of CNBr-Activated Sepharose immobilisation. This study also demonstrated that even conservative substitutions (Lys to Arg) can compromise both free-solution and immobilised stability. The important stabilising role of helical secondary structure is evidenced again.

Recombinant HRP functionality in two sensor configurations was explored. Electron transfer was evident in the screen-printed electrode; however, the optimal concentration of HRP required for this sensor configuration was beyond this study's current *E. coli* production rate and, as such, further investigation was abandoned. Use of an etched microelectrode permitted use of low-concentration rHRP. A clear difference between the recombinant and plant HRPs' direct electron transfer is apparent using an etched Pt microelectrode. The resulting rHRP data fitted a Michaelis-Menten kinetic model, and subsequent Eadie-Hofstee analysis yielded a K'_m calculation of 17.2 x 10⁻³ M for H₂O₂. The mutants generated in this study remain to be analysed in terms of biosensor performance.

7.1 Summary and Future Work.

The work described in this thesis has achieved the following successes:

- Directional cloning of PelB and HRP gene, with C-terminal His₍₆₎ tag, into pQE60.
- Optimal expression of functional rHRP using XL10 Gold *E. coli* strain.
- IMAC purification of rHRP to single-band homogeneity, as judged by SDS-PAGE.
- Characterisation (thermal, solvent, H₂O₂ tolerance and kinetic analysis) of rHRP.
- Generation of a number of rational lysine mutants based on prior experimentation.
- Characterisation of lysine mutants and comparison to wildtype.
- Further elucidation of the stabilising roles of K174, K232, E238 and K241.
- Development of *ProteinParser* programme for amino acid frequency counting.
- Creation of a number of rational consensus mutants based on *ProteinParser* predictions.
- Characterisation of consensus mutants and comparison to wildtype.
- Validation of frequency counting algorithm and development of archetype peroxidase.
- Elucidation of the key stabilising role of the helical secondary structure with HRP.
- Establishment of orientatable HRP immobilisation via additional lysine incorporation.
- Stability investigation of both free and CNBr-immobilised HRP mutants
- Application of rHRP to screen-print electrodes and Pt microelectrodes for H₂O₂ detection.

Future work in this area should address:

- Expression of HRP in eukaryotic host or use of co-expression systems (Varnado and Goodwin, 2004) to increase yield (particularly important for sensor development).
- Chemical modification of rHRP and introduction of chemically modifiable groups (e.g. lysine) to allow for selectable chemical modification.
- Use of phage display techniques to directionally evolve HRP towards increased stability.
- Synthesis and expression of archetype peroxidase protein, comparison with modern day HRP.
- Rapid reaction kinetics for rHRP and mutants.
- Physical characterisation studies: NMR, Raman spectroscopy, crystallisation of notable mutants.
- Incorporation into H₂O₂ sensors and catalase studies for H₂O₂-tolerant T110V mutant.
- Continued development of rHRP in etched platinum electrode, mutant investigation.

Chapter Eight.

References.

8.0 References.

Abad J.M, Mertens S.F.L, Pita M, Fernandez V.M. and Schiffrin D.J. (2005). Functionalization of Thioctic Acid-capped gold nanoparticles for specific immobilisation of Histidine-tagged proteins. *Journal of the American Chemical Society*, **127**, 5689-5694.

Abian O, Grazu V, Hermoso J, Gonzalez R, Garcia J.L, Fernandez-Lafuente R. and Guisan JM. (2004). Stabilization of penicillin G acylase from *Escherichia coli*: site-directed mutagenesis of the protein surface to increase multipoint covalent attachment. *Applied Environmental Microbiology*, **70**, (2), 1249-51.

Adak S, Mazumder A. and Banerjee R.K. (1996). Probing the active site residues in aromatic donor oxidation in HRP: involvement of an arginine and a tyrosine residue in aromatic donor binding. *Journal of Biochemistry (Tokyo)*, **314**, 985-991.

Aibara S, Kobayashi T. and Morita Y. (1981). Isolation and properties of basic isoenzymes of horseradish peroxidase. *Journal of Biochemistry (Tokyo)*, **90**, (2), 489-496.

Aibara S, Yamashita H, Mori E, Kato M. and Morita Y. (1982). Isolation and characterization of five neutral isoenzymes of horseradish peroxidase. *Journal of Biochemistry (Tokyo)*, **92**, (2), 531-539.

Allard L, Cheynet V, Oriol G, Mandrand B, Delair T. and Mallet F. (2002). Versatile method for production and controlled polymer-immobilization of biologically active recombinant proteins. *Biotechnology and Bioengineering*, **80**, (3), 341-348.

Alonso Lomillo M. A, Ruiz J.G. and Pascual F.J.M. (2005). Biosensor based on platinum chips for glucose determination. *Analytica Chimica Acta*, **547**, (2), 209-214.

Alltamirano M, Blackburn J.M, Aguayo C. and Fersht A. (2000). Directed evolution of new catalytic activity using the α/β barrel scaffold. *Nature*, **403**, 617-622.

Amin N, Liu A.D, Ramer S, Aehle W, Meijer D, Metin M, Wong S, Gualfetti P. and Schellenberger. (2004). Construction of stabilised proteins by combinatorial consensus mutagenesis. *Protein Engineering, Design and Selection*, **17**, (11), 787-793.

Andriex C.P., Garreau D, Hapiot, P. and Saveant J. (1998) Fast sweep cyclic voltammetry at ultra-microelectrodes: Evaluation of the method for fast electron-transfer kinetic measurements. *Journal of Electroanalytical Chemistry*, **243**, 321-335.

Anh D.T.V, Olthuis W. and Bergveld P. (2003). Hydrogen peroxide detection with improved selectivity and sensitivity using constant current potentiometry. *Sensors and Actuators B: Chemical*, **91**, (1), 1-4.

Arnao M.B, Acosta M, del Rio J.A, Varon R. and Garcia-Canovas F. (1990). A kinetic study on the suicide inactivation of peroxidase by hydrogen peroxide. *Biochimica et Biophysica Acta*, **1041**, 43-47.

- Arnold F.H. and Lin, Z. (2000). California Institute Of Technology "Expression of Functional Eukaryotic Proteins". Worldwide Patent: PCT/US99/17127, WO 00/006718.
- Arnold F.H. (1990). Engineering enzymes for non-aqueous solvents. *Trends in Biotechnology*, **8**, 244-249.
- Asokan A, De Ropp J.S, Newmyer S.L, De Montellano P.R.O. and La Mar G.N. (2001). Solution H NMR of the molecular and electronic structure of the heme cavity and substrate binding pocket of high-spin ferric horseradish peroxidase. Effect of His42Ala mutation. *Journal of the American Chemical Society*, **123**, (18), 4243-4254.
- Ayyagari M.S.R, Kaplan D.L, Chatterjee S, Walker J.E. and Akkara J.A. (2002). Solvent effects in horseradish peroxidase-catalysed polyphenol synthesis. *Enzyme and Microbial Technology*, **30**, 3-9.
- Azevedo A. M, Prazeres D.M, Cabral J.M. and Fonseca L.P. (2005). Ethanol biosensors based on alcohol oxidase. *Biosensors and Bioelectronics*, **21**, (2), 235-247.
- Azevedo A.M, Vojinovic V, Cabral J.M.S, Gibson T.D. and Fonseca L.P. (2004). Operational stability of immobilised horseradish peroxidase in mini-packed bed reactors. *Journal of Molecular Catalysis B: Enzymatic*, **28**, 121-128.
- Azevedo A.M, Martins V.C, Prazeres D.M.F, Vojinovic V, Cabral J.M.S. and Fonseca L.P. (2003). Horseradish peroxidase: a valuable tool in biotechnology. *Biotechnology Annual Review*, **9**, 199-247.
- Azevedo A.M, Prazeres D.M.F, Cabral J.M.S and Fonseca L.P. (2001). Stability of free and immobilised peroxidase in aqueous-organic solvents mixtures. *Journal Molecular Catalysis B*, **15**, 147-153.
- Bakalovic N, Passardi F, Ioannidis V, Cosio C, Penel C, Falquet L. and Dunand C. (2006). PeroxiBase: A class III plant peroxidase database. *Phytochemistry*, **67**, (6), 534-539.
- Baker C.J, Deahl K, Domek J. and Orlandi E.W. (2000). Scavenging of H₂O₂ and production of oxygen by Horseradish Peroxidase. *Archives of Biochemistry and Biophysics*, **382**, (2), 232-237.
- Barik S. (1997). "Mutagenesis and Gene Fusion by Mega primer method". IN: White B.A (ed). PCR Cloning Protocols, Methods in Molecular Biology. *Humana Press*, New Jersey, USA, pp 173-183.
- Bartonek-Roxa E. and Eriksson H. (1994) Expression of a neutral HRP in *E.coli*. *Journal of Biotechnology*, **37**, 133-142.
- Barth S, Huhn M, Matthey B, Klimka A, Galinski E.A. and Engert A. (2000). Compatible-solute-supported periplasmic expression of functional recombinant proteins under stress conditions. *Applied Environmental Microbiology*, **66**, 1572-1579.

- Bateman L, Leger C, Goodin D.B. and Armstrong F.A. (2001). A distal histidine mutant (H52Q) of Yeast Cytochrome *c* Peroxidase catalyses the oxidation of H₂O₂ instead of its reduction. *Journal of the American Chemical Society*, **123**, 9260-9263.
- Batra R. Tyagi R. and Gupta M.N. (1997). Influence of immobilization on enzyme activity in aqueous-organic cosolvent mixtures. *Biocatalysis and Biotransformation*, **15**, 101-119.
- Berglund G.I, Carlsson G.H, Smith A.T, Szoke H, Henriksen A. and Hajdu J. (2002). The catalytic pathway of Horseradish peroxidase at high resolution. *Nature*. **417**, 463-468.
- Berkowitz D.B. and Weibert D.W. (1981), The inactivation of HRP by a polystyrene surface. *Journal of Immunological Methods*, **47**, 121-124.
- Betts M.J. and Russell R.B. (2003). Amino acid properties and consequences of substitutions. *IN* Bioinformatics for Geneticists, M.R. Barnes, I.C. Gray (eds). John Wiley and Sons Inc, New York, USA.
- Birnboim H. and Doly J. (1979). A rapid alkaline extraction procedure for screening recombinant plasmid DNA. *Nucleic Acids Research*, **7**, 1513-1523.
- Bonnaffé D, Therisod M. and Seris JL. (1993). Chemical deglycosylation of horseradish peroxidase and surglycosylation using a new glycosylating reagent: effects on catalytic activity and stability. *IN*: van den Twell WJJ, Harder A, Buitelarr RM (eds), Stability and Stabilisation of Enzymes. Elsevier, Amsterdam, pp. 223-227.
- Bonfils C, Charasse S, Bonfils J. P. and Larroque C. (1995). Luminescent Visualization of Low Amounts of Cytochrome P450 and Hemoproteins by Luminol in Acrylamide Gels. *Analytical Biochemistry*, **226**, (2), 302-306.
- Borns M, Vaillancourt P, Hogrefe H. and Braman J. (2000). High-efficiency site directed mutagenesis of large plasmid vectors. *Strategies*, **13**, 106-107.
- Bornscheuer U.T. and Pohl M. (2001). Improved biocatalysts by directed evolution and rational design. *Current Opinion in Chemical Biology*, **5**, 137-143
- Brannigan J.A. and Wilkinson A.J. (2002). Protein Engineering 20 years on. *Nature Reviews*, **3**, 964-970.
- Brosnan J.T. and Brosnan M.E. (2006), Branched-chain amino acids: enzyme and substrate regulation. *Journal of Nutrition*, **136** (1), 207S-11S.
- Blattner F.R, Plunkett G, Bloch C.A, Perna N.T, Burland V, Riley M, ColladoVides J, Glasner J.D, Rode C.K, Mayhew G.F, et al. (1997). The complete genome sequence of *Escherichia coli* K-12. *Science*, **277**, (5331), 1453-1474.
- Bos E.S, van der Doelen A.A, van Rooy N. and Schuurs A.H. (1981). 3,3',5,5' - Tetramethylbenzidine as an Ames test negative chromogen for horse-radish peroxidase in enzyme-immunoassay. *Journal of Immunoassay*, **2**, 187.

Butler L.G. (1979). Enzymes in non-aqueous solvents. *Enzyme Microbial Technology*, **1**, 253-259.

Campanella L, De Luca S, Favero G, Persi L. and Tomassetti M. (2001). Superoxide dismutase biosensors working in non-aqueous solvent. *Fresenius J Anal Chem.*, **369**, (7-8), 594-600.

Cassidy J.F, Doherty A.P. and Vos J.G. (1998). Amperometric methods of detection. *IN: Diamond D. Principles of chemical and biological sensors*. John Wiley and Sons Inc, New York, pp 73-132.

Castillo J, Ferapontova E.E, Hushpulian D, Tasca F, Tishkov V, Chubar T, Gazaryan I. and Gorton L. (2006). Direct electrochemistry and bioelectrocatalysis of H₂O₂ reduction of recombinant tobacco peroxidase on graphite. Effect of peroxidase single point mutation on Ca²⁺ modulated catalytic activity. *Journal of Electroanalytical Chemistry*, **588**, 112-121.

Castillo TJ, Sotomayor Md P.T. and Kubota LT. (2005). Amperometric biosensor based on horseradish peroxidase for biogenic amine determinations in biological samples. *Journal of Pharmaceutical and Biomedical Analysis*, **37**, 785-791.

Carolan N. (2004). "The use of soybean peroxidase in amperometric biosensors". PhD Thesis, Dublin City University, Republic of Ireland.

Cedrone F, Menez A. and Quemeneur E. (2000) Tailoring new enzyme functions by rational design. *Current opinion in Structural Biology*, **10**, 405-410.

Cha T, Guo A. and Zhu X-Y. (2005). Enzymatic activity on a chip: The critical role of protein orientation. *Proteomics*, **5**, (2), 416-419.

Chance B. and George P. (1949). The enzyme-substrate compounds of Horseradish Peroxidase and peroxides. Kinetics of formation and decomposition of the primary and secondary complexes. *Archives of Biochemistry and Biophysics*, **22**, 224-252.

Chang B.S, Park K.H. and Lund D.B. (1988). Thermal inactivation kinetics of HRP. *Journal of Food Science*, **53**, 920-923.

Chakrabarti A. and Basak S. (1996). Structural alterations of HRP in the presence of low concentrations of guanidium chloride. *European Journal of Biochemistry*, **241**, 462-467.

Chakravarty S. and Varadarajan R. (2002). Elucidation of factors responsible for enhanced thermal stability of proteins: A structural genomics based study. *Biochemistry*, **41**, 8152-8161.

Chattopadhyay K. and Mazumdar S. (2000). Structural and conformational stability of HRP: effect of temperature and pH. *Biochemistry*, **39**, 263-270.

- Chen H. and Vierling R.A. (2000). Molecular cloning and characterisation of soybean peroxidase gene families. *Plant Science*, **150**, 129-137.
- Chen K. and Arnold F.H. (1993). Tuning the Activity of an Enzyme for Unusual Environments: Sequential Random Mutagenesis of Subtilisin E for Catalysis in Dimethylformamide. *Proceedings from the National Academy of Science, USA*, **90**, 5618-5622.
- Chen, R. (2001). Enzyme Engineering; Rational design versus directed evolution. *Trends in Biotechnology*, **19**, (1), 13-14.
- Chenna R, Sugawara H, Koike T, Lopez R, Gibson, T.J, Higgins, D.G. and Thompson J.D. (2003). Multiple sequence alignment with the Clustal series of programs. *Nucleic Acids Research*, **31**, (13), 3497-500.
- Cherry J. R, Lamsa M. H, Schneider P, Vind J, Svendsen A, Jones A. and Pedersen A. H. (1999). Directed evolution of a fungal peroxidase. *Nature Biotechnology*, **17**, 379-384.
- Childs R.E. and Bardsley W.G. (1975). The steady state kinetics of peroxidase with 2,2'-Azino-di-(3-ethyl-benzthiazoline-6-sulphonic acid) as chromagen. *Journal of Biochemistry*, **145**, 93-103.
- Chou P.Y. and Fasman G.D. (1978) Empirical Predictions of Protein Conformation. *Annual Review of Biochemistry*, **47**, 251-276.
- Clemente M.T. and Marquez A.J. (2000). Site directed mutagenesis of Cys-92 from the α -polypeptide of *Phaseolus vulgaris* glutamine synthetase reveals that this highly conserved residue is not essential for enzyme activity but it is involved in thermal stability. *Plant Science*, **154**, 189-197.
- Coates A.I, Cook M.P, Feezor R and Schuh M.D. (1998). Dependence of Heme accessibility in HRP on Ca^{2+} . *Journal of Inorganic Biochemistry*, **72**, 63-69.
- Colonna S, Gaggero N, Richelmi C. and Pasta P. (1999). Recent biotechnological developments in the use of peroxidases, *Trends in Biotechnology*, **17**, 163-168.
- Conyers S.M and Kidwell D.A. (1991). Chromogenic substrates for horseradish peroxidase. *Analytical Biochemistry*, **192**, (1), 207-11.
- Costantini S, Colonna G. and Facchiano A. M. (2006). Amino acid propensities for secondary structures are influenced by the protein structural class. *Biochemical and Biophysical Research Communications*, **342**, (2), 441-451.
- Cornelis P. (2000). Expressing genes in different *Escherichia coli* compartments. *Current Opinion in Biotechnology*. **11**, 450-454.
- Cornish V.W, Kaplan M.I, Veenstra D.L, Kollman P.A. and Schultz P.G. (1994). Stabilizing and destabilizing effects of placing beta-branched amino acids in protein alpha-helices. *Biochemistry*, **33**, (40), 12022-12031.

Cregg J.M., Vedvick T.S. and Raschke W.C. (1993). Recent advances in the expression of foreign genes in *Pichia pastoris*. *Bio/Technology*, **11**, 905-910.

Creighton T.E. (1993). "Proteins Structures and Molecular Properties". 2nd Ed. W.H Freeman and Company, New York, pp. 7-8.

Cretich M, Damin F, Pirri G. and Chiari M. (2006). Protein and Peptide arrays, Recent trends and new directions. *Biomolecular Engineering*, **23**, 77-88.

Dahiyat B.I. (1999), In silico design for protein stabilisation. *Current Opinion in Biotechnology*, **10**, 387-390.

Dai L. and Klibanov A.M. (1999). Striking activation of oxidative enzymes suspended in non-aqueous media. *Proceedings from the National Academy of Science*, **96**, 9475-9478.

Daugherty P.S, Iverson B.L. and Georgiou G. (2000), Flow cytometric screening of cell-based libraries. *Journal of Immunological Methods*, **243**, 211-227.

Davidson V.L. (2003). Probing mechanisms of catalysis and electron transfer by methylamine dehydrogenase by site directed mutagenesis of α Phe55. *Biochimica et Biophysica Acta*, **1647**, 230-233.

Dordick J. (1991). Non-aqueous Enzymology. IN Applied Biocatalysis. Blanch H.W. and Clark D.S (eds). Marcel Dekker Inc., New York, pp. 8-30.

Dotsikas Y. and Loukas Y.L. (2004). Employment of 4-(1-imidazolyl)phenol as a luminol signal enhancer in a competitive-type chemiluminescence immunoassay and its comparison with the conventional antigen-horseradish peroxidase conjugate-based assay. *Analytica Chimica Acta*, **509**, (1), 103-109.

Doyle W.A and Smith A.T. (1996). Expression of lignin peroxidase H8 in *Escherichia coli*: folding and activation of the recombinant enzyme with Ca^{2+} and heme. *Biochemistry Journal*, **315**, 15-19.

Dunford H.B. (1999). "Heme Peroxidases". Vol I, Wiley and Sons, New York, pp 1-23, 92-111.

Dunford H.B. (1991). Horsereadish peroxidase: structure and kinetic properties. IN: J.E. Everse, K.E. Everse, M.B. Grisham, (eds). *Peroxidases in Chemistry and Biology*, Vol II, CRC Press, Florida, pp 1-24.

Dunford B.H and Hewson W.D. (1977). Effect of mixed solvents on the formation of HRP Compound I. The importance of Diffusion-controlled reactions. *Biochemistry*, **16**, (13), 2949-2957.

Duroux L. and Welinder K.G. (2003), The Peroxidase Gene Family in Plants: A Phylogenetic Overview. *Journal of Molecular Evolution*, **57**, 397-407.

Egorov A.M, Gazaryan I.G, Savelyev S.V, Fechina V.A, Veryovkin A.N, Kim B.B. (1991). Horseradish peroxidase gene expression in *E.coli*. *Annals of New York Academy of Sciences*, **646**, 35-40.

Egorov A.M, Gazaryan I.G, Kim B.B, Doseyeva V.V, Kapeljuch J.L, Veryovkin A.N. and Ferchina V.A. (1994). HRP Isozyme C: A comparative study of Native and Recombinant enzyme produced by *E. coli* transformants. *Annals of New York Academy of Sciences*, **721**, 73-81.

Eijsink V.G.H, Bjork A, Gaseidnes S, Sirevag R, Synstad B, van der Berg B. and Vriend G. (2004). Rational design of enzyme stability. *Journal of Biotechnology*, **113**, 105-120.

Elcock A.H. (1998), The stability of salt bridges at high temperatures: Implications for hyperthermophilic proteins. *Journal of Molecular Biology*, **284**, 489-502.

Endo T, Okuyama A, Matsubara Y, Nishi K, Kobayashi M, Yamamura S, Morita Y, Takamura Y, Mizukami H. and Tamiya E. (2005). Fluorescence-based assay with enzyme amplification on a micro-flow immunosensor chip for monitoring coplanar polychlorinated biphenyls. *Analytica Chimica Acta*, **531**, (1), 7-13.

Eremin A.N, Budnikova L.P, Sviridov O.V. and Metelitsa D.I. (2002). Stabilisation of diluted aqueous solutions of HRP. *Applied Journal of Biochemistry and Microbiology*, **38**, (2), 151-158.

Ermolenko D.N, Zherdev A.V, Dzantiev B.B. and Popov V.O. (2002). Antiperoxidase antibodies enhance refolding of HRP. *Biochemical and Biophysical Research Communications*, **291**, 959-965.

Farinas T.E, Butler T. and Arnold F.H. (2001). Directed Enzyme Evolution. *Current Opinion in Biotechnology*, **12**, 545-551.

Feis A, Rodriguez-Lopez J.N, Thorneley R.N.F. and Smulevich G. (1998). The distal cavity structure of carbonyl horseradish peroxidase as probed by the resonance Raman spectra of His 42 Leu and Arg 38 Leu mutants. *Biochemistry*, **37**, (39), 13575-13581.

Ferapontova E.E. and Dominguez E. (2004). Adsorption of differently charged forms of horseradish peroxidase on metal electrodes of different nature: effect of surface charge. *Bioelectrochemistry*, **55**, 127-130.

Ferapontova E. (2004a). Direct peroxidase bioelectrocatalysis on a variety of electrode materials. *Electroanalysis*, **16**, (13), 1101-1112.

Ferapontova E.E, Schmengler K, Borchers T, Ruzgas T. and Gorton L. (2002), Effect of Cysteine mutations on direct electron transfer of HRP on gold. *Biosensors and Bioelectronics*, **17**, 953-963.

Ferapontova E. and Gorton L. (2002a). Effect of pH on direct electron transfer in the system gold electrode-recombinant horseradish peroxidase. *Bioelectrochemistry*, **55**, (1-2), 83-87.

Ferapontova E.E, Grigorenko V.G, Egorov A.M, Borchers T, Ruzgas T. and Gorton L. (2001). Mediatorless biosensor for H₂O₂ based on recombinant forms of horseradish peroxidase directly adsorbed on polycrystalline gold. *Biosensors and Bioelectronics*, **16**, 147-157.

Fernandes K.F, Lima C.S, Lopes F.M. and Collins C.H. (2004). Properties of horseradish peroxidase immobilised onto polyaniline. *Process Biochemistry*, **39**, 957-962.

Fersht A.R. and Serrano L. (1993). Principles of Protein Stability derived from Protein Engineering and experiments. *Current opinion in Structural Biology*, **3**, 75-83.

Fields R. (1971). The measurement of amino groups in proteins and peptides. *Biochemical Journal*, **124**, 581-590.

Filizola M. and Loew G.H. (2000). Role of protein environment in Horseradish peroxidase compound I formation: molecular dynamics simulations of horseradish peroxidase-HOOH complex. *Journal of the American Chemical Society*, **122**, 18-25.

Fishman A, Levy H, Cogan U. and Shoseyov O. (2002). Stabilization of HRP in aqueous-organic media by immobilisation into cellulose using a cellulose-binding-domain. *Journal of Molecular Catalysis B*, **18**, 121-131.

Flores H. and Ellington A.D. (2005). A modified consensus approach to mutagenesis inverts the co-factor specificity of *Bacillus stearothermophilus* lactate dehydrogenase. *Protein Engineering, Design and Selection*, **18**, (8), 369-377.

Freire R.S, Pessoa C.A, Mello L.D. And Kubota L.T. (2003). Direct Electron Transfer: An approach for Electrochemical Biosensors with higher selectivity and sensitivity. *Journal of the Brazilian Chemical Society*, **14**, (2), 230-243.

French C, Keshavarz-Moore E. and Ward J.M. (1996). Development of a simple method for the recovery of recombinant proteins from the *E.coli* periplasm. *Enzyme Microbial Technology*, **19**, 332-338.

Folkes L.K and Candeias L.P. (1997). Interpretation of the reactivity of peroxidase compounds I and II with phenols by the Marcus equation. *FEBS Letters*, **412**, 305-308.

Fuentes M, Mateo C, Fernández-Lafuente R, and Guisán J. M. (2006). Detection of Polyclonal Antibody Against Any Area of the Protein-Antigen Using Immobilized Protein-Antigens: The Critical Role of the Immobilization Protocol. *Biomacromolecules*, **7**, (2), 540-544.

Funashashi J, Sugita Y, Kitao A. and Yutani K. (2003). How can free energy component analysis explain the difference caused by amino acid substitutions? Effect of three hydrophobic mutations at the 56th residue on the stability of human lysozyme. *Protein Engineering*, **16**, (9), 665-671.

Garcia D, Ortéga F. and Marty J-L. (1998), Kinetics of thermal inactivation of HRP: Stabilising effect of methoxypoly(ethylene glycol). *Biotechnology and Applied Biochemistry*, **27**, 49-54.

Gajhede M, Schuller D, Henriksen A, Smith A, Poulos T.L. (1997), Crystal structure of HRPC at 2.15 Å resolution. *Nature Structural Biology*, **4**, (12), 1032-1038.

Gazaryan I.G, Chubar T.A, Ignatenko O.V, Mareeva E.A, Orlova M.A, Kapeliuch Y.L, Savitsky P.A, Rojkova A.M. and Tishkov V.I. (1999) Tryptophanless recombinant horseradish peroxidase. Stability and catalytic properties. *Biochemical and Biophysical Research Communications*, **262**, (1), 297-301.

Gazaryan I.G, Lagriminr L.M, Mellons F.A, Naldrett M.J, Ashby G.A. and Thornley R.N.F. (1998). Identification of skatolyl hydroperoxide and its role in the peroxidase-catalysed oxidation of indol-3-yl acetic acid. *Biochemical Journal*, **333**, 223-232.

Gazaryan I.G, Klyachko N.L, Dulkis Y.K, Ouporov I.V. and Levashov A.V. (1997). Formation and properties of dimeric recombinant horseradish peroxidase in a system of reversed micelles. *Biochemical Journal*, **328**, (2), 643-647.

Gazaryan I.G, Doseeva V.V, Galkin A.G. & Tishkov V.I. (1995) Production and catalytic properties of Phe41 to His and Phe143 to Glu single-point mutants of horseradish peroxidase expressed in *E.coli*. *Biochemistry (Moscow)*, **60**, (10), 1187-1192.

Gazaryan I.G, Doseeva V.V, Galkin A.G. and Tishkov V.I. (1994). Effect of single-point mutations Phe-41-His and Phe-143-Glu on folding and catalytic properties of recombinant horseradish peroxidase expressed in *E. coli*. *FEBS Letters*. **354**, (3), 248-250

Gelo-Pujic M, Kimm H.H, Butlin N.G. and Palmore G.T. (1999). Electrochemical studies of a truncated laccase produced in *Pichia pastoris*. *Applied Environmental Microbiology*, **65**, 5515-5521.

Gerasimas V.B, Chernoglazov V.M. and Klesov A.A. (1980) Effect of progressive chemical modification on the activity and thermal stability of soluble and immobilized glucoamylase. *Biokhimiia*, **45**, (6), 1086-92.

Gilabert M.A, Hiner A.N.P, García-Ruiz P.A, Tudela J., García-Molina F., Acosta M., García-Cánovas F. and Rodríguez-López J.N. (2004). Differential substrate behaviour of phenol and aniline derivatives during oxidation by horseradish peroxidase: kinetic evidence for a two-step mechanism. *Biochimica et Biophysica Acta*. **1699**, (1-2), 235-243.

Gilardi G. and Fantuzzi A. (2001), Manipulating Redox systems: Applications to nanotechnology. *Trends in Biotechnology*, **19**, (11), 468-475.

Gilardi G, den Blaauwen T. and Canters G. W. (1994). Molecular recognition – design of a biosensor with genetically engineered azurin as a redox mediator. *Journal of Control Release*, **29**, 231-238.

- Gonera A, Mischnick P. and Ukeda H. (2004). The application of O-aminopropyl amylose for the stabilisation of HRP via addition and crosslinking. *Enzyme and Microbial Technology*, **34**, 248-254.
- Gorman L.A.S. and Dordick J.S. (1992), Organic-solvents strip water off enzymes. *Biotechnology and Bioengineering*, **39**, (4), 392-397.
- Greco O, Rossiter S, Kanthou C, Folkes L.K, Wardman P, Tozer G.M. and Dachs G.U. (2001). Horseradish Peroxidase-mediated gene therapy: choice of prodrugs on oxic and anoxic conditions. *Molecular Cancer Therapeutics*, **1**, 151-160.
- Gregoret L.M. and Sauer R.T (1998). Tolerance of a protein helix to multiple alanine and valine substitutions. *Folding and Design*, **3**, (2), 119-26.
- Grennan K, Killard A.J, Hanson C.J, Cafolla A.A. and Smyth M.R. (2006). Optimisation and Characterisation of biosensors based on polyaniline. *Talanta*, **68**, 1591-1600.
- Grennan K, Killard A.J. and Smyth M.R. (2005). Chemically polymerised films for the mass-production of biosensor devices. *Electroanalysis*, **17**, (15-16), 1360 -1370.
- Grigorenko V, Chubar T, Kapeliuch Y, Borchers T, Spencer F. and Egorov A. (1999). New approaches for functional expression of recombinant horseradish peroxidase in *Escherichia coli*. *Biocatalysis and Biotransformation*, **17**, 359-379.
- Gromhina M.M. (2003). Factors influencing the thermal stability of buried protein mutants. *Polymer*, **44**, 4061-4066.
- Guex N. and Peitsch M.C. (1997) SWISS-MODEL and the Swiss-Pdb Viewer: An environment for comparative protein modelling. *Electrophoresis*, **18**, 2714-2723.
- Guruprasad K, Bhasker Reddy B.V. and Pandit M.W. (1990). Correlation between stability of a protein and its dipeptide composition: a novel approach for predicting in vivo stability protein from its primary sequence. *Protein Engineering*, **4**, (2), 155-161.
- Gustafsson C, Govindarajan S. and Minshull J. (2004). Codon Bias and heterologous protein expression. *Trends in Biotechnology*, **22**, (7), 346-353.
- Gustafsson C, Govindarajan S. and Minshull J. (2003). Putting engineering back into protein engineering: bioinformatic approaches to catalyst design. *Current Opinion in Biotechnology*, **14**, 366-370.
- Hakamada Y, Hatada Y, Ozawa T, Ozaki K, Kobayashi T. and Ito S. (2001). Identification of thermostabilising residues in a *Bacillus* alkaline cellulase by construction of chimeras from mesophilic and thermostable enzymes and site directed mutagenesis. *FEMS Microbiology Letters*, **195**, 67-72.
- Hall B.G. (2006). Simple and accurate estimation of ancestral protein sequences. *Proceedings of the National Academy of Science USA*, **103**, (14), 5431-5436.

- Haney P.J, Badger J.H, Buldak G.L, Reich C.I, Woese C.R. and Olsen G.J. (1999). Thermal adaptation analysed by comparison of protein sequences from mesophilic and extremely thermophilic *methanococcus species*. *Proceedings of the National Academy of Science USA*, **96**, (7), 3578-3583.
- Haque M. E, Debnath D, Basak S. and Chakrabarti A. (1999). Structural changes of HRP in presence of low concentrations of urea. *European Journal of Biochemistry*, **259**, 269-274.
- Hartmann C. and Ortiz de Montellano P.R. (1992). Baculovirus expression and characterisation of catalytically active HRP. *Archives of Biochemistry and Biophysics*, **297**, 1, 61-72.
- Haschke R.H. and Friedhoff J.M. (1978). Calcium-related properties of horseradish peroxidase. *Biochemical and Biophysical Research Communications*. **80**, (4), 1039-1042
- Hassani L, Ranjbar B, Khajeh K, Naderi-Manesh H, Naderi-Manesh M. and Sadeghi M. (2006). Horseradish peroxidase thermostabilization: The combinatorial effects of the surface modification and the polyols. *Enzyme and Microbial Technology*, **38**, (1-2), 118-125.
- Henriksen A, Schuller D.J, Meno K, Welinder K.G, Smith A.T. and Gajhede M. (1998). Structural interactions between HRP and the substrate Benzhydroxamic Acid determined by X-ray crystallography. *Biochemistry*, **37**, 8054-8060.
- Hernández-Ruiz J, Arnao M.B, Hiner A.N.P, Garcia-Cánovas F. and Acosta M. (2001). Catalase-like activity of horseradish peroxidase: relationship to enzyme inactivation by H₂O₂. *Biochemical Journal*, **354**, (107-114).
- Hiner A.N.P, Raven E.L, Thorneley R.N.F, Garcia-Canovas F. and Rodriguez-Lopez J.N. (2002). Mechanisms of Compound I formation in heme peroxidases. *Journal of Inorganic Biochemistry*, **91**, 27-34.
- Hiner A.N. P, Hernández Ruiz J, Rodríguez López J.N, García Cánovas F, Brisset N.C, Smith A.T, Arnao M. B. and Acosta M. (2002a) Reactions of the Class II Peroxidases, Lignin Peroxidase and *Arthromyces ramosus* Peroxidase, with Hydrogen Peroxide. Catalase like activity, compound III formation, and enzyme inactivation. *Journal of Biological Chemistry*, **277**, 26879-26885.
- Hiner A.N, Hernández-Ruiz J, Rodríguez-López J, Arnao M.B, Varón R, García-Cánovas F and Acosta M. (2001). The inactivation of horseradish peroxidase isoenzyme A2 by hydrogen peroxide: an example of partial resistance due to the formation of a stable enzyme intermediate. *Journal of Biological Inorganic Chemistry*, **6**, 504-516.
- Hiner A.N.P., Hernandez-Ruiz J., Garcia-Canovas F., Smith A.T., Arnao M.B. and Acosta M. (1995). A comparative study of the inactivation of wild-type, recombinant and two mutant horseradish peroxidase isoenzymes C by hydrogen peroxide and m-chloroperoxybenzoic acid. *European Journal of Biochemistry*, **234**, (2), 506-512.

Hoffmann F, van der Heuvel J, Zidek N. and Rinas U. (2004). Minimising inclusion body formation during recombinant protein production in E.coli at bench and pilot scale. *Enzyme and Microbial Technology*, **34**, 235-241.

Holmes D.S. and Quigley M. (1981). The rapid boiling method for preparation of bacterial plasmid. *Analytical Biochemistry*, **114**, 193-197.

Howes B.D, Brissett N.C, Doyle W.A, Smith A.T. and Smulevich G. (2005). Spectroscopic and kinetic properties of the horseradish peroxidase mutant T171S. *FEBS Journal*, **272**, 5514-5521.

Howes B.D, Feis A. Raimondi L. Indiani C. and Smulevich G. (2001a). The Critical Role of the Proximal Calcium Ion in the Structural Properties of Horseradish Peroxidase. *Journal of Biological Chemistry*, **276**, (44), 40704-40711.

Howes B.D, Veitch N.C, Smith A.T, White C.G. and Smulevich G. (2001b). Heme-linked interactions in horseradish peroxidase revealed by spectroscopic analysis of the Phe-221 to Met mutant. *Biochemical Journal*, **353**, (2), 181-191.

Howes B.D, Heering H.A, Roberts T.O, Schneider-Belhadadd F, Smith A.T. and Smulevich G. (2001c). Mutation of residues critical for benzohydroxamic acid binding to horseradish peroxidase isoenzyme C. *Biopolymers*, **62**, (5), 261-267.

Howes B.D, Rodriguez-Lopez J.N, Smith A.T. and Smulevich G. (1997). Mutation of distal residues of horseradish peroxidase. Influence on substrate binding and cavity properties. *Biochemistry*, **36**, (6), 1532-1543

Hoyle M.C. (1977). High-resolution of peroxidase-indoleacetic acid oxidase isoenzymes from horseradish by isoelectric-focusing. *Plant Physiology*, **60**, 787-793.

Huang W, Wang J, Bhattacharyya D. and Bachas L.G. (1997). Improving the Activity of Immobilized Subtilisin by Site-Specific Attachment to Surfaces. *Analytical Chemistry*, **69**, (22), 4601-4607.

Huddleston S, Robertson S, Dobson C, Kwong F.Y.P. and Charalambous B.M. (1995). Structural and functional stability of HRP. *Biochemical Society Transactions*, **23**, 108s.

Hudson E.P, Eppler R.K. and Clark D.S. (2005). Biocatalysis in semi-aqueous and nearly anhydrous conditions. *Current Opinion in Biotechnology*, **16**, (6), 637-643.

Ignatenko O.V, Gazaryan I.G, Mareeva E.A, Chubar T.A, Fechina V.A, Savitsky P.A, Rojkova A.M. and Tishkov V.I. (2000). Catalytic properties of tryptophanless recombinant horseradish peroxidase. *Biochemistry (Moscow)*, **65**, (5), 583-587.

Inoue H, Najima H and Okayama H. (1990). High efficiency transformation of *Escherichia coli* with plasmids. *Gene*, **96**, 23-28.

- Ishii K, Mussmann M, MacGregor B.J. and Amann R. (2004). An improved fluorescence in situ hybridization protocol for the identification of bacteria and archaea in marine sediments. *FEMS Microbiology Ecology*, **50**, (3): 203-212.
- Iwuoha E, de Villaverde D, Garcia N, Smyth M.R. and Pingarron J. (1997). Reactivities of organic phase biosensors. The amperometric behaviour of horseradish peroxidase immobilised on a platinum electrode modified with an electrosynthetic polyaniline film. *Biosensors and Bioelectronics*, **12**, 749-761.
- Jamnicky B, Derkossojak V. and Gamulin S. (1988). Application of horseradish peroxidase to glucose determination in body-fluids. *Acta Pharmaceutica Jugoslavica*, **38**, (1), 53-59.
- Jermutus L. and Pelletier J. (2001). Creating and evaluating protein diversity. *Current Opinion in Biotechnology*, **12**, (4), 331-333.
- Jestin J.L and Kaminski P.A. (2004). Directed enzyme evolution and selection for catalysis based on product formation. *Journal of Biotechnology*, **113**, (1), 85-103.
- Josephy P.D, Eling T. and Mason R.P. (1982). The horseradish peroxidase-catalysed oxidation of 3,3,3',5'-tetramethylbenzidine. Free radical and charge-transfer complex intermediates. *Journal of Biological Chemistry*, **257**, (7), 3669-3675.
- Jones D.H and Winistorfer S.C. (1997). "Recombination and Site Directed Mutagenesis of DNA". IN: White B.A (ed). PCR Cloning Protocols, Methods in Molecular Biology. (1997). *Human Press New Jersey*, USA, pp 131-141.
- Jones H.E, Holland I.B and Campbell A.K. (2002). Direct measurement of free Ca^{2+} shows different regulation of Ca^{2+} between the periplasm and the cytosol of *E.coli*. *Cell Calcium*, **32**, (4), 183-192.
- Jung Y, Kwak J. and Lee Y. (2001). High-level production of heme-containing holoproteins in *E.coli*. *Applied Microbiological Biotechnology*, **55**, 187-191.
- Kamin R.A. and Wilson G. S. (1980). Rotating ring-disk enzyme electrode for biocatalysis kinetic studies and characterization of the immobilized enzyme layer. *Analytical Chemistry*, **52**, (8), 1198-1205.
- Kaposi A.D, Fidy J, Manas E.S, Vanderkooi J.M. and Wright W.W. (1999), HRP monitored by infrared spectroscopy: effect of temperature, substrate and calcium. *Biochimica et Biophysica Acta*, **1435**, 41-50.
- Kazlauskas R. (2005). Biological chemistry: Enzymes in focus. *Nature*, **436**, 1096-1097.
- Kerby K and Sommerville C. (1996). Purification of an infection related extracellular peroxidase from barley. *Plant Physiology*, **62**, 397-402.

- Keyhani J, Keyhani E, Zarchipour S, Tayefi-Nasrabadi H. and Einollahi N. (2005). Stepwise binding of nickel to horseradish peroxidase and inhibition of the enzymatic activity. *Biochimica et Biophysica Acta*, **1722**, (3), 312-323.
- Keyhani J, Keyhani E, Einollahi N, Minai-Tehrani D. and Zarchipour S. (2003). Heterogeneous inhibition of horseradish peroxidase activity by cadmium. *Biochimica et Biophysica Acta*, **1621**, (2), 140-148.
- Khmelnitsky Y.L, Mozhaev V.V, Belova A.B, Sergeeva M.V. and Martinek K. (1991a). Denaturation capacity: a new quantitative criterion for selection of organic solvents as reaction media in biocatalysis. *European Journal of Biochemistry*, **198**, (1), 31-41.
- Khmelnitsky Y.L, Belova A.B, Levashov A.V. and Mozhaev V.V. (1991b). Relationship between surface hydrophobicity of a protein and its stability against denaturation by organic solvents. *FEBS Letters*, **284**, (2), 267-269.
- Killard A.J, Zhang S, Zhao H, John R, Iwuoha E.I. and Smyth M.R. (1999). Development of an electrochemical flow injection immunoassay (FIIA) for the real-time monitoring of biospecific interactions. *Analytica Chimica Acta*, **400**, 109-119.
- Kim J.R, Choi Y.S. and Yoo Y.J. (2000). Reactivation of HRP in organic solvent using extraction. *Biotechnology Letters*, **22**, 485-489.
- Kim S.S. and Lee D.J. (2005) Purification and characterization of a cationic peroxidase C-S in *Raphanus sativus*. *Journal of Plant Physiology*, **162** (6): 609-617.
- Kis M, Burbridge E, Brock I.W, Heggie L, Dix P.J. and Kavanagh T.A. (2004). An N-terminal peptide extension results in efficient expression, but not secretion of a synthetic horseradish peroxidase gene in transgenic tobacco. *Annals of Botany*, **93**, 303-310.
- Konash A. and Magner E. (2006). Characterization of an organic phase peroxide biosensor based on horseradish peroxidase immobilized in Eastman AQ. *Biosensors and Bioelectronics*, **22**, (1), 116-23.
- Kondo A, Kohda J, Endo Y, Shiromizu T, Kurokawa Y, Nishihara K, Yanagi H, Yura T. and Fukuda H. (2000). Improvement of Productivity of Active HRP in *E.coli* by Coexpression of Dsb Proteins. *Journal of Bioscience and Bioengineering*, **90**, (6), 600-606.
- Krowarsch D. and Otlewski J. (2001). Amino acid substitutions at the fully exposed P₁ site of bovine pancreatic trypsin inhibitor affect its stability. *Protein Science*, **10**, 715-724.
- Kuhlmeyer C. and Klein J. (2003). Stabilisation of enzymes with polyvinylsaccharides I: physical stabilisation of horseradish peroxidase. *Enzyme and Microbial Technology*, **32**, 99-106.
- Kumar S, Tsai C-J. and Nussinov R. (2000), Factors effecting protein thermostability. *Protein Engineering*, **13**, (3), 179-191.

Kurokawa Y, Yanagi H. and Yura T. (2000). Overexpression of Protein Disulfide Isomerase DSBC stabilises multiple disulphide bonded recombinant protein produced and transported to the periplasm in *E.coli*. *Applied and Environmental Microbiology*, **66**, (9), 3960-3965.

Kwasigroch J. M, Gilis D, Dehouck Y. and Rooman M. (2002) PoPMuSiC, rationally designing point mutations in protein structures. *Bioinformatics*, **18**, 1701-1702.

Kwon K.S, Kim J, Shin H.S. and Yu M-H. (1994). Single amino acid substitutions of α_1 -Antitrypsin that confer enhancement in thermal stability. *Journal of Biological Chemistry*, **269**, 9627-9631.

Ladbury J.E, Wynn R, Thompson J.A. and Sturtevant J.M. (1995). Substitution of charged residues into the hydrophobic core of *E.coli* thioredoxin results in a change in heat capacity of the active protein. *Biochemistry*, **3**, 54-58.

Laemmli U.K. (1970). "Cleavage of structural proteins during the assembly of the head of bacteriophage T4." *Nature*, **227**, 680-685.

Lai Y-C. and Lin S-C. (2005). Application of immobilised horseradish peroxidase for the removal of *p*-chlorophenol from aqueous solution. *Process Biochemistry*, **40**, 1167-1174.

Lambrechts W. and Sansen W. (1996). Biosensors: microelectrochemical devices. Institute of Physics Publishing, Philadelphia, USA.

Ledru S, Ruille N. and Boujtita M. (2006). One-step screen printed electrode modified in its bulk with HRP based on direct electron transfer for hydrogen peroxide detection in flow injection mode. *Biosensors and Bioelectronics*, **21**, 1591-1598.

Lee B. and Vasmatzis G. (1997). Stabilisation of Protein Structures. *Current Opinion in Biotechnology*, **8**, 423-428.

Lehmann M, Loch C, Middendorf A, Studer D, Lassen S.F, Pasamontes L, van Loon A.P.G.M. and Wyss M. (2002). The consensus concept for thermostability engineering of proteins: further proof of concept. *Protein Engineering*, **15**, (5), 403-411.

Lehmann M. and Wyss M. (2001) Engineering proteins for thermostability: the use of sequence alignments versus rational design and directed evolution. *Current Opinion in Biotechnology*, **12**, 371-375.

Lehmann M, Pasamontes L, Lassen S.F. and Wyss M. (2000). The consensus concept for thermostability engineering of proteins. *Biochimica et Biophysica Acta*, **1543**, 408-415.

Lei S.P, Lin H.C, Wang S.S, Callaway J. and Wilcox G. (1987). Characterisation of the *Erwinia carotovora* pelB gene and its product pectate lyase. *Journal of Bacteriology*, **169**, 9, 4379-4383.

- Leonard P. (2003). "Production of antibodies for use in a biosensor-based assay for *Listeria monocytogenes*". PhD Thesis, Dublin City University, Republic of Ireland.
- Lemos M.A, Oliveira J.C. and Saraiva J.A. (2000) Influence of pH on the Thermal Inactivation Kinetics of HRP in aqueous solution. *Lebensmittel-Wissenschaft und Technologie*, **33**, 362-368.
- Lesk, A.M., (2004) Introduction to Protein Science: architecture, function and Genomics. A.M. Lesk (ed), Oxford University Press New York. pp 310.
- Lett C.M, Rosu-Myles M, Frey H.E. and Guillemette G. (1999). Rational design of a more stable yeast iso-1-Cytochrome *c*. *Biochimica et Biophysica Acta*, **1432**, 40-48.
- Levitt M. and Gerstein M. (1998). A unified statistical framework for sequence comparison and structure comparison. *Proceedings of the National Academy of Science, USA*, **95**, 5913-5920.
- Li C.X, Hu S-H, Gao N, Shen G.L. and Yu R-Q. (2004). An amperometric hydrogen peroxide biosensor based on immobilizing horseradish peroxidase to a nano-Au monolayer supported by sol-gel derived carbon ceramic electrode. *Bioelectrochemistry*, **65**, (1), 33-39.
- Lichty J.J, Malecki J.L, Agnew H.D, Michelson-Horowitz D.J and Tan S. (2005). Comparison of affinity tags for protein purification. *Protein expression and Purification*, **41**, 98-105.
- Limoges B. and Savéant J-M. (2003). Cyclic voltammetry of immobilized redox enzymes. Interference of steady-state and non-steady-state Michaelis-Menten kinetics of the enzyme-redox cosubstrate system. *Journal of Electroanalytical Chemistry*, **15**, 61-70.
- Lin J. and Ju H. (2005). Electrochemical and chemiluminescent immunosensors for tumour markers. *Biosensors and Bioelectronics*, **20**, (8), 1461-1470.
- Lindgren A, Ruzgas T, Gorton L, Csoregi E, Ardila G.B, Sakharov I.Y. and Gazaryan I.G. (2000). Biosensors based on novel peroxidases with improved properties in direct and mediated electron transfer. *Biosensors and Bioelectronics*, **15**, 491-497.
- Lindgren A, Tanaka M, Ruzgas T, Gorton L, Gazaryan I, Ishimori K. and Morishima I. (1999). Directed electron transfer catalysed by recombinant forms of horseradish peroxidase: insight into the mechanism. *Electrochemistry Communications*, **1**, 171-175.
- Lindgren A, Munteanu I.G, Ruzgas T, Gazaryan I. and Gorton L. (1998). Comparison of rotating disk and wall-jet electrode systems for studying the kinetics of direct and mediated electron transfer for horseradish peroxidase on a graphite electrode. *Journal of Electroanalytical Chemistry*, **458**, (1-2), 113-120.
- Liu J-Z, Wang T-L, Huang M-T, Song H-Y, Weng L-P. and Ji L-N. (2006). Increased thermal and organic solvent tolerance of modified horseradish peroxidase. *Protein Engineering, Design and Selection*, **19**, (4), 169-173.

- Liu, Y.-L. et al. (2005). Nanosized flower-like ZnO synthesized by a simple hydrothermal method and applied as matrix for horseradish peroxidase immobilization for electro-biosensing. *Journal of Inorganic Biochemistry*, **99**, (10), 2046-2053.
- Liu J-Z, Song H-Y, Weng L-P and Ji L-N. (2002). Increased thermostability and phenol removal efficiency by chemical modified HRP. *Journal of Molecular Catalysis B*, **18**, 225-232.
- Liu X, Zhang S, Pan X. and Wang C. (1999). A novel method for increasing production of mature proteins in the periplasm of *Escherichia coli*. *Protein Science*, **8**, 2085-2089.
- Loladze V.V, Ibarra-Molero B, Sanchez-Ruiz J.M. and Makhatadze G.I. (1999). Engineering a thermostable protein via optimisation of charge-charge interactions on the protein surface. *Biochemistry*, **38**, 16419-16423.
- Lopez-Gallego F, Montes T, Fuentes M, Alonso N, Grazu V, Betancor L, Guisan J.M. and Fernandez-Lafuente R. (2005). Improved stabilization of chemically aminated enzymes via multipoint covalent attachment on glyoxyl supports. *Journal of Biotechnology*, **116**, (1), 1-10.
- Loprasert S, Negoro S. and Okada H. (1989). Cloning, Nucleotide sequence and Expression in *E.coli* of the *Bacillus stearothermophilus* Peroxidase gene (perA). *Journal of Bacteriology*, **171**, 4871-4875.
- Lori J.A, Morrin A, Killard A.J. and Smyth M.R. (2006). Development and characterisation of Nickel-NTA-Polyaniline modified electrodes. *Electroanalysis*, **18**, (1), 77-81.
- Loughran S. T, Loughran N. B, Ryan B. J, D'Souza B. N, Walls D. (2006). Expression and purification of His-tagged recombinant human Bfl-1: use of a modified *E. coli* expression vector enables purification by Immobilised Metal Affinity Chromatography. *Analytical Biochemistry*, **355**, (1), 148-150.
- Lu U, Hu B.C-P, Shih Y-C, Wu C-Y. and Yang Y-S. (2004). The design of a novel complementary metal oxide semiconductor detection system for biochemical luminescence. *Biosensors and Bioelectronics*, **19**, (10), 1185-1191.
- Luong J.H.T, Brown R.S, Male K.B, Cattaneo M.V. and Zhao S. (1995). Enzyme reactions in the presence of cyclodextrins: biosensors and enzyme assays. *Trends in Biotechnology*, **13**, 457-463.
- Luo W, Liu H, Deng H, Sun K, Zhao C, Qi D. and Deng J. (1997) Biosensing of hydrogen peroxide at carbon paste electrode incorporating N-methyl phenazine methosulphate, fused-silica and horseradish peroxidase. *Analytical Letters*, **30**, (2), 205-220.
- Machado M.F and Saraiva J.M. (2005). Thermal stability and activity regain of HRP in aqueous mixtures of imidazolium-based ionic liquids. *Biotechnology Letters*, **27**, 1233-1239.

- Machado MF. and Saraiva J. (2002). Inactivation and reactivation kinetics of HRP in phosphate buffer and buffer-dimethylformamide solutions. *Journal of Molecular Catalysis B*, **19-20**, 451-457.
- Machicado C, Bueno M. and Sancho J. (2002). Predicting the structure of protein cavities created by mutation. *Protein Engineering*, **15**, (8), 669-675.
- Mader M. and Fussel R. (1982). Role of peroxidase in lignification of tobacco cells. *Plant Physiology*, **43**, 1037-1041.
- Maeda Y. Fujihara M. and Ikeda I. (2002). Spectroscopic study on structure of Horseradish Peroxidase in water and DMSO. *Biopolymers (Biospectroscopy)*, **67**, 107-112.
- Magliery T.J and Regan L. (2004). Beyond consensus: statistical free energies reveal hidden interactions in the design of TPR Motif. *Journal of Molecular Biology*, **343**, 731-745.
- Maniatis T, Fritsch E.F. and Sambrook I. (1989) "Molecular Cloning- A laboratory Manual" Cold Spring Harbour Laboratory, Cold Spring Harbour, New York.
- Marcus R.A. and Sutin N. (1985). Electron transfers in chemistry and biology. *Biochimica et Biophysica Acta*, **811**, 265-322.
- Martinek K. and Mozhaev V.V. (1985). Immobilisation of enzymes: An approach to fundamental studies in Biochemistry. *Advances in Enzymology and Related Areas of Molecular Biology*, **57**, 179-249.
- Martinez P. and Arnold F.H. (1991). Surface change substitutions increase the stability of α -lytic protease in organic solvents. *Journal of the American Chemical Society*, **113**, 6336-6337.
- Mateo C, Abian O, Fernandez-Lafuente R. and Guisan J.M. (2000). Increase in conformational stability of enzymes immobilised on epoxy-activated supports by favouring additional multipoint covalent attachment. *Enzyme and Microbial Technology*, **26**, 509-515.
- Matthews B.W. (1993). Structural and genetic analysis of protein stability. *Annual Reviews in Biochemistry*, **62**, 139-160.
- Mayo S.L, Ellis W, Crutchley R. and Gray H.B. (1986) Long-range electron transfer in heme proteins. *Science*, **233**, 948-952.
- McEldoon J.P. and Dordick J.S. (1996). Unusual thermal stability of soybean peroxidase. *Biotechnology Progress*, **12**, 555-558.
- Mdluli K.M. (2005). Partial purification and characterisation of polyphenol oxidase and peroxidase from marula fruit (*Sclerocarya birrea subsp Caffra*). *Food Chemistry*, **92**, (2), 311-323.

Mergulhão F.J.M, Summers D.K. and Monteiro G.A. (2005). Recombinant protein secretion in *Escherichia coli*. *Biotechnology Advances*, **23**, (3), 177-202.

Metelitzka D.I, Karasyova E.I, Grintsevich E.E. and Thorneley R.N.F. (2004), Peroxidase-catalysed co-oxidation of 3,3',5,5'-tetramethylbenzidine in the presence of substituted phenols and their polydisulfides. *Journal of Inorganic Biochemistry*, **98**, 1-9.

Meunier B, Rodriguez-Lopez J.N, Smith A.T, Thorneley R.N.F. and Rich P.R. (1998). Redox- and anion-linked protonation sites in horseradish peroxidase. analysis of distal haem pocket mutants. *Biochemistry Journal*, **330**, (1), 303-309.

Meunier B, Rodriguez-Lopez J.N, Smith A.T, Thorneley R.N, & Rich P.R. (1995). Laser photolysis behavior of ferrous horseradish peroxidase with carbon monoxide and cyanide: effects of mutations in the distal heme pocket. *Biochemistry*, **34**, (45), 14687-14692

Miland E. (1996). "Stability characteristics and applications of native and chemically-modified Horseradish Peroxidase". PhD Thesis, Dublin City University, Dublin City University, Republic of Ireland.

Miland E, Smyth M.R. and O'Fágáin, C. (1996a). Modification of HRP with bifunctional N-hydroxysuccinimide esters: effects on molecular stability. *Enzyme and Microbial Technology*, **19**, 242-249.

Miland E, Smyth M.R and O'Fágáin, C. (1996b). Increased thermal and solvent tolerance of acetylated HRP. *Enzyme and Microbial Technology*, **19**, 63-67.

Miller V.P, Goodin D.B, Friedman A.E, Hartmann C. and Ortiz de Montellano P.R. (1995). Horseradish peroxidase Phe172 to Tyr mutant. Sequential formation of compound I with a porphyrin radical cation and a protein radical. *Journal of Biological Chemistry*, **270**, (31), 18413-18419.

Miyazaki C. and Takahashi H. (2001). Engineering of the H₂O₂-binding pocket region of a recombinant manganese peroxidase to be resistant to H₂O₂. *FEBS Letters*, **509**, 111-114.

Miyazaki J, Nakaya S, Suzuki T, Tamakoshi M, Oshima T. and Yamagishi A. (2001). Ancestral residues stabilising 3-Isopropylmalate Dehydrogenase of an extreme thermophile: Experimental evidence supporting the thermophilic common ancestor hypothesis. *Journal of Biochemistry*, **129**, 777-782.

Miyazaki K, Wintrode P.L, Grayling R.A, Rubingh D.N. and Arnold F.H. (2000). Directed evolution study of temperature adaption in a psychrophilic enzyme. *Journal of Molecular Biology*, **297**, 1015-1026.

Mohanty A.K. and Wiener M.C. (2004). Membrane protein expression and production: effects of polyhistidine tag length and position. *Protein Expression and Purification* **33**, (2), 311-25.

- Moore J. and Arnold F.H. (1996). Directed Evolution of a para-Nitrobenzyl Esterase for Aqueous-Organic Solvents. *Nature Biotechnology*, **14**, 458-467.
- Moosavi-Movahedi A.A. and Nazari K. (1994), Denaturation of HRP with Urea and Guanidine Hydrochloride. *International Journal of Biological Macromolecules*, **17**, 43-47.
- Morawski B, Lin Z.L, Cirino P, Joo H, Bandara G. and Arnold F.H. (2000a). Functional expression of horseradish peroxidase in *Saccharomyces cerevisiae* and *Pichia pastoris*. *Protein Engineering*, **13**, (5), 377-384.
- Morawski B, Zhanglin L, Cirino P, Joo H. and Bandara G. (2000b), Functional Expression of HRP in *S. cerevisiae* and *P. pastoris*. *Protein Engineering*, **13**, (5), 377-384.
- Morawski B, Quan S, Arnold F.H, (2001), Functional expression and stabilisation of HRP by directed evolution in *S. cerevisiae*. *Biotechnology and Bioengineering*, **76**, (2), 99-107.
- Morrin A. (2003). "Developments in modified electrodes for sensing applications". PhD Thesis, Dublin City University, Republic of Ireland.
- Morrin A, Guzman A, Killard A.J, Pingarron J.M. and Smyth M.R. (2002). Characterisation of horseradish peroxidase immobilisation on an electrochemical biosensor by colorimetric and amperometric techniques. *Biosensors and Bioelectronics*, **18**, (5-6), 715-720.
- Morimoto A, Tanaka M, Takahashi S, Ishimori K, Hori H. and Morishima I. (1998). Detection of a tryptophan radical as an intermediate species in the reaction of horseradish peroxidase mutant (Phe-221 to Trp) and hydrogen peroxide. *Journal of Biological Chemistry*, **273**, (24), 14753-14760.
- Morton C.L, Potter P.M. (2000). Comparison of *Escherichia coli*, *Saccharomyces cerevisiae*, *Pichia pastoris*, *Spodoptera frugiperda*, and COS7 Cells for recombinant gene expression. *Molecular Biology*, **16**, 193-202.
- Mössner E. and Pluckthün A. (2001), Directed evolution with fast and efficient selection technologies. *Chimia*, **55**, 324-328.
- Mozhaev V.V. (1993). Mechanism-based strategies for protein thermostabilization. *Trends in Biotechnology*, **11**, (3), 88-95.
- Mozhaev V.V, Siksnis V.A, Melik-Nubarov N.S, Galkantaite N.Z, Denis G.J, Butkus E.P, Zaslavsky B.Y, Mestechkina N.M. and Martinek K. (1988). Protein stabilization via hydrophilization: covalent modification of trypsin and α -chymotrypsin. *European Journal of Biochemistry*, **173**, 47-154.
- Mukai M, Nagano S, Tanaka M, Ishimori K, Morishima I, Ogura T, Watanabe Y. and Kitagawa T. (1997). Effects of concerted hydrogen bonding of distal histidine on active

- site structures of horseradish peroxidase. Resonance Raman studies with Asn70 mutants. *Journal of the American Chemical Society*, **119**, (7), 1758-1766.
- Mullis K.B and Faloona F.A. (1987). Specific synthesis of DNA in vitro via a polymerase catalysed chain reaction. *Methods in Enzymology*, **155**, 335-350.
- Munoz V, Cronet P, Lopez-Hernandez E. and Serrano L. (1996). Analysis of the effect of local interactions on protein stability. *Folding and Design*, **1**, (3), 167-178.
- Nagano S, Tanaka M, Ishimori K, Watanabe Y. and Morishima I. (1996). Catalytic roles of the distal site asparagine-histidine couple in peroxidases. *Biochemistry*, **35**, (45), 14251-14258.
- Nagano S, Tanaka M, Watanabe Y. and Morishima I. (1995). Putative hydrogen bond network in the heme distal site of horseradish peroxidase. *Biochemical and Biophysical Research Communications*, **207**, (1), 417-423.
- Nahar P. and Bora U. (2004). Microwave-mediated rapid immobilisation of enzymes onto an activated surface through covalent bonding. *Analytical Biochemistry*, **328**, 81-83.
- Newmyer S.L, Sun J, Loehr T.M. and De Montellano P.R.O. (1996a). Rescue of the horseradish peroxidase His-170 to Ala mutant activity by imidazole. Importance of proximal ligand tethering. *Biochemistry*, **35**, (39), 12788-12795.
- Newmyer S.L. and De Montellano P.R.O. (1996b). Rescue of the catalytic activity of an H42A mutant of horseradish peroxidase by exogenous imidazoles. *Journal of Biological Chemistry*, **271**, (25), 14891-14896.
- Newmyer S.L. and Ortiz de Montellano P.R. (1995). Horseradish peroxidase His-42 to Ala, His-42 to Val, and Phe-41 to Ala mutants. Histidine catalysis and control of substrate access to the heme iron. *Journal of Biological Chemistry*, **270**, (33), 19430-19438
- Nicell J.A. and Wright H. (1997). A model of peroxidase activity with inhibition by hydrogen peroxide. *Enzyme and Microbial Technology*, **21**, 302-310.
- Nielsen, K-L, Indiani, C, Henriksen, A, Feis, A, Becucci, M, Gajhede, M, Smulevich, G. and Welinder K.G. (2001) Differential activity and structure of highly similar peroxidases. Spectroscopic, crystallographic and enzymatic analyses of lignifying *Arabidopsis thaliana* peroxidase A2 and horseradish peroxidase A2. *Biochemistry*, **40**, 11013-11021.
- Nosoh Y. and Sekiguchi T. (1990). Protein Engineering for thermostability. *Trends in Biotechnology*, **8**, 16-20.
- Novagen (2003), "pET System Manual 10th Edition", Novagen Technical Literature.
- Numata K, Hayashi-Iwasaki Y, Kawaguchi J, Sakurai M, Moriyama H, Tanaka N. and Oshima T. (2001). Thermostabilisation of a chimeric enzyme by residue substitutions:

four amino acid residues in loop regions are responsible for the thermostability of *Thermus thermophilus* isopropylmalate dehydrogenase. *Biochimica et Biophysica Acta*, **1545**, 174-183.

Nys P.S, Savitskaia E.M. and Shellenberg N.N. (1977). Penicillin amidase from *E. coli*. A comparative study of the stability of penicillin amidase immobilized by various means. *Antibiotiki*, **22**, (2), 130-6.

O'Brien A.M, Smith A.T. and O'Fágáin C. (2003), Effects of phthalic anhydride modification on HRP stability and activity. *Biotechnology and Bioengineering*, **81**, (2), 233-240.

O'Brien A.M, O'Fágáin C, Nielsen P.F. and Welinder K.G. (2001), Location of Crosslinks in chemically stabilised HRP. Implications for design of crosslinks. *Biotechnology and Bioengineering*, **76**, (4), 277-284.

O'Brien A.M. (1997). "Chemical modification and characterisation of Horseradish Peroxidase and derivatives for environmental applications". PhD Thesis, Dublin City University, Dublin, Republic of Ireland.

O'Fágáin, C. (2003). Enzyme stabilisation- recent experimental progress. *Enzyme and Microbial Technology*, **33**, 137-149.

O'Fágáin, C. (1997). Protein stability and its measurement. *IN: C O' Fágáin, Stabilising protein function*. Springer Press, Berlin, pp 1-14, 69-75, 81-107.

Ogino H. and Ishikawa H. (2001). Enzymes that are stable in the presence of organic solvents. *Journal of Bioscience and Bioengineering*, **91**, (2), 109-116.

Olsen M.J, Iverson B. and Georgiou G. (2000), High-throughput screening of enzyme libraries. *Current Opinion in Biotechnology*, **11**, 331-337.

O'Maille P.E, Bakhtina M. and Tsai M-D. (2002). Structure-based Combinatorial Protein Engineering, SCOPE. *Journal of Molecular Biology*, **321**, 677-691.

Orlaova MA, Chubar TA, Fechina V.A, Ignatenko O.V, Badun G.A, Ksenofontov A.L, Uporov I.V. and Gazaryan IG. (2003). Conformational differences between native and recombinant HRP revealed by Tritium Planigraphy. *Biochemistry (Moscow)*, **68**, (11), 1225-1230.

Orlaova M.A, Kost O.A, Gribkov V.A, Gazaryan I.G, Dubrovsky A.V, Egorov V.A. and Troshina N.N. (2000). Enzyme activation and inactivation induced by low doses of irradiation. *Applied Biochemistry and Biotechnology*, **88**, 243-255.

Ozaki S. and Ortiz de Montellano P.R. (1995). Molecular engineering of horseradish peroxidase. Thioether sulfoxidation and styrene epoxidation by Phe-41 leucine and threonine mutants. *Journal of the American Chemical Society*, **117**, (27), 7056-7064.

- Ozaki S.-I. and Ortiz de Montellano P.R. (1994). Molecular engineering of horseradish peroxidase. Highly enantioselective sulfoxidation of aryl alkyl sulfides by the Phe-41-Leu mutant. *Journal of the American Chemical Society*, **116**, (10), 4487-4488.
- Pace N, Horn G, Hebert E.J, Bechert J, Shaw K, Urbanikova L, Scholtz M. and Sevcik J. (2001). Tyrosine hydrogen bonds make a large contribution to protein stability. *Journal of Molecular Biology*, **312**, (2), 393-404.
- Pace N, Alston R.W. and Shaw K.L. (2000). Charge-charge interactions influence the denatured state ensemble and contribute to protein stability. *Protein Science*, **9**, 1395-1398.
- Padmakumar V.C and Varadarajan R. (2003). A gradient PCR-based screen for use in site-directed mutagenesis. *Analytical Biochemistry*, **314**, 310-315.
- Padmanabhan S, Marqusee S, Ridgeway T, Laue T.M. and Baldwin RL. (1990). Relative helix-forming tendencies of nonpolar amino acids. *Nature*, **344**, (6263), 268-70.
- Palma R. and Curmi P.M.G. (1999). Computational studies on mutant protein stability: the correlation between surface thermal expansion and protein stability. *Protein Science*, **8**, 913-920.
- Pantoliano M.W, Whitlow M, Wood J.F, Dodd S.W, Hardman K.D, Rollence M.L. and Bryan P.N. (1989). Large increases in general stability for Subtilisin BPN through incremental changes in free energy of unfolding. *Biochemistry*, **28**, 7205-7213.
- Pappa H.S. and Cass A.E.G. (1993). A step towards understanding the folding mechanism of HRP. *European Journal of Biochemistry*, **212**, 227-235.
- Penalva J, Puchades R, Maquieira A. (1999). Analytical properties of immunosensors working in organic media. *Analytical Chemistry*; **71**, (17), 3862-72.
- Perry R.D, Shah J, Bearden S.W, Thompson J.M and Fetherston J.D. (2003). *Yersinia pestis* TonB: Role in Iron, Heme, and Hemoprotein Utilization. *Infection and Immunity*, **71**, (7), 4159-4162.
- Petrounia I.P. and Arnold F.H. (2000), Designed evolution of enzymatic properties. *Current Opinion in Biotechnology*, **11**, 325-330.
- Pina D.G, Shnyrova A.V, Gavilanes F, Rodriguez A, Leal F, Roig M.G, Sakharov I.Y, Zhadan G.G, Villar E. and Shnyrov V.L. (2001). Thermally induced conformational changes in HRP. *European Journal of Biochemistry*, **268**, 120-126.
- Presnova G, Grigorenko V, Egorov A, Ruzgas T, Lindgren A, Gorton L. and Börchers T. (2000). Direct heterogeneous electron transfer of recombinant horseradish peroxidases on gold. *Faraday Discussions*, **116**, 281 – 289.
- Priori A.M, Indiani C, de Sanctis G. and Marini S. (2000). Anion and pH-linked conformational transition in HRP. *Journal of Inorganic Biochemistry*, **79**, 25-30.

Qiagen, (2003). "The QIAexpressionist, A handbook for high level expression and purification of 6X His tagged proteins". Qiagen technical literature.

Rodriguez-Lopez J, Gilabert M.A, Tudela J, Thorneley R.N.F. and Garcia-Canovas F. (2000). Reactivity of Horseradish peroxidase Compound II toward substrates: Kinetic evidence for a two step mechanism. *Biochemistry*, **39**, 13201-13209.

Rodriguez-Lopez J.N, Smith A.T. and Thorneley R.N.F. (1997a). Effect of distal cavity mutations on the binding and activation of oxygen by ferrous horseradish peroxidase. *Journal of Biological Chemistry*, **272**, (1), 389-395

Rodriguez-Lopez J.N, Hernández-Ruiz J, Garcia-Cánovas F, Thorneley R.N.F, Acosta M. and Arnao M.B. (1997b). The Inactivation and Catalytic Pathways of Horseradish Peroxidase with *m*-Chloroperoxybenzoic Acid. A spectroscopic and transient kinetic study. *Journal of Biological Chemistry*, **272**, 5469-5476.

Rodriguez-Lopez J.N, Smith A.T. and Thorneley R.N.F. (1996) Role of Arginine 38 in horseradish peroxidase a critical, residue for substrate binding and catalysis. *Journal of Biological Chemistry*, **271**,(8), 4023-4030.

Rojas-Melgarejo F, Marín-Iniesta F, Rodríguez-López J.N, García-Cánovas F. and García-Ruiz P. A. (2006). Cinnamic carbohydrate esters show great versatility as supports for the immobilization of different enzymes. *Enzyme and Microbial Technology*, **38**, 6, 748-755.

Rojas-Melgarejo F, Rodriguez-Lopez J, García-Cánovas F. and García -Ruiz P.A. (2004) Immobilisation of Horseradish peroxidase on cinnamic carbohydrate esters. *Process Biochemistry*, **39**, 1455-1464.

Rojkova A.M, Galkin A.G, Kulakova L.B, Serov A.E, Savitsky P.A, Fedorchuk V.V. and Tishkov V.I. (1999). Bacterial formate dehydrogenase. Increasing the enzyme thermal stability by hydrophobization of alpha helices. *FEBS Letters*, **445**, 183-188.

Roy J.J, Sumi S, Sangeetha K. and Abraham TE. (2005). Chemical modification and immobilization of papain. *Journal of Chemical Technology and Biotechnology*, **80** (2), 184-188.

Rudrappa T. Neelwarne B, Kumar V, Lakshmanan V, Venkataramareddy S.R. and Aswathanarayana R.G. (2005). Peroxidase production from hairy root cultures of red beet (*Beta vulgaris*). *Electronic Journal of Biotechnology*, **8**, (2), 185-196.

Ruzgas T, Csogregi E, Emneus J, Gorton L. and Marko-Varga G. (1996). Peroxidase modified electrodes: fundamentals and applications. *Analytica Chimica Acta*, **330**, 123-138.

Ryan B, Carolan N. and O'Fágáin C. (2006). Horseradish and Soybean Peroxidases: Comparable Tools for Alternative Niches? *Trends in Biotechnology*, **24**, (8), 355-363.

- Ryan O, Smyth M.R. and O'Fágáin C. (1994) HRP: the analyst's friend. *IN: K.F. Tipton (ed), Essays in Biochemistry*, **28**, London, Portland Press, pp 129-146.
- Ryan O, Smyth M. R. and O'Fágáin C. (1994a), Thermostabilised chemical derivatives of HRP. *Enzyme Microbial Technology*, **16**, 501-505.
- Ryan O. (1992). "Studies on native and modified peroxidases". MSc Thesis, Dublin City University, Republic of Ireland.
- Ryu K. and Dordick J.S. (1989). Free energy relationships of substrate and solvent hydrophobicities with enzymatic catalysis in organic media. *Journal of the American Chemical Society*, **111**, 8026-8027.
- Saito R, Momma N. and Naito M. (1985). Dual Diffusion of Gold and Platinum into Silicon. *Journal of the Electrochemical Society*, **132**, 225-229.
- Sanchez P.D, Blanco P.T, Fernandez-Alvarez J.M, Smyth M.R. and O'Kennedy R. (1990). Flow-injection analysis of hydrogen-peroxide using a horseradish peroxidase-modified electrode detection system. *Electroanalysis*, **2**, (4), 303-308.
- Sanchez-Ruiz J.M. and Makhatadze G.I. (2001). To charge or not to charge? *Trends in Biotechnology*, **19**, (4), 132-135.
- Sanders S.A, Bray R.C. and Smith A.T. (1994). pH-dependent properties of a mutant horseradish peroxidase isoenzyme C in which 38-Arg has been replaced with lysine. *European Journal of Biochemistry*, **224**, (3), 1029-1037.
- Santucci R, Laurenti E, Sinibaldi F. and Ferrari R.P. (2002). Effect of dimethyl sulfoxide on the structure of the functional properties of HRP as observed by spectroscopy and cyclic voltammetry. *Biochimica et Biophysica Acta*, **1596**, 225-233.
- Sato K, Hasumi H, Tsukidate A, Sakurada J, Nakamura S. and Hosoya T. (1995), Effects of mixed solvents on three elementary steps in the reactions of HRP and lactoperoxidase. *Biochimica et Biophysica Acta*, **1253**, 94-102.
- Savenkova M.I. and de Montellano P.R.O. (1998a). Horseradish peroxidase. Partial rescue of the His-42 to Ala mutant by a concurrent Asn-70 to Asp mutation. *Archives of Biochemistry and Biophysics*, **351**, (2), 286-293.
- Savenkova M.I., Kuo J.M. and de Montellano P.R.O. (1998b). Improvement of peroxygenase activity by relocation of a catalytic histidine within the active site of horseradish peroxidase. *Biochemistry*, **37**, (30), 10828-10836.
- Savenkova M.I., Newmyer S.L. and de Montellano P.R.O. (1996). Rescue of His-42 to Ala horseradish peroxidase by a Phe-41 to His mutation - Engineering of a surrogate catalytic histidine. *Journal of Biological Chemistry*, **271**, (40), 24598-24603.
- Schmidt A, Schumacher J.T, Reichelt J, Hecht H-J. and Bilitewski U. (2002). Mechanistic and molecular investigation on stabilisation of HRPC. *Analytical Chemistry* **74**, 3037-3045.

Schumacher J.T, Hecht H-J, Dengler U, Reichelt J. and Bilitewski U. (2001). Direct electron transfer for peroxidase to screen-printed graphite electrodes. *Electroanalysis*, **13**, 779-785.

Schuhmann W. (2002). Amperometric enzyme biosensor based on optimised electron-transfer pathways and non-manual immobilisation procedures. *Reviews in Molecular Biotechnology*, **82**, 425-441.

Schwede T, Kopp J, Guex N. and Peitsch M.C. (2003) SWISS-MODEL: an automated protein homology-modelling server. *Nucleic Acids Research*, **31**, 3381-3385

Segura M de L.M, Levin G, Miranda M, Mendive F.M, Targovnik H.M. and Cascone O. (2005). High-level expression and purification of recombinant horseradish peroxidase isozyme C in SF-9 insect cell culture. *Process Biochemistry*, **40**, 795-800.

Shannon L.M, Kay E. and Lew J.Y. (1966). Peroxidases isoenzymes from Horseradish roots. *Journal of Biological Chemistry*, **241**, (9), 2166-2172.

Shigeaki H. (1998). Artificial evolution by DNA shuffling. *Trends In Biotechnology*, **16**, 76-82.

Shipovskov S, Ferapontova E.E, Gazaryan I. and Ruzgas T. (2004). Recombinant horseradish peroxidase - and cytochrome c-based two-electrode system for detection of superoxide radicals. *Bioelectrochemistry*, **63**, (1-2), 277-80.

Shrivastav T.G. (2003). Preparation of horseradish peroxidase hydrazide and its use in immunoassay. *Journal of Immunoassay & Immunochemistry*, **24** (3), 301-309.

Sigma Aldrich: Enzyme Substrate Index Enzyme Explorer.
http://www.sigmaaldrich.com/Area_of_Interest/Biochemicals/Enzyme_Explorer/Substrate_Index.html. [Accessed on 12/03/2005].

Singh N. and Singh J. (2002). An enzymatic method for the removal of phenol from effluent. *Preparatory Biochemistry and Biotechnology*, **32**, (2), 127-133.

Smeller L. and Fidy J. (2002). The enzyme HRP is less compressible at higher pressures. *Biophysical Journal*, **82**, (1), 426-436.

Smith A.T. and Veitch N.C. (1998), Substrate binding and catalysis in heme peroxidases. *Current Opinion in Chemical Biology*, **2**, pg 269-278.

Smith A.T, Sanders S.A, Thorneley R.N.F, Burke J.F. and Bray R.R.C. (1992). Characterisation of a heme active-site mutant of horseradish peroxidase, 41-Phe-Val, with altered reactivity towards hydrogen peroxide and reducing substrates. *European Journal of Biochemistry*, **207**, (2), 507-519.

Smith AT, Santama N, Dacey S, Edwards M, Bray R, Thorneley R. and Burke J. (1990). Expression of a synthetic gene for HRPc in E. coli and folding and activation of

the recombinant enzyme with Ca²⁺ and Heme. *Journal of Biological Chemistry*, **265**, (22), 13335-13343.

Smith, P.K, Krohn R.I, Hermanson G.T, Mallia A.K, Gartner F.H, Provenzano M.D, Fujimoto E.K, Goeke N.M, Olson B.J. and Klenk D.C. (1985). Measurement of protein using bicinchoninic acid. *Analytical Biochemistry*, **150**, 76-85.

Smulevich G, Paoli M, Burke J.F, Sanders S.A, Thorneley R.N.F. and Smith A.T. (1994). Characterization of recombinant horseradish peroxidase C and three site-directed mutants, F41V, F41W, and R38K, by resonance Raman spectroscopy. *Biochemistry*, **33**, (23), 7398-7407.

Spector S, Wang M, Carp S.A, Robblee J, Hendsch Z, Fairman R, Tidor B. and Raleigh D.P. (2000). Rational modification of protein stability by the mutation of charged surface residues. *Biochemistry*, **39**, 872-879.

Steipe B, Schiller B, Pluckthun A. and Steinbacher S. (1994). Sequence statistics reliably predict stabilising mutations in a protein domain. *Journal of Molecular Biology*, **240**, 188-192.

Stempfer G, Höll-Neugebauer B, Kopetzki E. and Rudolph R. (1996). A fusion protein designed for non covalent immobilisation: stability, enzymatic activity, and use in an enzyme reactor. *Nature Biotechnology*, **14**, 481-484.

Sterner R. and Liebl W. (2001). Thermophilic adaption of Proteins. *Critical Reviews in Biochemistry and Molecular Biology*, **36**, (1), 39-106.

Stratagene Quick Change[®] XL Site Directed Mutagenesis Kit Instruction Manual. (2003). Revision Number 063003m.

Stratagene, (2004). "XL10-Gold [®] Ultracompetent cells Technical Information, 200314-11, Revision 0740003" U.S. Patent Nos.5,512,468 and 5,707,841. Stratagene Technical Literature.

Studier F. W. (2005). Protein production by auto-induction in high-density shaking cultures. *Protein Expression and Purification*, **41**, (1), 207-234

Sun D, Cai C, Li X, Xing W. and Lu T. (2004). Direct electrochemistry and bioelectrocatalysis of horseradish peroxidase immobilised on active carbon. *Journal of Electroanalytical Chemistry*, **566**, 415-421.

Tams J.W. and Welinder K.G. (1998). Glycosylation and thermodynamic versus kinetic stability of HRP. *FEBS Letters*, **421**, 234-236.

Tanaka M, Ishimori K. and Morishima I. (1999). Luminol activity of horseradish peroxidase mutants mimicking a proposed binding site for luminol in *Arthromyces ramosus* peroxidase. *Biochemistry*, **38**, (32), 10463-10473.

- Tanaka M, Ishimori K, Mukai M, Kitagawa T. and Morishima I. (1997a). Catalytic activities and structural properties of horseradish peroxidase distal His42 to Glu or Gln mutant. *Biochemistry*, **36**, (32), 9889-9898.
- Tanaka M, Nagano S, Ishimori K. and Morishima I. (1997b). Hydrogen bond network in the distal site of peroxidases. Spectroscopic properties of Asn70 to Asp horseradish peroxidase mutant. *Biochemistry*, **36**, (32), 9791-9798.
- Tanaka M, Ishimori K. and Morishima I. (1996). The distal glutamic acid as an acid-base catalyst in the distal site of horseradish peroxidase. *Biochemical and Biophysical Research Communications*, **227**, (2), 393-399.
- Tang J.L, Wang B.Q, Wu Z.Y, Han X.J, Dong S.J. and Wang E.K. (2003). Lipid membrane immobilized horseradish peroxidase biosensor for amperometric determination of hydrogen peroxide. *Biosensors & Bioelectronics*, **18**, (7), 867-872.
- Taverna D.M. and Goldstein R.A. (2002a). Why are proteins marginally stable? *Proteins: structure, function and genetics*, **46**, 105-109.
- Taverna D.M. and Goldstein R.A. (2002b). Why are proteins so robust to site mutations? *Journal of Molecular Biology*, **315**, 479-484.
- Tawfik D.S. and Wells J.A. (1999). Man-made cell like compartments for molecular evolution. *Nature Biotechnology*, **16**, 652-656.
- Teilum K, Ostergaard L. and Welinder KG. (1999). Disulphide bond formation and folding of plant peroxidases expressed as inclusion body protein in *E.coli* thioredoxin reductase negative strains. *Protein Expression and Purification*, **15**, (1), 77-82.
- Temino de D.M.R., Hartmeier W. and Ansorge-Schumacher M.B. (2005). Entrapment of the alcohol dehydrogenase from *Lactobacillus kefir* in polyvinyl alcohol for the synthesis of chiral hydrophobic alcohols in organic solvents, *Enzyme Microbial Technology*, **36**, 3-9.
- Theorell H. (1957). The nature and mode of action of oxidation enzymes. *Experientia*, **13**, (1), 2-8.
- Thévenot D.R, Toth K, Durst R.A. and Wilson G.S. (1999). Electrochemical biosensors: recommended definitions and classification. *Pure and Applied Chemistry*, **71**, 2333-2348.
- Thompson J.D, Higgins D.G. and Gibson T.J. (1994). CLUSTAL W: improving the sensitivity of progressive multiple sequence alignment through sequence weighting, position-specific gap penalties and weight matrix choice. *Nucleic Acids Research*, **22**, (22), 4673-4680.
- Tobin M.B, Gustafsson C. and Huisman G.W. (2000). Directed evolution: the 'rational' basis for 'irrational' design. *Current Opinion Structure Biology*, **10**, (4), 421-427.

- Tønning E, Sapelnikova S, Christensen J, Carlsson C, Winther-Nielsen M, Dock E, Solna R, Skladal P, Norgaard L, Ruzgas T. and Emneus J. (2005). Chemometric exploration of an amperometric biosensor array for fast determination of wastewater quality. *Biosensors and Bioelectronics*, **21**, (4), 608-617.
- Torrez M, Schultehenrich M. and Livesay D.R. (2003). Conferring thermostability to mesophilic proteins through optimised electrostatic surfaces. *Biophysical Journal*, **85**, 2845-2853.
- Tupper J, Greco O, Tozer G.M. and Dachs G.U. (2004). Analysis of the horseradish peroxidase/indole-3-acetic acid combination in a three dimensional tumor model. *Cancer Gene Therapy*, **11**, 508-513.
- Ugarova N.N, Rozhkova G.D. and Berezin I.V. (1979). Chemical modification of the ϵ -aminogroups solflysine residues in HRP and its effect on the catalytic properties and thermostability. *Biochemica et Biophysica Acta*, **570**, 31-42.
- Valderrama B, Ayala M. and Vazquez-Duhalt R. (2002). Suicide inactivation of peroxidases and the challenge of engineering more robust enzymes. *Chemistry and Biology*, **9**, 555-565.
- van de Velde F, van Rantwijk F. and Sheldon R.A. (2001), Improving the catalytic performance of peroxidase in organic solvents. *Trends in Biotechnology*, **19**, (2), 73-80.
- van den Berg B. and Eijsink V.G.H. (2002) Selection of Mutations for increased protein stability. *Current Opinion in Biotechnology*, **13**, 333-337.
- van Gijlswijk R.P.M, van de Corput M.P.C, Bezrookove V, Wiegant J, Tanke H.J. and Raap A.K. (2000). Synthesis and purification of horseradish peroxidase-labeled oligonucleotides for tyramide-based fluorescence in situ hybridization. *Histochemistry and Cell Biology*, **113** (3): 175-180.
- van Haandel M.J.H, Primus J-L, Tenuis C, Boersma M.G, Osman A.H, Veeger C. and Rietjens I.M.C.M. (1998). Reversible formation of high-valent-iron-oxo-porphyrin intermediates in heme based catalysis: revisiting the kinetic model for Horseradish Peroxidase. *Inorganica Chimica Acta*, **275-276**, 98-105.
- van Haandel M.J.H, Claassems M.J.M, van der Hout N, Boersma M.G, Vervoort J. and Rietjens I.M.C.M. (1999). Differential substrate behaviour of phenol and aniline derivatives during conversion by HRP. *Biochimica et Biophysica Acta*, **435**, 22-29.
- van Regenmortel M.H.V. (2000). Are there two distinct research strategies for developing biologically active molecules: rational design and empirical selection? *Journal of Molecular Recognition*, **13**, (1), 1-4.
- Vazquez-Duhalt R. Fedorak P.M. and Westlake D.W.S. (1992). Role of enzyme hydrophobicity in biocatalysis in organic solvents. *Enzyme Microbial Technology*, **14**, 837-841.

- Varnado C.L and Goodwin D.C. (2004). System for the expression of recombinant hemoproteins in *Escherichia coli*. *Protein Expression and Purification*, **35**, 76-83.
- Veitch N.C. (2004). HRP: a modern view of a classic enzyme. *Phytochemistry*, **65**, 249-259.
- Veitch N.C and Smith A.T. (2000). Horseradish Peroxidase. *Advances in Inorganic Chemistry*, **51**, 107-162.
- Veitch N.C, Gao Y, Smith A.T. and White C.G. (1997). Identification of a critical phenylalanine residue in horseradish peroxidase, Phe179, by site-directed mutagenesis and H-NMR. Implications for complex formation with aromatic donor molecules. *Biochemistry*, **36**, (48), 14751-14761.
- Veitch N.C, Williams R.J.P, Bone N.M, Burke J.F. and Smith A.T. (1995). Solution characterisation by NMR spectroscopy of two horseradish peroxidase isoenzyme C mutants with alanine replacing either Phe142 or Phe143. *European Journal of Biochemistry*, **233**, (2), 650-658.
- Veitch N.C, Williams R.J.P, Bray R.C, Burke J.F, Sanders S.A, Thorneley R.N.F. and Smith A.T. (1992). Structural studies by proton-NMR spectroscopy of plant horseradish peroxidase C, the wild-type recombinant protein from *Escherichia coli* and two protein variants, 41-Phe-Val and 38-Arg-Lys. *European Journal of Biochemistry*, **207**, (2), 521-531.
- Vendruscolo M. (2002). Energetics of Enzyme Stability. *Trends in Biotechnology*, **20**, (1), 1-2.
- Verheart R.M.D, Beekwilder J, Olsthoorn R, van Duin J. and Quax W. J. (2002). Phage display selects for amylases with improved low pH starch binding. *Journal of Biotechnology*, **96**, 103-118.
- Veille C. and Zeikus G.J. (2001). Hyperthermophilic Enzymes: Sources, Uses and Molecular Mechanism for Thermostability. *Microbiology and Molecular Biology Reviews*, **65**, (1), 1-43.
- Vlami-Gardikas A, Smith A.T, Clements J.M. and Burke J.F. (1992), Expression of active HRP in *Saccharomyces cerevisiae*. *Biochemical Society Transactions*, **20**, 111.
- Vlassi M, Cesareni G. and Kokkinidis M. (1999). A correlation between the loss of hydrophobic core packing interactions and protein stability. *Journal of Molecular Biology*, **285**, (2), 817-827.
- Vriend G. (1990). WHAT IF: a molecular modelling and drug design program. *Journal of Molecular Graphics*, **8**, 52-56.
- Wallace G, Spinks G, Kane-Maguire L. (2003). *Conductive Electroactive Polymers*. 2 Ed, CRC Press, London.

- Wandersman C. and Stojiljkovic I. (2000). Bacterial heme sources: the role of heme, hemoprotein receptors and hemophores. *Current Opinion in Microbiology*, **3**, (2), 215-220
- Wang J, Tian B, Nascimento V.B. and Angnes L. (1998). Performance of screen-printed carbon electrodes fabricated from different carbon inks. *Electrochimical Acta*, **43**, 3459-3465.
- Wang L, Jackson W.C, Steinbach P.A. and Tsien R.Y. (2004). Evolution of new nonantibody proteins via iterative somatic hypermutation. *Proceedings of the National Academy of Science, USA*, **101**, (48), 16745-16749.
- Wang W. and Malcom B.A. (1999). Two-stage PCR protocol allowing introduction of multiple mutations, deletions and insertions using QuickChange™ site-directed mutagenesis. *BioTechniques*, **26**, (4), 680-682.
- Wang XQ, Li LS, Van der Meer B.W, Jin J, Tang D, Hu Zi, Li Y. and Li TJ. (2001) Comparison of photovoltaic behaviors for horseradish peroxidase and its mimicry by surface photovoltage spectroscopy. *Biochimica et Biophysica Acta (BBA) - Protein Structure and Molecular Enzymology*, **1544**, (1-2), 333-340.
- Wanger M. and Nicell J.A. (2002). Detoxification of phenolic solutions with horseradish peroxidase and hydrogen peroxide. *Water Research*, **36**, 4041-4052.
- Wells J.A. (1990). Additivity of Mutational Effects in proteins. *Biochemistry*, **29**, (37), 8509-8517.
- Welinder K.G, Justesen A.F, Kjærsgård I.V.H, Jensen R.B, Rasmussen S.K, Jespersen H.M. and Duroux L. (2002). Structural diversity and transcription of class III peroxidases from *Arabidopsis thaliana*. *European Journal of Biochemistry*, **269**, 6063-6081.
- Welinder K.G. (1992). Superfamily of Plant, fungal and bacterial peroxidases. *Current opinion in Structural Biology*, **2**, 388-393.
- Welinder K G. (1979). Amino Acid sequence studies of HRPc. *European Journal Biochemistry*, **96**, 483-502.
- Welinder, K.G, Justesen A.F, Kjærsgård I.V.H, Jensen R.B, Rasmussen S.K, Jespersen H.M and Duroux L. (2002). Structural diversity and transcription of class III peroxidases from *Arabidopsis thaliana*. *European Journal of Biochemistry*, **269**, (24), 6063-6081.
- Wilcheck M. and Miron T. (2002). Orientated versus random protein immobilisation. *Journal of Biochemistry and Biophysical Methods*, **55**, 67-70.
- Wong T.S, Arnold F.H. and Schwaneberg U. (2004). Laboratory Evolution of Cytochrome P450 BM-3 Monooxygenase for Organic Co-Solvents. *Biotechnology and Bioengineering*, **85**, (3), 351-358.

- Wong T.S. and Schwaneberg U. (2003). *Protein Engineering* in bioelectrocatalysis. *Current Opinion in Biotechnology*, **14**, 590-596.
- Woodard S. I. and Dailey H. A. (1995). Regulation of Heme Biosynthesis in *Escherichia coli*. *Archives of Biochemistry and Biophysics*, **316**, (1), 110-115.
- Wuhrer M. Balog C.I, Koeleman C.A, Deelder A.M. and Hokke C.H. (2005). New features of site-specific horseradish peroxidase (HRP) glycosylation uncovered by nano-LC-MS with repeated ion-isolation/fragmentation cycles. *Biochimica et Biophysica Acta*, **1723**, (1-3), 229-239.
- Xu Y, Peng W, Liu X. and Li G. (2004). A new film for the fabrication of an unmediated H₂O₂ biosensor. *Biosensors and Bioelectronics*, **20**, 533-537.
- Yamasaki H, Sakihama Y. and Ikehara N. (1997). Flavonoid-Peroxidase Reaction as a Detoxification Mechanism of Plant Cells against H₂O₂. *Plant Physiology*, **115**, 1405-1412.
- Yang M, Yang Y, Shen G. and Yu R. (2004). Bionzymatic amperometric biosensor for choline based on mediator thionine *in situ* electropolymerized within a carbon paste electrode. *Analytical Biochemistry*, **334**, 127-134.
- Yang S, Huang H, Li S.Y, Ye Y.Z, Wan L, Zhang F.W. and Yuan Z.Y. (2000). Enhancing Penicillin G Acylase Stability by Site-directed Mutagenesis. *Biochimica et Biophysica Sinica*, **32**, (6), 581-585.
- Yang, Z.H. (1997). PAML: a program package for phylogenetic analysis by maximum likelihood. *Computer Applications in the Biosciences*, **13**, (5), 555-556.
- Yang Z.H, Kumar S, and Nei M. (1995). A new method of inference of ancestral nucleotide and amino acid sequences. *Genetics*, **141**, (4), 1641-50.
- Yoshitsune S.Y, Aye H.N, Hong K.J. and Kajiuchi K. (2005). Efficacy of amphiphile-modified laccase in enzymatic oxidation and removal of phenolics in aqueous solution. *Enzyme and Microbial Technology*, **36**, (1), 147-152.
- Zambonelli C, Morandi P, Vanoni M.A, Tedeschi G, Servi S. and Curti B. (2003). Cloning and expression in *Escherichia coli* of the gene encoding *Streptomyces* PMF PLD, a phospholipase D with high transphosphatidyltransferase activity. *Enzyme Microbial Technology*. **33**, 676-688.
- Zaton A.M and de Aspuru E.O. (1995). Horseradish peroxidase inhibition by thiouracils. *FEBS Letters*, **374**, 192-194.
- Zhang K, Diehl M.R. and Tirrell D.A. (2005). Artificial Polypeptide Scaffold for Protein Immobilization. *Journal of the American Chemical Society*, **127**, (29), 10136-10137.

Zhang Y, Olsen D.R, Nguyen K.B, Olson P.S, Rhodes E.T. and Mascarenhas D. (1998). Expression of eukaryotic proteins in soluble form in *Escherichia coli*. *Protein Expression and Purification*, **12**, 159-165.

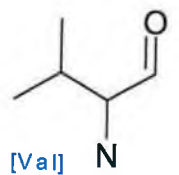
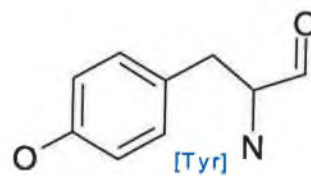
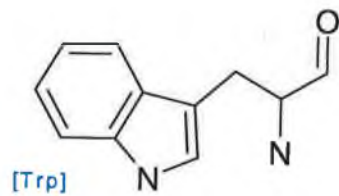
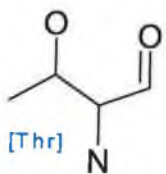
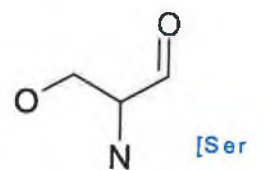
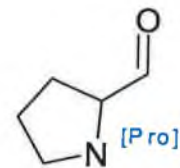
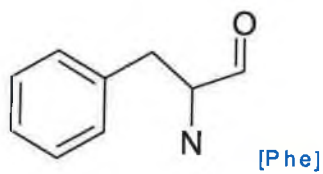
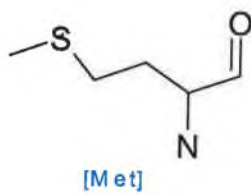
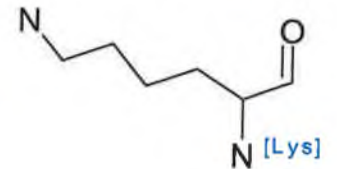
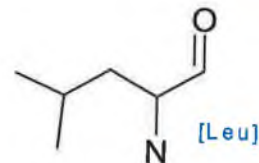
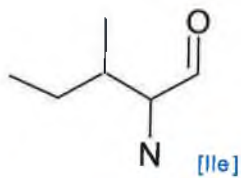
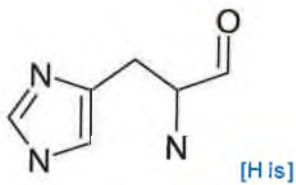
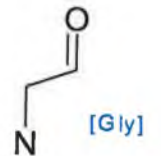
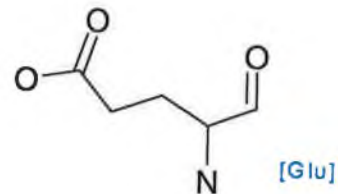
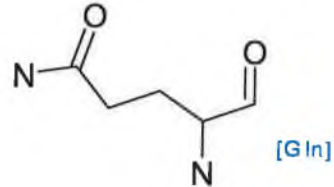
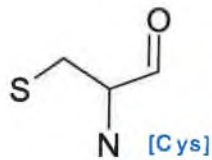
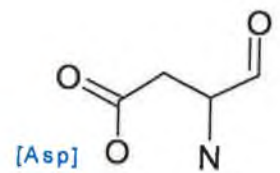
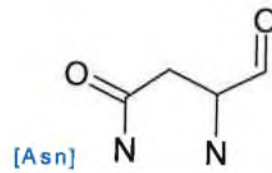
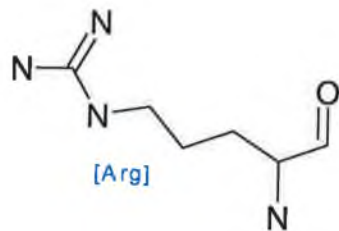
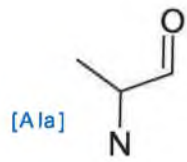
Zhanglin L, Thorsen T. and Arnold F.H (1999). Functional Expression of HRP in *E. coli* by directed evolution. *Biotechnology Progress*, **15**, 467-471.

Zhao H. Giver L. Shao Z. Affholter J.A. and Arnold F.H. (1998). Molecular Evolution by Staggered Extension Process (StEP) in vitro Recombination. *Nature Biotechnology*, **16**, 258-261.

Zhen G, Eggli V, Vörös J, Zammaretti P, Textor M, Glockshuber R. and Kuennemann E. (2004). Immobilization of the Enzyme β -Lactamase on Biotin-Derivatized Poly(L-lysine)-*g*-poly(ethylene glycol)-Coated Sensor Chips: A study on oriented attachment and surface activity by enzyme kinetics and *in-situ* optical sensing. *Langmuir*, **20**, (24), 10464-10473.

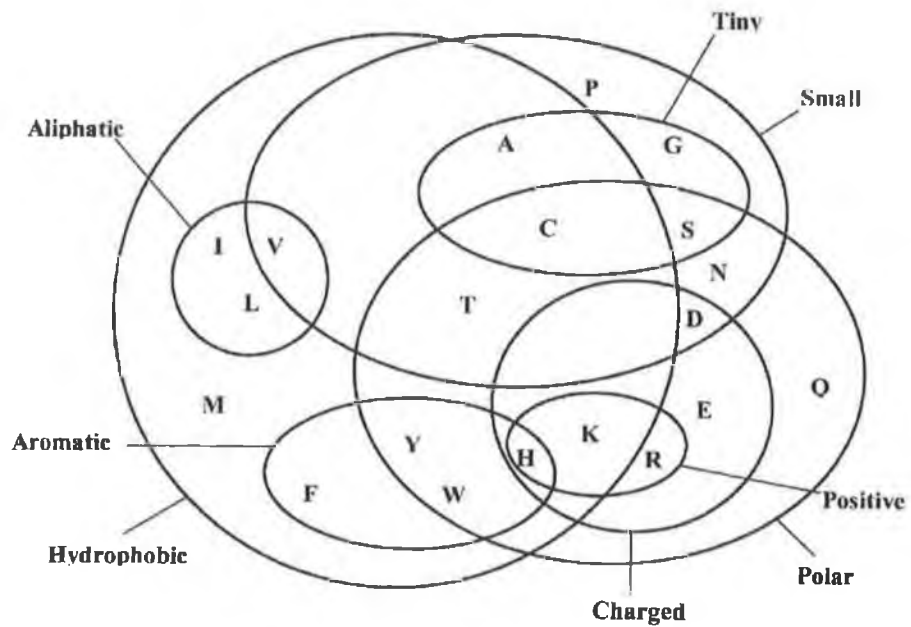
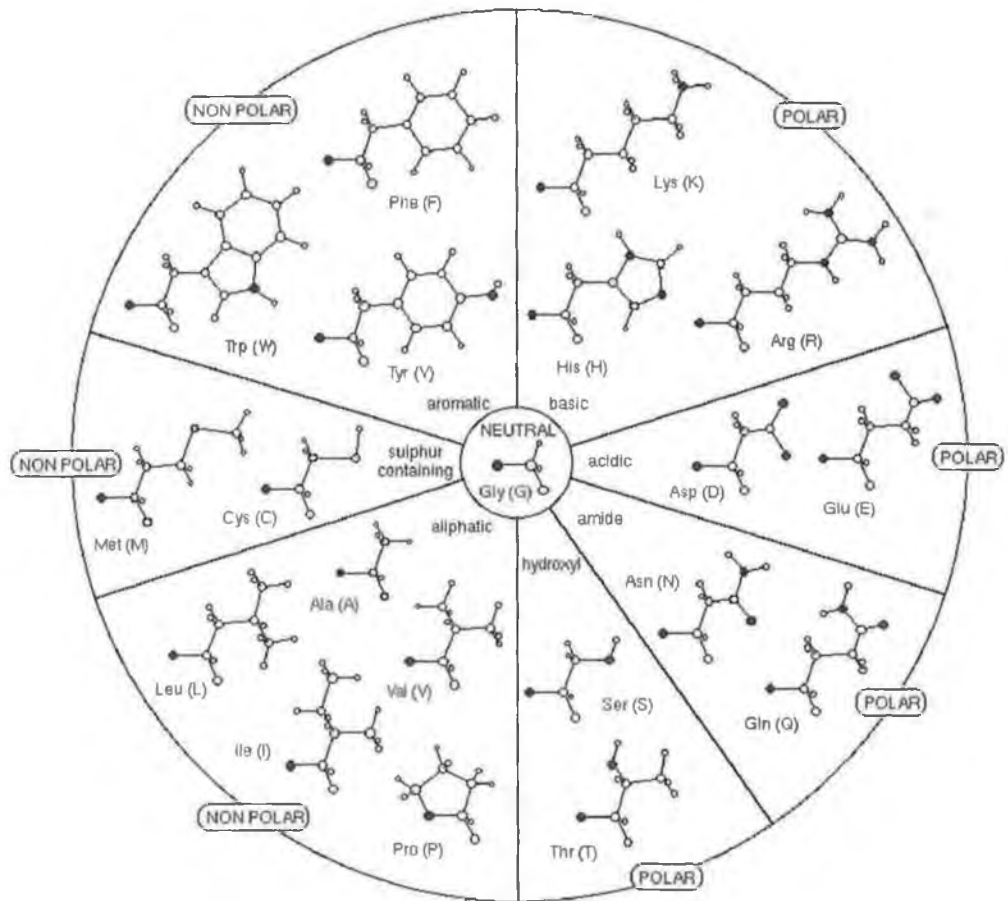
Appendices.

A1. Amino Acid R-groups.



A1 Images generated using ChemDraw (www.cambridgesoft.com).

A2 Amino Acid Characteristics.



A2 images adapted from Protein Design Group, Centro Nacional de Biotecnología, Campus Universidad Autónoma, Cantoblanco, Madrid, Spain. (www.somosierra.cnb.uam.es/wwwPDG/index.php).